AN EFFICIENT ALGORITHM FOR SIMULATION OF THE TIME-DOMAIN MAXWELL SYSTEM

by

Justin Praast

A thesis submitted to the Faculty and the Board of Trustees of the Colorado School of Mines in partial fulfilment of the requirements for the degree of Master of Science (Applied Mathematics and Statistics).

Golden, Colorado

Date _____

Signed: _____
Justin Praast

Signed: _____
Dr. Mahadevan Ganesh
Thesis Advisor

Golden, Colorado

Date _____

Signed: _____
Dr. Willy Hereman
Professor and Head
Department of Applied Mathematics and Statistics

ABSTRACT

The finite-difference time-domain (FDTD) method for computational electromagnetics is a versatile family of schemes and provides an efficient framework for the parallel implementation we consider. FDTD is a popular method for computing approximate solutions of the time-domain Maxwell system that may include a variety of heterogeneous material types and network elements. Extensions to the standard FDTD method have enabled the modeling of processes in unbounded domains such as far-field responses.

We investigate a FDTD formulation that is capable of handling linear, isotropic, nondispersive, non-hysteretical materials and also consider the implementation of two common useful network elements. We discuss the derivation of absorbing boundary conditions, techniques for obtaining far-field responses, and the inclusion of incident plane waves from distant sources. We compare our simulation results for selected transmission-line, antenna, and scattering problems with theory and previous work. We develop and implement a single-program multiple-data parallel computing scheme for efficient computation of FDTD solutions and provide details of the implementation and overhead of each of the several techniques considered in the thesis. We demonstrate that our parallel implementation provide competitive values for speedup for a class of scattering and far-field simulations. We observed that the scalability of our implementation of the FDTD scheme is in particular efficient for long time simulation of Maxwell systems on large size electromagnetic domains.

TABLE OF CONTENTS

LIST OF FIGURES

LIST OF TABLES

ACKNOWLEDGMENTS

I would like to acknowledge my advisor, Dr. Mahadevan Ganesh for his exceptional guidance and patience, and Crystal for unending support.

CHAPTER 1

INTRODUCTION

As there are a multitude of applications for detailed solutions to Maxwell's equations, we will examine one popular scheme from computational electromagnetics. The Finite-Difference Time-Domain (FDTD) method is a scheme for approximating solutions to the first-order coupled Maxwell system in the time domain. Kane Yee described and demonstrated the method in a 1966 paper [22] though its usage was somewhat limited for some time after its introduction. Many notable extensions to the method have been developed, such as circuit elements and sources with suitably realistic behavior [19], boundaries which simulate unbounded domains [2, 16], and techniques to obtain far-field data from the simulated near-field [7]. These and many other extensions, together with the general increase of availability of computing power, has led to increasing utilization of FDTD schemes.

Our focus is on the second-order convergent, explicit formulation of the scheme originally proposed by Yee [22]. In Chapter 2 we develop the scheme to conform to a Cartesian grid. The simulation of objects which do not conform to such a grid then necessarily entails a compromise in the accuracy of the object model itself, known as the "staircasing" effect. A variety of averaging schemes exist to allay this problem, and we will examine one of the simpler schemes to reduce the staircasing effect.

As our FDTD derivation is an explicit method, it is subject to a stability condition. In Chapter 3 we derive the numerical dispersion relation and find its relationship with the stability condition for this scheme. One main advantage of a time-domain scheme is that it inherently provides a broadband response. Many popular frequency-domain solution schemes exist to solve Maxwell's equations, however, they must be run separately for each frequency of interest. In comparison, a broadband pulse can be introduced and multiple frequency responses extracted from one FDTD simulation. So in Chapter 3 we also consider some widely used broadband pulse waveforms and their impacts on simulation accuracy.

In Chapter 4 we consider a few other lumped elements as in [7, 19] which add to the number of network simulations possible in FDTD. We also consider the sampling of voltage and current from

field data. We review the calculation of scattering parameters using these sampled values in [13], and observe their utility in characterizing high-frequency networks through simulation.

One of the most challenging issues with FDTD simulations is simulating an unbounded domain without incurring excessive computational cost. FDTD's inherently confined simulation domain is one of its disadvantages, especially paired with reflective Dirichlet boundaries. In Chapter 5 we examine three of the most-used absorbing boundary conditions, which simulate the radiation of EM waves outward across the simulation boundary. We derive the Mur radiative boundary condition for first-order and show how the second-order and higher derivations can proceed. The Mur boundary scheme was superseded by the split-field perfectly matched layer introduced in 1994-1996 by Berenger [1, 2]. In turn, we describe an improvement to Berenger's split-field perfectly matched layer (PML) absorbing boundary condition (ABC) includes the convolutional PML (CPML) introduced by Kuzuoglu and Mittra in 1996, and an implementation described by Roden and Gedney in 2000 in [16].

One popular application of computational electromagnetics is to obtain the scattering profile of arbitrary objects, for example to compute radar profiles. Obtaining such a scattering profile in FDTD is not so straightforward; simulating far field results directly is very often infeasible due to constraints in computer memory and computation time. In Chapter 6 we consider an alternative scheme, in which we terminate the simulation domain nearer to the scattering objects and use equivalent current techniques to estimate the far field using only near field simulation results. We also consider the implementation of very distant sources, and the scattered field and incident field formulation for scattering problems. We develop a technique to simulate a plane wave incident field which impinges on the domain from arbitrary direction.

In Chapter 7 we consider one of the most significant advantages of the FDTD method, its suitability for parallel computation. Modest local data dependence allows the straightforward construction of single-program multiple-data parallel programs for simulation, with modest interprocess communication requirements and significant reduction in computation time for large enough simulation domains. We will develop and demonstrate a parallel-computing implementation and show its efficacy in reducing computation times.

We begin Chapter 2 with a review and brief description of Maxwell's equations.

CHAPTER 2

DERIVATION OF STANDARD FDTD UPDATING EQUATIONS

Maxwell's laws fully describe the relations between electric charge, electric fields, and magnetic fields. Symbols used include ρ, the charge density function in a space, $\vec{J}$, the current density or amount of charge passing through a cross-sectional area of space per unit time; $\vec{E}$, the electric field, $\vec{B}$, the magnetic field, ε_0, a constant denoting the measured permittivity of freespace, and μ_0, a constant denoting the measured permeability of freespace. We will use the values $\varepsilon_0 = 8.854187817 \times 10^{-12} C^2/Nm^2$ and $\mu_0 = 4\pi \times 10^{-7} N/A^2$. Some find Maxwell's laws clearest in their integral forms; however, our finite difference scheme will directly make use of the differential forms of Maxwell's laws.

2.1 Maxwell's Laws

We repeat and briefly explain Maxwell's laws in their integral formulations.

- Ampere's law with Maxwell's Correction: Time-varying electric field flux, and the movement of electric charge, both induce a magnetic field that encircles the current and flux change. For a simple surface S and the closed loop C:

$$\oint_C \vec{B} \cdot ds = \mu_0 \left[\int_S \vec{J} \cdot da + \varepsilon_0 \int_S \frac{\partial \vec{E}}{\partial t} \cdot da \right],$$

  where applying the right-hand-rule to the direction of traversal of C agrees with the positive sense of da.

- Faraday's law: A magnetic flux that changes in time will induce an encircling electric field:

$$\oint_c \vec{E} \cdot ds = -\int_S \frac{\partial \vec{B}}{\partial t} \cdot da.$$

- Gauss's law for electricity: The total outward flux of an electric field across a closed simple surface is proportional to the total electric charge enclosed by the surface:

$$\int_S \vec{E} \cdot da = \frac{1}{\varepsilon_0} \int_V \rho \, dv.$$

- Gauss's law for magnetism: The total outward flux of a magnetic field across a closed simple surface is equal to the total magnetic charge enclosed by the surface; as no magnetic charge has ever been observed and recorded,

$$\int_S \vec{B} \cdot da = 0.$$

The above integral formulations also yield the boundary conditions which must hold at material boundaries, which will be derived below. First, we may employ Stokes's theorem and the divergence theorem repeatedly to find the differential format of Maxwell's laws.

2.1.1 Differential Formulations

- Ampere's Law with Maxwell's Correction: Apply Stokes's theorem to the left hand side path integral to obtain $\int_S \nabla \times \vec{B} \cdot da$; combine the two terms on the right to obtain a single surface integral $\int_S \vec{J} + \varepsilon_0 \frac{\partial \vec{E}}{\partial t} \cdot da$. As the surface of integration is arbitrary, we have that the integrands are equal:

$$\nabla \times \vec{B} = \mu_0 \vec{J} + \mu_0 \varepsilon_0 \frac{\partial \vec{E}}{\partial t}.$$

- Faraday's Law: A very similar process yields that the curl of the electric field equals the negative of the change of enclosed magnetic flux:

$$\nabla \times \vec{E} = -\frac{\partial \vec{B}}{\partial t}.$$

- Gauss's law for electricity: Employ the divergence theorem on the left hand side of Gauss's Law to obtain $\int_V \nabla \cdot \vec{E} \, dv$. Then recognize that the volumes are arbitrary, hence the integrands are equal. Thus the divergence of the electric field equals the charge density field:

$$\nabla \cdot \vec{E} = \frac{1}{\varepsilon_0} \rho.$$

- Gauss's law for magnetism: Analogously to Gauss's Law, we obtain

$$\nabla \cdot \vec{B} = 0.$$

Integral and differential forms of Maxwell's Laws completely describe the behavior of $\vec{E}$ and $\vec{B}$ fields. However, we choose to reformulate to emphasize the quantity of free or imposed (as opposed to bound) charge in the system. Charge terms occur in Gauss' law and in the modified Ampere's law, and so these are altered by the reformulation, but Gauss's laws remain the same.

To clarify the manipulations which lead to our governing FDTD equations, we should briefly consider the effect of fields on dielectric and magnetic media. A dielectric is as an insulating material which responds to an electric field with a strong dipole tendency but no current flow. On the molecular scale the response is a significant charge shift which opposes and diminishes the imposed electric field. The strength of this response is dependent on the material, and of course can vary within an object. In more complicated materials the polarization response or, indeed, the permittivity or permeability may display nonlinearity (response cannot be captured by a constant times field strength), inhomogeneity (response differs in space), hysteresis (response differs based on fields in the past), dispersivity (response differs based on frequency of a time varying field), or anisotropy (response differs based on direction of imposed field). At any given time, independent of how it originated, the polarization is characterized as a *polarization field* $\vec{P}$. The magnitude of the field is proportional to the existing charge separation and the direction of negative charge gives the direction of the field.

The material structure is on average fixed, so in the direction of $\vec{P}$ and within the dielectric, the negative charge concentration of one particle cancels out the positive concentration of the next. However, a variation of $\vec{P}$ in space implies that locally there is not exact cancellation. The divergence of $\vec{P}$ is related to the bound charge density:

$$-\nabla \cdot \vec{P} = \rho_b$$

We may write the total charge density field as the sum of free and bound charges; $\rho = \rho_f + \rho_b$.

This is the first of the constitutive equations which will help to reformulate Maxwell's equations. Substituting the bound charge term in Gauss's law for electricity, we obtain

$$\nabla \cdot \vec{E} = \frac{1}{\varepsilon_0}\left(\rho_f - \nabla \cdot \vec{P}\right)$$

Moving the divergence of polarization to the left side and combining the divergence operators, we obtain $\nabla \cdot \vec{D} \equiv \nabla \cdot \left(\varepsilon_0 \vec{E} + \vec{P}\right) = \rho_f$, where $\vec{D}$ is the electric displacement. For materials which have all the 'nice' properties of linearity, homogeneity, isotropy, and no hysteresis or dispersivity, there is a compact way to express the electric displacement: in these materials, $\vec{P} = \varepsilon_0 \chi_e \vec{E}$ for a constant χ_e called the electric susceptibility. Hence, within these simple materials (and empty space) we have $\vec{D} = \varepsilon_0(1+\chi_e)\vec{E} = \varepsilon \vec{E}$ for the convenience constant $\varepsilon = \varepsilon_0(1+\chi_e)$ which is named the permittivity.

Currents are also represented by a combination of free and bound charge; to fully account for $\vec{J}$ we must split it into three fields, each of which is a flux density term, like $\vec{J}$: $\vec{J_f}$, the current of free charge, $\vec{J_b}$, the bound current existing in a magnet, and $\vec{J_p}$, the polarization current that arises from a change in $\vec{P}$ over time and the resulting redistribution of bound charge. Sources [12], [9] or similar electromagnetics texts should contain more detail on the effects and behavior of these terms $\vec{J_b}$, $\vec{J_f}$.

The bound current is related to the magnetization of the object in which it occurs by: $\vec{J_b} = \nabla \times \vec{M}$ where M is the magnetization field. The polarization current is related to the change in polarization as $\vec{J_b} = \frac{\partial \vec{P}}{\partial t}$. With these substitutions into Ampere's law with Maxwell's corrections,

$$\nabla \times \vec{B} = \mu_0 \left(\vec{J_f} + \nabla \times \vec{M} + \frac{\partial \vec{P}}{\partial t}\right) + \mu_0 \varepsilon_0 \frac{\partial \vec{E}}{\partial t}.$$

Reorganizing in terms of both $\vec{D}$ and a new field definition

$$\vec{H} \equiv \frac{1}{\mu_0}\vec{B} - \vec{M}$$

we obtain Ampere's law with Maxwell's correction in terms of the free current and the electric displacement:

$$\nabla \times \vec{H} = \vec{J_f} + \frac{\partial \vec{D}}{\partial t}.$$

These expressions of Maxwell's equations naturally have their integral forms as well. The derivations are very similar to those above.

$$\int_S \vec{D} \cdot da = q_{f\cdot enc}, \qquad \int_S \vec{B} \cdot da = 0,$$
$$\oint_C \vec{E} \cdot ds = -\frac{d}{dt}\int_S \vec{B} \cdot da, \qquad \oint_c \vec{H} \cdot ds = I_{f\cdot enc} + \frac{d}{dt}\int_S \vec{D} \cdot da,$$

where $I_{f\cdot enc} \equiv \int_S \vec{J}_f \cdot da$, the enclosed free current.

We will also use the law of conservation of charge

$$-\int_S \vec{J} \cdot da = \frac{\partial}{\partial t}\int_V \rho dv$$

or in differential form,

$$\nabla \cdot \vec{J} = -\frac{\partial \rho}{\partial t}.$$

In our FDTD formulation, fictional magnetic charges are allowed to exist, and we consider the related magnetic conductivity and imposed magnetic current. This mainly simplifies the inclusion of certain absorbing boundary conditions and the expression of far-field calculations, and allows magnetic current driving sources.

We will now reformulate Maxwell's equations assuming linear, isotropic, non-dispersive, non-ferromagnetic, non-hysteretical conditions, possibly including conductivity. We will use fields $\vec{E}$ and $\vec{H}$; as derived above, the constitutive equations become $\vec{D} = \varepsilon\vec{E}$ and $\vec{B} = \mu\vec{H}$ for permittivity ε and permeability μ. Two conductivity properties of the material must be considered: electric, signified σ_e, and magnetic, σ_m. The free electric current is a sum of impressed current density $\vec{J}_i$ with the product of the electric conductivity and existing electric field: $\vec{J}_f = \sigma_e\vec{E} + \vec{J}_i$. Magnetic current is modeled similarly: the current density field $\vec{M}_c = \sigma_m\vec{H} + \vec{M}_i$. Then we may write curl equations:

$$\nabla \times \vec{H} = \varepsilon\frac{\partial \vec{E}}{\partial t} + \sigma_e\vec{E} + \vec{J}_i, \tag{2.1}$$

$$\nabla \times \vec{E} = -\mu\frac{\partial \vec{H}}{\partial t} - \sigma_m\vec{H} - \vec{M}_i. \tag{2.2}$$

2.1.2 Boundary Conditions

The following conditions are not expressly implemented as part of the FDTD algorithm, but are derived and included for completeness. At the transition from one material to another, the scalar fields of material properties may be discontinuous. However, applying Maxwell's laws across a discontinuity yields conditions that the fields must obey across a material boundary. These boundary conditions are derived without consideration of the fictitious magnetic charges that are incorporated into the FDTD formulation.

The first is most easily expressed using the integral statement of Gauss's law: consider using as a Gaussian surface a very thin cuboid, with some fixed length and width parallel to the material boundary, and a thickness which crosses the material boundary perpendicular to the surface. As the thickness approaches zero, consider the closed surface integral $\oint_S \vec{D} \cdot da$. The contributions of the sides perpendicular to the material boundary (components of $\vec{D}$ parallel to the material boundary) vanish as thickness goes to zero. This leaves only the components of $\vec{D}$, on each side of the boundary, which are perpendicular to the material boundary. Supposing we orient $\vec{a}$ upward, and label the top face of our Gaussian surface as 1, and the bottom face 2; then we may say that component of $\vec{D}$ which is above the boundary, perpendicular to and pointing away from the boundary, contributes positively to the integral; label this $D_1^{\perp}$. Similarly, that component of $\vec{D}$ which is below the boundary, perpendicular to and pointing toward the boundary, contributes negatively to the integral; label this $D_2^{\perp}$.

Finally, recall the right side of the equation of Gauss's law: free charge enclosed. Considering that as thickness goes to 0, the only charge density which always contributes to the overall charge enclosed is free surface charge density, typically labeled σ_f; the total charge then enclosed by our Gaussian surface is $\sigma_f \cdot a$. Hence, after cancelling the total area from both sides, we have the first boundary condition:

$$D_1^{\perp} - D_2^{\perp} = \sigma_f$$

A very similar calculation applied to Maxwell's fourth equation yields the second boundary condition:

$$B_1^{\perp} - B_2^{\perp} = 0$$

Similarly, consider a rectangular closed path across the material boundary. Take its thickness to zero, then the enclosed magnetic flux approaches zero; likewise the only terms that contribute to a path integral are those parallel to the boundary. Using Faraday's law, then, we obtain

$$\vec{E}_1^{\parallel} - \vec{E}_2^{\parallel} = 0.$$

In a similar calculation with Ampere's law, the electric flux goes to zero but the current term may not: we must consider free surface current density. This results in a fourth boundary condition of

$$\vec{H}_1^{\parallel} - \vec{H}_2^{\parallel} = \vec{K}_f \times \hat{n},$$

where $\vec{K}_f$ is the free *surface* current density field, and $\hat{n}$ is the local normal to the material boundary. Here, note that the sign convention is important; $\hat{n}$ is directed toward the $\vec{H}_1$ side of the boundary.

The conservation law gives us one more boundary condition, by way of examining a thin cuboid Gaussian surface crossing the boundary of a material: a discontinuity of current density arises only where there is a time-varying surface current:

$$J_1^{\perp} - J_2^{\perp} = -\frac{\partial \vec{\sigma}}{\partial t},$$

where $\vec{\sigma}$ is a surface describing surface charge density at the material boundary.

2.2 EM Waves in Simple Materials

For a linear, isotropic, homogeneous, non-dispersive, non-hysteretical, non-ferromagnetic material we have constant values of ε and μ in the definitions $\vec{D} = \varepsilon\vec{E}$ and $\vec{H} = \frac{1}{\mu}\vec{B}$. Suppose also that the material is perfectly non-conducting and there is a constant zero net charge distribution everywhere. Take Faraday's law $\nabla \times \vec{E} = -\frac{\partial \vec{B}}{\partial t}$ and apply the curl and the curl-curl vector identity:

$$\nabla \times \left(\nabla \times \vec{E}\right) = \nabla\left(\nabla \cdot \vec{E}\right) - \nabla^2\vec{E} = \nabla \times \left(-\frac{\partial \vec{B}}{\partial t}\right).$$

Pass the time derivative across the spatial derivatives and we obtain Ampere's law with Maxwell's correction:

$$\nabla \times \left(-\frac{\partial \vec{B}}{\partial t} \right) = -\frac{\partial}{\partial t} \left(\nabla \times \vec{B} \right) = -\frac{\partial}{\partial t} \left(\mu\varepsilon \frac{\partial \vec{E}}{\partial t} \right).$$

Using Gauss's law and that the space is free of net charge density, we obtain the wave equation

$$\nabla^2 \vec{E} = \mu\varepsilon \frac{\partial^2 \vec{E}}{\partial t^2}.$$

A similar process using Ampere's law with Maxwell's correction $\nabla \times \vec{H} = \frac{\partial \vec{D}}{\partial t}$. We may move the constant μ to the right hand side and pull constant ε out of the $\vec{D}$ term. We obtain a very similar result regarding the magnetic field. Using the curl-curl vector identity, Faraday's law and Gauss's law for magnetism:

$$\nabla \times \left(\nabla \times \vec{B} \right) = -\nabla^2 \vec{B} = \frac{\partial}{\partial t} \left(\mu\varepsilon \nabla \times \vec{E} \right) = \frac{\partial}{\partial t} \left(-\mu\varepsilon \frac{\partial \vec{B}}{\partial t} \right),$$

resulting in

$$\nabla^2 \vec{B} = \mu\varepsilon \frac{\partial^2 \vec{B}}{\partial t^2}.$$

Comparing with the wave equation, we may recognize a constant wavespeed term in the coefficient $\mu\varepsilon$; treating it as a coefficient $\frac{1}{v^2}$ we may solve for phase speed

$$v_p = \frac{1}{\sqrt{\mu\varepsilon}},$$

the speed of light in the material. Of course, notice that if the domain is vacuum, then $\mu = \mu_0$ and $\varepsilon = \varepsilon_0$, and we obtain

$$v_p = \frac{1}{\sqrt{\mu_0 \varepsilon_0}} = c.$$

The wave nature of fields $\vec{E}$ and $\vec{B}$ under the prior assumptions will be useful in showing the stability criterion of FDTD in Chapter 3.

2.3 Finite Difference Time Domain Modeling

Faraday's and modified Ampere's laws are vector equalities; thus in 3D they constitute a system of six first-order differential equations, which can be approximated with finite difference operators.

At this point we make use of the differential formulations of Maxwell's equations.

2.3.1 Finite Difference Operators

We replace the derivatives in Maxwell's curl equations with discrete approximations. Let us briefly develop the central difference operator and see that it is a second-order approximation. Choosing and fixing a small value for Δx in each of the one-sided limit definitions of the derivative, obtain

$$\frac{\partial f}{\partial x}(a) = \lim_{\Delta x \to 0} \frac{f(a+\Delta x) - f(a)}{\Delta x} \approx \frac{f(a+\Delta x) - f(a)}{\Delta x}$$

$$\frac{\partial f}{\partial x}(a) = \lim_{\Delta x \to 0} \frac{f(a) - f(a-\Delta x)}{\Delta x} \approx \frac{f(a) - f(a-\Delta x)}{\Delta x}$$

The arithmetic mean of these two operators is itself an operator, and a more accurate approximation. Taking the Taylor expansions of the forward and backward difference operators,

$$f(a+\Delta x) = f(a) + \Delta x f'(a) + \frac{(\Delta x)^2}{2!} f''(a) + \frac{(\Delta x)^3}{3!} f'''(a) + \dots$$

$$f(a-\Delta x) = f(a) - \Delta x f'(a) + \frac{(\Delta x)^2}{2!} f''(a) - \frac{(\Delta x)^3}{3!} f'''(a) + \dots$$

we may assemble the forward difference operator:

$$\frac{f(a+\Delta x) - f(a)}{\Delta x} = f'(a) + \frac{\Delta x}{2} f''(a) + \frac{(\Delta x)^2}{6} f'''(a) + \dots$$

Observe that the exact derivative $f'(a)$ occurs, and that the following terms constitute error which is dominated by argument Δx. Since Δx is degree 1, the error is $\mathcal{O}(\Delta x)$. The backward difference operator expansion is

$$\frac{f(a-\Delta x) - f(a)}{\Delta x} = f'(a) - \frac{\Delta x}{2} f''(a) + \frac{(\Delta x)^2}{6} f'''(a) + \dots$$

Now, the arithmetic mean of these operators looks like

$$\frac{1}{2}\left(\frac{f(a+\Delta x) - f(a) + f(a) - f(a-\Delta x)}{\Delta x}\right) = \frac{f(a+\Delta x) - f(a-\Delta x)}{2\Delta x}$$

$$\frac{f(a+\Delta x)-f(a-\Delta x)}{2\Delta x} = f'(a) + \frac{(\Delta x)^2}{12} f'''(a) + \ldots$$

Error in this central difference approximation is $\mathcal{O}(\Delta x^2)$. Note that this approximation is accurate at point a despite referencing function values only at $a + \Delta x$ and $a - \Delta x$. This is key in the formulation of the staggered grid.

2.3.2 The Yee cell

In 1966 Kane Yee published a paper describing the FDTD scheme modeling the evolution of $\vec{E}$ and $\vec{H}$ fields in 3 dimensions in the time domain [22]. The Yee cell is the spatial organization of the scalar components E_x, E_y, E_z, H_x, H_y, H_z relative to each other and to the grid or node points which partition the spatial domain.

Field elements are placed to surround one another, so that the curl about one field element is easily captured by the others nearby. Physical properties of the domain – the permittivity ε, for example – are specified at the same points in space as the field elements they directly affect – the electric field $\vec{E}$, for example. This design simplifies indexing and reduces averaging error.

The Yee cell is employed as the finest element into which a problem domain is divided, and identified by node index triplet (i, j, k). For a given domain that we wish to model, we first choose a grid size in each dimension, at which to divide the domain into cells. The partitioning is regular, cell indexing is referred to by 'nodes', and each is assigned the Yee cell layout for field components and material property coefficients.

For convenience we repeat equation (2.1):

$$\nabla \times \vec{H} = \varepsilon \frac{\partial \vec{E}}{\partial t} + \sigma^e \vec{E} + \vec{J_i}$$

Now consider just the x components of the vector quantities:

$$\frac{\partial H_z}{\partial y} - \frac{\partial H_y}{\partial z} = \varepsilon \frac{\partial E_x}{\partial t} + \sigma^e E_x + J_{ix}$$

Substitute central finite difference operators for space and time derivatives in the scalar equation above. Examining the Yee cell, it is clear that a central difference approximation in y using $H_y(i, j, k)$ and $H_y(i, j, k-1)$ components is centered, and most accurate, at the location of $E_x(i, j, k)$.

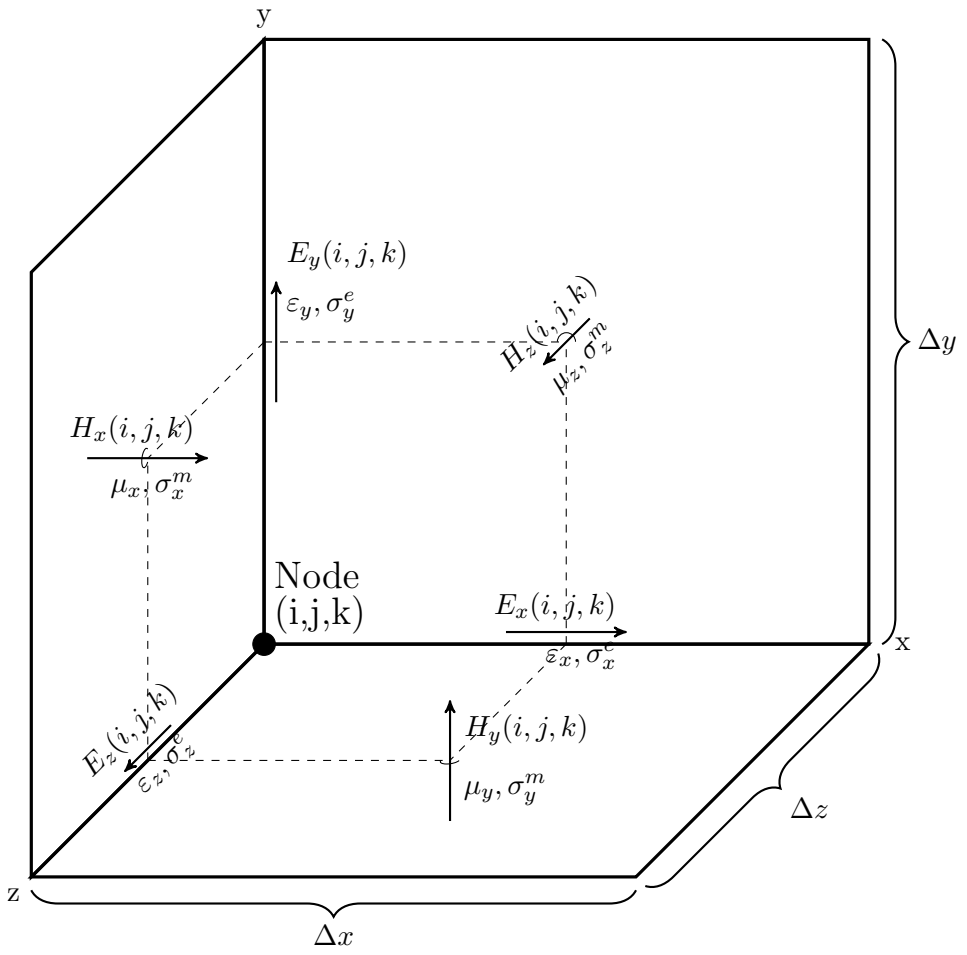

Figure 2.1: Diagram of Yee cell with field components and their associated material properties

Likewise a central difference in z using $H_z(i,j,k)$ and $H_z(i,j-1,k)$ should be most accurate at the location of $E_x(i,j,k)$. Similarly for the other central difference operators which we will use, the positioning of the magnetic field components makes the central difference operators most accurate at the locations of the corresponding electric field components.

Updates are staggered in time as well:

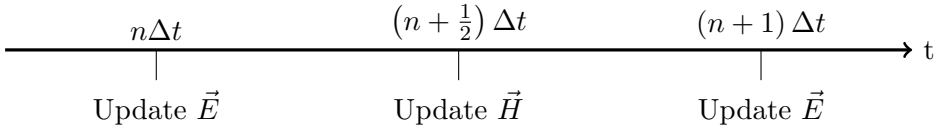

Figure 2.2: Diagram of updates staggered in time

A central difference formulation applied to $\vec{E}$ at $\left(n+\frac{1}{2}\right)\Delta t$ depends upon $n\Delta t$ and $(n+1)\,\Delta t$, which motivates the choice of updating $\vec{H}$ at half-integer time steps.

Assume we locate node index $(0,0,0)$ at the origin. We adopt notation for field values at the points represented on the Yee cell as follows. For example, the $\vec{E}$ field's x component function defined for node (i,j,k) at time n, and its label:

$$\vec{E}((i+\frac{1}{2})\Delta x, j\Delta y, k\Delta z, n\Delta t)\cdot\hat{i} \equiv E_x^n(i,j,k).$$

We use analogous notation for $\vec{H}$. A spatial offset to the domain can be applied to the continuous fields on the left hand side while the labeling on the right remains unchanged.

2.3.3 Discretization and Updating Equations

Now we finish substituting difference operators. We repeat the scalar x component equation listed previously:

$$\frac{\partial H_z}{\partial y} - \frac{\partial H_y}{\partial z} = \varepsilon\frac{\partial E_x}{\partial t} + \sigma^e E_x + J_{ix}$$

Substitute central difference operators for derivatives in time and space:

$$\frac{H_z^{n+\frac{1}{2}}(i,j,k) - H_z^{n+\frac{1}{2}}(i,j-1,k)}{\Delta y} - \frac{H_y^{n+\frac{1}{2}}(i,j,k) - H_y^{n+\frac{1}{2}}(i,j,k-1)}{\Delta z} = \tag{2.3}$$
$$\varepsilon_x(i,j,k)\frac{E_x^{n+1}(i,j,k) - E_x^n(i,j,k)}{\Delta t} + \sigma_x^e(i,j,k)E_x^{n+\frac{1}{2}}(i,j,k) + J_{ix}^{n+\frac{1}{2}}(i,j,k).$$

Notice the last two terms on the right hand side, both referring to the time $t_{n+\frac{1}{2}}$. The current density term $J_{ix}(i,j,k)$ is effectively a parameter, so we allow it without modification. However, the electric component is not chosen to be defined at any half-integer time steps. We replace the term with the mean of the values at times $t = n\Delta t$ and $t = (n+1)\Delta t$. This incurs error that is second-order accurate in Δt:

$$E_x(x, t + \frac{1}{2}\Delta t) = E_x(x,t) + \frac{\Delta t}{2}\partial_t E_x(x,t) + \frac{\Delta t^2}{4}\frac{\partial_t^2 E_x(x,t)}{2} + \mathcal{O}(\Delta t^3),$$

$$E_x(x, t - \frac{1}{2}\Delta t) = E_x(x,t) - \frac{\Delta t}{2}\partial_t E_x(x,t) + \frac{\Delta t^2}{4}\frac{\partial_t^2 E_x(x,t)}{2} + \mathcal{O}(\Delta t^3).$$

Sum and halve these equations to form the mean, then cancel terms to obtain:

$$\frac{E_x(x, t + \frac{1}{2}\Delta t) + E_x(x, t - \frac{1}{2}\Delta t)}{2} = \frac{1}{2}\left[2E_x(x,t) + \Delta t^2 \frac{\partial_t^2 E_x(x,t)}{4} + \mathcal{O}(\Delta t^4)\right].$$

which is second-order error in Δt to the value $E_x(x,t)$.

Rewriting the discretized equation (2.3) with the preceding substitution:

$$\frac{H_z^{n+\frac{1}{2}}(i,j,k) - H_z^{n+\frac{1}{2}}(i,j-1,k)}{\Delta y} - \frac{H_y^{n+\frac{1}{2}}(i,j,k) - H_y^{n+\frac{1}{2}}(i,j,k-1)}{\Delta z} =$$
$$\frac{\varepsilon_x(i,j,k)}{\Delta t}\big(E_x^{n+1}(i,j,k) - E_x^n(i,j,k)\big) + \frac{\sigma_x^e(i,j,k)}{2}\big(E_x^{n+1}(i,j,k) + E_x^n(i,j,k)\big) + J_{ix}^{n+\frac{1}{2}}(i,j,k)$$

Collect both E_x terms defined at $t = (n+1)\Delta t$:

$$\left(\frac{\varepsilon_x(i,j,k)}{\Delta t} + \frac{\sigma_x^e(i,j,k)}{2}\right) E_x^{n+1}(i,j,k) =$$
$$\frac{1}{\Delta y}\big(H_z^{n+\frac{1}{2}}(i,j,k) - H_z^{n+\frac{1}{2}}(i,j,k-1)\big) + \frac{1}{\Delta x}\big(H_y^{n+\frac{1}{2}}(i,j,k-1) - H_y^{n+\frac{1}{2}}(i,j,k)\big) +$$
$$\left(\frac{\varepsilon_x(i,j,k)}{\Delta t} - \frac{\sigma_x^e(i,j,k)}{2}\right) E_x^n(i,j,k) - J_{ix}^{n+\frac{1}{2}}(i,j,k).$$

Combining fractions and dividing through by the coefficient on the left side:

$$E_x^{n+1}(i,j,k) = \left(\frac{2\Delta t}{(2\varepsilon_x(i,j,k) + \sigma_x^e(i,j,k)\Delta t)\Delta y}\right)\big(H_z^{n+\frac{1}{2}}(i,j,k) - H_z^{n+\frac{1}{2}}(i,j-1,k)\big) + \qquad (2.4)$$
$$+ \left(\frac{2\Delta t}{(2\varepsilon_x(i,j,k) + \sigma_x^e(i,j,k)\Delta t)\Delta z}\right)\big(H_y^{n+\frac{1}{2}}(i,j,k-1) - H_y^{n+\frac{1}{2}}(i,j,k)\big) +$$

$$+\left(\frac{2\varepsilon_x(i,j,k)-\sigma_x^e(i,j,k)\Delta t}{2\varepsilon_x(i,j,k)+\sigma_x^e(i,j,k)\Delta t}\right)E_x^n(i,j,k)+\left(\frac{-2\Delta t}{2\varepsilon_x(i,j,k)-\sigma_x^e(i,j,k)\Delta t}\right)J_{ix}^{n+\frac{1}{2}}(i,j,k)$$

Equation (2.4) is the updating equation for E_x and under most conditions, is employed to calculate the E_x component array at each time step.

A Note on Labels and Usage

The coefficients on each term will be referred to collectively as updating coefficients. Where needed, we will label them following the naming scheme used in [7]: the subscript has the format 'component, term'. For example, from the previously listed E_x updating equation,

$$C_{exe}=\left(\frac{2\varepsilon_x(i,j,k)-\sigma_x^e(i,j,k)\Delta t}{2\varepsilon_x(i,j,k)+\sigma_x^e(i,j,k)\Delta t}\right),$$

$$C_{exhy}=\left(\frac{2\Delta t}{(2\varepsilon_x(i,j,k)+\sigma_x^e(i,j,k)\Delta t)\Delta z}\right),$$

$$C_{exhz}=\left(\frac{2\Delta t}{(2\varepsilon_x(i,j,k)+\sigma_x^e(i,j,k)\Delta t)\Delta y}\right),$$

$$C_{exj}=\left(\frac{-2\Delta t}{2\varepsilon_x(i,j,k)-\sigma_x^e(i,j,k)\Delta t}\right).$$

The other five standard updating equations have analogously labeled updating coefficients. These will not be explicitly listed here for brevity, but the naming scheme should be understood for future reference. In addition, we will see in Chapter 4 that some common lumped elements and a thin wire approximation are implemented by modifying the values of these updating coefficients, most often the imposed current term.

For most problems, we note that most or all of the domain is free from imposed current $\vec{J}_i$, that is, $\vec{J}_i = 0$ for most (i,j,k). We save significantly on computational resources by not storing an array containing nearly all zeros. For that reason, the standard updating equations contain no $\vec{J}_i$ term and no $\vec{J}_i$ arrays are stored in implementation. We will see that the imposed current term is used exclusively in modeling certain standard circuit elements including sources, and that it is most efficient and convenient to store a small array customized to the circuit element in question.

In addition, there is the potential for ambiguity in referring to ε and μ values. The most common usage is to specify relative permittivity and relative permeability, ε_r and μ_r, where $\varepsilon = \frac{\varepsilon_r}{\varepsilon_0}$

and $\mu = \frac{\mu_r}{\mu_0}$. That is, $\varepsilon_r = \mu_r = 1$ in vacuum. This document will follow the convention of specifying relative values of permittivity and permeability, but omit the r subscript. Where these material properties occur in text, the reader should assume they are relative values unless otherwise specified. Where they are listed in formulas, context determines whether they are absolute or relative. For example, the appropriate scaling is applied in code before the absolute versions of the values are used in updating coefficients.

Now we will resume deriving updating equations. Once more, consider equation (2.1):

$$\nabla \times \vec{H} = \varepsilon \frac{\partial \vec{E}}{\partial t} + \sigma^e \vec{E} + \vec{J}_i.$$

Now we consider just the y components of the vector quantities:

$$\frac{\partial H_x}{\partial z} - \frac{\partial H_z}{\partial x} = \varepsilon \frac{\partial E_y}{\partial t} + \sigma^e E_y + J_{iy}.$$

Substitute central difference operators for space and time derivatives in the scalar equation above:

$$\frac{H_x^{n+\frac{1}{2}}(i,j,k) - H_x^{n+\frac{1}{2}}(i,j,k-1)}{\Delta z} - \frac{H_z^{n+\frac{1}{2}}(i,j,k) - H_z^{n+\frac{1}{2}}(i-1,j,k)}{\Delta x} =$$
$$\varepsilon_y(i,j,k)\frac{E_y^{n+1}(i,j,k) - E_y^n(i,j,k)}{\Delta t} + \sigma_y^e(i,j,k)E_y^{n+\frac{1}{2}}(i,j,k) + J_{iy}^{n+\frac{1}{2}}(i,j,k).$$

As before, replace the $E_y^{n+\frac{1}{2}}$ by its mean across the previous and future timestep. Then, solving for the E_y^{n+1} term proceeds much the same as before, and we obtain

$$\begin{aligned} E_y^{n+1}(i,j,k) = &\left(\frac{2\Delta t}{(2\varepsilon_y(i,j,k) + \sigma_y^e(i,j,k)\Delta t)\Delta z}\right)\left(H_x^{n+\frac{1}{2}}(i,j,k) - H_x^{n+\frac{1}{2}}(i,j,k-1)\right) + \\ &+ \left(\frac{2\Delta t}{(2\varepsilon_y(i,j,k) + \sigma_y^e(i,j,k)\Delta t)\Delta x}\right)\left(H_z^{n+\frac{1}{2}}(i-1,j,k) - H_z^{n+\frac{1}{2}}(i,j,k)\right) + \\ &+ \left(\frac{2\varepsilon_y(i,j,k) - \sigma_y^e(i,j,k)\Delta t}{2\varepsilon_y(i,j,k) + \sigma_y^e(i,j,k)\Delta t}\right)E_y^n(i,j,k) + \left(\frac{-2\Delta t}{2\varepsilon_y(i,j,k) - \sigma_y^e(i,j,k)\Delta t}\right)J_{iy}^{n+\frac{1}{2}}(i,j,k) \end{aligned} \tag{2.5}$$

This is the updating equation for E_y components, with updating coefficients labeled C_{eyhx}, C_{eyhz}, C_{eye}, C_{eyj}. Starting from equation (2.1) and taking the z component equation:

$$\frac{\partial H_y}{\partial x} - \frac{\partial H_x}{\partial y} = \varepsilon \frac{\partial E_z}{\partial t} + \sigma^e E_z + J_{iz}.$$

The process is as above. Replace the $E_z^{n+\frac{1}{2}}$ by its mean across the previous and future timestep, and solve for the E_z^{n+1} term to find:

$$E_z^{n+1}(i,j,k) = \left(\frac{2\Delta t}{(2\varepsilon_z(i,j,k)+\sigma_z^e(i,j,k)\Delta t)\Delta x}\right)\left(H_y^{n+\frac{1}{2}}(i,j,k) - H_y^{n+\frac{1}{2}}(i-1,j,k)\right)+ \tag{2.6}$$
$$+\left(\frac{2\Delta t}{(2\varepsilon_z(i,j,k)+\sigma_z^e(i,j,k)\Delta t)\Delta y}\right)\left(H_x^{n+\frac{1}{2}}(i,j-1,k) - H_x^{n+\frac{1}{2}}(i,j,k)\right)+$$
$$+\left(\frac{2\varepsilon_z(i,j,k)-\sigma_z^e(i,j,k)\Delta t}{2\varepsilon_z(i,j,k)+\sigma_z^e(i,j,k)\Delta t}\right)E_z^n(i,j,k)+\left(\frac{-2\Delta t}{2\varepsilon_z(i,j,k)-\sigma_z^e(i,j,k)\Delta t}\right)J_{iz}^{n+\frac{1}{2}}(i,j,k)$$

This is the updating equation for E_z components.

Now we consider the $\vec{H}$ field. For convenience we repeat equation (2.2):

$$\nabla\times\vec{E} = -\mu\frac{\partial\vec{H}}{\partial t} - \sigma_m\vec{H} - \vec{M}_i.$$

Consider the x equation from this vector equation:

$$\frac{\partial E_z}{\partial y} - \frac{\partial E_y}{\partial z} = -\mu\frac{\partial H_x}{\partial t} - \sigma^m H_x - M_{ix}.$$

Observing the placement of the H_x component on the Yee cell, a central difference operator in y using $E_y(i,j+1,k)$ and $E_y(i,j,k)$ is centered and most accurate at H_x. Similarly for the central difference operators in x and z which we will use, the electric field components are placed to make the central difference operators accurate at the magnetic field component locations.

$$\frac{1}{\Delta y}\left(E_z^n(i,j+1,k) - E_z^n(i,j,k)\right) - \frac{1}{\Delta z}\left(E_y^n(i,j,k+1) - E_y^n(i,j,k)\right) =$$
$$-\frac{\mu_x(i,j,k)}{\Delta t}\left(H_x^{n+\frac{1}{2}}(i,j,k) - H_x^{n-\frac{1}{2}}(i,j,k)\right) - \sigma_x^m(i,j,k)H_x^n(i,j,k) - M_{ix}^n(i,j,k).$$

The last two terms on the right occur at time t_n. The $\vec{M}_i$ field is a user-defined parameter, and we allow it to remain as-is. However, H_x is to be defined at half-integer time steps, and so we substitute the mean over $t_{n-\frac{1}{2}}$ and $t_{n+\frac{1}{2}}$, incurring second-order error in doing so. Substituting this, obtain

$$\frac{1}{\Delta y}\left(E_z^n(i,j+1,k) - E_z^n(i,j,k)\right) + \frac{1}{\Delta z}\left(E_y^n(i,j,k) - E_y^n(i,j,k+1)\right) =$$

$$
\begin{aligned}
&- \frac{\mu_x(i,j,k)}{\Delta t}\big(H_x^{n+\frac{1}{2}}(i,j,k) - H_x^{n-\frac{1}{2}}(i,j,k)\big) - \\
&- \frac{\sigma_x^m(i,j,k)}{2}\big(H_x^{n-\frac{1}{2}}(i,j,k) + H_x^{n+\frac{1}{2}}(i,j,k)\big) - M_{ix}^n(i,j,k).
\end{aligned}
$$

Collect $H_x^{n+\frac{1}{2}}$ terms on the left to find

$$
\begin{aligned}
&\left(\frac{2\mu_x(i,j,k) + \sigma_x^m(i,j,k)\Delta t}{2\Delta t}\right) H_x^{n+\frac{1}{2}}(i,j,k) = \\
&\quad \frac{1}{\Delta y}\big(E_z^n(i,j,k) - E_z^n(i,j+1,k)\big) + \frac{1}{\Delta z}\big(E_y^n(i,j,k+1) - E_y^n(i,j,k)\big) + \\
&\quad + \left(\frac{2\mu_x(i,j,k) - \sigma_x^m(i,j,k)\Delta t}{2\Delta t}\right) H_x^{n-\frac{1}{2}}(i,j,k) - M_{ix}^n(i,j,k).
\end{aligned}
$$

Divide through by the coefficient on the left and simplify to find

$$
\begin{aligned}
H_x^{n+\frac{1}{2}}(i,j,k) = &\left(\frac{2\Delta t}{(2\mu_x(i,j,k) + \sigma_x^m(i,j,k)\Delta t)\Delta y}\right)\big(E_z^n(i,j,k) - E_z^n(i,j+1,k)\big) + \\
&\left(\frac{2\Delta t}{(2\mu_x(i,j,k) + \sigma_x^m(i,j,k)\Delta t)\Delta z}\right)\big(E_y^n(i,j,k+1) - E_y^n(i,j,k)\big) + \\
&+ \left(\frac{2\mu_x(i,j,k) - \sigma_x^m(i,j,k)\Delta t}{2\mu_x(i,j,k) + \sigma_x^m(i,j,k)\Delta t}\right) H_x^{n-\frac{1}{2}}(i,j,k) + \left(\frac{-2\Delta t}{2\mu_x(i,j,k) + \sigma_x^m(i,j,k)\Delta t}\right) M_{ix}^n(i,j,k).
\end{aligned} \tag{2.7}
$$

This is the updating equation for H_x. From this we can see the parallels with the $\vec{E}$ updating equations, and that deriving the remaining two updating equations goes similarly: using the next scalar equation from (2.2), substitute central difference operators, solve for the magnetic component defined at future time step $t_{n+\frac{1}{2}}$, and simplify:

$$
\begin{aligned}
H_y^{n+\frac{1}{2}}(i,j,k) = &\left(\frac{2\Delta t}{(2\mu_y(i,j,k) + \sigma_y^m(i,j,k)\Delta t)\Delta z}\right)\big(E_x^n(i,j,k) - E_x^n(i,j,k+1)\big) + \\
&\left(\frac{2\Delta t}{(2\mu_y(i,j,k) + \sigma_y^m(i,j,k)\Delta t)\Delta x}\right)\big(E_z^n(i+1,j,k) - E_z^n(i,j,k)\big) + \\
&+ \left(\frac{2\mu_y(i,j,k) - \sigma_y^m(i,j,k)\Delta t}{2\mu_y(i,j,k) + \sigma_y^m(i,j,k)\Delta t}\right) H_y^{n-\frac{1}{2}}(i,j,k) + \left(\frac{-2\Delta t}{2\mu_y(i,j,k) + \sigma_y^m(i,j,k)\Delta t}\right) M_{iy}^n(i,j,k),
\end{aligned} \tag{2.8}
$$

and

$$
H_z^{n+\frac{1}{2}}(i,j,k) = \left(\frac{2\Delta t}{(2\mu_z(i,j,k) + \sigma_z^m(i,j,k)\Delta t)\Delta x}\right)\big(E_y^n(i,j,k) - E_y^n(i+1,j,k)\big) + \tag{2.9}
$$

$$\left(\frac{2\Delta t}{(2\mu_z(i,j,k)+\sigma_z^m(i,j,k)\Delta t)\Delta y}\right)\left(E_x^n(i,j+1,k)-E_x^n(i,j,k)\right)+$$
$$+\left(\frac{2\mu_z(i,j,k)-\sigma_z^m(i,j,k)\Delta t}{2\mu_z(i,j,k)+\sigma_z^m(i,j,k)\Delta t}\right)H_z^{n-\frac{1}{2}}(i,j,k)+\left(\frac{-2\Delta t}{2\mu_z(i,j,k)+\sigma_z^m(i,j,k)\Delta t}\right)M_{iz}^n(i,j,k),$$

which completes the system of updating equations.

Two Dimensional Updating Equations

Suppose we want to solve a problem modeled in two dimensions. We may let the physical domain be homogeneous in the z dimension, which leads to elimination of all derivatives with respect to z. Note that the following derivations can be rewritten to accomodate any pair of dimensions.

Once more, consider equation (2.1):

$$\nabla\times\vec{H}=\varepsilon\frac{\partial\vec{E}}{\partial t}+\sigma^e\vec{E}+\vec{J}_i.$$

The x component equation is

$$\frac{\partial H_z}{\partial y}-\frac{\partial H_y}{\partial z}=\varepsilon\frac{\partial E_x}{\partial t}+\sigma^e E_x+J_{ix}.$$

This reduces to

$$\frac{\partial H_z}{\partial y}=\varepsilon\frac{\partial E_x}{\partial t}+\sigma^e E_x+J_{ix}.$$

Similarly, the y component equation

$$\frac{\partial H_x}{\partial z}-\frac{\partial H_z}{\partial x}=\varepsilon\frac{\partial E_y}{\partial t}+\sigma^e E_y+J_{iy},$$

reduces to

$$-\frac{\partial H_z}{\partial x}=\varepsilon\frac{\partial E_y}{\partial t}+\sigma^e E_y+J_{iy}.$$

The z component equation is

$$\frac{\partial H_y}{\partial x}-\frac{\partial H_x}{\partial y}=\varepsilon\frac{\partial E_z}{\partial t}+\sigma^e E_z+J_{iz}$$

Now, considering equation (2.2), allow eliminating z derivatives from each of the scalar equations and obtain

$$\frac{\partial E_z}{\partial y}=-\mu\frac{\partial H_x}{\partial t}-\sigma^m H_x-M_{ix},$$

$$
\begin{aligned}
-\frac{\partial E_z}{\partial x} &= -\mu\frac{\partial H_y}{\partial t} - \sigma^m H_y - M_{iy}, \\
\frac{\partial E_y}{\partial x} - \frac{\partial E_x}{\partial y} &= -\mu\frac{\partial H_z}{\partial t} - \sigma^m H_z - M_{iz}.
\end{aligned}
$$

Observe that within the above six reduced equations, we have two isolated systems. The first which we examine is commonly termed the 'transverse-electric-z' TE_z mode. This is a reference to the fact that the involved electric field components E_x, E_y are transverse to the z axis.

$$
\begin{aligned}
\frac{\partial H_z}{\partial y} &= \varepsilon\frac{\partial E_x}{\partial t} + \sigma^e E_x + J_{ix}, \\
-\frac{\partial H_z}{\partial x} &= \varepsilon\frac{\partial E_y}{\partial t} + \sigma^e E_y + J_{iy}, \\
\frac{\partial E_y}{\partial x} - \frac{\partial E_x}{\partial y} &= -\mu\frac{\partial H_z}{\partial t} - \sigma^m H_z - M_{iz}.
\end{aligned}
$$

These three field components can be discretized and computed separately from the remaining three. For problems which are described exclusively by the TE_z mode, we may exclude the remaining three components from storage or calculation.

The remaining components form the transverse-magnetic-z or TM_z mode, for magnetic fields transverse to the z axis:

$$
\begin{aligned}
\frac{\partial E_z}{\partial y} &= -\mu\frac{\partial H_x}{\partial t} - \sigma^m H_x - M_{ix}, \\
-\frac{\partial E_z}{\partial x} &= -\mu\frac{\partial H_y}{\partial t} - \sigma^m H_y - M_{iy}, \\
\frac{\partial H_y}{\partial x} - \frac{\partial H_x}{\partial y} &= \varepsilon\frac{\partial E_z}{\partial t} + \sigma^e E_z + J_{iz}.
\end{aligned}
$$

A note on terminology: these modes are not directly related to TE, TM, TEM modes of propagation in transmission lines or waveguides.

After a process of discretization and solving for future timesteps which proceeds nearly identically to the above fully three-dimensional case, we obtain the TE_z updating equations. For E_x:

$$
\begin{aligned}
E_x^{n+1}(i,j) = &\left(\frac{2\Delta t}{(2\varepsilon_x(i,j) + \sigma_x^e(i,j)\Delta t)\Delta y}\right)\left(H_z^{n+\frac{1}{2}}(i,j) - H_z^{n+\frac{1}{2}}(i,j-1)\right) + \\
&+ \left(\frac{2\varepsilon_x(i,j) - \sigma_x^e(i,j)\Delta t}{2\varepsilon_x(i,j) + \sigma_x^e(i,j)\Delta t}\right) E_x^n(i,j) + \left(\frac{-2\Delta t}{2\varepsilon_x(i,j) - \sigma_x^e(i,j)\Delta t}\right) J_{ix}^{n+\frac{1}{2}}(i,j).
\end{aligned}
$$

For E_y:

$$E_y^{n+1}(i,j) = \left(\frac{2\Delta t}{(2\varepsilon_y(i,j)+\sigma_y^e(i,j)\Delta t)\Delta x}\right)\left(H_z^{n+\frac{1}{2}}(i-1,j) - H_z^{n+\frac{1}{2}}(i,j)\right) + \\ + \left(\frac{2\varepsilon_y(i,j)-\sigma_y^e(i,j)\Delta t}{2\varepsilon_y(i,j)+\sigma_y^e(i,j)\Delta t}\right)E_y^n(i,j) + \left(\frac{-2\Delta t}{2\varepsilon_y(i,j)-\sigma_y^e(i,j)\Delta t}\right)J_{iy}^{n+\frac{1}{2}}(i,j).$$

For H_z:

$$H_z^{n+\frac{1}{2}}(i,j) = \left(\frac{2\Delta t}{(2\mu_z(i,j)+\sigma_z^m(i,j)\Delta t)\Delta x}\right)\left(E_y^n(i,j) - E_y^n(i+1,j)\right) + \\ + \left(\frac{2\Delta t}{(2\mu_z(i,j)+\sigma_z^m(i,j)\Delta t)\Delta y}\right)\left(E_x^n(i,j+1) - E_x^n(i,j)\right) + \\ + \left(\frac{2\mu_z(i,j)-\sigma_z^m(i,j)\Delta t}{2\mu_z(i,j)+\sigma_z^m(i,j)\Delta t}\right)H_z^{n-\frac{1}{2}}(i,j) + \left(\frac{-2\Delta t}{2\mu_z(i,j,)+\sigma_z^m(i,j)\Delta t}\right)M_{iz}^n(i,j).$$

Similarly, after a process of discretization and solving, we obtain the TM_z updating equations.

For H_x:

$$H_x^{n+\frac{1}{2}}(i,j) = \left(\frac{2\Delta t}{(2\mu_x(i,j)+\sigma_x^m(i,j)\Delta t)\Delta y}\right)\left(E_z^n(i,j) - E_z^n(i,j+1)\right) + \\ + \left(\frac{2\mu_x(i,j)-\sigma_x^m(i,j)\Delta t}{2\mu_x(i,j)+\sigma_x^m(i,j)\Delta t}\right)H_x^{n-\frac{1}{2}}(i,j) + \left(\frac{-2\Delta t}{2\mu_x(i,j)+\sigma_x^m(i,j)\Delta t}\right)M_{ix}^n(i,j).$$

For H_y:

$$H_y^{n+\frac{1}{2}}(i,j) = \left(\frac{2\Delta t}{(2\mu_y(i,j)+\sigma_y^m(i,j)\Delta t)\Delta x}\right)\left(E_z^n(i+1,j) - E_z^n(i,j)\right) + \\ + \left(\frac{2\mu_y(i,j)-\sigma_y^m(i,j)\Delta t}{2\mu_y(i,j)+\sigma_y^m(i,j)\Delta t}\right)H_y^{n-\frac{1}{2}}(i,j) + \left(\frac{-2\Delta t}{2\mu_y(i,j)+\sigma_y^m(i,j)\Delta t}\right)M_{iy}^n(i,j).$$

For E_z:

$$E_z^{n+1}(i,j) = \left(\frac{2\Delta t}{(2\varepsilon_z(i,j)+\sigma_z^e(i,j)\Delta t)\Delta x}\right)\left(H_y^{n+\frac{1}{2}}(i,j) - H_y^{n+\frac{1}{2}}(i-1,j)\right) + \\ + \left(\frac{2\Delta t}{(2\varepsilon_z(i,j)+\sigma_z^e(i,j)\Delta t)\Delta y}\right)\left(H_x^{n+\frac{1}{2}}(i,j-1) - H_x^{n+\frac{1}{2}}(i,j)\right) + \\ + \left(\frac{2\varepsilon_z(i,j)-\sigma_z^e(i,j)\Delta t}{2\varepsilon_z(i,j)+\sigma_z^e(i,j)\Delta t}\right)E_z^n(i,j) + \left(\frac{-2\Delta t}{2\varepsilon_z(i,j)-\sigma_z^e(i,j)\Delta t}\right)J_{iz}^{n+\frac{1}{2}}(i,j).$$

If a problem allows, the remaining three components may be excluded from simulation.

One Dimensional Updating Equations

Suppose we want to solve a problem suited to modeling in one dimension. A simple example is to model the behavior between two parallel metal plates with large surface area and a small separation. Then the fields that exist between the plates near the center may be well-approximated by a one-dimensional model. Let the plates be normal to the x axis, and make the approximation that between the plates near their center points, fields only change with respect to x. Then in the scalar equations considered above, all partial derivatives with respect to y and z vanish.

Within the Yee cell, we may translate field components toward the x axis in a plane perpendicular to the $\vec{x}$ direction. By assumption, field magnitudes do not change with respect to such translations and we obtain the following cell design:

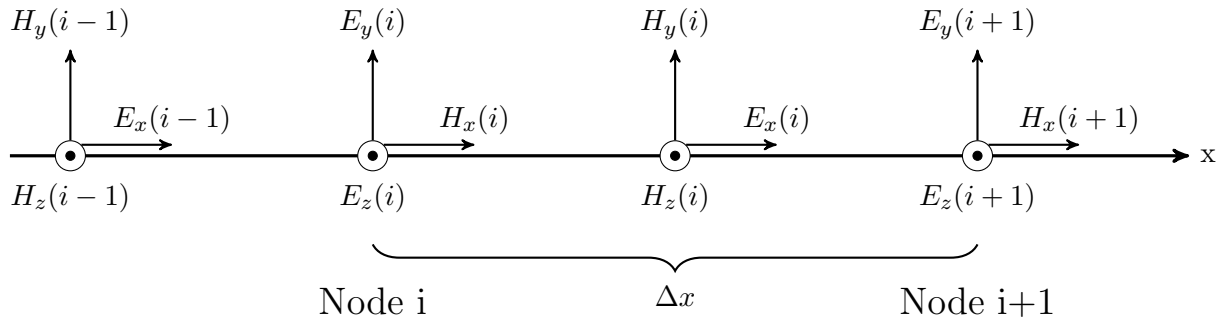

Figure 2.3: Diagram of field component spatial arrangement in 1D FDTD scheme

After canceling the y and z derivatives which are assumed to be 0, we discretize and solve for the future time step in the same way as above to find the updating equation for E_y:

$$E_y^{n+1}(i) = \left(\frac{2\Delta t}{(2\varepsilon_y(i) + \sigma_y^e(i)\Delta t)\Delta x}\right)\left(H_z^{n+\frac{1}{2}}(i-1) - H_z^{n+\frac{1}{2}}(i)\right) + \\ + \left(\frac{2\varepsilon_y(i) - \sigma_y^e(i)\Delta t}{2\varepsilon_y(i) + \sigma_y^e(i)\Delta t}\right)E_y^n(i) + \left(\frac{-2\Delta t}{2\varepsilon_y(i) - \sigma_y^e(i)\Delta t}\right)J_y^{n+\frac{1}{2}}(i).$$

The other updating equations are found to be

$$E_z^{n+1}(i) = \left(\frac{2\Delta t}{(2\varepsilon_z(i) + \sigma_z^e(i)\Delta t)\Delta x}\right)\left(H_y^{n+\frac{1}{2}}(i) - H_y^{n+\frac{1}{2}}(i-1)\right) + \\ + \left(\frac{2\varepsilon_z(i) - \sigma_z^e(i)\Delta t}{2\varepsilon_z(i) + \sigma_z^e(i)\Delta t}\right)E_z^n(i) + \left(\frac{-2\Delta t}{2\varepsilon_z(i) - \sigma_z^e(i)\Delta t}\right)J_z^{n+\frac{1}{2}}(i),$$

$$H_y^{n+\frac{1}{2}}(i) = \left(\frac{2\Delta t}{(2\mu_y(i) + \sigma_y^m(i)\Delta t)\Delta x}\right)\left(E_z^n(i+1) - E_z^n(i)\right) +$$
$$+ \left(\frac{2\mu_y(i) - \sigma_y^m(i)\Delta t}{2\mu_y(i) + \sigma_y^m(i)\Delta t}\right) H_y^{n-\frac{1}{2}}(i) + \left(\frac{-2\Delta t}{2\mu_y(i) + \sigma_y^m(i)\Delta t}\right) M_y^n(i),$$
$$H_z^{n+\frac{1}{2}}(i) = \left(\frac{2\Delta t}{(2\mu_z(i) + \sigma_z^m(i)\Delta t)\Delta x}\right)\left(E_y^n(i) - E_y^n(i+1)\right),$$
$$+ \left(\frac{2\mu_z(i) - \sigma_z^m(i)\Delta t}{2\mu_z(i) + \sigma_z^m(i)\Delta t}\right) H_z^{n-\frac{1}{2}}(i) + \left(\frac{-2\Delta t}{2\mu_z(i) + \sigma_z^m(i)\Delta t}\right) M_z^n(i).$$

Convergence

The central-difference approximations used in setting up these updating equations are second-order. By [7] we expect the method to converge to a solution at a rate consistent with second-order error.

2.4 Objects and Material Properties

Observe in Figure 2.1 the marked locations of the ε and μ component values. The focus of the previous section was constructing the updating coefficients given the material property values. We will now briefly consider a method of obtaining the material property values, keeping in mind that the material property grid is a discretization of the ideal domain. The aim is to reduce the impact of the 'staircasing' effect noted in [7], wherein the domain discretization forces all objects to conform to the grid of material properties. Curved and angled object surfaces which pass through part of a cell are represented as occupying the entire cell; by a considered averaging scheme we can reduce the impact of this approximation.

Material Property Averaging

Among the most straightforward methods of setting the material property values is to obtain the quantity directly from the corresponding point in the ideal domain. There is no mitigation of the staircasing effect in this scheme, however. An object could occupy 90% of a given cell, but if the surface-air interface excludes one of the material property points, the entire cell is treated as air for that property and that component.

We adopt a straightforward averaging scheme in code for this work. There are more sophisticated schemes for setting component values, but the method we will examine requires no customiza-

tion per-simulation, and by [7] yields adequate results. We describe a first step in the process of setting up the material property coefficients as the formation of a material index grid. This material index grid is colocated with and sized the same as the Yee cell; its indexing points are chosen to be at the center of each node. Each material used in the simulation is assigned an index, with an associated scalar value. This does limit us to homogeneous materials within this scheme, though inhomogeneous materials can be modeled by directly modifying the material property values on a per-simulation basis.

The material index data is obtained by sampling directly from the corresponding point in the ideal domain; each at the center of a Yee cell, each identified by the node index (i, j, k). Let us use the label $MI(i, j, k, r)$ to refer to the material index grid data for that node, where the r argument is μ or ε for the corresponding material. Consider the placement of μ material property values. Their positions on the centers of cell faces are directly between the neighboring material index points. So we choose to average the two corresponding material property values, and set the μ value accordingly. For example, fix $\mu_x(i, j, k)$. We set this value to $\frac{1}{2}\big(MI(i-1, j, k, \mu) + MI(i, j, k, \mu)\big)$. Similarly, $\mu_y(i, j, k) = \frac{1}{2}\big(MI(i, j-1, k, \mu) + MI(i, j, k, \mu)\big)$ and $\mu_z(i, j, k) = \frac{1}{2}\big(MI(i, j, k-1, \mu) + MI(i, j, k, \mu)\big)$. The same scheme is used to set electric conductivity values, using $MI(i, j, k, \sigma^e)$ and neighboring values.

The relative permittivity components ε lie on the edges of nodes, rather than the faces; this necessitates averaging across the four nearest material property indexes. Fix $\varepsilon_x(i, j, k)$; this value is set to $\frac{1}{4}\big(MI(i, j, k, \varepsilon) + MI(i, j-1, k, \varepsilon) + MI(i, j, k-1, \varepsilon) + MI(i, j-1, k-1, \varepsilon)\big)$.
Likewise, $\varepsilon_y(i, j, k) = \frac{1}{4}\big(MI(i, j, k, \varepsilon) + MI(i-1, j, k, \varepsilon) + MI(i, j, k-1, \varepsilon) + MI(i-1, j, k-1, \varepsilon)\big)$ and $\varepsilon_z(i, j, k) = \frac{1}{4}\big(MI(i, j, k, \varepsilon) + MI(i-1, j, k, \varepsilon) + MI(i, j-1, k, \varepsilon) + MI(i-1, j-1, k, \varepsilon)\big)$. The same scheme is used to set magnetic conductivity values, using $MI(i, j, k, \sigma^m)$ and neighboring values.

There are more sophisticated techniques for choosing discretized material property values to reduce the staircasing effect. These include finer sub-cell divisions and averaging, and more sophisticated intra-cell volume averaging, as described in [7]. However, the preceding description of material index averaging is the technique that will be used for all simulations developed in this thesis.

Thin Plates

One very useful technique is to allow conductive plates into simulation which are significantly thinner than the cell size. For example, very thin conducting traces such as those found on microstrip can be introduced into a simulation which uses a relatively coarse grid, and computational expense is reduced.

Modeling a thin plate is simple given our development so far, subject to the restriction that they conform closely to the grid. Consider a conducting plate object in the xy plane, between x indexes is and ie and between y indexes js and je. Suppose it is placed at the z index k. We can effectively model this plate in simulation by setting the material properties $\sigma^e(i,j,k)$ for $i = is, \ldots, ie$ and $j = js, \ldots, je$ to the plate conductivity. No further alteration of any material property is needed.

We encounter a limitation with the thin plate method if we attempt to model a thin wire - that is, if our plate has extent in only one dimension. As noted in [7, 11], the fields near thin wires vary dramatically and are not modeled well with this thin-plate method. A technique for introducing thin wires to simulation by alteration of the standard updating equations will be derived in Chapter 4.

CHAPTER 3

ACCURACY CONSIDERATIONS

We will consider the stability of our staggered-grid finite-difference scheme. The concept of stability in a numerical scheme does not have an easy parallel in analytical treatments of partial differential equations. Rather, stability of a particular FDTD simulation is a property that depends on the appropriate choice of space and time discretization applied within the context of a scheme.

3.1 Stability and dispersion

We will see that the stability condition for our scheme is that the chosen time step size must be less than or equal to a function of chosen spatial step sizes. Choosing a time step which exceeds this limit results in spurious, non-physical results, typically growing by many orders of magnitude within a few time steps. The dispersion of a numerical scheme also affects its accuracy. Different frequencies may propagate through the grid at different speeds even when the modeled material is nondispersive. This effect is also related to the choice of time step size.

Stability

Developed during World War 2 at Los Alamos [11], the von Neumann analysis is a standard approach to determine the stability and conditions of finite difference schemes. The method is to write the finite difference scheme applied to a spatial Fourier mode $C(t)\exp[\mathrm{i}kx]$ (using notation $\mathrm{i} = \sqrt{-1}$) and find step size conditions under which the amplification factor is not greater than one. It can be shown that the algorithm under analysis is stable under those conditions. However, because of the interleaved nature of the discretized $\vec{H}$, $\vec{E}$ system, the von Neumann analysis needs to be modified for the FDTD scheme. Consider a freespace, one-dimensional FDTD simulation in E_z and H_y; the updating equations with appropriate updating coefficients are

$$E_z^{n+1}(i) = E_z^n(i) + \frac{\Delta t}{\Delta x}(H_y^{n+\frac{1}{2}}(i) - H_y^{n+\frac{1}{2}}(i)),$$

$$H_y^{n+\frac{1}{2}}(i) = H_y^{n-\frac{1}{2}}(i) + \frac{\Delta t}{\Delta x}(E_z^n(i+1) - E_z^n(i)).$$

Now let $E_z^n = k(\Delta t^n)\exp(\mathrm{i}k\, i\Delta x)$ and $H_y^n = L(\Delta t^{n+\frac{1}{2}})\exp(\mathrm{i}k(i+\frac{1}{2})\Delta x)$. We can simplify,

$$\begin{aligned}
E_z^{n+1}(i) &= E_z^n(i) + (H_y^{n+\frac{1}{2}}(i) - H_y^{n+\frac{1}{2}}(i) \cdot \exp(-\mathrm{i}k\Delta x)) \\
&= E_z^n(i) + H_y^{n+\frac{1}{2}}(i)(1 - \exp(-\mathrm{i}k\Delta x)) \\
&= E_z^n(i) + H_y^{n+\frac{1}{2}}(i)(\exp(\mathrm{i}k\frac{\Delta x}{2}) - \exp(\mathrm{i}k\frac{\Delta x}{2}) \cdot (\exp(-\mathrm{i}k\frac{\Delta x}{2})) \\
&= E_z^n(i) - 2H_y^{n+\frac{1}{2}}(i) \cdot \mathrm{i}\sin(k\frac{\Delta x}{2}) \cdot \exp(-\mathrm{i}k\frac{\Delta x}{2}).
\end{aligned}$$

Likewise,

$$\begin{aligned}
H_y^{n+\frac{1}{2}}(i) &= H_y^{n+\frac{1}{2}}(i) + (E_z^n(i)\exp(\mathrm{i}k\Delta x) - E_z^n(i)) \\
&= H_y^{n-\frac{1}{2}}(i) + (E_z^n(i)(\exp(\mathrm{i}k\Delta x) - E_z^n(i)) \\
&= H_y^{n-\frac{1}{2}}(i) + E_z^n(i)((\exp(\mathrm{i}k\frac{\Delta x}{2}) - \exp(-\mathrm{i}k\frac{\Delta x}{2}))\exp(\mathrm{i}k\frac{\Delta x}{2})) \\
&= H_y^{n-\frac{1}{2}}(i) + E_z^n(i)(2\mathrm{i}\sin(k\frac{\Delta x}{2})\exp(\mathrm{i}k\frac{\Delta x}{2})).
\end{aligned}$$

For many other types of finite difference schemes, the next step would be to rewrite this system in matrix notation, as (with certain detail omitted),

$$\begin{bmatrix} E_z & H_y \end{bmatrix} = A \begin{bmatrix} E_z & H_y \end{bmatrix},$$

where then we would find the conditions under which the eigenvalues of A are bounded by 1. Note that the vectors $\vec{E}, \vec{H}$ are not labeled with timesteps in the above equations, because the fields are always staggered by a half timestep. That is the core problem we encounter which prevents us from writing a complete matrix-notation version of this system and proceeding with the Von Neumann method.

We proceed to derive the dispersion relation for the finite difference scheme; the stability condition will be revealed from that. These analyses are conducted for freespace conditions, following [7, 11].

Dispersion

Where dispersion is present, a wave becomes deformed as it travels, as different Fourier modes shift phase relative to one another. We are interested in determining the numerical dispersion which results from the finite difference scheme. To that end, we consider simple simulation situations. The following calculations use values $\varepsilon = \varepsilon_0$, $\mu = \mu_0$, $\sigma^e = \sigma^m = 0$, and $J_i = M_i = 0$ everywhere.

Under these simpler conditions the Maxwell system can be separated into two wave equations, and the dispersion relation simplifies accordingly. We derive the dispersion relation for the PDEs first, and apply the same method to the finite-difference algorithm later.

We assume a one-dimensional domain in x, involving E_z and H_y components. Prior to eliminating the unused components, Equation (2.1), Faraday's law, contains scalar equation

$$\partial_x E_z - \partial_z E_x = \partial_x E_z = \mu_0 \partial_t H_y,$$

and Equation 2.2, Ampere's law with Maxwell's correction contains the scalar equation

$$\partial_x H_y - \partial_y H_x = \varepsilon_0 \partial_t E_z.$$

Now let each scalar component be a Fourier mode in space and time:

$$E_z = C_1 \exp[\mathrm{i}(kx + \omega t)] \text{ and } H_y = C_2 \exp[\mathrm{i}(kx + \omega t)],$$

Substituting this into the scalar Faraday's Law above and taking derivatives,

$$C_1 \mathrm{i}k \exp[\mathrm{i}(kx + \omega t)] = C_2 \mu_0 \mathrm{i}\omega \exp[\mathrm{i}(kx + \omega t)],$$

$$C_1 k - C_2 \mu_0 \omega = 0.$$

Substituting the Fourier mode into the scalar modified Ampere's law yields

$$C_2 \mathrm{i}k \exp[\mathrm{i}(kx + \omega t)] = C_1 \varepsilon_0 \mathrm{i}\omega \exp[\mathrm{i}(kx + \omega t)],$$

$$C_2 k = C_1 \varepsilon_0 \omega,$$

$$C_1\varepsilon_0\omega - C_2 k = 0.$$

Assembling the two equations into matrix form, we obtain

$$\begin{bmatrix} k & -u_0\omega \\ \varepsilon_0\omega & -k \end{bmatrix} \begin{bmatrix} C_1 \\ C_2 \end{bmatrix} = \vec{0}.$$

Taking the determinant of the coefficient matrix and setting this to zero expresses the fact that any nonconstant Fourier mode will have nonzero coefficients. This reveals the dispersion relation [11]:

$$\begin{vmatrix} k & -u_0\omega \\ \varepsilon_0\omega & -k \end{vmatrix} = -k^2 + \mu_0\varepsilon_0\omega^2 = 0,$$

$$\omega = \pm\frac{k}{\sqrt{\mu_0\varepsilon_0}} = \pm ck,$$

where as usual c is the speed of light in a vacuum. Notice we only needed the TM_z system to show this complete result; we could obtain the same using the TE_z system.

Now we can apply the same process directly to the updating equations in the FDTD mode to obtain the numerical dispersion. The updating equations for E_y and H_z are respectively

$$\begin{aligned} E_y^{n+1}(i) = &\left(\frac{2\Delta t}{(2\varepsilon_y(i) + \sigma_y^e(i)\Delta t)\Delta x}\right)\left(H_z^{n+\frac{1}{2}}(i) - H_z^{n+\frac{1}{2}}(i-1)\right) + \\ &+ \left(\frac{2\varepsilon_y(i) - \sigma_y^e(i)\Delta t}{2\varepsilon_y(i) + \sigma_y^e(i)\Delta t}\right) E_y^n(i) + \left(\frac{-2\Delta t}{2\varepsilon_y(i) - \sigma_y^e(i)\Delta t}\right) J_{iy}^{n+\frac{1}{2}}(i), \end{aligned}$$

and

$$\begin{aligned} H_z^{n+\frac{1}{2}}(i) = &\left(\frac{2\Delta t}{(2\mu_z(i) + \sigma_z^m(i)\Delta t)\Delta x}\right)\left(E_y^n(i) - E_y^n(i+1)\right) + \\ &+ \left(\frac{2\mu_z(i) - \sigma_z^m(i)\Delta t}{2\mu_z(i) + \sigma_z^m(i)\Delta t}\right) H_z^{n-\frac{1}{2}}(i) + \left(\frac{-2\Delta t}{2\mu_z(i) + \sigma_z^m(i)\Delta t}\right) M_{iz}^n(i). \end{aligned}$$

Under the assumptions that $\varepsilon = \varepsilon_0$, $\mu = \mu_0$, $\sigma^e = \sigma^m = 0$, and $J_i = M_i = 0$, we obtain

$$E_y^{n+1}(i) = E_y^{n+1}(i) + \frac{\Delta t}{\varepsilon_0 \Delta x}\left(H_z^{n+\frac{1}{2}}(i) - H_z^{n+\frac{1}{2}}(i-1)\right)$$

and

$$H_z^{n+\frac{1}{2}}(i) = H_z^{n-\frac{1}{2}}(i) + \frac{\Delta t}{\mu_0 \Delta x}\big(E_y^n(i) - E_y^n(i-1)\big).$$

Recall the offset of $H_z(i)$ in space as $(i+1/2)\Delta x$. Then allow $E_y^n(i) = C_1 \exp[\mathrm{i}(ki\Delta x + \omega n \Delta t)]$ and $H_z^{n+1/2} = C_2 \exp[\mathrm{i}(k(i+1/2)\Delta x + \omega(n+1/2)\Delta t)]$. Substituting these into the first updating equation above and factoring, obtain

$$\begin{aligned} &C_1 \exp[\mathrm{i}\omega\Delta t] \exp[\mathrm{i}(ki\Delta x + \omega n \Delta t)] = \\ &\exp[\mathrm{i}(ki\Delta x + \omega n \Delta t)] \left[C_1 + C_2 \frac{\Delta t}{\varepsilon_0 \Delta x} \exp[\mathrm{i}\omega\Delta t/2] \left(\exp[\mathrm{i}k\Delta x/2] - \exp[-\mathrm{i}k\Delta x/2]\right)\right]. \end{aligned}$$

Dividing through by the common factor $\exp[\mathrm{i}(ki\Delta x + \omega n \Delta t)]$ and rearranging terms gives

$$C_1(\exp[\mathrm{i}\omega\Delta t] - 1)\exp[-\mathrm{i}\omega\Delta t/2] = C_2 \frac{\Delta t}{\varepsilon_0 \Delta x}\left(\exp[\mathrm{i}k\Delta x/2] - \exp[-\mathrm{i}k\Delta x/2]\right).$$

Rearranging once more and using the definition of sine, we obtain

$$\frac{C_1}{\Delta t} 2\mathrm{i}\sin(\mathrm{i}\omega\Delta t/2) - \frac{C_2}{\varepsilon_0 \Delta x} 2\mathrm{i}\sin(k\Delta x/2) = 0,$$

or simply

$$\frac{C_1}{\Delta t}\sin(\mathrm{i}\omega\Delta t/2) - \frac{C_2}{\varepsilon_0 \Delta x}\sin(k\Delta x/2) = 0. \tag{3.1}$$

Now with the second updating equation above, repeat the process. Substituting the Fourier modes and pulling out common factors yields

$$\begin{aligned} &C_2 \exp[\mathrm{i}k\Delta x/2] \exp[\mathrm{i}\omega\Delta t/2] \exp[\mathrm{i}(ki\Delta x + \omega n \Delta t)] = \\ &C_2 \exp[\mathrm{i}k\Delta x/2] \exp[-\mathrm{i}\omega\Delta t/2] \exp[\mathrm{i}(ki\Delta x + \omega n \Delta t)] + \\ &+ \frac{\Delta t}{\mu_0 \Delta x} C_1(\exp[\mathrm{i}k\Delta x] - 1)\exp[\mathrm{i}(ki\Delta x + \omega n \Delta t)]. \end{aligned}$$

Dividing out the common mode term $\exp[\mathrm{i}(ki\Delta x + \omega n \Delta t)]$ and a factor of $\exp[\mathrm{i}k\Delta x/2]$, then rearranging:

$$C_2(\exp[\mathrm{i}\omega\Delta t/2] - \exp[\mathrm{i}\omega\Delta t/2]) = C_1 \frac{\Delta t}{\mu_0 \Delta x}(\exp[\mathrm{i}k\Delta x/2] - \exp[-\mathrm{i}k\Delta x/2]).$$

Rearranging and writing sine terms:

$$-\frac{C_1}{\mu_0 \Delta x} 2\mathrm{i} \sin(k\Delta x/2) + \frac{C_2}{\Delta t} 2\mathrm{i} \sin(\omega \Delta t/2) = 0,$$

or simply

$$-\frac{C_1}{\mu_0 \Delta x} \sin(k\Delta x/2) + \frac{C_2}{\Delta t} \sin(\omega \Delta t/2) = 0. \tag{3.2}$$

Construct the matrix equation defined by Equations 3.2 and 3.1:

$$\begin{bmatrix} \frac{1}{\Delta t} \sin(\omega \Delta t/2) & \frac{-1}{\varepsilon_0 \Delta x} \sin(k\Delta x/2) \\ \frac{-1}{\mu_0 \Delta x} \sin(k\Delta x/2) & \frac{1}{\Delta t} \sin(\omega \Delta t/2) \end{bmatrix} \begin{bmatrix} C_1 \\ C_2 \end{bmatrix} = \vec{0}.$$

Take the determinant of the first matrix, as before, and set to zero since any nonconstant Fourier mode will have nonzero coefficients. We obtain the dispersion relation for the FDTD scheme in 1D:

$$\det \begin{bmatrix} \frac{1}{\Delta t} \sin(\omega \Delta t/2) & \frac{-1}{\varepsilon_0 \Delta x} \sin(k\Delta x/2) \\ \frac{-1}{\mu_0 \Delta x} \sin(k\Delta x/2) & \frac{1}{\Delta t} \sin(\omega \Delta t/2) \end{bmatrix} = \frac{1}{\Delta t^2} \sin^2(\omega \Delta t/2) - \frac{1}{\Delta x^2} \frac{1}{\mu_0 \varepsilon_0} \sin^2(k\Delta x/2) = 0,$$

or simply

$$\sin^2(\omega \Delta t/2) = c^2 \left(\frac{\Delta t}{\Delta x} \right)^2 \sin^2(k\Delta x/2). \tag{3.3}$$

3.1.1 A Variant Form of Stability Analysis

Equation (3.3) reveals the stability condition of the 1-d FDTD for freespace, after some manipulation. This section follows [11]. Solving for ω,

$$\sin(\omega \Delta t/2) = \pm c\Delta t \sqrt{\frac{1}{\Delta x^2} \sin^2(k\Delta x/2)}$$

$$\omega = \pm \frac{2}{\Delta t} \sin^{-1} \left(c\Delta t \sqrt{\frac{1}{\Delta x^2} \sin^2(k\Delta x/2)} \right).$$

At this point, recall that we are assured of stability as long as the growth in the Fourier mode is less than or equal to one in absolute value. Considering the formulation (for example) $E_y = C_1 \exp[I(kx + \omega t)]$, if ω is complex, this may be rewritten as $E_y = C_1 \exp[\omega_i t] \exp[I(kx + \omega_r t)]$. If ω_i is positive, this leads to an unstable growth situation. To avoid this situation, we require that

ω remain purely real ($\omega_i = 0$).

With this requirement on ω we reconsider the preceding term $\sin^{-1}\left(c\Delta t\sqrt{\frac{1}{\Delta x^2}\sin^2(k\Delta x/2)}\right)$. The issue is not that the term inside the square root may become negative; it does not. Instead, if the argument to $\sin^{-1}$ becomes greater than 1, the solution becomes complex. Taking 1 as a maximum on the sin term, this drops out and we obtain the condition

$$c\Delta t\sqrt{\frac{1}{\Delta x^2}} = \frac{c\Delta t}{\Delta x} \leq 1.$$

For three dimensions, we take a different approach; the two-dimensional case is omitted, but would parallel the following. As noted in Chapter 2, we can obtain that in simple (non-conductive, non-dispersive, isotropic, non-hysteretical, homogeneous) dielectric materials free of net charge, $\vec{B}$ and $\vec{E}$ fields each satisfy the wave equation. Assume a three dimensional domain consisting of such a simple dielectric. Note that the phase speed v_p is then $\frac{1}{\sqrt{\varepsilon\mu}}$ where ε and μ are the permittivity and permeability of the dielectric.

Allow a plane wave with wavefront normal to $\vec{k} =< k_x, k_y, k_z >$. Without loss of generality, suppose that the plane wave is oriented such that the component E_x is nonzero. Then we can write that this component satisfies the wave equation, and discretize the differential operators as

$$\frac{E_x^n(i+1,j,k) - 2E_x^n(i,j,k) + E_x^n(i-1,j,k)}{\Delta x^2} + \frac{E_x^n(i,j+1,k) - 2E_x^n(i,j,k) + E_x^n(i,j-1,k)}{\Delta y^2}$$
$$+\frac{E_x^n(i,j,k+1) - 2E_x^n(i,j,k) + E_x^n(i,j,k-1)}{\Delta z^2} - \frac{1}{v_p^2}\frac{E_x^{n+1}(i,j,k) - 2E_x^n(i,j,k) + E_x^{n-1}(i,j,k)}{\Delta t^2} = 0.$$

Following [11], this discretization scheme is numerically equivalent to the FDTD formulation discussed in the previous chapter. Taking the Fourier mode expression

$$E_x(x,y,z,t) = C\exp \mathrm{i}(\omega t + k_x x + k_y y + k_z z),$$

$$\frac{1}{\Delta x^2}\big(\exp \mathrm{i}(\omega n\Delta t + k_x(i+1)\Delta x + j\Delta y + k\Delta z) - 2\exp \mathrm{i}(\omega n\Delta t + k_x i\Delta x + j\Delta y + k\Delta z)$$
$$+ \exp \mathrm{i}(\omega n\Delta t + k_x(i-1)\Delta x + j\Delta y + k\Delta z)\big)$$
$$+ \frac{1}{\Delta y^2}\big(\exp \mathrm{i}(\omega n\Delta t + k_x i\Delta x + (j+1)\Delta y + k\Delta z) - 2\exp \mathrm{i}(\omega n\Delta t + k_x i\Delta x + j\Delta y + k\Delta z)$$

$$
\begin{aligned}
&+ \exp \mathrm{i}(\omega n\Delta t + k_x i\Delta x + (j-1)\Delta y + k\Delta z)\big) \\
&+ \frac{1}{\Delta z^2}\big(\exp \mathrm{i}(\omega n\Delta t + k_x i\Delta x + j\Delta y + (k+1)\Delta z) - 2\exp \mathrm{i}(\omega n\Delta t + k_x i\Delta x + j\Delta y + k\Delta z) \\
&+ \exp \mathrm{i}(\omega n\Delta t + k_x i\Delta x + j\Delta y + (k-1)\Delta z)\big) \\
&- \frac{1}{v_p^2\Delta t^2}\big(\exp \mathrm{i}(\omega (n+1)\Delta t + k_x i\Delta x + j\Delta y + k\Delta z) - 2\exp \mathrm{i}(\omega n\Delta t + k_x i\Delta x + j\Delta y + k\Delta z) \\
&+ \exp \mathrm{i}(\omega (n-1)\Delta t + k_x i\Delta x + j\Delta y + k\Delta z)\big) = 0.
\end{aligned}
$$

Factoring and dividing out the common exponential term leaves

$$
\begin{aligned}
&\frac{1}{\Delta x^2}\big(\exp \mathrm{i}(k_x\Delta x) - 2 + \exp \mathrm{i}(-k_x\Delta x)\big) + \frac{1}{\Delta y^2}\big(\exp \mathrm{i}(k_y\Delta y) - 2 + \exp \mathrm{i}(-k_y\Delta y)\big) \\
&+ \frac{1}{\Delta z^2}\big(\exp \mathrm{i}(k_z\Delta z) - 2 + \exp \mathrm{i}(-k_z\Delta z)\big) + \frac{1}{v_p^2\Delta t^2}\big(\exp \mathrm{i}(\omega\Delta t) - 2 + \exp \mathrm{i}(-\omega\Delta t)\big) = 0.
\end{aligned}
$$

Taking the definition of cosine,

$$
\begin{aligned}
&\frac{2}{\Delta x^2}\big(\cos(k_x\Delta x) - 1\big) + \frac{2}{\Delta y^2}\big(\cos(k_y\Delta y) - 1\big) + \\
&\quad + \frac{2}{\Delta z^2}\big(\cos(k_z\Delta z) - 1\big) - \frac{2}{v_p^2\Delta t^2}\big(\cos(\omega\Delta t) - 1\big) = 0.
\end{aligned}
$$

Collecting and using the trigonometric identity $\cos(2t) - 1 = \sin^2(t)$,

$$
\begin{aligned}
&\left(\frac{v_p\Delta t}{\Delta x}\right)^2 \sin^2\left(\frac{k_x\Delta x}{2}\right) + \left(\frac{v_p\Delta t}{\Delta y}\right)^2 \sin^2\left(\frac{k_y\Delta y}{2}\right) + \left(\frac{v_p\Delta t}{\Delta z}\right)^2 \sin^2\left(\frac{k_z\Delta z}{2}\right) = \sin\left(\frac{\omega\Delta t}{2}\right) \\
&\pm v_p\Delta t\sqrt{\left(\frac{1}{\Delta x}\sin\left(\frac{k_x\Delta x}{2}\right)\right)^2 + \left(\frac{1}{\Delta y}\sin\left(\frac{k_y\Delta y}{2}\right)\right)^2 + \left(\frac{1}{\Delta z}\sin\left(\frac{k_z\Delta z}{2}\right)\right)^2} = \sin\left(\frac{\omega\Delta t}{2}\right).
\end{aligned}
$$

Solving for the frequency ω,

$$
\omega = \frac{2}{\Delta t}\sin^{-1}\left(v_p\Delta t\sqrt{\left(\frac{1}{\Delta x}\sin\left(\frac{k_x\Delta x}{2}\right)\right)^2 + \left(\frac{1}{\Delta y}\sin\left(\frac{k_y\Delta y}{2}\right)\right)^2 + \left(\frac{1}{\Delta z}\sin\left(\frac{k_z\Delta z}{2}\right)\right)^2}\right).
$$

Due to convention of positive frequency, we choose the positive root. As $v_p > 0$ and $\Delta t > 0$ by convention, we obtain that the argument to arcsine is positive. If the argument exceeds 1, then the equality only holds if ω is complex. As in the previous argument, a complex frequency leads to instability in the scheme, so we require ω to be real and thus the argument to arcsine must be

between 0 and 1. The condition that ensures this while allowing the greatest Δt value is

$$v_p \Delta t \sqrt{\frac{1}{\Delta x^2} + \frac{1}{\Delta y^2} + \frac{1}{\Delta z^2}} \leq 1$$

This is the stability condition in three dimensions for simple media which follows a similar form to the one-dimensional case. The convention which will be adopted in all simulation designs in this thesis is to assume vacuum when checking the stability condition.

3.2 Pulsed Signals

FDTD simulations are sensitive to the frequencies that compose a driving EM signal. In fact, given the assumption of linearity, one of the main advantages to the time-domain method is that we can introduce a broadband signal and obtain results for many frequencies simultaneously.

Pulsed signals typically contain a controllable broadband frequency content, and are suited to time-stepping algorithms by their short duration. To ensure that we do introduce the frequencies we desire and avoid introducing spurious frequencies, we will consider three of the most commonly used pulsed signals and describe how to set their parameters based on desired bandwidth. Since jumps and kinks in a source waveform almost always introduce high-frequency artifacts, we will also take care that our sampled waveforms do not contain significant jumps in value.

Gaussian

One waveform which is used frequently as a signal is the Gaussian function

$$a \exp(-(\frac{t - t_0}{b})^2).$$

The function is a smooth strictly positive pulse, with maximum amplitude a and centered at time t_0. It falls off toward zero rapidly, but asymptotically. Constrain the signal to start at a small enough value, and the discontinuity will be acceptable for our calculations. A jump of $\exp(-20) \approx 2.06 \times 10^{-9}$ V is taken to be acceptable, see for example [7].

We must find an appropriate time offset t_0 to satisfy this requirement of small starting value. So, setting $t = 0$ we need to find t_0 such that $1 \exp(-(\frac{t_0}{b})^2) \leq \exp(-20)$, so

$$t_0^2/b^2 \geq 20 \qquad \Rightarrow \qquad t_0 \geq \sqrt{20}b. \tag{3.4}$$

We know the Fourier transform

$$\mathcal{F}\left(\exp(-(t/b)^2)\right) = b\sqrt{\pi}\exp\left(-\frac{(b\omega)^2}{4}\right).$$

This is a broadband function, in fact there are nonzero components at all frequencies.

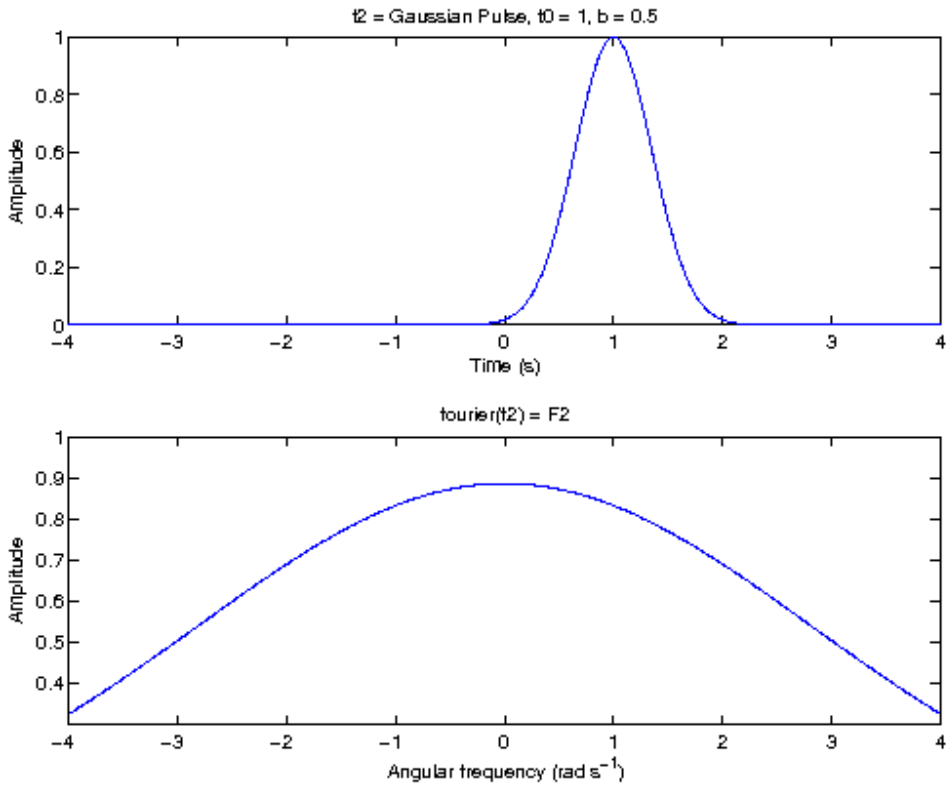

Figure 3.1: Shifted, scaled Gaussian function in time, with its Fourier transform

Grid choice constrains the upper frequency limit at which FDTD simulations will yield acceptable results. We will follow two constraints here: first, the minimum wavelength should span ten or more grid cells in the coarsest of dx, dy, or dt; this guideline for maintaining solution quality is explained in [7, 11] as the result of numerical experimentation. Second, in a Gaussian pulse f, we will consider a frequency ω to be negligible if its magnitude $F(\omega)$ is $< 10\%$ of the maximum magnitude of $\mathcal{F}(f)$, as used in [7]. We will refer to the largest and smallest non-negligible frequencies in a signal as the cutoff frequencies.

So, to find that 10% mark we want to solve for $\omega_{\max}$:

$$0.1 = \exp\left(-\frac{(b\omega_{\max})^2}{4}\right) \qquad \Rightarrow \qquad \sqrt{4\ln 10} = b\omega_{\max},$$

$$\omega_{\max} = 2\pi f_{\max},$$

$$\frac{\sqrt{\ln 10}}{\pi f_{\max}} = b. \tag{3.5}$$

The 'b' in the preceding is also often labeled τ or T.

We note that the t_0 calculated above is approximately $4.5T$, however, setting $t_0 = 3T$ is another common choice.

For a typical EM simulation, we need a relatively narrow pulse so that the simulation is operating over reasonable timescales of ns and frequencies in GHz ranges. We may examine a pulse with parameters suitable for inclusion in simulation:

$$b = \frac{\sqrt{\ln 10}}{\pi 7.5E9} \approx 6.44E-11,$$

$$t_0 = \sqrt{20}b \approx 2.88E-10 \text{ s}.$$

Cosine Modulated Gaussian Pulse

Following [7] we have that multiplying a Gaussian by $\cos(\omega_s t)$ shifts the Fourier transform right by ω_s. This product $\cos(\omega_s t)\exp\left(-\frac{(t-t_0)^2}{b^2}\right)$ is visualized below. Note that most of the remainder of this work uses Hz frequency units, so we will work with $f_{\text{s}} = \frac{1}{2\pi}\omega_s$. Note that the symmetry of the transform for a real function means that the negative frequency magnitudes carry the same information as the positive frequency magnitudes.

To be able to specify a bandwidth parameter, we observe that the range of significant frequencies is controlled by the pure Gaussian pulse's $f_{\max}$, as: $\Delta f \equiv 2f_{\max}$. Referring to equation (3.5), we have

$$b = \frac{2\sqrt{\ln 10}}{\pi\Delta f}.$$

The resulting signal has a bandwidth between $f_{\text{s}} - \frac{\Delta f}{2}$ and $f_{\text{s}} + \frac{\Delta f}{2}$.

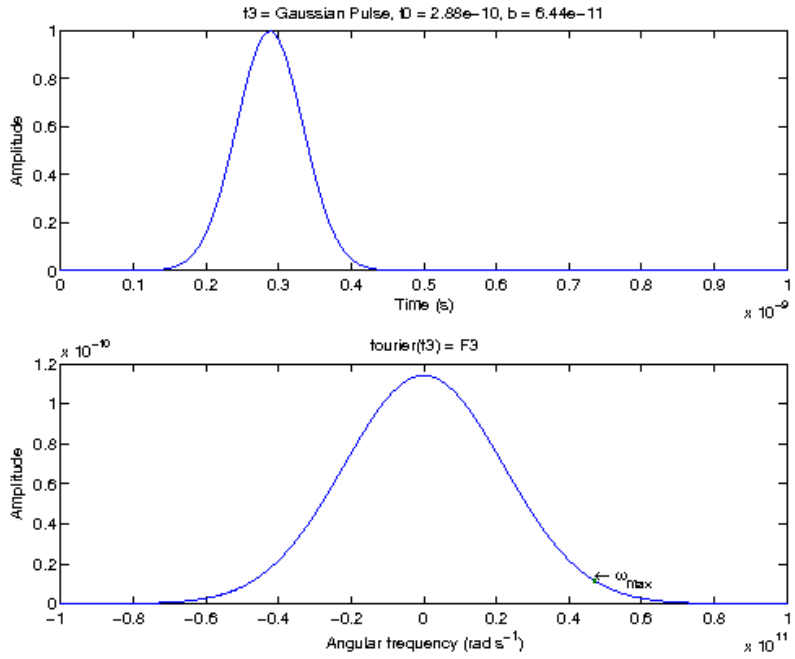

Figure 3.2: Shifted, scaled Gaussian function in time, with its Fourier transform. Chosen frequency cutoff in rad / s is calculated and indicated.

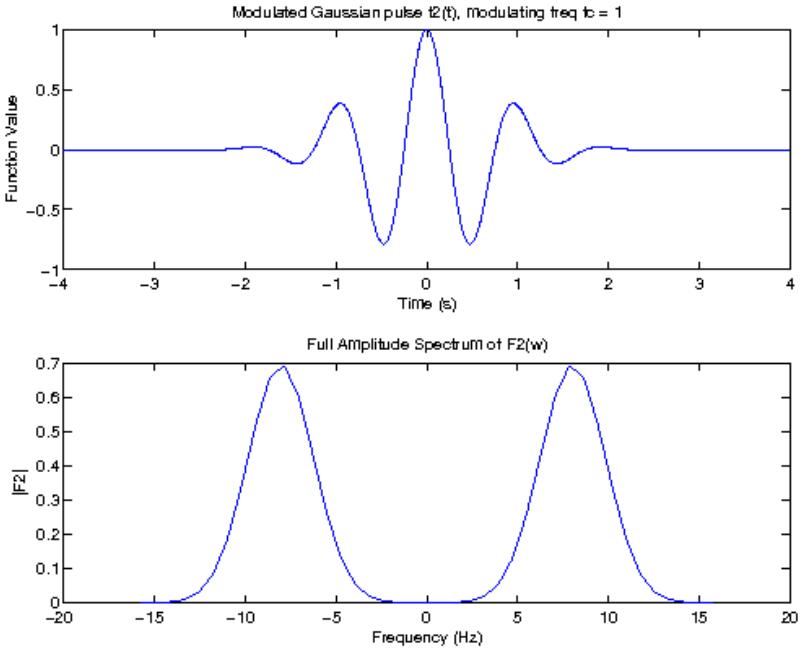

Figure 3.3: Cosine-modulated Gaussian pulse function in time, with its shifted Fourier transform.

Derivative Gaussian

Another pulse signal which we consider is the normalized derivative of the Gaussian. This pulse type is broadband and captures low frequencies while excluding zero- and very low frequencies. The normalization is necessary because the factor b which emerges as a coefficient is often small enough to cause issues with the amplitude of the resulting time-domain signal. As a result, following [7], after normalization the Derivative Gaussian function used in simulation is

$$-\frac{\sqrt{2e}}{b} \cdot (t - t_0) \exp\left(-\frac{(t - t_0)^2}{b^2}\right),$$

and the corresponding Fourier transform is [7]

$$\frac{I\omega b^2\sqrt{\pi e}}{\sqrt{2}} \exp\left(-\frac{b^2\omega^2}{4}\right).$$

Again following [7], we recognize that the formulas (3.5) and (3.4) for b and t_0 are applicable to the Derivative Gaussian as well. The calculated b value yields a signal with the same cutoff frequency $f_{\max}$ as the corresponding pure Gaussian. The corresponding t_0 time offset yields a signal with a negligible jump, just as with the corresponding Gaussian.

Discretization of the Waveform

The inclusion of the chosen signal in simulation is a considerable matter, with possibilities including voltage and current sources, and imposition of incident waves. These are covered in later chapters. Now, though, we still can examine the discretization process of the waveform. For each of the above pulses, the code proceeds the same. The number of timesteps allotted to the simulation governs the size of the one-dimensional array which stores the waveform. The analytical expression for the chosen wave is evaluated for each half-integer timestep, and the result placed into the waveform array.

We choose to evaluate at half-integer timesteps due to the usage of the waveform in updating. Recall the updating equations for $\vec{E}$, and the formulation of the imposed current $\vec{J}$ term. The sources which will be examined next chapter use various manipulations of $\vec{J}$. The $\vec{J}$ components are represented at half-integer timesteps, so we wish to discretize the waveforms at half-integer

timesteps as well for maximum accuracy.

The incident plane wave source, on the other hand, requires tailoring to each grid point. Hence the waveform discretization per timestep is handled differently. This is explored in Chapter 6.

3.2.1 Charging and Grid Capacitance

We see in [19] that for the FDTD formulation used here, a source-free domain will maintain zero divergence in E and H fields. However, the same source also shows that sources which simulate a net nonzero current flow can produce significant divergence in simulated E and H fields. The Gaussian pulse is one such signal.

The deposition of charge density between cells is explored in [19], where it is demonstrated that a one-cell electric current filament subject to a Gaussian pulse will retain its charge for 300 timesteps, and is expected to retain it indefinitely. The divergence of the resulting E field corresponds to a nonconstant charge density field, while the H field is unaffected. A magnetic current filament driven by a Gaussian source has a parallel effect on the H field, depositing opposing magnetic monopole charge density on opposite ends of the filament. The H field exhibits the corresponding divergence while the E field is unaffected in that case.

We note that the Gaussian pulse has this effect, however, we will not entirely forego its use. It has precedent; for example in a published result [15] considered in part in Chapter 5, a Gaussian pulse was effectively employed to drive the simulation of a dielectric resonating antenna.

The grid capacitance and inductance effects are examined in [19] as well. In three dimensions, the capacitance between adjacent nodes is shown in [19] to be $3\varepsilon_0\Delta$, and the inductance to be $\frac{\mu_0\Delta}{4}$, for uniform spatial step Δ. For a simulation which involves the lumped-element capacitors or inductors examined next chapter, the simulation designer must keep these effects in mind. Grid capacitance and inductance values are comparatively small in terms of common circuit element parameters. Yet [19] shows that when lumped-element capacitors or inductors are given parameters on the same order, the grid capacitance or inductance effects have a predictable and significant effect on the simulation. We will not examine any simulations which use these elements, and so our focus will not be on the phenomena of grid capacitance and inductance.

CHAPTER 4

SAMPLING, LUMPED ELEMENTS, AND THIN WIRES

We will examine a few of the extensions to the FDTD scheme which allow improved modeling of electrical networks. Several different element types can be implemented in FDTD using their idealized governing equations. We also observe a straightforward method of sampling voltage and current from the full-field data produced in simulation.

4.1 Sampling of Voltage and Current

Voltage

We develop a way of sampling the voltage between grid nodes, subject to a constraint: the voltage difference between the two should involve one component only. The method is based on a discretization of the integral $V = -\int_c \vec{E} \cdot dl$ on the domain grid, where path c is constrained to a straight line parallel to one of the axes.

Sampling regions are defined in cuboids, and one orientation is selected from among $\pm x, \pm y, \pm z$. We will examine the $+z$ orientation case, as x and y orientation cases follow easily. The sampled voltage result is measured and averaged across each individual z-oriented column. However, this gives rise to the constraint mentioned above; we obtain the voltage for each column using only the E_z component. The E_x and E_y components are not considered. This is equivalent to making the assumption that the two sampled faces of the region are expected to be equipotential surfaces. Any net contribution to the voltage integral by x and y components in the ideal case is lost using this sample method.

We can obtain accurate results using this sampling method by careful simulation design. For instance, later in this chapter we will develop an example in which we sample the voltage difference between a trace and a ground plane, both of which are parallel and conform to the domain gridding. In that case we expect the fields tangential to the conductors to average to zero in the space between them.

Suppose a simple case first: that a cuboid voltage sampling region occupies a single z column of grid cells, $k = ks$ to ke, with x and y cell indexes i, j. Observe that due to E_z component placement, this represents a physical region which occupies between $ks \cdot dz$ and $(ke + 1)dz$ in the z dimension, plus a fixed domain offset. The potential difference $V_{ke} - V_{ks}$ is the discretized field integral $-\sum_{k=ks}^{ke-1} E_z(i, j, k) \cdot dz = -dz \sum_{k=ks}^{ke-1} E_z(i, j, k)$ which is the sum of potential differences across individual grid cells from ks to ke.

Consider a slightly more general case, that a cuboid voltage sampling region occupies grid points as follows: in the x dimension, the region spans cell indexes from $i = is$ to $i = ie$; in y, $j = js$ to je; in z, $k = ks$ to ke. Again, observe that E_z components occupy between $ks \cdot dz$ and $(ke+1)dz$ in the z dimension, plus a fixed domain offset, but the parallel does not hold for the other dimensions of the region. In the x and y extents our components only occupy $(ie - is)dx$ and $(je - js)dy$, plus respective offsets, in the simulated physical space.

The column sampling method is extended to find the average z-oriented voltage difference between the $\pm z$ surfaces of the region. There are $(ie - is + 1)$ and $(je - js + 1)$ rows of z-oriented columns in x and y, respectively. We take the average of the $(ie - is + 1) \cdot (je - js + 1)$ sampling columns to find the result:

$$V_{ke} - V_{ks} = \frac{-dz}{(ie - is + 1)(je - js + 1)} \sum_{i=is}^{ie} \sum_{j=js}^{je} \sum_{k=ks}^{ke-1} E_z(i, j, k).$$

Of course, the coefficient $\frac{-dz}{(ie-is+1)(je-js+1)}$ is not time-dependent and may be stored and reused at each time step to avoid some recalculation.

Current

We employ a very similar method of discretizing a suitable integral in order to find the current flowing through a sample region. The current measurement method we use is also restricted to the three axes in orientation. We discretize Ampere's Law

$$I_{f \cdot enc} = \oint_c \vec{H} \cdot ds,$$

with a rectangular loop fit to the grid, and sum the appropriate magnetic components around the four loop legs. We note that $I_{f \cdot enc}$ is as in Chapter 2, the free charge enclosed by the loop c. We

also note that we are neglecting Maxwell's correction $\frac{\partial}{\partial t}\vec{D}$, as in [7]. In simulation we do not store the polarization density.

Consider a region of current sampling spanning cell indexes from $i = is$ to $i = ie$; in y, $j = js$ to je; in z, suppose it is a single cell thick between k and $k+1$, with a declared orientation of $+z$. The physical layout of the enclosing loop needs careful consideration; we must ensure that we enclose the entirety of the volume of the sampling region. We take leg $+x$ along y from js to je, at x index ie. Likewise leg $+y$ is along x from is to ie, at y index je. Recalling that the H components lie in the centers of cell faces, we must include an additional cell as spacing to each leg on the $-x$ and $-y$ ends. This causes the $-x$ leg to be summed along y from js to je, at x index $is - 1$. Also $-y$ is taken along x from is to ie, at y index $js - 1$.

We must also duly account for the orientation of the H components, so that our loop integral is summed in the correct orientation. For our $+z$-oriented sampling, this requires a factor of -1 on the $+x$ and $-y$ legs.

All of these legs are at z index k. So, the discretized integral summed in the CCW leg order $+x, -y, -x, +y$ is represented as

$$I_{f\cdot enc} = -\sum_{i=is}^{ie} H_x(i, je, ks) \cdot dx - \sum_{j=js}^{je} H_y(is - 1, j, ks) \cdot dy + \\ + \sum_{i=is}^{ie} H_x(i, js - 1, ks) \cdot dx + \sum_{j=js}^{je} H_y(ie, j, ks) \cdot dy.$$

Consider a region of current sampling spanning cell indexes from $i = is$ to $i = ie$; in y, $j = js$ to je; in z, $k = ks$ to ke, with a declared orientation of $+z$. We need consider only one of the $(ke - ks)$ possible loops for this more general case.

4.1.1 Discrete Fourier Transform

We will have cause to take the Fourier transform of a variety of measurements obtainable from simulation. Sampled voltages and currents are the first example we encounter. We calculate a discretization of the complex Fourier integral as a running sum, updated with each timestep. This technique is limited to a preselected set of frequencies f_c, chosen before the simulation begins. For a simulation with N timesteps:

$$\mathcal{F}(V(t)) \equiv V^*(\omega) = \int_{t=-\infty}^{\infty} V(t) \exp\left(-\mathrm{i}\omega t\right)\, dt,$$

$$V^*(f_c) \approx \sum_{n=1}^{N} V(n\Delta t)\Delta t \cdot \exp\left(-\mathrm{i}2\pi f_c n\Delta t\right).$$

As the time-domain voltage values are not expensive to store, we may choose to store the value at each timestep and take the discrete transform after timestepping is complete. Similarly, the current can be transformed as

$$I^*(f_c) \approx \sum_{n=1}^{N} I\left(\left(n-\frac{1}{2}\right)\Delta t\right)\Delta t \cdot \exp\left(-\mathrm{i}2\pi f_c n\Delta t\right).$$

Observe that the staggered grid formulation causes the V and I values to be offset in space and time. As noted in [8], this issue can significantly affect the Fourier transforms of sampled values, and can be addressed by taking an appropriate spatial average and multiplying by a time correction. We will explore this further in the stripline simulation example, later in the chapter.

The DFT will be revisited in later chapters, as we will have need of the frequency composition of other signals.

4.2 Lumped Circuit Elements

The term 'lumped circuit element' has a distinct definition in the FDTD scheme, referring to circuit elements which are effectively modeled in simulation using modification of the updating coefficients and minimal other overhead. We will explore a few types of linear elements which are broadly useful and generally applicable with minimum customization. Many more lumped element approximations have been derived than are explored here, for nonlinear and other more difficult types of elements.

This example demonstrates the inclusion of some common sources and other elements in the 3D derivation of the FDTD scheme, following [7, chapter 4].

4.2.1 Elements With Overhead

We may divide the lumped elements we examine into those which must use minor auxiliary fields, which we will examine first, and those which can be implemented with only modification of standard updating coefficient values. The various source types are here due to their dependence on a chosen waveform, and the inductor requires storage of the previous timestep's current value. Some overhead-free elements will be examined in the subsection after this one.

Soft voltage source

Setting the value of $\vec{E}$ fields directly is one of the simplest methods of driving a simulation, and is equivalent to modeling ideal voltage sources with zero internal resistance at each driven grid point. This type of source will be described below. Unfortunately these sources have drawbacks which we mention in brief: when forcing a given field value irrespective of surrounding field values, that component acts like a perfect reflector. This issue can corrupt a simulation with non-physical reflections if propagating waves happen to intersect the driven field values. Many network and antenna simulations are driven more accurately by a soft voltage source.

A more realistic or 'soft' voltage source includes nonzero internal resistance, modeled by a resistor placed in series after an ideal source. Following [19, 7], with imposed voltage signal V_s, internal resistance R_s, and voltage difference in the z direction V_z we can obtain the current by:

$$I = \frac{V_z + V_s}{R_s}.$$

Now as noted below in the section on sampling, V_z can be calculated from field values at time $n+\frac{1}{2}$ with the time average

$$V_z^{n+\frac{1}{2}}(i,j,k) = -\Delta z \cdot E_z^{n+1/2}(i,j,k) = -\frac{\Delta z}{2}(E_z^{n+1}(i,j,k) + E_z^n(i,j,k)).$$

With these expressions for current and voltage difference V_z on the grid, we obtain an expression for current density J_{iz} at time $n+1/2$ in terms of the imposed voltage:

$$J_{iz}^{n+\frac{1}{2}}(i,j,k) = \frac{\Delta z}{2\Delta x \Delta y R_s}(E_z^{n+1}(i,j,k) + E_z^n(i,j,k)) + \frac{1}{\Delta x \Delta y R_s} V_s^{n+\frac{1}{2}}.$$

Substituting this expression into the updating equation and solving for E_z^{n+1},

$$\begin{aligned}
E_z^{n+1}(i,j,k) = &\left(\frac{2\varepsilon_z(i,j,k) - \sigma_z^e(i,j,k)\Delta t - \frac{\Delta t \Delta z}{R_s \Delta x \Delta y}}{2\varepsilon_z(i,j,k) + \sigma_z^e(i,j,k)\Delta t + \frac{\Delta t \Delta z}{R_s \Delta x \Delta y}}\right) E_z^n(i,j,k) \\
&+ \left(\frac{2\Delta t}{\left(2\varepsilon_z(i,j,k) + \sigma_z^e(i,j,k)\Delta t + \frac{\Delta t \Delta z}{R_s \Delta x \Delta y}\right)\Delta x}\right)\left(H_y^{n+\frac{1}{2}}(i,j,k) - H_y^{n+\frac{1}{2}}(i-1,j,k)\right) \\
&+ \left(\frac{-2\Delta t}{\left(2\varepsilon_z(i,j,k) + \sigma_z^e(i,j,k)\Delta t + \frac{\Delta t \Delta z}{R_s \Delta x \Delta y}\right)\Delta y}\right)\left(H_x^{n+\frac{1}{2}}(i,j,k) - H_x^{n+\frac{1}{2}}(i,j-1,k)\right) \\
&+ \left(\frac{-2\Delta t}{\left(2\varepsilon_z(i,j,k) + \sigma_z^e(i,j,k)\Delta t + \frac{\Delta t \Delta z}{R_s \Delta x \Delta y}\right) R_s \Delta x \Delta y}\right) V_s^{n+\frac{1}{2}}(i,j,k),
\end{aligned}$$

in which we observe modified updating coefficients

$$\begin{aligned}
C_{eze} &= \left(\frac{2\varepsilon_z(i,j,k) - \sigma_z^e(i,j,k)\Delta t - \frac{\Delta t \Delta z}{R_s \Delta x \Delta y}}{2\varepsilon_z(i,j,k) + \sigma_z^e(i,j,k)\Delta t + \frac{\Delta t \Delta z}{R_s \Delta x \Delta y}}\right), \\
C_{ezhy} &= \left(\frac{2\Delta t}{\left(2\varepsilon_z(i,j,k) + \sigma_z^e(i,j,k)\Delta t + \frac{\Delta t \Delta z}{R_s \Delta x \Delta y}\right)\Delta x}\right), \\
C_{ezhx} &= \left(\frac{-2\Delta t}{\left(2\varepsilon_z(i,j,k) + \sigma_z^e(i,j,k)\Delta t + \frac{\Delta t \Delta z}{R_s \Delta x \Delta y}\right)\Delta y}\right), \\
C_{ezs} &= \left(\frac{-2\Delta t}{\left(2\varepsilon_z(i,j,k) + \sigma_z^e(i,j,k)\Delta t + \frac{\Delta t \Delta z}{R_s \Delta x \Delta y}\right) R_s \Delta x \Delta y}\right).
\end{aligned}$$

Hard voltage source

Expressing the hard source more precisely, we force the voltage V between two nodes to a specific value V_s; note also that this is forced during the $\vec{E}$ update, centered at half-integer timesteps. For example, we consider setting the $+z$-directed voltage V_z: using $V_z = V_s$ and taking the usual time average of $\vec{E}$, we expect $V_s^{n+\frac{1}{2}} = -\frac{\Delta z}{2}(E_z^{n+1}(i,j,k) + E_z^n(i,j,k))$. Solving for the future timestep, our forced field is

$$E_z^{n+1}(i,j,k) = -E_z^n(i,j,k) - \frac{2}{\Delta z} V_s^{n+\frac{1}{2}}(i,j,k).$$

We can confirm this expression another way: deriving the hard source by taking the limit of the soft-source expression as internal resistance drops to 0:

$$\lim_{R_s\to 0} E_z^{n+1}(i,j,k) = \lim_{R_s\to 0}\left(\frac{2R_s\varepsilon_z(i,j,k) - R_s\sigma_z^e(i,j,k)\Delta t - \frac{\Delta t\Delta z}{\Delta x\Delta y}}{2R_s\varepsilon_z(i,j,k) + R_s\sigma_z^e(i,j,k)\Delta t + \frac{\Delta t\Delta z}{\Delta x\Delta y}}\right) E_z^n(i,j,k)$$
$$+\left(\frac{2R_s\Delta t}{\left(2R_s\varepsilon_z(i,j,k) + R_s\sigma_z^e(i,j,k)\Delta t + \frac{\Delta t\Delta z}{\Delta x\Delta y}\right)\Delta x}\right)(H_y^{n+\frac{1}{2}}(i,j,k) - H_y^{n+\frac{1}{2}}(i-1,j,k))$$
$$+\left(\frac{-2R_s\Delta t}{\left(2R_s\varepsilon_z(i,j,k) + R_s\sigma_z^e(i,j,k)\Delta t + \frac{\Delta t\Delta z}{\Delta x\Delta y}\right)\Delta y}\right)(H_x^{n+\frac{1}{2}}(i,j,k) - H_x^{n+\frac{1}{2}}(i,j-1,k))$$
$$+\left(\frac{-2\Delta t}{\left(2R_s\varepsilon_z(i,j,k) + R_s\sigma_z^e(i,j,k)\Delta t + \frac{\Delta t\Delta z}{\Delta x\Delta y}\right)\Delta x\Delta y}\right) V_s^{n+\frac{1}{2}}(i,j,k)$$
$$= -1E_z^n(i,j,k) + 0(H_y^{n+\frac{1}{2}}(i,j,k) - H_y^{n+\frac{1}{2}}(i-1,j,k))$$
$$+ 0(H_x^{n+\frac{1}{2}}(i,j,k) - H_x^{n+\frac{1}{2}}(i,j-1,k)) - \frac{2}{\Delta z}V_s^{n+\frac{1}{2}}(i,j,k).$$

Non-ideal current source

A $+z$-facing current source within a cell is a source which conducts between the $\pm z$ faces. The lumped source is as a loop connecting an ideal current source with a resistor, the resistance of which is termed the internal resistance. Each leg of the loop is connected to a $\pm z$ face of the cell. An imposed current term $\vec{J}$ applied in simulation without modification acts as an ideal current source with infinite internal resistance. A more physically realistic current source has finite internal resistance, which requires alteration of the simulation's updating coefficients locally.

We need an expression for current which conforms to the grid in space and time, and which expresses total flux (A) rather than flux density ($\mathrm{A/m^2}$). At gridpoint i,j,k and time $n+1/2$,

$$I_z^{n+\frac{1}{2}}(i,j,k) = \Delta x\Delta y J_{iz}^{n+\frac{1}{2}}(i,j,k).$$

From [19], and assuming a $+z$-directed source, we have an expression for the total current in simulation $I_z^{n+\frac{1}{2}}(i,j,k) = I_s + V_z/R_s$ where I_s is the imposed current of the source, R_s is the internal resistance parameter of the source, and V_z is voltage difference between the nodes (i,j,k) and $(i,j,k+1)$ in the z direction.

Substituting the measured V_z and the flux expression for I_z, we obtain

$$\Delta x\Delta y J_{iz}^{n+\frac{1}{2}}(i,j,k) = I_s + \frac{\Delta z}{2}(E_z^{n+1}(i,j,k) + E_z^n(i,j,k)),$$

and hence

$$J_{iz}^{n+\frac{1}{2}}(i,j,k) = \frac{\Delta z}{2\Delta x \Delta y}(E_z^{n+1}(i,j,k) + E_z^n(i,j,k)) + \frac{1}{\Delta x \Delta y} I_s^{n+\frac{1}{2}}.$$

This expression for imposed current density can then be substituted into the updating equation in order to find modified coefficients. From the scalar component

$$\frac{\partial E_z}{\partial t} = \frac{1}{\varepsilon_z}\left(\frac{\partial H_y}{\partial x} - \frac{\partial H_x}{\partial y} - \sigma_z^e E_z - J_{iz}\right),$$

we discretize as usual and substitute the preceding expression for $J_{iz}(i,j,k)$:

$$\begin{aligned}
\frac{E_z^{n+1}(i,j,k) - E_z^n(i,j,k)}{\Delta t} &= \frac{1}{\varepsilon_z(i,j,k)} \frac{H_y^{n+\frac{1}{2}}(i,j,k) - H_y^{n+\frac{1}{2}}(i-1,j,k)}{\Delta x} \\
&- \frac{1}{\varepsilon_z i,j,k} \frac{H_x^{n+\frac{1}{2}}(i,j,k) - H_x^{n+\frac{1}{2}}(i,j-1,k)}{\Delta x} \\
&- \frac{\sigma_z^e(i,j,k)}{2\varepsilon_z(i,j,k)}(E_z^{n+1}(i,j,k) + E_z^n(i,j,k)) \\
&- \frac{1}{\varepsilon_z(i,j,k)}\left(\frac{\Delta z}{2\Delta x \Delta y}(E_z^{n+1}(i,j,k) + E_z^n(i,j,k)) + \frac{1}{\Delta x \Delta y} I_s^{n+\frac{1}{2}}\right).
\end{aligned}$$

Finally, this can be solved for $E_z^{n+1}(i,j,k)$, to find the modified updating equation:

$$\begin{aligned}
E_z^{n+1}(i,j,k) = &\left(\frac{2\varepsilon_z(i,j,k) - \sigma_z^e(i,j,k)\Delta t - \frac{\Delta t \Delta z}{R_s \Delta x \Delta y}}{2\varepsilon_z(i,j,k) + \sigma_z^e(i,j,k)\Delta t + \frac{\Delta t \Delta z}{R_s \Delta x \Delta y}}\right) E_z^n(i,j,k) \\
&+ \left(\frac{2\Delta t}{\left(2\varepsilon_z(i,j,k) + \sigma_z^e(i,j,k)\Delta t + \frac{\Delta t \Delta z}{R_s \Delta x \Delta y}\right)\Delta x}\right)(H_y^{n+\frac{1}{2}}(i,j,k) - H_y^{n+\frac{1}{2}}(i-1,j,k)) \\
&+ \left(\frac{-2\Delta t}{\left(2\varepsilon_z(i,j,k) + \sigma_z^e(i,j,k)\Delta t + \frac{\Delta t \Delta z}{R_s \Delta x \Delta y}\right)\Delta y}\right)(H_x^{n+\frac{1}{2}}(i,j,k) - H_x^{n+\frac{1}{2}}(i,j-1,k)) \\
&+ \left(\frac{-2\Delta t}{\left(2\varepsilon_z(i,j,k) + \sigma_z^e(i,j,k)\Delta t + \frac{\Delta t \Delta z}{R_s \Delta x \Delta y}\right)\Delta x \Delta y}\right) I_s^{n+\frac{1}{2}}(i,j,k).
\end{aligned}$$

from which we obtain modified updating coefficients

$$C_{eze} = \left(\frac{2\varepsilon_z(i,j,k) - \sigma_z^e(i,j,k)\Delta t - \frac{\Delta t \Delta z}{R_s \Delta x \Delta y}}{2\varepsilon_z(i,j,k) + \sigma_z^e(i,j,k)\Delta t + \frac{\Delta t \Delta z}{R_s \Delta x \Delta y}}\right)$$

$$C_{ezhy} = \left(\frac{2\Delta t}{\left(2\varepsilon_z(i,j,k) + \sigma_z^e(i,j,k)\Delta t + \frac{\Delta t \Delta z}{R_s \Delta x \Delta y}\right)\Delta x} \right)$$
$$C_{ezhx} = \left(\frac{-2\Delta t}{\left(2\varepsilon_z(i,j,k) + \sigma_z^e(i,j,k)\Delta t + \frac{\Delta t \Delta z}{R_s \Delta x \Delta y}\right)\Delta y} \right)$$
$$C_{ezs} = \left(\frac{-2\Delta t}{\left(2\varepsilon_z(i,j,k) + \sigma_z^e(i,j,k)\Delta t + \frac{\Delta t \Delta z}{R_s \Delta x \Delta y}\right)\Delta x \Delta y} \right),$$

with which the simulation can be run as usual.

Inductor

An inductor element can be simulated with the standard updating coefficients and an auxiliary field: the imposed current term becomes dependent on the simulated electric field. This element does have a dependency on two timesteps of total current through the cell.

For an inductor with L henrys inductance, we know the element obeys the fundamental relation

$$V = L\frac{dI}{dt}.$$

For a $+z$-facing inductor element one grid unit long, discretizing the time derivative in the usual way with a central difference operator centered at time n,

$$\Delta V^n = L\frac{I^{n+\frac{1}{2}} - I^{n-\frac{1}{2}}}{\Delta t}.$$

Substituting our flux definition for the current terms,

$$\Delta z E_z^n(i,j,k) = L\frac{\Delta x \Delta y \left(J_{iz}^{n+\frac{1}{2}}(i,j,k) - J_{iz}^{n-\frac{1}{2}}(i,j,k)\right)}{\Delta t}.$$

Solving this for the future imposed current term,

$$J_{iz}^{n+\frac{1}{2}} = \frac{\Delta z \Delta t}{L \Delta x \Delta y} E_z^n(i,j,k) + J_{iz}^{n-\frac{1}{2}}(i,j,k).$$

Then the above equation implies that to model an inductor at grid cell (i,j,k) we calculate the imposed current at that grid cell according to the above equation, and then update normally.

4.2.2 Elements Without Overhead

Resistor

A resistor can be modeled following one of the active sources already derived which includes internal resistance. Starting with either the expression for non-ideal current source or soft voltage source, allow the imposed signal (V_s or I_s respectively) to be 0 and in both cases the last term drops out. So, for a resistor element providing $R_s\,\Omega$ resistance, oriented along z between nodes (i,j,k) and $(i,j,k+1)$, the E_z updating equation is

$$\begin{aligned}
E_z^{n+1}(i,j,k) = &\left(\frac{2\varepsilon_z(i,j,k) - \sigma_z^e(i,j,k)\Delta t - \frac{\Delta t\Delta z}{R_s\Delta x\Delta y}}{2\varepsilon_z(i,j,k) + \sigma_z^e(i,j,k)\Delta t + \frac{\Delta t\Delta z}{R_s\Delta x\Delta y}}\right) E_z^n(i,j,k) \\
&+ \left(\frac{2\Delta t}{\left(2\varepsilon_z(i,j,k) + \sigma_z^e(i,j,k)\Delta t + \frac{\Delta t\Delta z}{R_s\Delta x\Delta y}\right)\Delta x}\right)\left(H_y^{n+\frac{1}{2}}(i,j,k) - H_y^{n+\frac{1}{2}}(i-1,j,k)\right) \\
&+ \left(\frac{-2\Delta t}{\left(2\varepsilon_z(i,j,k) + \sigma_z^e(i,j,k)\Delta t + \frac{\Delta t\Delta z}{R_s\Delta x\Delta y}\right)\Delta y}\right)\left(H_x^{n+\frac{1}{2}}(i,j,k) - H_x^{n+\frac{1}{2}}(i,j-1,k)\right).
\end{aligned}$$

Capacitor

We know that the effect a capacitor has on voltage and current follows the equation

$$I = C\frac{d\Delta V}{dt},$$

where C is the capacitance of the element in farads, and I and V are as usual, current and voltage in amps and volts respectively. Setting this equation up across two neighboring gridpoints (i,j,k) and $(i,j,k+1)$ in the $+z$ direction and discretizing the d/dt operator with a central difference in time yields

$$I^{n+\frac{1}{2}} = C\frac{\Delta V^{n+1} - \Delta V^n}{\Delta t},$$

where $\Delta V^n = \Delta z E_z^n(i,j,k)$. In terms of the electric field and imposed current J, then, we obtain

$$\Delta x\Delta y J_{iz}^{n+\frac{1}{2}}(i,j,k) = \frac{C\Delta z}{\Delta t}(E_z^{n+1}(i,j,k) - E_z^n(i,j,k)),$$

which implies the substitution

$$J_{iz}^{n+\frac{1}{2}}(i,j,k) = \frac{C\Delta z}{\Delta t \Delta x \Delta y}(E_z^{n+1}(i,j,k) - E_z^n(i,j,k)).$$

Substituting this into the standard updating equation for E_z,

$$\begin{aligned} E_z^{n+1}(i,j,k) = &\left(\frac{2\varepsilon_z(i,j,k) - \sigma_z^e(i,j,k)\Delta t + \frac{2C\Delta z}{\Delta x \Delta y}}{2\varepsilon_z(i,j,k) + \sigma_z^e(i,j,k)\Delta t + \frac{2C\Delta z}{\Delta x \Delta y}}\right) E_z^n(i,j,k) \\ &+ \left(\frac{2\Delta t}{\left(2\varepsilon_z(i,j,k) + \sigma_z^e(i,j,k)\Delta t + \frac{2C\Delta z}{\Delta x \Delta y}\right)\Delta x}\right)(H_y^{n+\frac{1}{2}}(i,j,k) - H_y^{n+\frac{1}{2}}(i-1,j,k)) \\ &+ \left(\frac{-2\Delta t}{\left(2\varepsilon_z(i,j,k) + \sigma_z^e(i,j,k)\Delta t + \frac{2C\Delta z}{\Delta x \Delta y}\right)\Delta y}\right)(H_x^{n+\frac{1}{2}}(i,j,k) - H_x^{n+\frac{1}{2}}(i,j-1,k)), \end{aligned}$$

from which we obtain the modified updating coefficients

$$\begin{aligned} C_{ez} &= \frac{2\varepsilon_z(i,j,k) - \sigma_z^e(i,j,k)\Delta t + \frac{2C\Delta z}{\Delta x \Delta y}}{2\varepsilon_z(i,j,k) + \sigma_z^e(i,j,k)\Delta t + \frac{2C\Delta z}{\Delta x \Delta y}}, \\ C_{ezhx} &= \frac{2\Delta t}{\left(2\varepsilon_z(i,j,k) + \sigma_z^e(i,j,k)\Delta t + \frac{2C\Delta z}{\Delta x \Delta y}\right)\Delta x}, \\ C_{ezhy} &= \frac{-2\Delta t}{\left(2\varepsilon_z(i,j,k) + \sigma_z^e(i,j,k)\Delta t + \frac{2C\Delta z}{\Delta x \Delta y}\right)\Delta y}. \end{aligned}$$

4.2.3 Distributed Lumped Elements

We need a way to express lumped elements which are larger than a single grid node. Following the approach of [7, 11], we observe that a cuboid, contiguous group of single-node lumped elements of any one of the types derived above will satisfy the same ideal, fundamental equation or approximating relation as governs each of its individual elements. However, the simulation can locally be idealized as a network rather than a single element. The network of like elements acts as a single element, but we must carefully develop ways to choose the parameter of each element such that the network displays the desired parameter value. Correspondingly, we must examine how the various parameters act in a network.

Suppose a voltage source oriented toward $+z$ occupies grid points as follows: in the x dimension, the element spans node indexes from $i = is$ to $i = ie$; in y, $j = js$ to je; in z, $k = ks$ to ke. Note

that this represents a physical element which also occupies up to $(ke+1)dz$ in the z dimension, plus a fixed domain offset. Suppose the element is to have a total voltage difference of V_s. Note that there are $ke-ks+1$ rows of source elements. Potential difference between V_{ks} and V_{ke} is the discretized field integral $-\sum E_z dz$ which is the sum of potential differences across individual grid cells from ks to ke. Since we want the total potential difference to be V_s, this corresponds to a value

$$V_{is} = \frac{V_s}{ke-ks+1}.$$

We must also determine how to set the individual source elements' internal resistance parameter R_{is} so that the network displays a chosen resistance. Noting that the same fundamental relation governs both lumped soft voltage sources and resistors, the source network can be thought of as a network of resistors. Within each 'slab' of $(ie-is+1)\times(je-js+1)$, the elements are connected in parallel; each of the $ke-ks+1$ slabs is connected in serial. Using standard equations for resistors in serial and parallel, $R_{total}=\sum R_{is}$ and $\frac{1}{R_{total}}=\sum\frac{1}{R_{is}}$ respectively, we find that

$$R_{is} = R_s\frac{(ie-is+1)\times(je-js+1)}{ke-ks+1}$$

determines the correct internal resistance parameter for each individual source. Of course, for a lumped resistor network, precisely the same derivation applies.

For a distributed lumped capacitor with total capacitance C we use equivalent parallel capacitance $C_{total}=\sum C_i$ and serial capacitance $\frac{1}{C_{total}}=\sum\frac{1}{C_i}$. These provide the capacitance parameter

$$C_i = C\frac{ke-ks+1}{(ie-is+1)(je-js+1)}.$$

For a distributed lumped inductor with total inductance L we use equivalent series inductance $L_{total}=\sum L_i$ and equivalent parallel inductance $\frac{1}{L_{total}}=\sum\frac{1}{L_i}$. This yields inductance parameter

$$L_i = L\frac{(ie-is+1)(je-js+1)}{ke-ks+1}.$$

For a non-ideal current source with total current I_s and internal resistance R_s, we forego the derivation steps but recognize that they closely parallel that of the soft voltage source. We obtain

individual current and resistance parameters I_{is} and R_{is} as

$$I_{is} = \frac{I_s}{(ie - is + 1)(je - js + 1)},$$

and

$$R_{is} = R_s \frac{(ie - is + 1)(je - js + 1)}{ke - ks + 1}.$$

Hence for each of these types of elements, we have a way to incorporate distributed versions spanning cuboid groups of nodes.

4.3 Example: Stripline, Terminating Resistor

In this example, we demonstrate a practical implementation of the soft voltage source and resistor elements in a transmission line. Note that our results for this simulation are recognized as inconclusive – the fine-tuning of resistive load implementation in FDTD simulations is not our focus, and we will return to this example in Chapter 5 when we are equipped with absorbing boundary conditions.

Triplate stripline is a type of transmission line used in integrated circuit interconnects and power distribution. A dielectric substrate fills the space between two parallel conducting plates, with a thin conducting trace sandwiched between the plates inside the dielectric. The outer plates serve as ground reference voltage, and the voltage on the stripline is the potential difference between the center trace and ground.

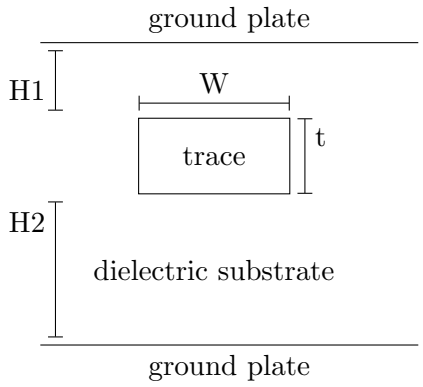

Figure 4.1: Diagram of asymmetric stripline structure.

This category of transmission line has the property of characteristic impedance, Z_0, which is a function of frequency expressing the ratio of voltage to current for a wave traveling in a set direction without reflection. The function $Z_0(\omega)$ is complex-valued with the real part expressing resistance and the imaginary part expressing phase delay.

The value of Z_0 in stripline is a complicated function of substrate thickness and permittivity, as well as trace thickness, cross-sectional shape, and position between the ground plates. Several approximation approaches have been developed to find Z_0 for parameter ranges; they vary in accuracy and ease of use. This situation also holds for several other categories of transmission line such as microstrip and coaxial cable, as noted in [23, 10].

The chosen stripline category simulated here has a trace with rectangular cross-section, which is thin in comparison to its width and the substrate thickness. This is most suited to the FDTD cuboid grid discretization. The spatial steps chosen are $\Delta x = \Delta z = 0.25 \times 10^{-3}$ m and $\Delta y = 0.10325 \times 10^{-3}$ m. These values allow conformation to chosen ratios of trace thickness to dielectric thickness and trace width to dielectric thickness.

We orient the stripline so that the trace's cross-section is in the yz plane, x is the axis of propagation, and the ground plates are on $\pm z$ sides of the domain, separated by 5 mm. The dielectric is homogeneous with permittivity 4. The trace thickness t is 0.25 mm, its width W 1.652 mm, and is located asymmetrically between the ground plates: H_1 is 2.75 mm, the distance from the $+z$ trace edge to the $+z$ ground plate, and H_2 is 2 mm, the distance from the $-z$ trace edge to the $-z$ plate. The $\pm z$ extents of the domain are bounded by Dirichlet conditions on E_x, E_y fields, which acts equivalent to PEC plates. These serve as ground plates for the simulation, and the voltage quantity is measured between the edge of the trace and the corresponding domain edge. Ideal stripline supports pure TEM wave propagation, wherein all fields involved in wave propagation are perpendicular to the direction of propagation. We do not expect to see significant E_x or H_x fields; the voltage is expressed in E_y and E_z, and current expressed as H_y and H_z curl about the trace. In addition, the ideal stripline is dispersion-free, which implies that $Z_0(\omega)$ for the line should be purely real. Using [10] as a starting point, after experimentation with the effect of asymmetry on simulations with other geometry, we choose an estimate Z_0 for this stripline configuration to be a constant, real 53.9Ω, and compare simulation results to this value.

Driving and Timing

So, for an excitation method for stripline analogous to those found in [23, 5], we use two voltage sources to excite an approximation to the TEM propagation mode for the stripline. The sources have zero internal resistance and are assigned a Gaussian waveform. They are the same width as the trace and extending from the edge of the trace to the corresponding y-domain edge in $\pm z$, and one cell thickness in x. This method neglects the fringing E fields, and the circulating H fields entirely, as well as introducing high frequency signal due to the discontinuity at the edge of each voltage source. Hence we allow approximately 10mm of simulation domain between the source and the first sampling area so that the fields take on a more representative, physical character. In fact, at this stage we allow 20mm of simulation domain before sampling. Two sample points will be needed for developments explained below.

We intend to obtain $Z_0(\omega)$ for ω from 0 to $40\pi \times 10^9$, or 0 to 20 GHz. A Gaussian waveform with time parameter $\tau \approx 2.0848 \times 10^{-11}$ sec and offset $t_0 \approx 9.3815 \times 10^{-11}$ sec provides frequency content to modestly over 20 GHz, corresponding to approximately 50 cells per wavelength for this choice of dx, dy, dz.

In the dielectric with permittivity 4, wave propagation speed is $\frac{1}{\sqrt{\varepsilon_r \varepsilon_0 \cdot \mu_r \mu_0}} = \frac{c}{\sqrt{4 \cdot 1}} = \frac{c}{2}$, so that a point on the source waveform takes about 1.3343×10^{-10} sec to travel the 20mm from the source location to the final sample point. Finally, by [24] we want at least one complete cycle of the lowest frequency of interest. We choose to calculate frequency domain results in steps of 10MHz from 0 to 20GHz. The time component required to allow the 10MHz component one full cycle is of course $\frac{1}{10 \times 10^6} = 1 \times 10^{-7}$ sec, which dominates the other terms. However, due to other observed issues explained below, we will investigate the result of allowing only enough time for one cycle of a 1GHz component, 1×10^{-9} sec. For a timestep $dt \approx 2.6765 \times 10^{-13}$, these correspond to about 37500 timesteps and 5000 timesteps respectively.

Measurement of Characteristic Impedance

Our first approach to finding Z_0 for this stripline structure is to apply the definition directly: we take the discrete Fourier transform of sampled voltage and current values at a point 20mm from the source. We note that the offset of E and H fields in space and time can strongly affect the

DFT of each, per [8], and lead to significant error when we take the quotient of the functions. The authors of [8] use a polar derivation of FDTD in a similar setting to confirm the expected Z_0 of a coaxial transmission line, by calculating Z_0 directly from the definition. To address the offset-field issue, the authors found that taking the spatial average of one field prior to calculating the DFT adequately addressed the spatial offset. Multiplying the other field DFT by $\exp(-\mathrm{i}\Delta t/2)$ effectively addressed the time offset.

In [8] the authors chose to spatially average the measured current value, and adjust the time sampling of the voltage measure. In our simulation, and all further voltage and current DFTs, the current sample, which is calculated from H fields at half-integer timesteps, is advanced by a half-timestep instead.

The voltage spatial average is implemented by choosing a voltage-sample cuboid with a two-cell thicknness in the appropriate dimension – in this case the x-dimension – chosen so that the sampled E components surround the plane of sampled H components. The averaging involved in voltage sampling then matches the spatial averaging described above. This technique will also be used to improve the accuracy of scattering parameters, described later.

Termination

Now, recall the definition of Z_0 involved a wave traveling in one direction with no reflection. However, the Dirichlet boundary conditions on $\pm x$ boundaries will perfectly reflect any wave traveling along the transmission line, if it reaches the domain boundary.

The naive option is to expand the domain so that the reflected wave does not reach the sampling point. But when we recall the time scales required to resolve the low-frequency components of interest, we take it as clear that the required domain size is prohibitive.

The standard motivation we discover, then, is to eliminate waves which approach domain boundaries – we will find that unbounded-domain scattering problems and far-field problems also need such a solution. In the stripline case, as we are equipped with a resistor lumped element of arbitrary resistance, we may attempt to terminate the stripline with a matched load at the domain edge. A poorly matched load will reflect some signal, which limits the usefulness of the method – we cannot expect to obtain a good value of Z_0 without a good initial estimate of Z_0. Since we approach the problem with an expected value of Z_0 we may test the performance of a well-matched load for

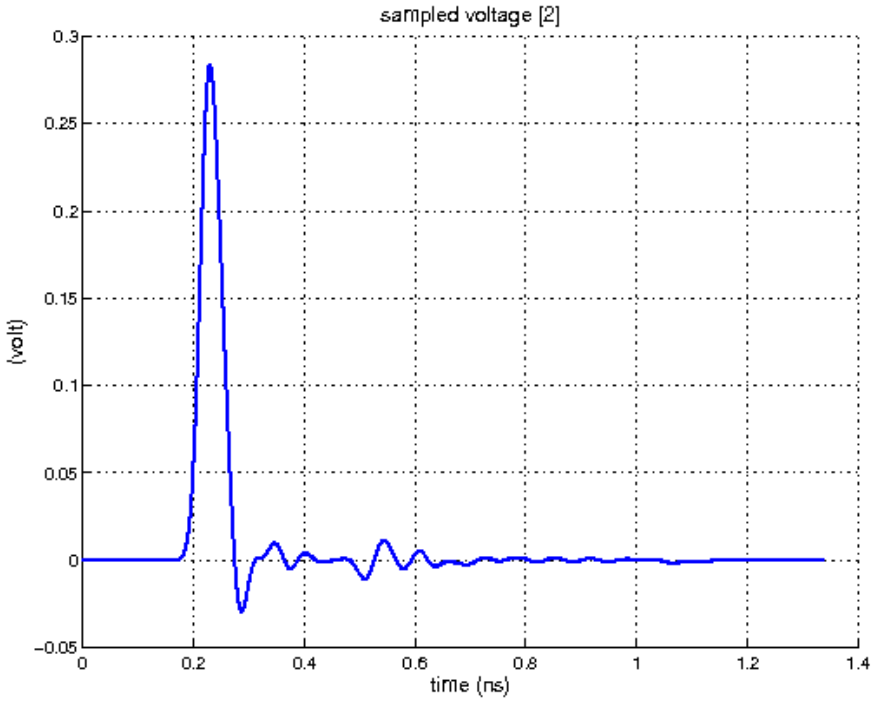

Figure 4.2: Resistor-terminated stripline sampled voltage 20mm from source, time domain

absorbing transmission line signal.

The results indicate that our terminating load is ineffective at absorbing the traveling wave. It should be clear that using a terminating resistor will not suffice for this example; this configuration is nearly ineffective at absorbing the signal. We will need a more effective wave absorbing mechanism; this prompts the consideration of absorbing boundary conditions in the next chapter.

4.4 Additional Lumped Elements

Many more elements have been developed, such as the diode featured in [7, 19] and the transistor featured in [19]. We will not develop these elements here, but we will note a limitation of each. The diode implementation is not readily extended to a distributed element.

Implementing the diode as developed in [7] involves the approximation of a nonlinear equation for current flow,

$$-I_d = -I_0[\exp(qV_d/kT) - 1]$$

where q, k are universal parameters, T is fixed during simulation, and the variable $V_d = -\nabla V$.

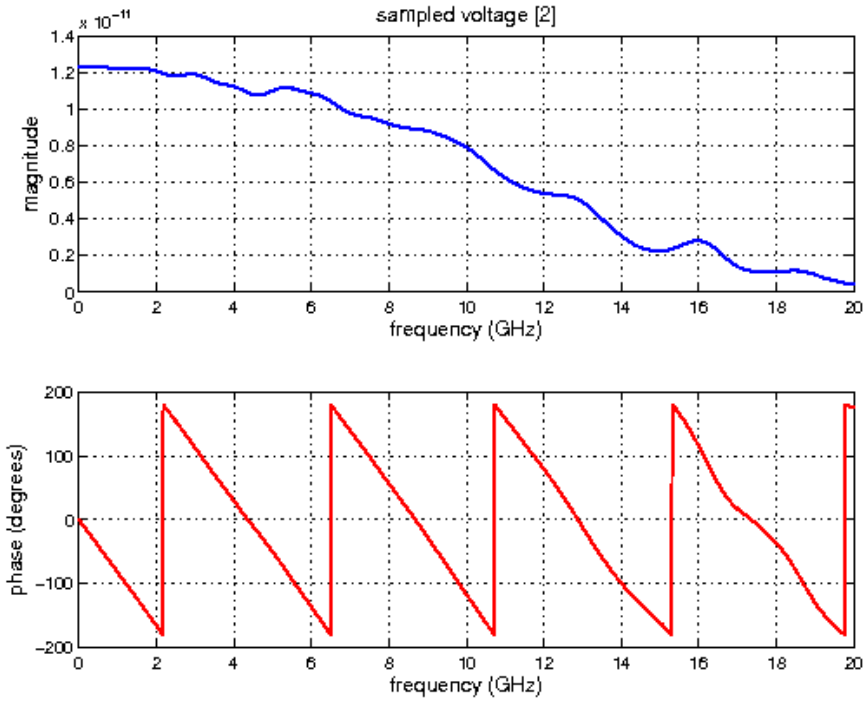

Figure 4.3: Resistor-terminated stripline sampled voltage 20mm from source, frequency domain

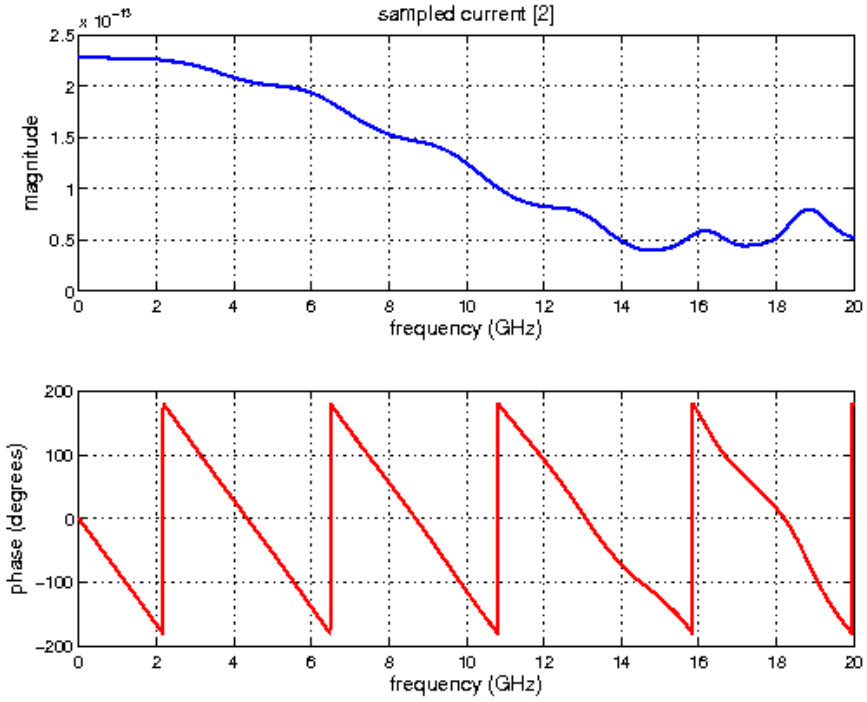

Figure 4.4: Resistor-terminated stripline sampled current 20mm from source, frequency domain

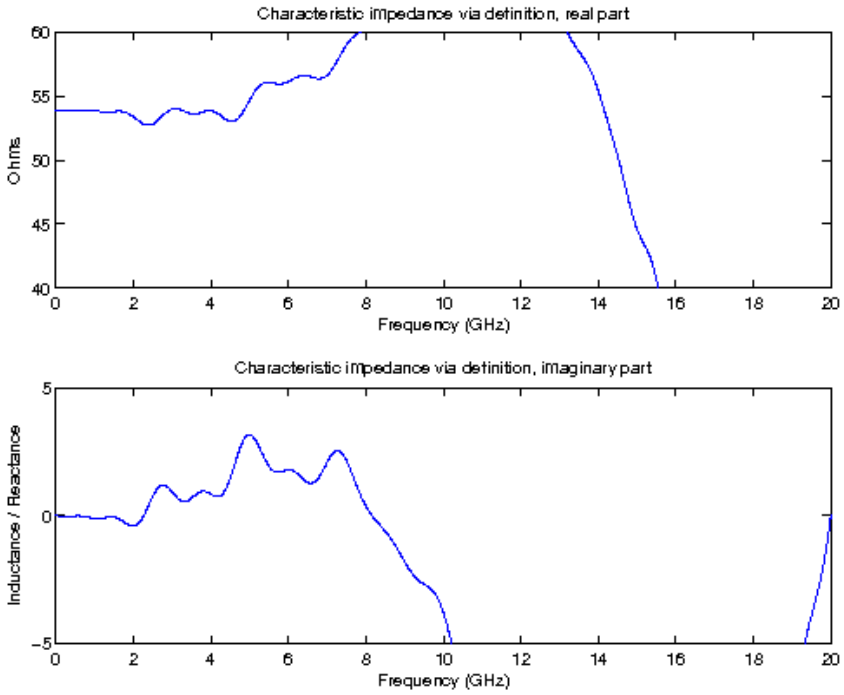

Figure 4.5: Resistor-terminated stripline, characteristic impedance real and imaginary parts as calculated from definition

The discretization and approximation method used for this equation are not straightforward to extend to multiple grid cells, so we are limited to a single grid cell per diode element. The transistor element described in [19] is also implemented using nonlinear diode equations. As such, it is unlikely that implementing a distributed transistor element would be convenient.

One popular analog circuit simulatior named SPICE offers an alternative to the lumped-element approach. Rather than laboriously deriving a model suitable for FDTD for each element we wish to include, [19] shows that FDTD and SPICE methods can be interfaced. Though the method is not examined in detail here, its essential idea is that a circuit SPICE simulations provide voltage and current values at selected ports, which drive selected $\vec{E}$ components in the FDTD space. The FDTD calculations and the SPICE calculations are timestepped alternately, and the results of each applied to the other at each timestep.

4.5 Scattering Parameters

For electrical networks which are expected to operate on microwave frequencies and higher, finding certain operational parameters of the network can be done by the FDTD simulation. We examine the simulation and use of scattering parameters, abbreviated S-parameters.

4.5.1 Definitions

S-parameters are defined in the context of electrical networks with indexed ports and well-defined measurement methods for voltage and current. We assume that the network's response to an impulse at any given port is linear at all ports. Note that this characterization of the physical network is usually appropriate for low voltages. For a network with two or more ports, S_{21} would describe the response of port 2 to a low-voltage, varying excitation at port 1.

Kurokawa in [13] defines an inbound power wave $a_i(\omega)$ and a reflected power wave $b_i(\omega)$ at port i, as

$$a_i = \frac{V_i + Z_i \times I_i}{2\sqrt{|\Re[Z_i]|}} \quad \text{and} \quad b_i = \frac{V_i - Z_i^* \times I_i}{2\sqrt{|\Re[Z_i]|}},$$

where V_i, I_i are frequency-domain voltage and current, and Z_i is the outward-looking frequency-domain impedance at the i'th port. Then if only port j is excited, we may define

$$S_{ij} = \frac{b_i}{a_j}, \qquad \Rightarrow \qquad S\vec{a} = \vec{b},$$

where we rely on the assumption that the network operates linearly at low-power to assemble the system, and $[S]_{ij} \equiv S_{ij}$, $[a]_i = a_i$ and $[b]_i = b_i$. Then, under the assumption of linearity, once the S-parameters are known, the response of the circuit to a small excitation at any or all ports can be calculated for any or all ports.

4.5.2 Simulation of S-Parameters

We already have access to the Fourier-transformed voltage and current values. The above definition of a_i and b_i are applied to calculate S_{ij} for any pair of sampled ports (i, j). Note that the scattering parameters are calculated using Fourier-transformed voltage and current values which are intended to be colocated in space and time. As such, we take care to obtain the same space and time averages as mentioned in the previous section regarding characteristic impedance.

The scattering parameters are in fact useful for the calculation of characteristic impedance of a transmission line, as in the previous example. A transmission line can be considered as a two-port network when two ports are separated by a length of the transmission line. Noted in [6], under these circumstances, the characteristic impedance can be obtained from S parameters using the

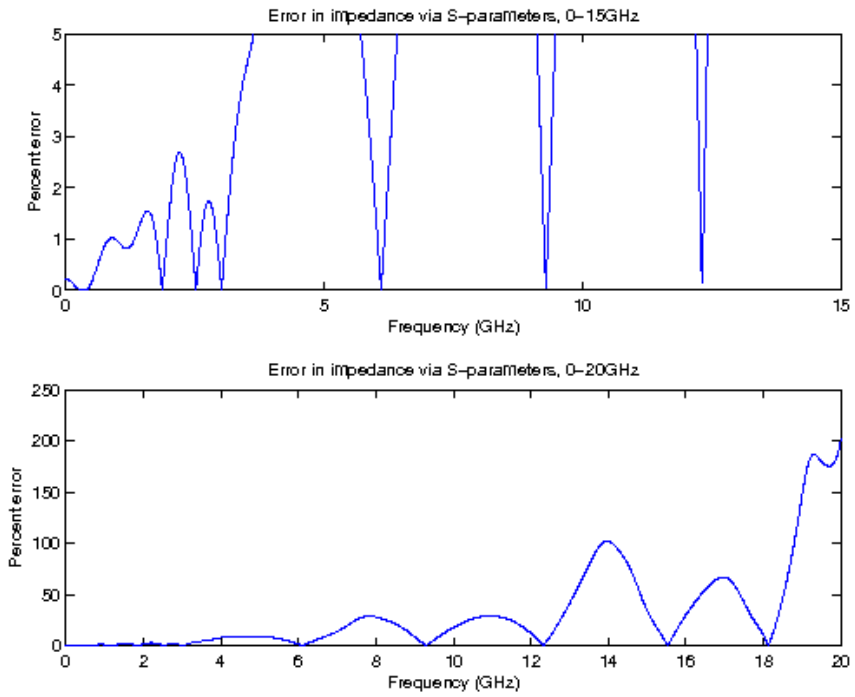

Figure 4.6: Resistor-terminated stripline, characteristic impedance real and imaginary parts as calculated from S-parameters.

formula

$$Z_0 = Z_r \sqrt{\frac{(1+S_{11})^2 - S_{21}^2}{(1-S_{11})^2 - S_{21}^2}},$$

where Z_r is a reference impedance, and we use 50Ω to match the value used for Z_1, Z_2.

Using this method to calculate the stripline Z_0 with terminating load, unfortunately, fares no better than applying the definition of Z_0.

Example: Low-Pass Filter S-Parameters

The purpose of this simulation is twofold; first, to verify the usefulness of scattering parameters in characterizing printed elements, and second, to emphasize the usefulness of the absorbing boundary conditions developed in Chapter 5. A simple layout for a microstrip low-pass filter is found in [18]. All traces are modeled as thin plates using the method described in Chapter 2. The entry and exit ports are 2.4384 mm wide; the center strip is 2.5398 mm $\times$ 20.32 mm. The substrate is 0.795 mm thick with a permittivity of 3.2 and a permeability of 1.4. This gives an expected impedance of 50Ω for both entry and exit ports. We also give the substrate small electric

and magnetic conductivity values of 0.5 and 0.3 respectively, so it is not a perfect dielectric.

We use the $-z$ PEC domain boundary as ground. In contrast to the stripline, sources, resistor elements, and sampling planes only occupy the $-z$ side of the trace. A soft voltage source is assigned a resistance of 50Ω and a waveform of a Gaussian pulse with bandwidth between 0 and over 20GHz; the source is placed near the termination of the entry port. A resistor is placed near the termination of the exit port. Voltage and current sampling elements are placed inward of the source and terminating load with care taken to orient the current sampling of the exit port inward, by S-parameter convention. All other faces $+z$, $\pm x$, $\pm y$ are allowed ten cells gap between the closest object and the boundary. The simulation is run for 25000 timesteps, which corresponds to a simulated final time of about 14.75 ns.

We observe that in this simulation, the terminating resistor functions well to minimize reflections. Experimentation with using an absorbing boundary to absorb voltage directly off the trace were not as effective.

The graphs of voltage by frequency and S_{11}, S_{21} are included here, for simulations without and without an absorbing boundary. In these results we can pick out strong resonance effects at about 8 GHz, 13 GHz, and 17 GHz. The fact that it is a cavity resonance interfering with our simulation is significant. Even if we were to perfect a terminating resistor to apply to each port in this simulation, the cavity resonance would remain. This introduces the necessity of an absorbing boundary condition that can absorb waves propagating through more general media than transmission lines. The CPML absorbing boundary used is developed in Chapter 5, applied here for illustration.

For the calculated S_{21} parameter, we observe real values nearly zero between 0 and 6 GHz. This indicates that the signal is transmitted from the source port 1 to port 2 with nearly no loss for these frequencies. The S_{21} real part drops to large negative values for a range of frequencies above 6 GHz, which indicates that signals in this range are expected to strongly attenuate. Rephrased, this element is expected to pass low frequencies from 0-6 GHz and block higher frequencies, within an operating range of approximately 0–10 GHz. As we can see, the undesired resonance effects strongly impact the S parameter results.

Let us view the results of the same simulation with absorbing boundary conditions applied – see Chapter 5 for more detail on the CPML used to reduce cavity resonance. A CPML with standard

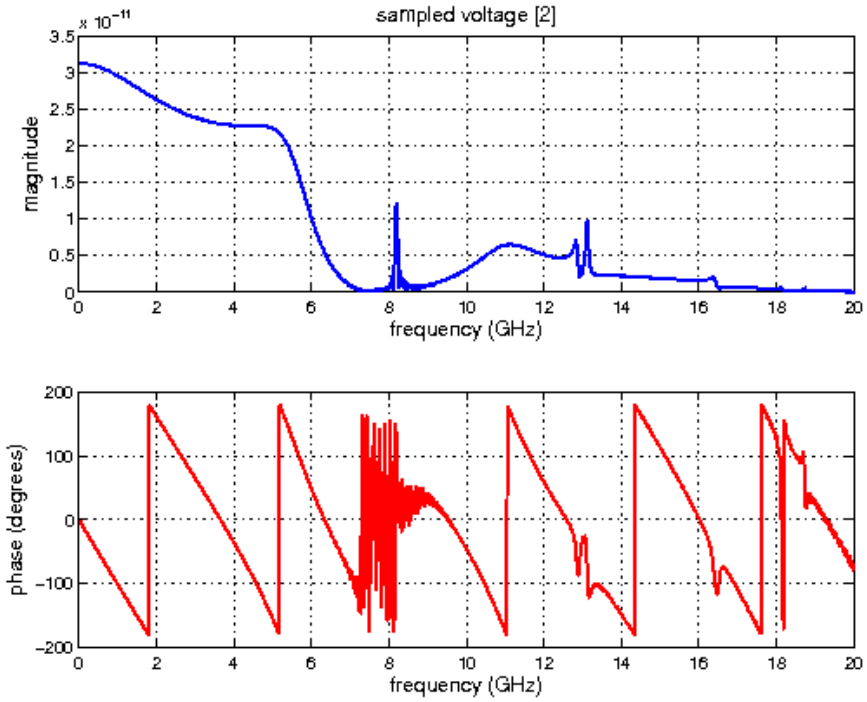

Figure 4.7: Low-pass filter, frequency-domain sampled voltage at exit port, PEC boundaries.

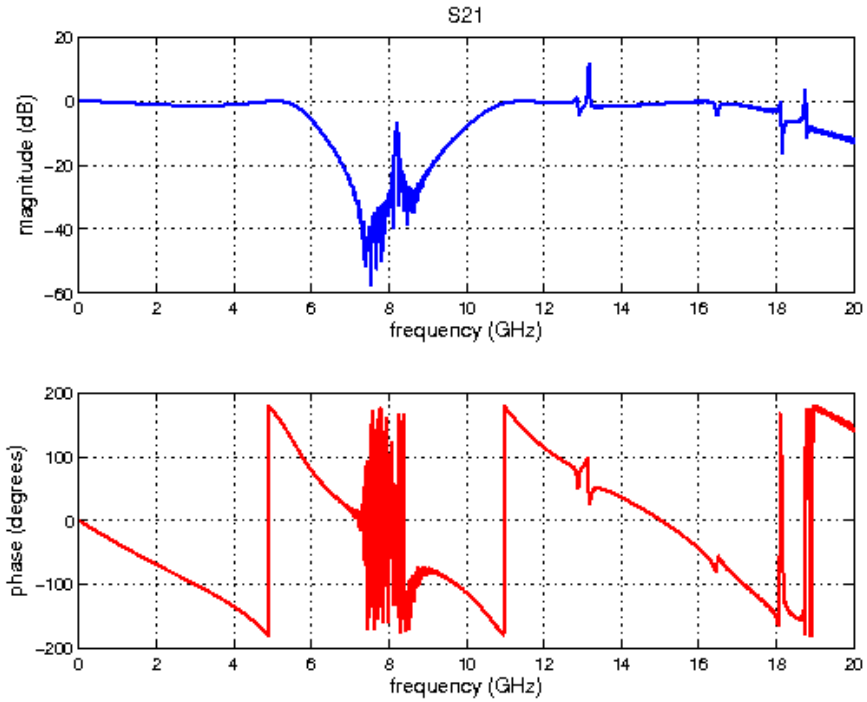

Figure 4.8: Low-pass filter S21 simulation result, PEC boundaries.

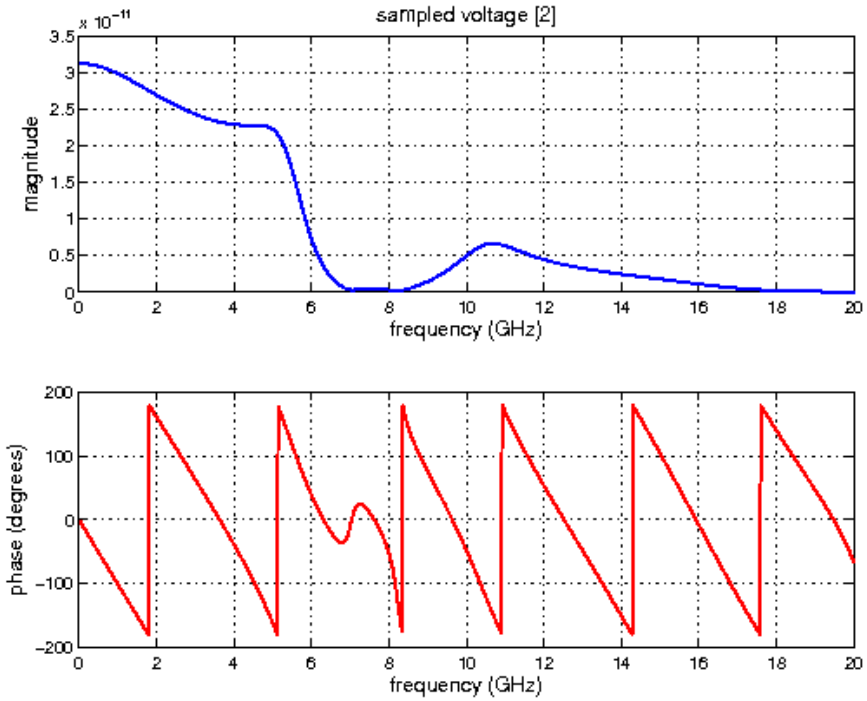

Figure 4.9: Low-pass filter, frequency-domain sampled voltage, absorbing boundaries.

parameters is applied to $\pm x$, $\pm y$, $+z$ domain faces, while the $-z$ face is left as PEC to serve as ground. The simulation is run for the same number of timesteps; we see that the applied CPML has suppressed the cavity resonance effect and our S-parameter results clearly indicate an effective low-pass filter element.

4.5.3 Other applications of S-Parameters

FDTD simulation of S-parameters is a cheap alternative to printing networks with the discontinuities we may wish to characterize, as noted in [23]; for microwave and higher frequency applications, there may not exist physical tools capable of making the desired measurements. As observed and developed in [19], S-parameters for a network can be used to form an equivalent circuit for other kinds of discontinuities such as vias; this may be an easier or more effective method of characterizing such discontinuities than direct simulation. We will not consider these applications in detail, however.

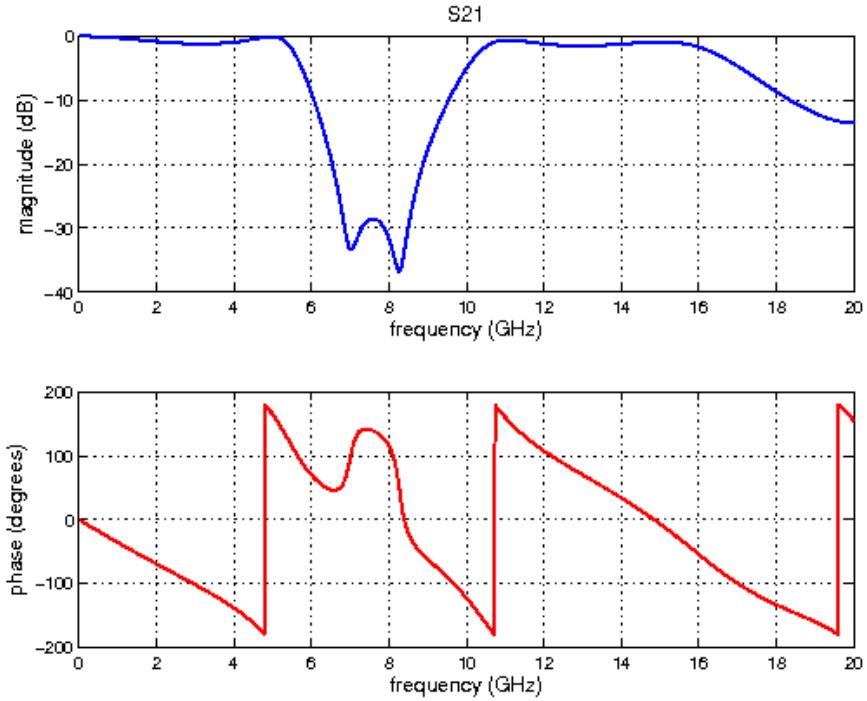

Figure 4.10: Low-pass filter S11 simulation result, absorbing boundaries.

4.6 Thin Wire Approximation

We may desire to model a network wherein the overall dimensions of the network are very much larger than the dimensions of some conductors. We already developed the technique to include thin plates in simulation, but thin wires are not approximated well by this method. Determining the grid cell size by the size of thin wires can lead to an impractically large computational domain. We resort to approximations to model conductors much smaller than a grid cell.

The following approximation provides modified updating coefficients for the magnetic field circulating about a thin current-carrying wire. We require the wire to conform to a straight line parallel to one of x, y, or z axes, with no turns. Note that the electric field is updated normally outside the wire, and within the wire itself we set the electric field to zero; hence we seek only magnetic field updating equations.

Consider a straight thin wire running along the x axis, aligned with nodes (i, j, k) and $(i+1, j, k)$. Let the surface S be a rectangle with corners at nodes (i, j, k), $(i + 1, j, k)$, $(i + 1, j + 1, k)$, and $(i, j + 1, k)$. Note that the field components $E_x(i, j, k)$, $E_x(i, j + 1, k)$, lie along the x-oriented sides

of S, and the field components $E_y(i,j,k)$, $E_y(i+1,j,k)$ lie along the y-oriented sides of S.

Note that the magnetic field component H_z is located at the center of S, pointing upward. Now as noted in [21], the fields E_y and H_z vary as $1/r$ near the wire, with r the distance from the wire center. We find a precedent for this in [21]. This allows us to relate the continuous field component to its value on the grid; for example set constant H_{z0} such that $H_z(i,j,k) = \frac{H_{z0}}{\Delta y/2}$. Then within the plane of S, labeling$y' \equiv j\Delta y + r$, we may say that the continuous field is

$$H_z(y') = \frac{H_{z0}}{r} = \frac{H_z(i,j,k)\Delta y}{2r},$$

down to the radius of the wire. We set two such equalities for the electric field, one for each side of S. Let $\frac{E_{y0}}{\Delta y/2} = E_y(i,j,k)$, and let $\frac{E_{y1}}{\Delta y/2} = E_y(i+1,j,k)$, then within the plane of S we have

$$E_y(y') = \frac{E_{y0}}{r} = \frac{E_y(i,j,k)\Delta y}{2r},$$

along the side of S at $x = i\Delta x$, and

$$E_y(y') = \frac{E_{y1}}{r} = \frac{E_y(i+1,j,k)\Delta y}{2r}$$

along the side of S at $x = (i+1)\Delta x$, down to the radius of the wire.

Now apply Faraday's law in its integral form to S. Allow the sense of da to be upward $(+z)$, and the outer edge of S to be labeled loop C traversed in the counter-clockwise direction as viewed from above, to obtain

$$-\mu \int_S \frac{\partial H}{\partial t} \cdot da = \oint_C E \cdot dl.$$

Applying this to S the surface integral on the LHS becomes

$$-\mu \int_{x=i\Delta x}^{(i+1)\Delta x} \int_{y=j\Delta y}^{(j+1)\Delta y} \frac{\partial}{\partial t} \frac{H_z(i,j,k)\Delta y}{2y} dx\, dy.$$

For the path integral on the RHS, we take the four sides of S separately:

$$= \int_{y=j\Delta y}^{(j+1)\Delta y} \frac{E_y(i+1,j,k)\Delta y}{2y} dy \; + \; \int_{x=(i+1)\Delta x}^{i\Delta x} E_x(i,j+1,k) dx \; +$$

$$+\int_{y=(j+1)\Delta y}^{j\Delta y}\frac{E_y(i,j,k)\Delta y}{2y}dy\ +\ \int_{x=i\Delta x}^{(i+1)\Delta x}E_x(i,j,k)dx.$$

Now we observe and apply the fact that within the conductor, the electric field should be negligible. The last integral $\int_{x=i\Delta x}^{(i+1)\Delta x}E_x(i,j,k)dx$ is taken entirely within the wire, so it drops out entirely. The two integrals involving E_y have limits which extend from the center of the wire to the limit of S; we may neglect the segments which lie inside the wire radius. Label the wire radius R, and write the y integral in terms of distance from wire center, then we have

$$\begin{aligned}-\mu\int_{x=i\Delta x}^{(i+1)\Delta x}\int_{r=R}^{\Delta y}\frac{\partial}{\partial t}\frac{H_z(i,j,k)\Delta y}{2r}dx\,dr=\\ =\int_{r=R}^{\Delta y}\frac{E_y(i+1,j,k)\Delta y}{2r}dr\ +\ \int_{x=(i+1)\Delta x}^{i\Delta x}E_x(i,j+1,k)dx\ +\\ +\int_{r=\Delta y}^{R}\frac{E_y(i,j,k)\Delta y}{2r}dr.\end{aligned}\tag{4.1}$$

Taking these integrals results in

$$\begin{aligned}-\mu\frac{\Delta x\Delta y}{2}\ln\left(\frac{\Delta y}{R}\right)\frac{\partial H_z(i,j,k)}{\partial t}=\frac{\Delta y}{2}\ln\left(\frac{\Delta y}{R}\right)E_y(i+1,j,k)-\\ -\Delta xE_x(i,j+1,k)-\frac{\Delta y}{2}\ln\left(\frac{\Delta y}{R}\right)E_y(i,j,k).\end{aligned}\tag{4.2}$$

We can discretize the time derivative at this point and obtain an updating equation for the H_z component from this equation. As usual we take a central difference, which for the magnetic field is centered about whole-integer timesteps,

$$\begin{aligned}-\mu_z(i,j,k)\frac{\Delta x\Delta y}{2}\ln\left(\frac{\Delta y}{R}\right)\frac{H_z^{n+\frac{1}{2}}(i,j,k)-H_z^{n-\frac{1}{2}}(i,j,k)}{\Delta t}=\frac{\Delta y}{2}\ln\left(\frac{\Delta y}{R}\right)E_y(i+1,j,k)-\\ -\Delta xE_x(i,j+1,k)-\frac{\Delta y}{2}\ln\left(\frac{\Delta y}{R}\right)E_y(i,j,k).\end{aligned}$$

Solving for future timestep, obtain

$$\begin{aligned}H_z^{n+\frac{1}{2}}(i,j,k)=H_z^{n-\frac{1}{2}}(i,j,k)+\frac{\Delta t}{\mu\Delta x}\left(E_y^n(i,j,k)-E_y^n(i+1,j,k)\right)+\\ +\frac{2\Delta t}{\mu_z(i,j,k)\Delta y\ln\left(\frac{\Delta y}{R}\right)}E_x^n(i,j+1,k).\end{aligned}\tag{4.3}$$

Now in fact the updating equation above fits into the standard updating equation (2.9) with appropriately modified coefficients. For reference, (2.9) is

$$H_z^{n+\frac{1}{2}}(i,j,k) = \left(\frac{2\Delta t}{(2\mu_z(i,j,k)+\sigma_z^m(i,j,k)\Delta t)\Delta x}\right)\big(E_y^n(i,j,k) - E_y^n(i+1,j,k)\big)+$$
$$\left(\frac{2\Delta t}{(2\mu_z(i,j,k)+\sigma_z^m(i,j,k)\Delta t)\Delta y}\right)\big(E_x^n(i,j+1,k) - E_x^n(i,j,k)\big)+$$
$$+\left(\frac{2\mu_z(i,j,k)-\sigma_z^m(i,j,k)\Delta t}{2\mu_z(i,j,k)+\sigma_z^m(i,j,k)\Delta t}\right)H_z^{n-\frac{1}{2}}(i,j,k) + \left(\frac{-2\Delta t}{2\mu_z(i,j,k)+\sigma_z^m(i,j,k)\Delta t}\right)M_{iz}^n(i,j,k).$$

Zeroing the impressed magnetic current term, recognizing that the term $E_x^n(i,j,k)$ is already fixed at 0, and labeling the coefficients separately, we use the standard

$$H_z^{n+\frac{1}{2}}(i,j,k) = C_{hzey}(i,j,k)\big(E_y^n(i,j,k) - E_y^n(i+1,j,k)\big)+$$
$$C_{hzex}(i,j,k)\big(E_x^n(i,j+1,k) - E_x^n(i,j,k)\big)+$$
$$+ C_{hzh}(i,j,k)H_z^{n-\frac{1}{2}}(i,j,k) + C_{hzm}M_{iz}^n(i,j,k),$$

with

$$C_{hzh}(i,j,k) = 1, \quad C_{hzm}(i,j,k) = 0, \quad C_{hzey}(i,j,k) = \frac{-\Delta t}{\mu_z(i,j,k)\Delta x},$$
$$\text{and } C_{hzex}(i,j,k) = \frac{2\Delta t}{\mu_z(i,j,k)\Delta y \ln\left(\frac{\Delta y}{R}\right)}.$$

Now, the magnetic field about a straight wire will be encircling the wire, prompting us to use similar processes to obtain the updating equations for the other surrounding field components $H_y(i,j,k)$, $H_z(i,j-1,k)$, $H_y(i,j,k-1)$. As the other derivations are very similar, they are omitted here and only the updating coefficients are listed. Using the same nomenclature for the neighboring components:

For $H_z(i,j-1,k)$:

$$C_{hzh}(i,j-1,k) = 1, \quad C_{hzm}(i,j-1,k) = 0, \quad C_{hzey}(i,j-1,k) = \frac{-\Delta t}{\mu_z(i,j-1,k)\Delta x},$$
$$C_{hzex}(i,j-1,k) = \frac{2\Delta t}{\mu_z(i,j,k)\Delta y \ln\left(\frac{\Delta y}{R}\right)}$$

For $H_y(i,j,k)$:

$$C_{hyh}(i,j,k) = 1, \quad C_{hym=0}, \quad C_{hyex}(i,j,k) = \frac{-2\Delta t}{\mu_y(i,j,k)\Delta z \ln\left(\frac{\Delta z}{R}\right)}$$

$$C_{hyez}(i,j,k) = \frac{\Delta t}{\mu_y(i,j,k)\Delta x}$$

For $H_y(i,j,k-1)$:

$$C_{hyh}(i,j,k-1) = 1, \quad C_{hym}(i,j,k-1) = 0, \quad C_{hyex}(i,j,k-1) = \frac{-2\Delta t}{\mu_y(i,j,k-1)\Delta z \ln\left(\frac{\Delta z}{R}\right)}$$

$$C_{hyez}(i,j,k-1) = \frac{\Delta t}{\mu_y(i,j,k-1)\Delta x}$$

Recall that the wire in the preceding derivation is oriented parallel to the x axis; still the results for wire orientations parallel to y and to z are similar. The other sets of updating coefficients are not listed here, but can be found similarly.

Note that there is an example simulation of a dipole antenna which uses the thin wire approximation in Chapter 6, after the far field method is developed.

CHAPTER 5

DOMAIN BOUNDARY CONDITIONS

We have seen in previous examples how reflections from a domain boundary can compromise the results we desire from a given simulation. Several schemes have been formulated to approximate unbounded domains and minimize reflections from the boundaries. This chapter examines three of the schemes intended to minimize such reflections, including the CPML scheme which is used in our simulations where absorbing boundary conditions are called for. First, we briefly consider the homogeneous Dirichlet boundary condition.

Perfect electric conductor

Homogeneous Dirichlet conditions force the tangential E components to zero everywhere they lie on a domain boundary. This condition is equivalent to a perfectly conductive plate with $\sigma^e = \infty$ bounding the domain and containing the outermost tangential $\vec{E}$ components. We may limit the condition to the tangential components because the perpendicular component is removed from the boundary by the structure of the Yee cell, and may be updated with information available in simulation. We arrive at the conclusion that the electric field has only a normal component approaching the boundary. The result is that waves incident on the boundary are completely reflected. For most simulations, this is not desired, so we must examine other conditions on the boundary.

Absorbing and Radiative boundary conditions

Due to its high performance in reducing reflections, the Perfectly Matched Layer and its extensions have become commonly used in many FDTD applications. Before Berenger's description of PML for two-dimensional simulations in 1994 [1] and three-dimensional simulations in 1996 [2], the set of boundary condition formulations named for Gerrit Mur saw frequent use from 1981 to the early 1990s. A Mur boundary condition is a partial differential operator formed from a weighted sum of derivatives, and acting directly on the tangential components at the boundary. As noted

in [11], these are examples of a radiation operators which approximate the unimpeded passage of waves across the domain boundary in order to reduce reflection. There is a tradeoff between accuracy and complexity of implementation in these radiative BCs.

5.0.1 Mur boundary conditions

Mur BCs apply an approximation to the convection equation at the simulation boundary. The family of BCs is separated into first-order, second-order, and so on. This category arises from the number of terms retained in a Taylor approximation as part of the derivation. The order also dictates both the performance of the BC and the overhead required for its numeric implementation. As shown in [11], the performance of Mur boundary conditions in absorbing incident waves is strongly a function of their angle of incidence. Incident plane waves which travel normal to the boundary are absorbed completely, and as the angle of incidence approaches 90° the wave approaches complete reflection. As the order of the Mur boundary increases, the absorption per fixed angle of incidence, as well as the difficulty and overhead of implementation, also increase. There is an exception for the 1D case, which does not have an order classification for this boundary type because the corresponding Taylor expansion is not necessary during derivation. We will derive the first-order case in 1D and 2D only.

Assume a domain of vacuum and consider a plane wave traveling in the $-x$ direction, polarized to involve only components E_y and H_z. Then the convection equation

$$(\partial_t - c\partial_x)E_y = 0.$$

is satisfied for all time and space. Consider the equivalent 1D FDTD simulation domain in x involving components E_y and H_z. Assume the standard domain composition such that the E_y components are the bounding components, at the domain edges; allow these nodes to be labeled 0 and $N+1$ for $-x$ and $+x$ boundaries respectively. Of course all H_z components can be updated from the usual updating equations, and need no additional conditions.

Consider a central-difference discretization of the convection equations which is centered halfway between nodes 0 and 1 in space, and halfway between steps n and $n+1$ in time, which is at

$(\Delta x/2, (n+1/2)\Delta t)$:

$$\frac{1}{\Delta t}(E_y^{n+1}(1/2) - E_y^n(1/2)) = \frac{c}{\Delta x}(E_y^{n+1/2}(1) - E_y^{n+1/2}(0)).$$

As E_y is computed at whole integer time and space steps, following [11] we take the appropriate average for every term:

$$\frac{1}{2\Delta t}\big((E_y^{n+1}(0) + E_y^{n+1}(1)) - (E_y^n(0) + E_y^n(1))\big) = \frac{c}{2\Delta x}\big((E_y^{n+1}(1) + E_y^n(1)) - (E_y^{n+1}(0) + E_y^n(0))\big),$$

Solving for the leftmost E_y component at the future time step t_{n+1},

$$E_y^{n+1}(0) = E_y^n(1) + \frac{c\Delta t - \Delta x}{c\Delta t + \Delta x}(E_y^{n+1}(1) - E_y^n(0)).$$

In contrast to updates on the staggered grid, here we have E_y future terms depending on both E_y present and E_y future terms. In implementation, this requires that the boundary be updated after the interior of the simulation space.

At the $+x$ boundary, we find an updating equation for the $N+1$th gridpoint by using the convection equation solved by a wave traveling in the $+x$ direction,

$$(\partial_t + c\partial_x)E_y = 0.$$

Discretization, averaging, and obtaining the update equation then proceed as before, and we obtain

$$E_y^{n+1}(N+1) = E_y^n(N) + \frac{c\Delta t - \Delta x}{c\Delta t + \Delta x}(E_y^{n+1}(N) - E_y^n(N+1)).$$

Note that in a one-dimensional simulation space, any wave which reaches the boundary is normally incident. So the nearly ideal performance of even first-order Mur boundaries paired with their ease of implementation make these BCs a good choice for a 1D simulation.

For 2D simulation space, it will be most convenient to consider a simulation in the TM_z system where the E_z field is outermost on all boundaries. For the TE_z case wherein the $y = y_{min}$ and $y = y_{max}$ boundaries have an outermost E_x component, and $x = 0$ and $x = x_{max}$ boundaries have an outermost E_y component, we would carry through a derivation similar to the following for each

of the boundaries separately. For ease of notation, let the grid indexes be such that $x_i = i\Delta x$ for $i = 0, \ldots, N+1$, and $y_j = j\Delta y$ for $j = 0, \ldots, M+1$.

The following is the derivation for the Mur BC along the $+x$ boundary x_{N+1}. Starting with the wave equation for continuous E_z, rearrange the operator:

$$\left[\frac{\partial^2}{\partial x^2} - \left(\frac{1}{c^2}\frac{\partial^2}{\partial t^2} - \frac{\partial^2}{\partial y^2}\right)\right] E_z = 0,$$

$$\left(\frac{\partial}{\partial x} + \sqrt{\frac{1}{c^2}\frac{\partial^2}{\partial t^2} - \frac{\partial^2}{\partial y^2}}\right)\left(\frac{\partial}{\partial x} - \sqrt{\frac{1}{c^2}\frac{\partial^2}{\partial t^2} - \frac{\partial^2}{\partial y^2}}\right) E_z = 0,$$

where we define this "factored" operator in terms of a Fourier transform. Let E_z be the inverse Fourier transform in y and t of a function $\mathbf{E_z}(x, k_y, \omega)$. As noted in [11], a time derivative of a time-domain function becomes a multiplication under the Fourier transform; likewise a spatial derivative becomes multiplication by the wavenumber:

$$\frac{\partial}{\partial t}\mathcal{F}^{-1}\mathbf{E_z} = \mathcal{F}^{-1}(\mathrm{i}\omega\mathbf{E_z}) \text{ and } \frac{\partial}{\partial y}\mathcal{F}^{-1}\mathbf{E_z} = \mathcal{F}^{-1}(\mathrm{i}k_y\mathbf{E_z}).$$

Now define the square-root operator in the preceding factorization by

$$\sqrt{\frac{1}{c^2}\frac{\partial^2}{\partial t^2} - \frac{\partial^2}{\partial y^2}} E_z = \mathcal{F}^{-1}\left(\sqrt{\frac{1}{c^2}(\mathrm{i}\omega)^2 - (\mathrm{i}k_y)^2}\mathbf{E_z}\right).$$

However, this does not help define a numerical scheme yet, because the inverse transform needs $\mathbf{E_z}$ at all frequencies - we would need to know E_z internal to the domain for all timesteps before we could calculate any boundary values.

We turn to approximation of the operator itself. Within the square root, with the Fourier definition in mind, suppose we "factor out" $\frac{1}{c}\frac{\partial^2}{\partial t^2}$, obtaining a factor of

$$S^2 = c^2\frac{\partial^2/\partial y^2}{\partial^2/\partial t^2}.$$

Notice that the magnitude of S when applied to E_z is a function of angle of incidence. This can be visualized if we consider a plane wave. If S is small, the wave is nearly normal to the rightmost boundary. For a wave which travels normal to the $+x$ boundary, the wavefront is parallel to the y

axis, so $\frac{\partial}{\partial_y} = 0$ and $S = 0$. As the angle of incidence increases, so does $\frac{\partial}{\partial_y}$ and the value of S.

The square root quantity is approximated by Taylor expansion:

$$\sqrt{1 - S^2} = 1 - \frac{S^2}{2} - \frac{S^4}{8} - \dots$$

A first-order method retains only the first term of this expansion, and as S grows with angle of incidence, the approximation error increases.

For the first-order approximation to the square root term, we obtain

$$\left(\frac{\partial}{\partial x} + \frac{1}{c}\frac{\partial}{\partial t}\right)\left(\frac{\partial}{\partial x} - \frac{1}{c}\frac{\partial}{\partial t}\right) E_z = \mathcal{L}^+\mathcal{L}^- E_z = 0.$$

Now at this point, we follow [11] and apply only one of these operators, depending on which boundary we are considering. On the $+x$ boundary we choose to discretize and apply the $\mathcal{L}^+$ operator, since we assume no sources beyond the $+x$ boundary. So the first-order case reduces to the 1D expression applied at all nodes on the boundary.

$$E_z^{n+1}(N+1, j) = E_y^n(N, j) + \frac{c\Delta t - \Delta x}{c\Delta t + \Delta x}(E_z^{n+1}(N, j) - E_y^n(N+1, j)),$$

for $j = 1, \dots, M$.

The derivation for the other x boundary follows similarly, and we find for the $-x$ boundary

$$E_z^{n+1}(0, j) = E_y^n(1, j) + \frac{c\Delta t - \Delta x}{c\Delta t + \Delta x}(E_z^{n+1}(1, j) - E_y^n(0, j)),$$

for $j = 1, \dots, M$.

We obtain the equations for the $\pm y$ boundaries by forming the factored operators differently. Now we write

$$\left[\frac{\partial^2}{\partial y^2} - \left(\frac{1}{c^2}\frac{\partial^2}{\partial t^2} - \frac{\partial^2}{\partial x^2}\right)\right] E_z = \left(\frac{\partial}{\partial y} + \sqrt{\frac{1}{c^2}\frac{\partial}{\partial x} - \frac{\partial}{\partial x}}\right)\left(\frac{\partial}{\partial y} - \sqrt{\frac{1}{c^2}\frac{\partial}{\partial x} - \frac{\partial}{\partial x}}\right) E_z = 0$$

with analogous definitions by inverse Fourier transform. Again factoring $\frac{1}{c^2}\frac{\partial^2}{\partial t^2}$ out of the square root, we obtain

$$S^2 = c^2 \frac{\partial^2/\partial x^2}{\partial^2/\partial t^2}$$

and again a first-order approximation of the square root now leading to the convection equation

$$\frac{\partial}{\partial y} E_z + \frac{1}{c} \frac{\partial}{\partial t} E_z = 0$$

along the $\pm y$ boundaries. The usual discretization leads to the updating equations, for $-y$:

$$E_z^{n+1}(i,0) = E_y^n(i,1) + \frac{c\Delta t - \Delta y}{c\Delta t + \Delta y}(E_z^{n+1}(i,1) - E_y^n(i,0)),$$

for $i = 1, \ldots, N$; and for $+y$:

$$E_z^{n+1}(i,M+1) = E_y^n(i,M) + \frac{c\Delta t - \Delta y}{c\Delta t + \Delta y}(E_z^{n+1}(i,M) - E_y^n(i,M+1)),$$

for $i = 1, \ldots, N$.

However, the preceding updating equations do not address four elements, the domain corner nodes $(0,0)$, $(N+1,0)$, $(0,M+1)$, $(N+1,M+1)$. The simplest and most approximation-free way to address this is to alter the domain so that these corner nodes do not need to be addressed at all. If we extend the H_x and H_y fields to form the $\pm y$ and $\pm x$ domain boundaries, respectively, then there are no such corner nodes. The derivation relies only on the wave nature of the field it's applied to, which of course H fields satisfy. Hence we repeat the derivation almost verbatim, for the appropriate fields, per boundary. For a TE_z 2D system, the equivalent is to allow E_x and E_y to form the domain boundaries, and repeat the corresponding derivations. Mur boundaries can be applied to 3D domains as well; this derivation is similar to the 2D case but is quite lengthy and is omitted here.

5.0.2 Perfectly Matched Layer

We have seen how adding lossy material to the borders of a simulation could reduce unwanted reflections. The idea can be refined, and using a method introduced by Berenger in 1994 [1] we can obtain better absorption from boundaries a few grid cells thick. The Perfectly Matched Layer (PML) incorporates carefully selected conductivity coefficients, so that signal decays quickly in its

interior, as in a lossy material, while reflection from the layer boundary is also minimized.

Consider an EM plane wave in the transverse-E_z (TE_z) mode, that is, unvarying in the z dimension and involving only the field components E_x, E_y, H_z. A plane wave traveling in the θ_i direction can be described as

$$H_z = \mathrm{Re}\left\{H_{z0}\exp\left(\mathrm{i}(\omega t - k_{0x}x - k_{0y}y)\right)\right\}\hat{k},$$

where ω is the frequency and k_{0x}, k_{0y} are wave vector components which can be found as follows: By the relation in homogeneous media $|k_0| = \omega\sqrt{\mu\varepsilon}$ we obtain $k_{0x} = \omega\sqrt{\mu\varepsilon}\cos\theta_i$ and $k_{0y} = \omega\sqrt{\mu\varepsilon}\sin\theta_i$. The time-invariant formulation of the same wave is just

$$\vec{H}_{z0}\exp\left(\mathrm{i}\omega(-\sqrt{\mu\varepsilon}\cos\theta_i x - \sqrt{\mu\varepsilon}\sin\theta_i y)\right)\hat{k}.$$

By the wave impedance relation we can write the associated electric field as

$$\vec{E}_{x0} = -\sin(\theta_i)\sqrt{\frac{\mu}{\varepsilon}}H_{z0}\hat{i}, \quad \vec{E}_{y0} = \cos(\theta_i)\sqrt{\frac{\mu}{\varepsilon}}H_{z0}\hat{j}.$$

Let the preceding wave exist in a non-conductive half-space of $x < 0$, and let the $x > 0$ half-space be occupied by a uniform lossy material. Then there is reflection and transmission at $x = 0$ to consider, but our focus will be on the transmitted wave in $x > 0$ and specifying the nature of the $x > 0$ region. Both can be expressed in terms of the incident fields, but this is not essential for the PML description. Label the fields existing in the lossy material as

$$E_{x1} = -E_1\sin\theta_t\exp(\mathrm{i}\omega(t - \alpha x - \beta y)), \quad E_{y1} = E_1\cos\theta_t\exp(\mathrm{i}\omega(t - \alpha x - \beta y)),$$

$$H_{z1} = H_1\exp(\mathrm{i}\omega(t - \alpha x - \beta y)),$$

where θ_t is the angle of transmission (normal to surfaces of constant phase), and α and β are unknowns relating the transmitted to the incident wave.

Equations for the TE_z mode, after expanding the cross products in Faraday's and Ampere's Laws, reduce to

$$\varepsilon\frac{\partial E_{x1}}{\partial t} + \sigma^e E_{x1} = \frac{\partial H_{z1}}{\partial y},$$

$$\varepsilon\frac{\partial E_{y1}}{\partial t} + \sigma^e E_{y1} = -\frac{\partial H_{z1}}{\partial x},$$
$$\mu\frac{\partial H_{z1}}{\partial t} + \sigma^m H_{z1} = \frac{\partial E_{x1}}{\partial y} - \frac{\partial E_{y1}}{\partial x}.$$

However, as with Berenger's split-field formulation, suppose we define two components H_{zx} and H_{zy} such that $H_{z1} = H_{zx} + H_{zy}$ and the system is satisfied:

$$\begin{aligned}
\mu\frac{\partial H_{zx}}{\partial t} + \sigma_x^m H_{zx} &= -\frac{\partial E_{y1}}{\partial x}, \\
\mu\frac{\partial H_{zy}}{\partial t} + \sigma_y^m H_{zy} &= \frac{\partial E_{x1}}{\partial y}, \\
\varepsilon\frac{\partial E_{x1}}{\partial t} + \sigma_y^e E_{x1} &= \frac{\partial (H_{zx} + H_{zy})}{\partial y}, \\
\varepsilon\frac{\partial E_{y1}}{\partial t} + \sigma_x^e E_{y1} &= -\frac{\partial (H_{zx} + H_{zy})}{\partial x}.
\end{aligned} \tag{5.1}$$

Note that the split fields are not physical, and may not satisfy the wave equation independently. Also note that the conductivities in the above systems $\sigma_x^e, \sigma_y^e, \sigma_x^m, \sigma_y^m$ do *not* denote the material response to different field components. As H_{zx} is intended to describe the component of the H_z wave "traveling in the x direction", so σ_x^m is the conductivity associated with H_{zx}. Similar for H_{zy}.

The system describes an anisotropic medium which would formally require tensors for electric and magnetic conductivity. However, the derivation can be completed, including FDTD updating equations, using only the split field formulation.

Using the time-harmonic field expressions and taking derivatives, the system is then

$$\begin{aligned}
(\varepsilon \mathrm{i}\omega + \sigma_y^e) E_{x1} &= -\mathrm{i}\omega\beta(H_{zx} + H_{zy}), \\
(\varepsilon \mathrm{i}\omega + \sigma_x^e) E_{y1} &= -\mathrm{i}\omega\alpha(H_{zx} + H_{zy}), \\
(\mu \mathrm{i}\omega + \sigma_x^m) H_{zx} &= -(-\cos\theta_t \cdot \mathrm{i}\omega\alpha) E_1, \\
(\mu \mathrm{i}\omega + \sigma_y^m) H_{zy} &= (\sin\theta_t \cdot \mathrm{i}\omega\beta) E_1.
\end{aligned}$$

Multiplying all by i/ω and substituting E_1 field equalities,

$$\begin{aligned}
(\varepsilon - \mathrm{i}\sigma_y^e/\omega)\sin\theta_t E_1 &= \beta(H_{zx} + H_{zy}), \\
(\varepsilon - \mathrm{i}\sigma_x^e/\omega)\cos\theta_t E_1 &= \alpha(H_{zx} + H_{zy}),
\end{aligned} \tag{5.2}$$

$$(\mu - \mathrm{i}\sigma_x^m/\omega)H_{zx} = \alpha\cos\theta_t E_1,$$
$$(\mu - \mathrm{i}\sigma_y^m/\omega)H_{zy} = \beta\sin\theta_t E_1.$$

The last two equations can be substituted into the first to find

$$(\varepsilon - \mathrm{i}\sigma_y^e/\omega)\sin\theta_t E_1 = \beta\left[\frac{\alpha\cos\theta_t}{\mu - \mathrm{i}\sigma_x^m/\omega} + \frac{\beta\sin\theta_t}{\mu - \mathrm{i}\sigma_y^m/\omega}\right]E_1.$$

Then pull out factors of ε and μ and cancel E_1 to find

$$\varepsilon\mu(1 - \mathrm{i}\sigma_y^e/\varepsilon\omega)\sin\theta_t = \beta\left[\frac{\alpha\cos\theta_t}{1 - \mathrm{i}\sigma_x^m/\mu\omega} + \frac{\beta\sin\theta_t}{1 - \mathrm{i}\sigma_y^m/\mu\omega}\right].$$

A similar process for the second equation shows

$$\varepsilon\mu(1 - \mathrm{i}\sigma_y^e/\varepsilon\omega)\cos\theta_t = \alpha\left[\frac{\alpha\cos\theta_t}{1 - \mathrm{i}\sigma_x^m/\mu\omega} + \frac{\beta\sin\theta_t}{1 - \mathrm{i}\sigma_y^m/\mu\omega}\right].$$

After some computation we obtain for unknowns α, β:

$$\alpha = \frac{\sqrt{\varepsilon\mu}}{G}\left(1 - \mathrm{i}\frac{\sigma_x^e}{\omega\varepsilon}\right)\cos\theta_t,$$
$$\beta = \frac{\sqrt{\varepsilon\mu}}{G}\left(1 - \mathrm{i}\frac{\sigma_x^e}{\omega\varepsilon}\right)\sin\theta_t,$$

where we use

$$G = \sqrt{\frac{1 - \mathrm{i}\sigma_x^e/\omega\varepsilon}{1 - \mathrm{i}\sigma_x^m/\omega\varepsilon}\cos^2\theta_t + \frac{1 - \mathrm{i}\sigma_y^e/\omega\varepsilon}{1 - \mathrm{i}\sigma_y^m/\omega\varepsilon}\sin^2\theta_t}.$$

Now we insert α, β into the latter two equations of (5.2) and find

$$(\mu - \mathrm{i}\sigma_x^m/\omega)H_{zx} = \frac{\sqrt{\varepsilon\mu}}{G}\left(1 - \mathrm{i}\frac{\sigma_x^e}{\omega\varepsilon}\right)\cos^2\theta_t E_1,$$

$$H_{zx} = \sqrt{\frac{\varepsilon}{\mu}}\frac{1}{G}\left(\frac{1 - \mathrm{i}\sigma_x^e/\omega\varepsilon}{1 - \mathrm{i}\sigma_x^m/\omega\mu}\right)\cos^2\theta_t E_1.$$

Similarly

$$H_{zy} = \sqrt{\frac{\varepsilon}{\mu}}\frac{1}{G}\left(\frac{1 - \mathrm{i}\sigma_y^e/\omega\varepsilon}{1 - \mathrm{i}\sigma_y^m/\omega\mu}\right)\sin^2\theta_t E_1.$$

Then, as

$$H_{z1} = H_{zx} + H_{zy} = \sqrt{\frac{\varepsilon}{\mu}}\frac{1}{G}\left(\frac{1-\mathrm{i}\sigma_x^e/\omega\varepsilon}{1-\mathrm{i}\sigma_x^m/\omega\mu}\cos^2\theta_t + \frac{1-\mathrm{i}\sigma_y^e/\omega\varepsilon}{1-\mathrm{i}\sigma_y^m/\omega\mu}\sin^2\theta_t)\right)E_1$$
$$= \sqrt{\frac{\varepsilon}{\mu}}\frac{1}{G}G^2E_1,$$

we can use the definition of wave impedance $Z = \frac{E_1}{H_{z1}}$ to obtain

$$Z = \sqrt{\frac{\mu}{\varepsilon}}\frac{1}{G}$$

Now, requiring $G = 1$ causes the wave impedance to reduce to $\sqrt{\frac{\mu}{\varepsilon}}$. We can obtain $G = 1$ when

$$\frac{1-\mathrm{i}\sigma_x^e/\omega\varepsilon}{1-\mathrm{i}\sigma_x^m/\omega\mu} = \frac{1-\mathrm{i}\sigma_y^e/\omega\varepsilon}{1-\mathrm{i}\sigma_y^m/\omega\mu} = 1,$$

which is satisfied when

$$\frac{\sigma_x^e}{\varepsilon} = \frac{\sigma_x^m}{\mu} \tag{5.3}$$

and

$$\frac{\sigma_y^e}{\varepsilon} = \frac{\sigma_y^m}{\mu}.$$

Recall the domain setup wherein $x < 0$ is a dielectric and $x \geq 0$ is the PML medium we are considering. Label ε' and μ' to be the permittivity and permeability of the dielectric medium in $x < 0$. As one of the major conclusions of PML theory, choosing PML properties $\varepsilon = \varepsilon'$ and $\mu = \mu'$ means that $Z = \sqrt{\frac{\mu}{\varepsilon}} = \sqrt{\frac{\mu'}{\varepsilon'}}$ and the wave impedance of the PML medium matches that of the domain medium. Hence, in theory we expect zero reflection from the domain-PML interface. In most cases, the domain abutting the PML region is expected to be empty space and thus we desire $\varepsilon = \varepsilon_0$ and $\mu = \mu_0$, but as we have seen, we may use the PML to truncate the domain within a dielectric as well.

Finally, the next section will clarify why we choose certain conductivities to be 0: in a PML abutting an x-normal boundary, a standard choice is $\sigma_x^e = \sigma_x^m = 0$ and the two parameters σ_y large

and conforming to (5.3). In a PML abutting a y-normal boundary, the converse is usually applied; $\sigma_y^e = \sigma_y^m = 0$ and σ_x values nonzero and conforming to (5.3).

2D PML-PML interface

At any corner of a 2D domain, we have a choice of how to fill the space with a PML region. If the appropriate conductivities are chosen to be 0, it turns out, the regions may be allowed to overlap in the sense of holding nonzero conductivities constant. Choose the $+x$, $+y$ corner of a 2D domain; let the x-normal boundary PML region be denoted as region 1 and the y-normal boundary PML region be denoted as region 2. The corner where they would overlap is region 3.

Region 1's conductivities should be set $\sigma_y^e = \sigma_y^m = 0$ corresponding to no loss for the y-directed signal component, and region 2's conductivities should be $\sigma_x^e = \sigma_x^m = 0$ corresponding to no loss for the x-directed signal component. Then, in region 3 where both regions overlap, we apply the nonzero conductivities from both regions. This leads to PML-PML interfaces without reflections as follows.

Consider the boundary between regions 1 and 3, and allow a plane wave in TE_z to cross the boundary. Let the intrinsic wave impedances for regions 1, 2, and 3 be Z_1, Z_2, Z_3 as usual. Let the incident angle (in region 1) be θ_i and the transmitted angle (in region 3) be θ_t. Without derivation, the reflection coefficient for a signal is given by

$$r = \left|\frac{H_{z3}}{H_{z1}}\right| = \frac{Z_3 \cos\theta_t - Z_1 \cos\theta_i}{Z_3 \cos\theta_t + Z_1 \cos\theta_i}.$$

Under the assumption that each PML region is impedance-matched to freespace, $Z_1 = \sqrt{\frac{\mu_0}{\varepsilon_0}}\frac{1}{G_1}$ and $Z_3 = \sqrt{\frac{\mu_0}{\varepsilon_0}}\frac{1}{G_3}$, which obtains

$$r = \frac{G_1 G_3}{G_1 G_3} \frac{\sqrt{\frac{\mu_0}{\varepsilon_0}}\frac{1}{G_3}\cos\theta_t - \sqrt{\frac{\mu_0}{\varepsilon_0}}\frac{1}{G_1}\cos\theta_i}{\sqrt{\frac{\mu_0}{\varepsilon_0}}\frac{1}{G_3}\cos\theta_t + \sqrt{\frac{\mu_0}{\varepsilon_0}}\frac{1}{G_1}\cos\theta_i} = \frac{G_1\cos\theta_t - G_3\cos\theta_i}{G_1\cos\theta_t + G_3\cos\theta_i}.$$

Then, setting region 3's x conductivities to match region 1, and its y conductivities to match region 2, implies $G_3 = 1$. This means $r = \frac{\cos\theta_t - \cos\theta_i}{\cos\theta_t + \cos\theta_i}$, and to avoid reflections from the 1-3 interface entirely, we need only show that $\theta_t = \theta_i$.

Again the 1-3 interface is normal to y, so without derivation the Snell-Descartes law at the 1-3 interface is

$$\left(1 - \mathrm{i}\frac{\sigma_{x1}}{\varepsilon_0 \omega}\right) \frac{\sin\theta_i}{G_1} = \left(1 - \mathrm{i}\frac{\sigma_{x3}}{\varepsilon_0 \omega}\right) \frac{\sin\theta_t}{G_3}.$$

By our choice of allowing $\sigma_{x1} = \sigma_{x3}$ and $G_1 = G_3 = 1$, we obtain $\sin\theta_i = \sin\theta_t$ which by natural constraints on incident and transmission angles, means $\theta_i = \theta_t$.

Calculations run nearly identically for the 2-3 interface, justifying $\sigma_{y2} = \sigma_{y3}$.

Numerical artifacts and loss functions

Unfortunately the theory of the reflection-free air-PML interface does not translate perfectly into simulation. In test simulations it has been found that a homogeneous PML region still yields reflections at its air interface, even when implemented correctly according to theory. The standard solution is to define the PML region with graded properties, that is, nonconstant distributions of material properties within the PML region which still adhere to the reflectionless conditions stated above.

Two of the standard conductivity distribution functions use a pair of parameters: n_{pml} and $R(0)$. The n_{pml} parameter controls the spatial profile of the distribution function, and is usually decided by details of the simulation or optimized by testing. The $R(0)$ parameter is an acceptable reflection coefficient at incident angle 0 (normal to the boundary), usually very small such as 10^{-8} [7].

By attenuation calculations, [7] shows that the reflection coefficient at the domain interface for a wave which has traveled through a *uniform* PML medium is

$$R(\theta_i) = \exp\left(-2\delta \frac{\sigma \cos\theta_i}{\varepsilon_0 c}\right).$$

The parameters here are δ which is the thickness of the PML region and σ which is the electrical conductivity in the direction normal to the air-PML interface. Requiring $R(0)$ be a fixed acceptably small value allows us to find the required σ_{max}. Note that the PML which follows a graded conductivity distribution function will not absorb as strongly as the theoretical uniform PML. So, the choice of $R(0)$ parameter is an ideal, not met by actual simulations.

Two standard conductivity distribution functions used are the geometric and the power (or polynomial) profiles, following [7, 11]. Conductivity should increase from zero to σ_{max} as the distance from the air-PML interface according to one of these functions:

$$\text{Power: } \sigma(x) = \left(\frac{x}{d}\right)^m \cdot \sigma_{x,\max},$$

where d is the depth of the PML region,

$$\text{Geometric: } \sigma(x) = \sigma_0 g^{\frac{x}{\Delta s}},$$

where Δs is the grid step corresponding to the dimension normal to the interface (substitute Δx or Δy as appropriate).

We can set σ_{max} by solving for the conductivity in the above reflection coefficient expression. For the power conductivity distribution, the coefficient σ_{max} is set according to

$$\sigma_{max} = -\frac{(n_{pml}+1)\varepsilon_0 c \ln(R(0))}{2\Delta s N},$$

where Δs is the grid cell size as before and N is the number of cells depth in the PML region.

In the geometric distribution, find

$$\sigma_0 = -\frac{\varepsilon_0 c \ln(g)}{2\Delta s g^N - 1} \ln R(0),$$

where g is the 'base' parameter for the geometric function.

In the above cases, we can use the condition (5.3) to set the corresponding magnetic conductivity distribution, to maintain the reflection-free property throughout the region.

2D FDTD PML Updating Equations

Updating equations for PML regions are obtained by discretizing the system derived such as (5.1) for the TE_z case. We keep the split-field components such as H_{zx}, H_{zy} and calculate the total field H_z afterward.

To update $H_{zx}(i,j)$ at time $n+\frac{1}{2}$, discretize the first equation in (5.1):

$$\mu_0 \frac{H_{zx}^{n+\frac{1}{2}}(i,j) - H_{zx}^{n-\frac{1}{2}}(i,j)}{\Delta t} + \sigma_x^m(i,j) \frac{H_{zx}^{n+\frac{1}{2}}(i,j) + H_{zx}^{n-\frac{1}{2}}(i,j)}{2} = -\left[\frac{E_y^n(i+1,j) - E_y^n(i,j)}{\Delta x}\right],$$

which can be solved for time step $n+\frac{1}{2}$

$$H_{zx}^{n+\frac{1}{2}}(i,j) = \frac{2\Delta t}{(2\mu_0 + \Delta t \sigma_x^m(i,j))\Delta x}\left[E_y^n(i,j) - E_y^n(i+1,j)\right] + \left(\frac{\sigma_x^m(i,j)\Delta t - 2\mu_0}{\sigma_x^m(i,j)\Delta t + 2\mu_0}\right) H_{zx}^{n-\frac{1}{2}}(i,j).$$

By discretization of the equation for H_{zy} we obtain

$$H_{zy}^{n+\frac{1}{2}}(i,j) = \frac{2\Delta t}{(2\mu + \Delta t \sigma_y^m(i,j))\Delta y}\left[E_x^n(i,j+1) - E_x^n(i,j)\right] + \left(\frac{\sigma_y^m(i,j)\Delta t - 2\mu_0}{\sigma_y^m(i,j)\Delta t + 2\mu_0}\right) H_{zy}^{n-\frac{1}{2}}(i,j).$$

To discretize and update E_x and E_y within the PML region, we need H_z; this is calculated by adding the field components $H_{zx} + H_{zy}$. Since we center the time discretization about $n+\frac{1}{2}$, there are no issues with finding average field component values.

$$\varepsilon_0 \left[\frac{E_x^{n+1}(i,j) - E_x^n(i,j)}{\Delta t}\right] + \sigma_y^e(i,j)\left[\frac{E_x^{n+1}(i,j) + E_x^n(i,j)}{2}\right] = \frac{H_z^{n+\frac{1}{2}}(i,j) - H_z^{n+\frac{1}{2}}(i,j-1)}{\Delta y}.$$

Solve for time $n+1$ to find

$$E_x^{n+1}(i,j) = \left(\frac{2\varepsilon_0 - \Delta t \sigma_y^e(i,j)}{2\varepsilon_0 + \Delta t \sigma_y^e(i,j)}\right) E_x^n(i,j) + \frac{2\Delta t}{(2\varepsilon_0 + \Delta t \sigma_y^e(i,j))\Delta y}[H_z^{n+\frac{1}{2}}(i,j) - H_z^{n+\frac{1}{2}}(i,j-1)].$$

A similar process for E_y yields

$$E_y^{n+1}(i,j) = \left(\frac{2\varepsilon_0 - \Delta t \sigma_x^e(i,j)}{2\varepsilon_0 + \Delta t \sigma_x^e(i,j)}\right) E_y^n(i,j) + \frac{2\Delta t}{(2\varepsilon_0 + \Delta t \sigma_x^e(i,j))\Delta x}[H_z^{n+\frac{1}{2}}(i,j) - H_z^{n+\frac{1}{2}}(i-1,j)].$$

3D PML

The extension to 3D of the Berenger split-field PML derivation is straightforward. All fields are split; $E_x \equiv E_{xy} + E_{xz}$ and $H_x \equiv H_{xy} + H_{xz}$, $E_y \equiv E_{yx} + E_{yz}$ and $H_y \equiv H_{yx} + H_{yz}$, and so on. So, the six scalar Maxwell equations split to form a system of 12 equations:

$$\varepsilon \frac{\partial E_{xy}}{\partial t} + \sigma_y^e E_{xy} = \frac{\partial (H_{zx} + H_{zy})}{\partial y} \qquad \mu \frac{\partial H_{xy}}{\partial t} + \sigma_y^m H_{xy} = -\frac{\partial (E_{zx} + E_{zy})}{\partial y},$$

$$\varepsilon\frac{\partial E_{xz}}{\partial t}+\sigma_z^e E_{xz}=-\frac{\partial(H_{yz}+H_{yx})}{\partial z} \qquad \mu\frac{\partial H_{xz}}{\partial t}+\sigma_z^m H_{xz}=\frac{\partial(E_{yz}+E_{yx})}{\partial z},$$
$$\varepsilon\frac{\partial E_{yz}}{\partial t}+\sigma_z^e E_{yz}=\frac{\partial(H_{xy}+H_{xz})}{\partial z} \qquad \mu\frac{\partial H_{yz}}{\partial t}+\sigma_z^m H_{yz}=-\frac{\partial(E_{xy}+E_{xz})}{\partial z},$$
$$\varepsilon\frac{\partial E_{yx}}{\partial t}+\sigma_x^e E_{yx}=-\frac{\partial(H_{zx}+H_{zy})}{\partial x} \qquad \mu\frac{\partial H_{yx}}{\partial t}+\sigma_x^m H_{yx}=\frac{\partial(E_{zx}+E_{zy})}{\partial x},$$
$$\varepsilon\frac{\partial E_{zx}}{\partial t}+\sigma_x^e E_{zx}=\frac{\partial(H_{yz}+H_{yx})}{\partial x} \qquad \mu\frac{\partial H_{zx}}{\partial t}+\sigma_x^m H_{zx}=-\frac{\partial(E_{yz}+E_{yx})}{\partial x},$$
$$\varepsilon\frac{\partial E_{zy}}{\partial t}+\sigma_y^e E_{zy}=-\frac{\partial(H_{xy}+H_{xz})}{\partial y} \qquad \mu\frac{\partial H_{zy}}{\partial t}+\sigma_y^m H_{zy}=\frac{\partial(E_{xy}+E_{xz})}{\partial y}.$$

As Berenger showed in [2], the plane-wave analysis yielding matching conditions at the vacuum-PML interface can be repeated in an arbitrary plane of incidence in 3D. The condition that must hold for a matched layer parallel to $x = 0$ is $\frac{\sigma_x^e}{\varepsilon} = \frac{\sigma_x^m}{\mu}$ and other conductivities zero, just as in the 2D case. Similar conditions on σ_y^e, σ_y^m and σ_z^e, σ_z^m hold for layers parallel to $y = 0$ and $z = 0$. At domain edges and corners where two or three boundary planes meet, we have superimposed PML regions. These regions are defined analogously to the 2D case: along an edge, two of the three pairs of conductivity parameters are nonzero, and at a corner, all three pairs of conductivity parameters are nonzero. As in [2], matched layers defined in this way also theoretically yield zero reflection at PML-PML interfaces.

5.0.3 Convolutional PML

Berenger's split-field PML does not absorb evanescent waves reliably in implementation. As noted in [3], the theoretical absorption of evanescent waves may be so high within the split-field PML medium as to cause spurious numerical reflection. One way to avoid this issue is to choose the domain such that most evanescent waves die off to a sufficient degree before reaching the PML region, typically 1/3 of a wavelength of the largest significant evanescent wave present in simulation. This is undesirable, though, as the purpose of ABCs is to allow smaller domains and reduce computing resource consumption.

The Complex Frequency-Shifted PML (CFS-PML) is developed as a reformulation of split-field PML. The numerical implementation of CFS-PML, Convolutional PML developed below, can more efficiently absorb evanescent waves. CPML is a discretizable implementation of the complex frequency-shifted PML (CFS-PML) technique developed by Kuzuoglu and Mittra in [14]. Another of the authors' stated aims in [14] is to formulate a PML which is strongly causal; the original

split-field formulation is only weakly causal as noted in [3, 11, 20].

It turns out that a PML region can be regarded as a region of stretched coordinates in complex space. Assuming that the computational domain is surrounded by vacuum, the EM fields in vacuum at some sufficient distance from domain center correspond to a superposition of plane waves. As such we can analytically extend their solution into complex space and choose a contour that departs from the reals on which to find the solution. As noted in [20], the exact solution to a given simulation with PMLs is the solution of Maxwell's equations on a contour in complex space. Finally, note that although these derivations assume vacuum near the domain boundary, the CPML scheme has been shown to apply to domains which include objects contacting the boundary. The CPML functions to absorb waves traveling along transmission lines and through waveguides, so long as they do not vary tangentially within the CPML region.

Split-field derivation from stretched coordinates

Following [4], Maxwell's equations in the frequency domain with $\exp(\mathrm{i}\omega t)$ in a Cartesian coordinate-stretched space without conductivity, are

$$\begin{aligned} \nabla_e \times E &= -\mathrm{i}\omega\mu H, \\ \nabla_h \times H &= \mathrm{i}\omega\varepsilon E, \\ \nabla_h \cdot \varepsilon E &= \rho, \\ \nabla_e \cdot \mu H &= 0, \end{aligned} \tag{5.4}$$

where we use stretching coefficients $e_x(\vec{x}), e_y(\vec{x}), e_z(\vec{x}), h_x(\vec{x}), h_y(\vec{x}), h_z(\vec{x})$ to build the custom operators

$$\begin{aligned} \nabla_e &= \frac{1}{e_x}\left(\frac{\partial}{\partial x}\right)\hat{i} + \frac{1}{e_y}\left(\frac{\partial}{\partial y}\right)\hat{j} + \frac{1}{e_z}\left(\frac{\partial}{\partial z}\right)\hat{k}, \\ \nabla_h &= \frac{1}{h_x}\left(\frac{\partial}{\partial x}\right)\hat{i} + \frac{1}{h_y}\left(\frac{\partial}{\partial y}\right)\hat{j} + \frac{1}{h_z}\left(\frac{\partial}{\partial z}\right)\hat{k}. \end{aligned}$$

Note that the stretching coefficients may be functions of position and may be complex-valued. As derived in [4], we use the matching condition that the stretching coefficients be equal by component, that is, $e_x = h_x$, $e_y = h_y$, $e_z = h_z$. Then we may relabel stretching coefficients component-wise; let

$e_x = h_x \equiv s_x$ and similar for s_y, s_z.

We can recover Berenger's split-field formulation from this coordinate-stretching formulation. Taking the first two equations in (5.4) and expanding the cross-products, (allowing notation $\partial_r \equiv \partial/\partial_r$ for $r \equiv x, y, z$)

$$\left(\frac{1}{s_y}\partial_y E_z - \frac{1}{s_z}\partial_z E_y\right)\hat{i} + \left(\frac{1}{s_z}\partial_z E_x - \frac{1}{s_x}\partial_x E_z\right)\hat{j} + \left(\frac{1}{s_x}\partial_x E_y - \frac{1}{s_y}\partial_y E_x\right)\hat{k} = -\mathrm{i}\omega\mu H,$$
$$\left(\frac{1}{s_y}\partial_y H_z - \frac{1}{s_z}\partial_z H_y\right)\hat{i} + \left(\frac{1}{s_z}\partial_z H_x - \frac{1}{s_x}\partial_x H_z\right)\hat{j} + \left(\frac{1}{s_x}\partial_x H_y - \frac{1}{s_y}\partial_y H_x\right)\hat{k} = \mathrm{i}\omega\varepsilon E.$$

Define the fields

$$\mathrm{i}\omega\mu H_{xy} = -\frac{1}{s_y}\partial_y E_z, \qquad \mathrm{i}\omega\mu H_{xz} = \frac{1}{s_z}\partial_z E_y,$$
$$\mathrm{i}\omega\varepsilon E_{xy} = \frac{1}{s_y}\partial_y H_z, \qquad \mathrm{i}\omega\varepsilon E_{xz} = -\frac{1}{s_z}\partial_z H_y.$$

and similar for H_{yx}, H_{yz}, H_{zx}, H_{zy}, E_{yx}, E_{yz}, E_{zx}, E_{zy}. Observe that these definitions correspond to each of the terms in the preceding cross-product expansions, such that

$$H_{xy} + H_{xz} = H_x, \qquad E_{xy} + E_{xz} = E_x,$$

and similar for the other component pairings. Now we will find that for the $\exp(\mathrm{i}\omega t)$ convention, taking

$$s_r = 1 + \frac{\sigma_r}{\mathrm{i}\omega\varepsilon} \text{ for } r \equiv x, y, z$$

is equivalent to the split-field formulation. Note that the three σ_r values should be considered to be parameters of the stretching coefficients, distinct from material conductivity values at this point; these parameters will be associated with conductivity values in what follows.

Allow notation $\partial_t \equiv \partial/\partial t$, and recall that with the $\exp(\mathrm{i}\omega t)$ convention of time dependence, rewriting in the time domain is achieved by substituting ∂_t for the coefficient $\mathrm{i}\omega$. Following [4]:

$$\left(\mu\partial_t + \frac{\sigma_y\mu}{\varepsilon}\right)H_{xy} = -\partial_y E_z, \qquad \left(\mu\partial_t + \frac{\sigma_z\mu}{\varepsilon}\right)H_{xz} = \partial_z E_y,$$

$$(\varepsilon\partial_t + \sigma_y)\, E_{xy} = \partial_y H_z, \qquad (\varepsilon\partial_t + \sigma_z)\, E_{xz} = -\partial_z H_y,$$

and similar for the other component pairings. We recognize the form of the updating equations for split-field components, which implies the role of conductivity for the σ_r parameters. Finally, to impose distinct σ_r^e and σ_r^m electric and magnetic conductivity parameters such that the preceding equations are satisfied, we observe the relation

$$\frac{\sigma_r^m \mu}{\varepsilon} = \sigma_r^e \equiv \sigma_r,$$

for $r \equiv x, y, z$. So, we find that the coordinate-stretching matching condition $e_r = h_r \equiv s_r$ is equivalent to the split-field matching condition derived in the preceding section, $\frac{\sigma_r^m}{\varepsilon} = \frac{\sigma_r^e}{\mu}$.

To recover the notation in [4] which uses the $\exp(-\mathrm{i}\omega t)$ convention for time dependence, substitute:

$$\begin{aligned} -H_{s_x} &= H_{yx} + H_{zx}, \qquad -E_{s_x} = E_{yx} + E_{zx}, \\ -H_{s_y} &= H_{xy} + H_{zy}, \qquad -E_{s_y} = E_{xy} + E_{zy}, \\ -H_{s_z} &= H_{xz} + H_{yz}, \qquad -E_{s_z} = E_{xz} + E_{yz}, \end{aligned}$$

and note that the stretching parameters must be defined slightly differently, as $s_r = 1 + \frac{\mathrm{i}\sigma_r}{\omega\varepsilon}$.

Complex frequency shifted PML

As a generalization of the formulation of PML, the coordinate-stretching coefficients are not limited to the preceding definitions. The first two of the coordinate-stretched, frequency domain Maxwell's equations for $\exp(\mathrm{i}t)$ convention are reiterated below, in scalar form. This restatement includes the matching condition that stretching coefficients are equal, and the conductivity properties of terminating media, as the σ^e and σ^m values on the RHS terms.

$$\begin{aligned} \left(\frac{1}{s_y}\partial_y E_z - \frac{1}{s_z}\partial_z E_y\right) &= -(\mathrm{i}\omega\mu_x + \sigma_x^m) H_x, \\ \left(\frac{1}{s_z}\partial_z E_x - \frac{1}{s_x}\partial_x E_z\right) &= -(\mathrm{i}\omega\mu_y + \sigma_y^m) H_y, \\ \left(\frac{1}{s_x}\partial_x E_y - \frac{1}{s_y}\partial_y E_x\right) &= -(\mathrm{i}\omega\mu_z + \sigma_z^m) H_z, \end{aligned}$$

$$\left(\frac{1}{s_y}\partial_y H_z - \frac{1}{s_z}\partial_z H_y\right) = (\mathrm{i}\omega\varepsilon_x + \sigma_x^e)E_x,$$
$$\left(\frac{1}{s_z}\partial_z H_x - \frac{1}{s_x}\partial_x H_z\right) = (\mathrm{i}\omega\varepsilon_y + \sigma_y^e)E_y,$$
$$\left(\frac{1}{s_x}\partial_x H_y - \frac{1}{s_y}\partial_y H_x\right) = (\mathrm{i}\omega\varepsilon_z + \sigma_z^e)E_z.$$

Kuzuoglu and Mittra in [14] use a more general definition for the stretching parameters:

$$s_r^e = \kappa_r^e + \frac{\sigma_{pr}^e}{\alpha_r^e + \mathrm{i}\omega\varepsilon_r}, \qquad s_r^m = \kappa_r^m + \frac{\sigma_{pr}^m}{\alpha_r^m + \mathrm{i}\omega\mu_r},$$

for $r \equiv x, y, z$. Values σ_{pr}^e, σ_{pr}^m are analogous to but distinct from conductivity values; σ_r^e, σ_r^m are maintained separately and terminating media (such as conducting traces) can be accommodated within the CPML layer. As part of the definition, it is stipulated that κ_r^e and κ_r^m are real scalar parameters ≥ 1, and α_r^e and α_r^m are real scalar parameters ≥ 0. The previous derivation of the reflection-free matching condition $s_r^e = s_r^m \equiv s_r$ applies, which leads to conditions [7]

$$\kappa_r^e = \kappa_r^m$$
$$\frac{\sigma_{pr}^e}{\alpha_r^e + \mathrm{i}\omega\varepsilon_r} = \frac{\sigma_{pr}^m}{\alpha_r^m + \mathrm{i}\omega\varepsilon_r},$$

which requires

$$\frac{\sigma_{pr}^e}{\varepsilon_r} = \frac{\sigma_{pr}^m}{\mu_r}, \qquad \frac{\alpha_r^e}{\varepsilon_r} = \frac{\alpha_r^m}{\mu_r}.$$

We use the following parameter definitions,

$$\sigma_{pr}^e \equiv \sigma_{pr},\ \alpha_r^e \equiv \alpha_r, \text{ and } \kappa_r^e \equiv \kappa_r.$$

However, for brevity, we will continue to use σ_{pr}^m interchangeably with $\sigma_{pr}\varepsilon_0/\mu_0$. The actual assignation of parameter values will be addressed in a following section regarding CPML grading; for the rest of this derivation the parameters remain fixed but unknown.

Now, by [14], translating into the time domain requires a convolution with the inverse Laplace transform of the new stretching parameter:

$$(S_y * \partial_y E_z - S_z * \partial_z E_y) = -(\mu_x\partial_t + \sigma_x^m)H_x,$$

$$(S_z * \partial_z E_x - S_x * \partial_x E_z) = -(\mu_y \partial_t + \sigma_y^m) H_y,$$
$$(S_x * \partial_x E_y - S_y * \partial_y E_x) = -(\mu_z \partial_t + \sigma_z^m) H_z,$$
$$(S_y * \partial_y H_z - S_z * \partial_z H_y) = (\varepsilon_x \partial_t + \sigma_x^e) E_x,$$
$$(S_z * \partial_z H_x - S_x * \partial_x H_z) = (\varepsilon_y \partial_t + \sigma_y^e) E_y,$$
$$(S_x * \partial_x H_y - S_y * \partial_y H_x) = (\varepsilon_z \partial_t + \sigma_z^e) E_z,$$

where $S_r = \mathcal{L}^{-1}\left(\frac{1}{s_r}\right)$ for $r \equiv x, y, z$, and the asterisk operator of course denotes convolution. By [7, 11],

$$\begin{aligned} S_r(t) &= \frac{\delta(t)}{\kappa_r} - \frac{\sigma_r}{\varepsilon_0 \kappa_r^2} \exp\left(\left(-\frac{\sigma_{pr}}{\varepsilon_0 \kappa_r} - \frac{\alpha_r}{\varepsilon_0}\right) \cdot t\right) \cdot \mathcal{U}(t) \\ &= \frac{\delta(t)}{\kappa_r} - \zeta_r(t). \end{aligned}$$

where $\delta(t)$ is the Dirac delta function and $\mathcal{U}(t)$ is the Heaviside step function, $r \equiv x, y, z$, and explicitly stated, $\zeta_r(t) = \frac{\sigma_r}{\varepsilon_0 \kappa_r^2} \exp\left(\left(-\frac{\sigma_r}{\varepsilon_0 \kappa_r} - \frac{\alpha_r}{\varepsilon_0}\right) \cdot t\right) \cdot \mathcal{U}(t)$. So, in convolving S_r with one of the field functions, the Dirac delta term simplifies to the field function itself, and the ζ term convolution can be written separately. The preceding time-domain equations become:

$$\left(\frac{\partial_y E_z}{\kappa_y} - \zeta_y * \partial_y E_z - \frac{\partial_z E_y}{\kappa_z} + \zeta_z * \partial_z E_y\right) = -(\mu_x \partial_t + \sigma_x^m) H_x,$$
$$\left(\frac{\partial_z E_x}{\kappa_z} - \zeta_z * \partial_z E_x - \frac{\partial_x E_z}{\kappa_x} + \zeta_x * \partial_x E_z\right) = -(\mu_y \partial_t + \sigma_y^m) H_y,$$
$$\left(\frac{\partial_x E_y}{\kappa_x} - \zeta_x * \partial_x E_y - \frac{\partial_y E_x}{\kappa_y} + \zeta_y * \partial_y E_x\right) = -(\mu_z \partial_t + \sigma_z^m) H_z,$$
$$\left(\frac{\partial_y H_z}{\kappa_y} - \zeta_y * \partial_y H_z - \frac{\partial_z H_y}{\kappa_z} + \zeta_z * \partial_z H_y\right) = (\varepsilon_x \partial_t + \sigma_x^e) E_x,$$
$$\left(\frac{\partial_z H_x}{\kappa_z} - \zeta_z * \partial_z H_x - \frac{\partial_x H_z}{\kappa_x} + \zeta_x * \partial_x H_z\right) = (\varepsilon_y \partial_t + \sigma_y^e) E_y,$$
$$\left(\frac{\partial_x H_y}{\kappa_x} - \zeta_x * \partial_x H_y - \frac{\partial_y H_x}{\kappa_y} + \zeta_y * \partial_y H_x\right) = (\varepsilon_z \partial_t + \sigma_z^e) E_z.$$

Now we discretize the convolution integrals, so that we can discretize and obtain updating equations from these time-domain equations. Consider the first equation above; as the ∂_t operator is applied to the H_x field, we seek an updating equation for H_x. In particular, we will focus on $H_x^{n+\frac{1}{2}}(i, j, k)$.

Recursive convolution technique

Consider the first convolution integral in the first equation above. Substitute the discretized E field derivative, split the integral into appropriate parts, and pull out constants where applicable to find

$$\int_{\tau=0}^{t} \zeta_y(\tau)\partial_y E_z(t-\tau)\,d\tau \approx \sum_{m=0}^{m=n-1} \left(\frac{E_z^{n-m}(i,j+1,k) - E_z^{n-m}(i,j,k)}{\Delta y}\right) \int_{\tau=m\Delta t}^{(m+1)\Delta t} \zeta_y(\tau)\,d\tau.$$

Substitute the definition of ζ_y into the integral and evaluate:

$$\begin{aligned}\int_{\tau=m\Delta t}^{(m+1)\Delta t} \zeta_y(\tau)\,d\tau &= -\frac{\sigma_{py}}{\varepsilon_0\kappa_y^2} \int_{\tau=m\Delta t}^{(m+1)\Delta t} \exp\left(\left(-\frac{\sigma_{py}}{\varepsilon_0\kappa_y} - \frac{\alpha_y}{\varepsilon_0}\right)\tau\right)\,d\tau \\ &= \Delta y\, a_y \exp\left[\left(\frac{\sigma_{py}}{\kappa_y} + \alpha_y\right)\left(\frac{m\Delta t}{\varepsilon_0}\right)\right],\end{aligned}$$

where, following [7, 11], we have defined a constant

$$a_y = \frac{\sigma_{py}}{\Delta y(\sigma_{py}\kappa_y + \kappa_y^2\alpha_y)}\left[\exp\left(\left(-\frac{\sigma_y}{\kappa_y} - \alpha_y\right)\frac{\Delta t}{\varepsilon_0}\right) - 1\right].$$

(Note that the factor of Δy will cancel with the divisor in the discretization of $\partial_y E_z$.) Altogether we can rewrite the summation as a discretized function,

$$\begin{aligned}\Psi_{hxy}^n(i,j,k) &= \sum_{m=0}^{n-1} \left(E_z^{n-m}(i,j+1,k) - E_z^{n-m}(i,j,k)\right) a_y \exp\left[\left(\frac{\sigma_{py}}{\kappa_y} + \alpha_y\right)\left(\frac{m\Delta t}{\varepsilon_0}\right)\right] \\ &\approx \zeta_y * \partial_y E_z.\end{aligned}$$

Similar definitions apply for functions Ψ_{hxz}, Ψ_{hyx}, Ψ_{hyz}, Ψ_{exy}, Ψ_{exz}. At this point, consider the discretized equation for H_x which we could obtain from the first of the preceding time domain equations. Discretizing in the usual fashion and substituting $\Psi_{hxy}^n(i,j,k)$ for $\zeta_y * \partial_y E_z$ in the equation

$$\left(\frac{\partial_y E_z}{\kappa_y} - \zeta_y * \partial_y E_z - \frac{\partial_z E_y}{\kappa_z} + \zeta_z * \partial_z E_y\right) = -(\mu_x\partial_t + \sigma_x^m)H_x,$$

we obtain

$$\frac{1}{\kappa_y}\left(\frac{E_z^n(i,j+1,k) - E_z^n(i,j,k)}{\Delta y}\right) - \Psi_{hxy}^n(i,j,k) - \frac{1}{\kappa_z}\left(\frac{E_y^n(i,j,k+1) - E_y^n(i,j,k)}{\Delta z}\right) + \Psi_{hxz}^n(i,j,k)$$

$$= -\mu_x(i,j,k)\frac{H_x^{n+\frac{1}{2}}(i,j,k) - H_x^{n-\frac{1}{2}}(i,j,k)}{\Delta t} - \frac{\sigma_x\varepsilon_x(i,j,k)}{\mu_x(i,j,k)}\frac{H_x^{n+\frac{1}{2}}(i,j,k) + H_x^{n-\frac{1}{2}}(i,j,k)}{2},$$

which could be solved for the future term $H_x^{n+\frac{1}{2}}$. But recall that in the definition of the two functions Ψ_{hxr}^n, there are summations of E field terms over all previous timesteps. Since we do not store this data, we must resort to a different method: recursive convolution. It turns out that we can continue to use the preceding definitions of the Ψ functions, after a little manipulation of the summation.

Consider this rearrangement and relabeling of terms:

$$\begin{aligned}\Psi_{hxy}^n &= a_y \sum_{m=0}^{n-1} \left[E_z^{n-m}(i,j+1,k) - E_z^{n-m}(i,j,k)\right] \cdot \exp\left[m\left(\frac{\Delta t}{\varepsilon_0}\right)\left(\frac{\sigma_{py}}{\kappa_y} + \alpha_y\right)\right] \\ &= a_y B(n-m)\cdot\exp(mT).\end{aligned}$$

Writing the summation term by term,

$$\begin{aligned}\Psi_{hxy}^n &= a_y B(n-0)\exp(0T) + a_y B(n-1)\exp(1T) + \ldots \\ &\qquad + a_y B(2)\exp((n-2)T) + a_y B(1)\exp((n-1)T) \\ &= a_y B(n-0)\exp(0T) + \exp(T)\cdot[a_y B(n-1)\exp(0T) + \ldots \\ &\qquad + a_y B(2)\exp((n-3)T) + a_y B(1)\exp((n-2)T)] \\ &= a_y B(n) + \exp(T)\Psi_{hxy}^{n-1} \\ &= a_y\left(E_z^n(i,j+1,k) - E_z^n(i,j,k)\right) + \exp\left[\left(\frac{\sigma_{py}}{\kappa_y} + \alpha_y\right)\left(\frac{\Delta t}{\varepsilon_0}\right)\right] \cdot \Psi_{hxy}^{n-1}.\end{aligned}$$

Hence our dependence on the complete time history of local E values is eliminated. Rather than needing to store the entire time history of two field values and recompute the entire sum for each gridpoint with an associated Ψ term, we can instead compute the current Ψ value using only the previous Ψ value and current field values.

The auxiliary Ψ functions need to be updated at each timestep, but we need to determine the correct order in which to update all fields. Observe that the Ψ_{hxy}^n data depends only on the electric field data at time $n\Delta t$, its previous value, and some constants. The dependence on Ψ of the magnetic field data $H_x^{n+\frac{1}{2}}$ is only at time $n\Delta t$ as well. So, at half-integer timestep updates associated with

magnetic field updates, the auxiliary $\Psi_{hxr}, \Psi_{hyr}, \Psi_{hzr}$ functions ($r \equiv x, y, z$ where appropriate) are updated immediately after the magnetic field data. At integer timestep updates associated with electric field updates, the auxiliary $\Psi_{exr}, \Psi_{eyr}, \Psi_{ezr}$ functions are updated immediately after the electric field data. These auxiliary fields are offset by a half-timestep relative to the fields they affect, just like the imposed current terms in the standard updating equations.

CPML Updating Equations

To reiterate, we are considering the discretization of:

$$\left(\frac{\partial_y E_z}{\kappa_y} - \zeta_y * \partial_y E_z - \frac{\partial_z E_y}{\kappa_z} + \zeta_z * \partial_z E_y\right) = -(\mu_x \partial_t + \sigma_x^m) H_x.$$

Discretized and with the auxiliary convolution terms applied:

$$\begin{aligned}
&\frac{1}{\kappa_y}\left(\frac{E_z^n(i,j+1,k) - E_z^n(i,j,k)}{\Delta y}\right) - \Psi_{hxy}^n(i,j,k) - \frac{1}{\kappa_z}\left(\frac{E_y^n(i,j,k+1) - E_y^n(i,j,k)}{\Delta z}\right) + \Psi_{hxz}^n(i,j,k) \\
&\quad = -\mu_x(i,j,k)\frac{H_x^{n+\frac{1}{2}}(i,j,k) - H_x^{n-\frac{1}{2}}(i,j,k)}{\Delta t} - \frac{\sigma_x \varepsilon_x(i,j,k)}{\mu_x(i,j,k)}\frac{H_x^{n+\frac{1}{2}}(i,j,k) + H_x^{n-\frac{1}{2}}(i,j,k)}{2}.
\end{aligned}$$

Now we solve for the future timestep $(n+\frac{1}{2})\Delta t$ for H_x to find an update equation:

$$\begin{aligned}
\left(\frac{\sigma_x^m}{2} + \frac{\mu_x(i,j,k)}{\Delta t}\right) H_x^{n+\frac{1}{2}}(i,j,k) &= -\frac{1}{\kappa_y}\left(\frac{E_z^n(i,j+1,k) - E_z^n(i,j,k)}{\Delta y}\right) + \\
&+ \frac{1}{\kappa_z}\left(\frac{E_y^n(i,j,k+1) - E_y^n(i,j,k)}{\Delta z}\right) + \mu_x(i,j,k)\frac{H_x^{n-\frac{1}{2}}(i,j,k)}{\Delta t} - \\
&- \frac{\sigma_x^m}{2} H_x^{n-\frac{1}{2}}(i,j,k) + \Psi_{hxy}^n(i,j,k) - \Psi_{hxz}^n(i,j,k) \\
H_x^{n+\frac{1}{2}}(i,j,k) &= \frac{1}{\kappa_y}\frac{-2\Delta t}{(2\mu_x(i,j,k) + \Delta t \sigma_x^m(i,j,k))\Delta y}(E_z^n(i,j+1,k) - E_z^n(i,j,k)) + \\
&+ \frac{1}{\kappa_z}\frac{2\Delta t}{(2\mu_x(i,j,k) + \Delta t \sigma_x^m(i,j,k))\Delta z}(E_y^n(i,j,k+1) - E_y^n(i,j,k)) + \\
&+ \frac{2\mu_x(i,j,k) - \Delta t \sigma_x^m(i,j,k)}{2\mu_x(i,j,k) + \Delta t \sigma_x^m(i,j,k)} H_x^{n-\frac{1}{2}}(i,j,k) + \\
&+ \frac{2\Delta t}{2\mu_x(i,j,k) + \Delta t \sigma_x^m(i,j,k)} \Psi_{hxy}^n(i,j,k) + \\
&+ \frac{-2\Delta t}{2\mu_x(i,j,k) + \Delta t \sigma_x^m(i,j,k)} \Psi_{hxz}^n(i,j,k).
\end{aligned}$$

So we have arrived at a simple method of updating H_x for the CPML region on the $\pm y$ boundaries subject to the complex coordinate stretching described above. Looking at this update equation, we find the standard updating coefficients up to a factor of $\frac{1}{\kappa_y}$, $\frac{1}{\kappa_z}$ on the E_y, E_z terms respectively. We also observe updating coefficients

$$C_{\Psi hxy} = \frac{2\Delta t}{2\mu_x(i,j,k) + \Delta t \sigma_x^m(i,j,k)}$$
$$C_{\Psi hxz} = \frac{-2\Delta t}{2\mu_x(i,j,k) + \Delta t \sigma_x^m(i,j,k)}$$

This derivation has so far accounted for any choice of CPML parameters subject to the matching condition. However, the standard parameter value choices cause us to drop one of the auxiliary fields - in the case of H_x at $\pm y$ boundaries, we will have no need to include the Ψ_{hxz} term. It is time to consider how to allocate the CPML parameters.

CPML parameter selection and distribution

Analogous to conductivities in the PML, standard usage of σ_p values is to set the CPML conductivity nonzero for the perpendicular component only. So in our H_x examination, for the $\pm y$ boundaries we set $\sigma_{pmz} = 0$. Also as with the PML, we grade parameters to increase smoothly between the inner domain-PML interface and the domain boundary. Following [7, 16], we grade the CPML parameters according to the following.

We select parameters n_{pml} as polynomial order and δ as the total thickness of the CPML layer; we will use ρ as the distance from the inner domain-CPML interface. For both σ_{pr}^e, σ_{pr}^m, we select σ_{factor} as the input parameter for CPML conductivity; then

$$\sigma_{max} = \sigma_{factor} \cdot \sigma_{opt}, \text{ where } \sigma_{opt} = \frac{n_{pml}+1}{150\pi\sqrt{\varepsilon_r}\Delta r},$$

for $r = x$, y, z to match the boundary under consideration. With σ_{max} calculated, we set the actual CPML conductivity values on a polynomial distribution, as a function of depth ρ.

$$\sigma_{pr}^e(\rho) = \sigma_{max}\left(\frac{\rho}{\delta}\right)^{n_{pml}}, \qquad \sigma_{pr}^m(\rho) = \frac{\mu_0}{\varepsilon_0}\sigma_{max}\left(\frac{\rho}{\delta}\right)^{n_{pml}},$$

which maintains the matching condition.

We choose κ_{max} as a parameter, and calculate the κ_r values as a function of depth. Recalling the matching condition between κ_r^e and κ_r^m is equality:

$$\kappa_r^e(\rho) = \kappa_r^m(\rho) = 1 + (\kappa_{max} - 1)\left(\frac{\rho}{\delta}\right)^{n_{pml}}.$$

We choose parameters α_{min} and α_{max}, and calculate the α_r^e and α_r^m values as functions of depth.

$$\alpha_r^e(\rho) = \alpha_{min} + (\alpha_{max} - \alpha_{min})\left(1 - \frac{\rho}{\delta}\right).$$

The matching condition for α is analogous to the CPML conductivity:

$$\alpha_r^m(\rho) = \frac{\mu_0}{\varepsilon_0}\left(\alpha_{min} + (\alpha_{max} - \alpha_{min})\left(1 - \frac{\rho}{\delta}\right)\right).$$

Updating CPML

So, updating the CPML layer in $\pm y$ regions becomes clear. The standard updating coefficients C_{Hxey}, C_{Hxez} are modified by multiplying by $\frac{1}{\kappa_y}$, $\frac{1}{\kappa_z}$ respectively. The H_x field is updated with the standard updating equation, leaving off the imposed current term as we do not expect sources in our absorbing layer. Then Ψ_{hxy} is calculated with the discrete convolution and $C_{\Psi hxy}(i,j,k) \cdot \Psi_{hxy}(i,j,k)$ term is added to $H_x(i,j,k)$.

The other CPML-region updating equations are derived and applied in a similar fashion. We note that the derived $C_{\Psi hxy} = C_{hxez} \cdot \Delta y$, and $C_{\Psi hxz} = C_{hxey} \cdot \Delta z$, and similar parallels hold for the other coefficients:

$$\begin{aligned}
C_{\Psi exy} &= C_{exhz} \cdot \Delta y, \qquad & C_{\Psi exz} &= C_{exhy} \cdot \Delta z,\\
C_{\Psi eyx} &= C_{eyhz} \cdot \Delta x, \qquad & C_{\Psi eyz} &= C_{eyhx} \cdot \Delta z,\\
C_{\Psi ezx} &= C_{ezhy} \cdot \Delta x, \qquad & C_{\Psi ezy} &= C_{ezhx} \cdot \Delta y,\\
C_{\Psi hyx} &= C_{hyez} \cdot \Delta x, \qquad & C_{\Psi hyz} &= C_{hyex} \cdot \Delta z,\\
C_{\Psi hzx} &= C_{hzey} \cdot \Delta x, \qquad & C_{\Psi hzy} &= C_{hzex} \cdot \Delta y.
\end{aligned}$$

We skip the derivation of the remaining Ψ formulas, but list them here. For $\vec{E}$ component Ψ functions, we will use definitions

$$a_{ex} = \frac{\sigma_{px}^e}{\Delta x(\sigma_{px}^e \kappa_x + \alpha_x^e \kappa_x^2)}[b_{ex} - 1],$$

$$
\begin{aligned}
a_{ey} &= \frac{\sigma^e_{py}}{\Delta y(\sigma^e_{py}\kappa_y + \alpha^e_y\kappa_y^2)}[b_{ey} - 1], \\
a_{ez} &= \frac{\sigma^e_{pz}}{\Delta z(\sigma^e_{pz}\kappa_z + \alpha^e_z\kappa_z^2)}[b_{ez} - 1], \\
b_{ex} &= \exp\left[-\left(\frac{\sigma^e_{px}}{\kappa_x} + \alpha^e_x\right)\frac{\Delta t}{\varepsilon_0}\right], \\
b_{ey} &= \exp\left[-\left(\frac{\sigma^e_{py}}{\kappa_y} + \alpha^e_y\right)\frac{\Delta t}{\varepsilon_0}\right], \\
b_{ez} &= \exp\left[-\left(\frac{\sigma^e_{pz}}{\kappa_z} + \alpha^e_z\right)\frac{\Delta t}{\varepsilon_0}\right].
\end{aligned}
$$

For E_x component Ψ functions,

$$
\begin{aligned}
\Psi^{n+\frac{1}{2}}_{exy}(i,j,k) &= b_{ey}\Psi^{n-\frac{1}{2}}_{exy}(i,j,k) + a_{ey}(H_z^{n+\frac{1}{2}}(i,j,k) - H_z^{n+\frac{1}{2}}(i,j-1,k)), \\
\Psi^{n+\frac{1}{2}}_{exz}(i,j,k) &= b_{ez}\Psi^{n-\frac{1}{2}}_{exz}(i,j,k) + a_{ez}(H_y^{n+\frac{1}{2}}(i,j,k) - H_y^{n+\frac{1}{2}}(i,j,k-1)).
\end{aligned}
$$

For E_y component Ψ functions,

$$
\begin{aligned}
\Psi^{n+\frac{1}{2}}_{eyz}(i,j,k) &= b_{ez}\Psi^{n-\frac{1}{2}}_{eyz}(i,j,k) + a_{ez}(H_x^{n+\frac{1}{2}}(i,j,k) - H_x^{n+\frac{1}{2}}(i,j,k-1)), \\
\Psi^{n+\frac{1}{2}}_{eyx}(i,j,k) &= b_{ex}\Psi^{n-\frac{1}{2}}_{eyz}(i,j,k) + a_{ex}(H_z^{n+\frac{1}{2}}(i,j,k) - H_z^{n+\frac{1}{2}}(i-1,j,k)).
\end{aligned}
$$

For E_z component Ψ functions,

$$
\begin{aligned}
\Psi^{n+\frac{1}{2}}_{ezx}(i,j,k) &= b_{ex}\Psi^{n-\frac{1}{2}}_{ezx}(i,j,k) + a_{ex}(H_z^{n+\frac{1}{2}}(i,j,k) - H_z^{n+\frac{1}{2}}(i-1,j,k)), \\
\Psi^{n+\frac{1}{2}}_{ezy}(i,j,k) &= b_{ey}\Psi^{n-\frac{1}{2}}_{ezy}(i,j,k) + a_{ey}(H_x^{n+\frac{1}{2}}(i,j,k) - H_x^{n+\frac{1}{2}}(i,j-1,k)).
\end{aligned}
$$

For $\vec{H}$ component Ψ functions, we will use definitions

$$
\begin{aligned}
a_{mx} &= \frac{\sigma^m_{px}}{\Delta x(\sigma^m_{px}\kappa_x + \alpha^m_x\kappa_x^2)}[b_{mx} - 1], \\
a_{my} &= \frac{\sigma^m_{py}}{\Delta y(\sigma^m_{py}\kappa_y + \alpha^m_y\kappa_y^2)}[b_{my} - 1], \\
a_{ez} &= \frac{\sigma^m_{pz}}{\Delta z(\sigma^m_{pz}\kappa_z + \alpha^m_z\kappa_z^2)}[b_{mz} - 1], \\
b_{mx} &= \exp\left[-\left(\frac{\sigma^m_{px}}{\kappa_x} + \alpha^m_x\right)\frac{\Delta t}{\mu_0}\right], \\
b_{my} &= \exp\left[-\left(\frac{\sigma^m_{py}}{\kappa_y} + \alpha^m_y\right)\frac{\Delta t}{\mu_0}\right],
\end{aligned}
$$

$$b_{mz} = \exp\left[-\left(\frac{\sigma_{pz}^m}{\kappa_z} + \alpha_z^m\right)\frac{\Delta t}{\mu_0}\right].$$

We covered the H_x component Ψ functions. For H_y component Ψ functions,

$$\Psi_{hxy}^n(i,j,k) = b_{my}\Psi_{hxy}^{n-1}(i,j,k) + a_{my}(E_z^n(i,j+1,k) - E_z^n(i,j,k)),$$
$$\Psi_{hxz}^n(i,j,k) = b_{mz}\Psi_{hxz}^{n-1}(i,j,k) + a_{mz}(E_y^n(i,j,k+1) - E_y^n(i,j,k)).$$

For H_y component Ψ functions,

$$\Psi_{hyz}^n(i,j,k) = b_{mz}\Psi_{hyz}^{n-1}(i,j,k) + a_{mz}(E_x^n(i,j,k+1) - E_x^n(i,j,k)),$$
$$\Psi_{hyx}^n(i,j,k) = b_{mx}\Psi_{hyx}^{n-1}(i,j,k) + a_{mx}(E_z^n(i+1,j,k) - E_z^n(i,j,k)).$$

Stripline with CPML

Now recall the simulations from Chapter 4, the stripline and the low-pass filter element. The low-pass filter results were already shown with a CPML boundary applied. The parameters used are as follows, and in fact these are the same parameter values as will be used in all other simulations, as they are functionally quite adequate. The chosen CPML layer is eight cells thick, with a third-order polynomial scaling. Parameter values are $\sigma_{max} = 1.3$, $\kappa_{max} = 7$, $\alpha_{min} = 0$, $\alpha_{max} = 0.05$.

Finding the characteristic impedance for the stripline example was hindered by reflection from the terminating load, a set of resistor lumped elements. However, we can apply CPML layers to greatly improve the results. The resistor elements can be removed entirely. The $\pm x$ and $\pm y$ boundaries are set to the above standard CPML properties. The stripline's trace layer and dielectric material both pass through the CPML layer and make contact with the Dirichlet boundary, so there is no material discontinuity. The $\pm z$ boundaries are PEC and serve as ground plates.

The CPML layer on the $\pm x$ boundaries absorb the pulse traveling along the trace quite effectively; the same simulation now produces Z_0 values within about 2% of the predicted value for frequencies from 0 to 15 GHz, using the direct definition of Z_0 for calculation. The calculation of Z_0 using S-parameters produces a comparable accuracy, within about 3% of the expected value for the same frequency range of 0 to 15 GHz. We observe two shortcomings of this simulation: the calculated Z_0 departs sharply from the expected value beyond 15 GHz, reaching about 5% error at

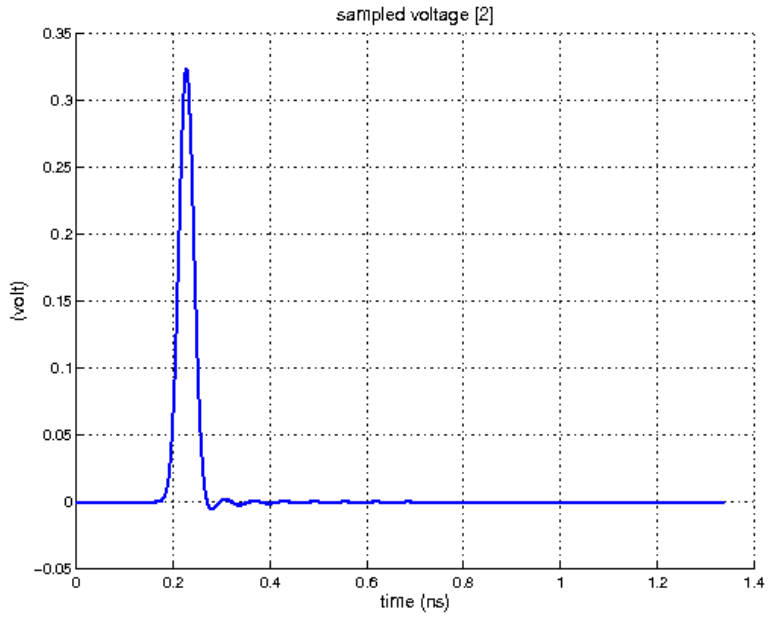

Figure 5.1: CPML-terminated stripline sampled voltage 20mm from source, time domain

20 GHz. This occurs with both methods of calculating Z_0, and it is known through test simulations that this is not an artifact of either the frequency distribution of the driving pulse, nor the 10 cell per wavelength limit. The error is possibly a result of the high frequency elements introduced at the driving voltage source edge discontinuity.

The second issue is that we wish to ensure we are obtaining reliable data for the 10 MHz - 1 GHz frequency spread. By [24], it is common to ensure that the simulation's final time allows at least one full cycle at each frequency of interest; in this case, that entails running the simulation up to a simulated 10 ns, about requiring 37500 timesteps. However, in attempting this, an oscillation artifact becomes evident in simulation. It is unclear what causes this abberation. Experimentation demonstrated that the effect is mitigated in an asymmetrical stripline with a relatively thin trace. The long-simulation time results shown below reflect the artifact described. They are not expected to be truly representative of the ideal stripline.

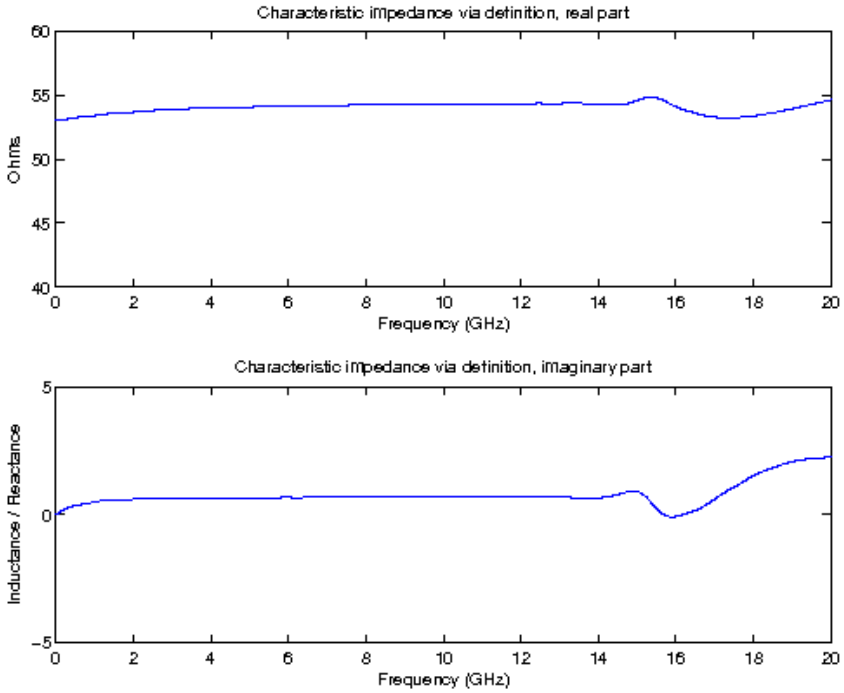

Figure 5.2: CPML-terminated characteristic impedance real and imaginary parts as calculated from definition

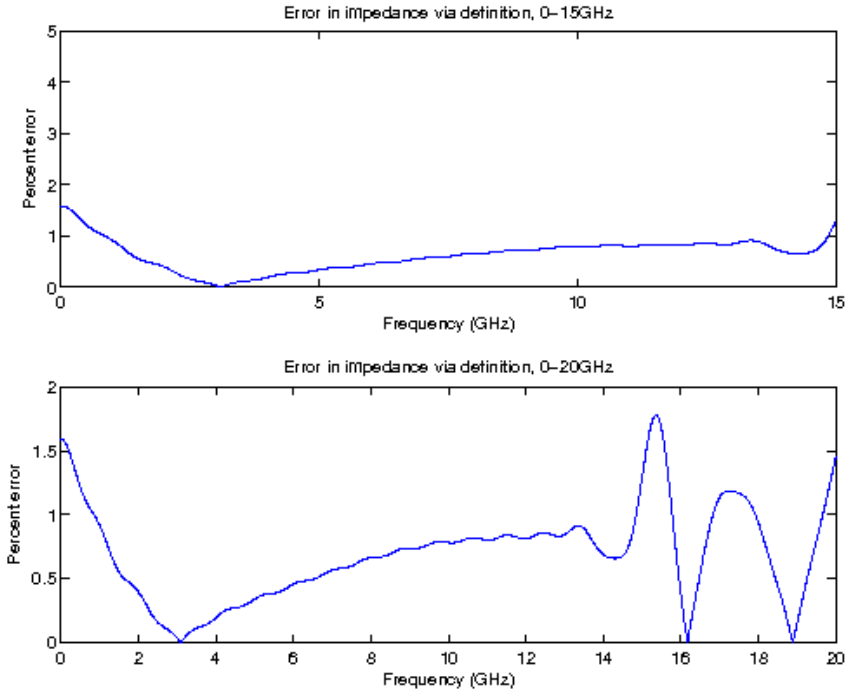

Figure 5.3: Error in CPML-terminated characteristic impedance real and imaginary parts as calculated from definition

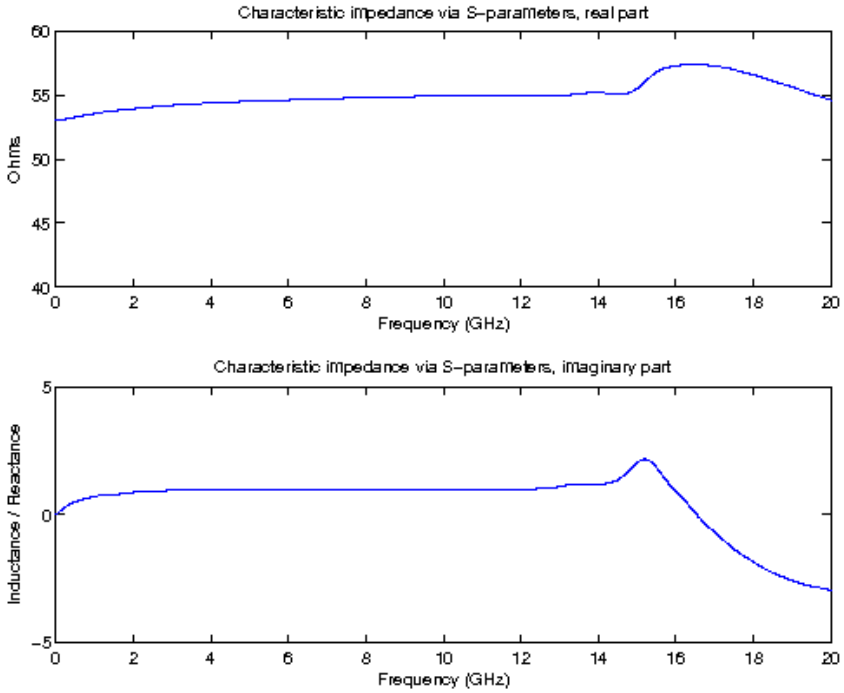

Figure 5.4: CPML-terminated characteristic impedance real and imaginary parts as calculated from S-parameters

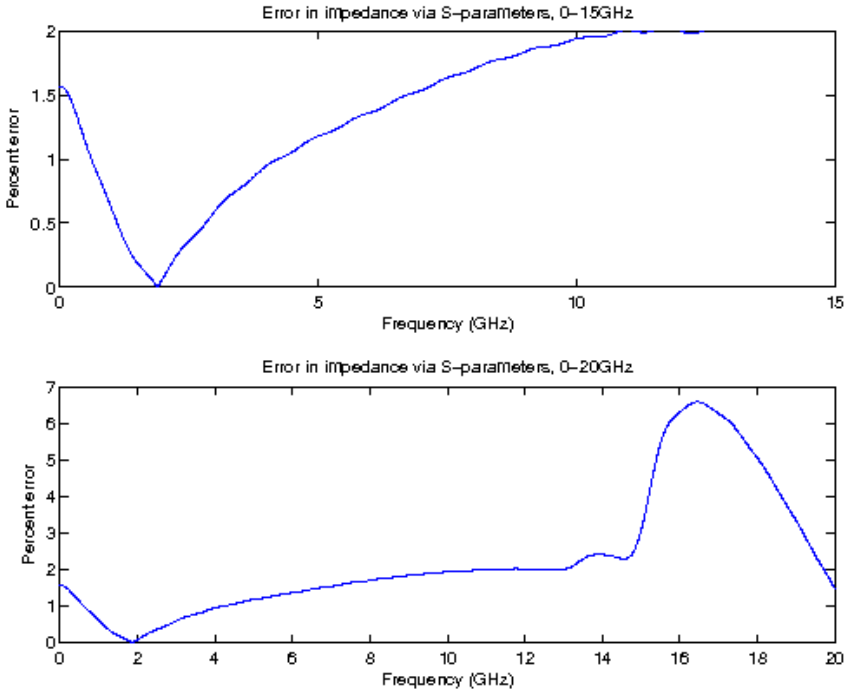

Figure 5.5: Error in CPML-terminated characteristic impedance real and imaginary parts as calculated from S-parameters

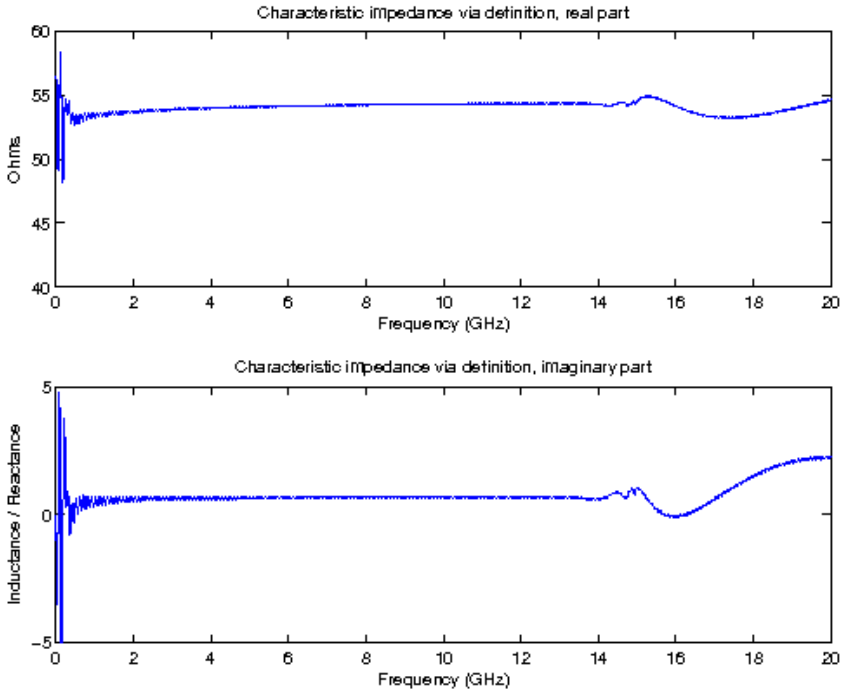

Figure 5.6: CPML-terminated characteristic impedance, long-duration simulation, real and imaginary parts as calculated from definition

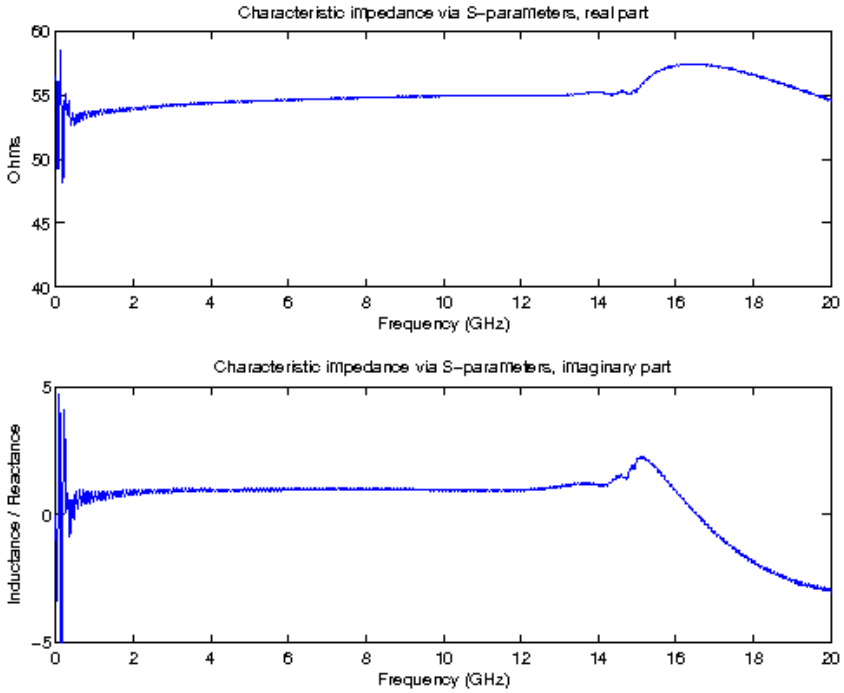

Figure 5.7: CPML-terminated characteristic impedance, long-duration simulation, real and imaginary parts as calculated from S-parameters

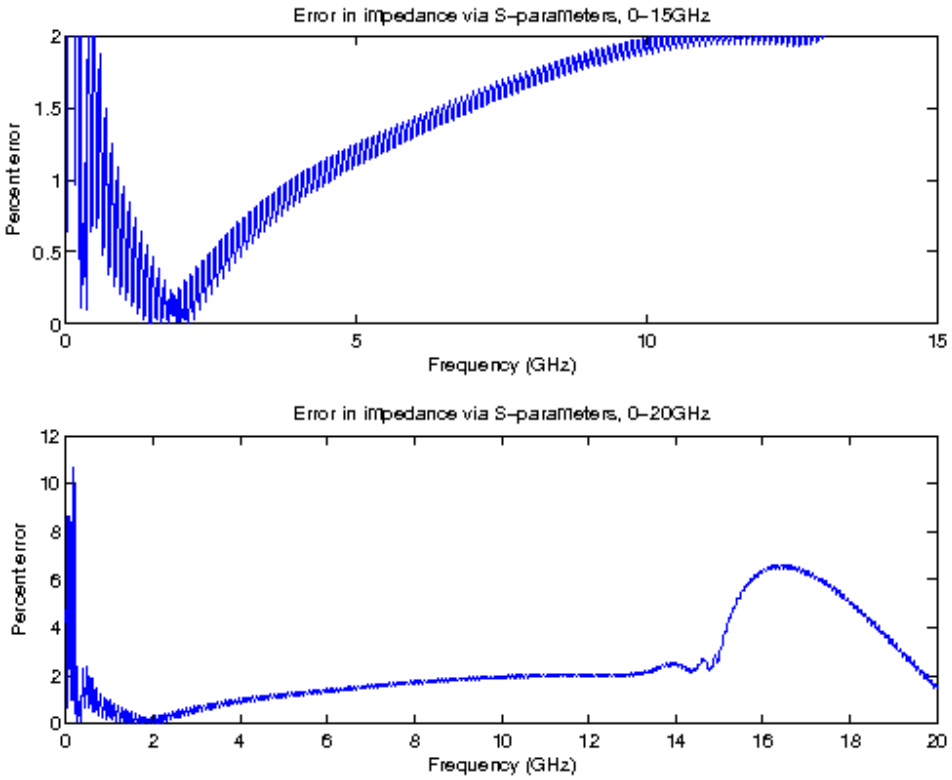

Figure 5.8: CPML-terminated characteristic impedance, long-duration simulation, error as calculated from S-parameters

CHAPTER 6

THE FAR-FIELD TRANSFORM

Now we turn our attention to scattering problems. A typical scattering problem has some object or collection of objects on which the domain is centered, and vacuum surrounding these objects out to the domain boundaries. Some form of source creates an incident field or excitation; obtaining the resultant scattered field associated with the simulated material configuration is the true goal of this simulation. This chapter is focused on the far-field transformation which yields information about the scattering properties of the simulated objects at large distances. We follow the development in [7].

There are two categories of data which can be obtained with the technique shown below. If we calculate equivalent currents in the time domain, we can obtain the broadband far-field data, only at chosen angles of observation. If we calculate equivalent currents in the frequency domain, we can obtain far-field data at all observation angles but only for chosen frequencies. This section focuses on the latter choice. For the developments below, set f_c in Hz to be a given frequency of interest; it is a feature of the scheme that all needed calculations can be repeated for multiple discrete frequencies in the same simulation. Let $\vec{k}$ correspond to the wave vector of a plane wave of frequency f_c traveling in freespace, using the angular wavenumber convention such that $|\vec{k}| = 2\pi f_c \sqrt{\mu_0 \varepsilon_0}$.

Commonly in scattering problems we assume that the region outside the domain is homogeneous, whether vacuum or a simple dielectric material. The governing assumption in this far-field transformation development is that the domain is surrounded by air on all sides.

6.0.4 Equivalent Surface Currents: Derivation

We consider far-field for the purposes of this transform, and require that an observation point be many wavelengths distant from the domain. Labeling that distance from the simulation center as R, we require

$$|\vec{k}|R = \frac{2\pi}{\lambda}R \gg 1.$$

Further we assume that there are no external sources. The fundamental idea on which the procedure rests is the surface equivalence theorem, first proposed by Schelkunoff in 1936 [17]. We introduce a

fictional surface, typically near simulation domain boundaries, and measure fields on this surface. These field measurements are converted uniquely into fictional electromagnetic currents on the surface from which the far field values are calculated. These currents define an equivalent problem wherein the fields inside the fictional surface are everywhere zero, and the fields outside the surface are identical to the original problem.

With $\vec{n}$ as the normal to the fictional surface, we apply the standard tangential boundary condition $\vec{n} \times \left[\vec{H}_{out} - \vec{H}_{in}\right] = \vec{J}_s$ where $\vec{J}_s$ is the fictional surface current density, and note that $\vec{H}_{in} = 0$ by our assumption of no external sources. Allow $\vec{H}_{out}$ to be represented by the field on the fictional boundary, $\vec{H}_{out} = \vec{H}$. Then our fictional surface electric current must be

$$\vec{J}_s = \vec{n} \times \vec{H},$$

The electric current boundary is usually shown without the presence of the fictional magnetic charges we include in simulation. The usual idea is to consider $\oint_C \vec{E} \cdot \vec{dl}$ with C a rectangle passing through the fictional surface and shrinking toward zero width normal to the surface. Allowing fictional magnetic charges, this integral equals $-\int_S \vec{M} \cdot \vec{ds} - \int_S \frac{\partial \vec{H}}{\partial t} \cdot \vec{ds}$. Following a similar derivation as the above, we obtain a similar expression for the fictional magnetic current:

$$\vec{M}_s = -\vec{n} \times \vec{E}$$

Now, in computation, the equivalence theorem technique is implemented directly, in the sense that the fictional currents are calculated on the grid for a specific fictional surface enclosing all sources and objects. Regarding the choice of that fictional surface, the derivation in [17] can be freely applied to non-smooth surfaces. So, we choose a cuboid following grid planes near the domain boundaries; care must be taken to choose the surface so that it does not intersect a CPML layer, if that is the choice of ABC implemented in the simulation. Given that choice, the fictional surface currents are calculated by a separate formula for each face of the cuboid. For example, on the $+z$ face with unit normal $\hat{k}$,

$$\vec{J}_s = \vec{k} \times (H_x\vec{i} + H_y\vec{j} + H_z\vec{k}) = -H_y\vec{i} + H_x\vec{j}.$$

Equating components,

$$J_{s,x} = -H_y \qquad \text{and} \qquad J_{s,y} = H_x \qquad \text{and} \qquad J_{s,z} = 0.$$

Similarly

$$\vec{M}_s = -\vec{k} \times (E_x\vec{i} + E_y\vec{j} + E_z\vec{k}) = E_y\vec{i} - E_x\vec{j},$$

leading to

$$M_{s,x} = E_y \qquad \text{and} \qquad M_{s,y} = E_x \qquad \text{and} \qquad M_{s,z} = 0$$

on the top face of the cuboid.

A repetition of these ideas applied to the other five faces yield the following equivalent surface currents. (For notational ease, in the following current terms, we omit the "S" subscript designation, so $\vec{J}_x \equiv J_{s,x}$ and so on.) On the bottom $(-z)$ face,

$$J_x = H_y,\ J_y = -H_x,\ J_z = 0,\ M_x = -E_y,\ M_y = E_x,\ M_z = 0.$$

Noting that these opposing surfaces identify the same field components with swapped signs, and that this holds for other face pairs, allow the grouping of face pairs such as $\pm z$ and the usual sign convention implied by the $\pm$ and $\mp$ symbols:

$$\text{face } \pm x \quad \Rightarrow \quad J_x = 0,\ J_y = \mp H_z,\ J_z = \pm H_y,\ M_x = 0,\ M_y = \pm E_z,\ M_z = \mp E_y,$$

$$\text{face } \pm y \quad \Rightarrow \quad J_x = \pm H_z,\ J_y = 0, J_z = \mp H_x,\ M_x = \mp E_z,\ M_y = 0,\ M_z = \pm E_x.$$

We note that the field equations which recover far field values are defined to depend on surface currents J and M located in the same position. So when considering discretization of these equivalent equations on the staggered grid, we will have to resort to spatial averaging of magnetic field components, in order to obtain collocated J and M values.

6.0.5 Transformation to Frequency Domain

As mentioned, we need the equivalent surface currents in the frequency domain to proceed. Recalling that on the top face of the imaginary surface $J_y = H_x$, recalling the selected frequency f_c (in Hz), we can write the transform

$$\mathcal{F}\{J_y(i,j,k;f_c)\} = J_y^*(i,j,k;f_c) = \int_{t=-\infty}^{\infty} H_x(i,j,k)\exp\left(-\mathrm{i}2\pi f_c t\right)$$

$$\approx \sum_{n=1}^{N} H_x(i,j,k) \exp\left(-\mathrm{i}2\pi f_c n \Delta t\right) \Delta t,$$

where N is the total time steps used in the simulation. Data from all time steps are needed, however we do not want to store the complete field history. So, this calculation progresses during the simulation, but is completed and usable only after the simulation is complete.

6.0.6 Potential definitions and far field equations

As noted in [7], the far field computation is based on vector potentials. We will use these labels for the remainder of the section, though we should note that the source and observation points p and q are not fixed but tailored to specific calculations. Fix the central node point of the computational domain as the center or 'origin' for this calculation, and call it p'. Also choose a point p lying on the surface S; due to spatial placement of field components, in this implementation we always choose p to lie in the center of a grid cell face which itself lies on S. As well, choose a point q for observation of far fields. Let $\vec{r}'$ point from the center p' to the source point p, let $\vec{R}$ point from the source point p to observation point q, and let r point from center p' to observation point q. Then let ψ be the angle between r and r', and let θ and ϕ be the usual angle measures in spherical coordinates locating q.

Now with the assumptions going in to our far-field approximation, the fields at observation points q are transverse only. The method used here formulates the far fields in spherical coordinates with linear polarization, so we can express the preceding condition as $E_r = H_r = 0$. The transverse components of the spherically radiating fields decay as $1/r$ and can be rewritten in terms of the vector potentials above. The auxiliary vector functions $\vec{N}$ and $\vec{L}$ will be expressed component-wise, with spherical components. Using the impedance of free space $\eta_0 = \left|\vec{E}\right| / \left|\vec{H}\right|$ and the functions

$$N_\theta = \int_S (J_x^* \cos\theta\cos\phi + J_y^* \cos\theta \sin\phi - J_z^* \sin\theta) \exp(-\mathrm{i}|\vec{k}|r' \cos\psi)\, dS,$$

$$N_\phi = \int_S (-J_x^* \sin\phi + J_y^* \cos\phi) \exp(-\mathrm{i}|\vec{k}|r' \cos\psi)\, dS,$$

$$L_\theta = \int_S (M_x^* \cos\theta\cos\phi + M_y^* \cos\theta \sin\phi - M_z^* \sin\theta) \exp(-\mathrm{i}|\vec{k}|r' \cos\psi)\, dS,$$

$$L_\phi = \int_S (-M_x^* \sin\phi + M_y^* \cos\phi) \exp(-\mathrm{i}|\vec{k}|r' \cos\psi)\, dS,$$

we have

$$E_\theta = \left[\frac{\exp(-\mathrm{i}|\vec{k}|r)}{4\pi r}\right] \cdot -\mathrm{i}|\vec{k}| \left[L_\phi + \eta_0 N_\theta\right],$$

$$E_\phi = \left[\frac{\exp(-\mathrm{i}|\vec{k}|r)}{4\pi r}\right] \cdot \mathrm{i}|\vec{k}| \left[L_\theta - \eta_0 N_\phi\right].$$

We can obtain the corresponding magnetic fields directly from these definitions by applying the equivalence

$$\vec{H} = \hat{r} \times \frac{\vec{E}}{\eta_0},$$

which simply expresses that the H field is rotated $\pi/2$ rad from the E field. Hence $\eta_0 H_\theta$ is the negative of E_ϕ, and $\eta_0 H_\phi = E_\theta$:

$$H_\theta = \left[\frac{\exp(-\mathrm{i}|\vec{k}|r)}{4\pi r}\right] \cdot \mathrm{i}|\vec{k}| \left[N_\phi - \frac{L_\theta}{\eta_0}\right],$$

$$H_\phi = \left[\frac{\exp(-\mathrm{i}|\vec{k}|r)}{4\pi r}\right] \cdot -\mathrm{i}|\vec{k}| \left[N_\theta + \frac{L_\phi}{\eta_0}\right].$$

The consideration of determining these equivalent currents in simulation is delayed until a later section.

Circularly polarized components and radiation efficiency

The preceding field components are linearly polarized, however as noted in [7] we can obtain the circularly polarized basis elements by using the identities

$$\hat{\theta} = \frac{\hat{\theta} - \mathrm{i}\hat{\phi}}{2} + \frac{\hat{\theta} + \mathrm{i}\hat{\phi}}{2} = \frac{\hat{E}_R}{\sqrt{2}} + \frac{\hat{E}_L}{\sqrt{2}},$$

$$\hat{\phi} = \frac{\hat{\theta} + \mathrm{i}\hat{\phi}}{2\mathrm{i}} - \frac{\hat{\theta} - \mathrm{i}\hat{\phi}}{2\mathrm{i}} = \frac{\hat{E}_L}{\mathrm{i}\sqrt{2}} - \frac{\hat{E}_R}{\mathrm{i}\sqrt{2}}.$$

where the right-hand circularly polarized electric field basis function is called $\hat{E}_R$, the left-hand circularly polarized electric field basis function is $\hat{E}_L$, and the corresponding circularly polarized magnetic fields can be found from the electric fields if needed. Then, rewriting the linearly polarized

basis functions:

$$\hat{\theta}E_\theta + \hat{\phi}E_\phi = \left(\frac{\hat{E}_R}{\sqrt{2}} + \frac{\hat{E}_L}{\sqrt{2}}\right) E_\theta + \left(\frac{\hat{E}_L}{\mathrm{i}\sqrt{2}} - \frac{\hat{E}_R}{\mathrm{i}\sqrt{2}}\right) E_\phi.$$

Collect in terms of circularly polarized basis functions. Then, using the same equivalences for the field components solved for E_R and E_L, we find

$$= \hat{E}_R \left(\frac{E_\theta}{\sqrt{2}} - \frac{E_\phi}{J\sqrt{2}}\right) \hat{E}_L \left(\frac{E_\theta}{\sqrt{2}} + \frac{E_\phi}{J\sqrt{2}}\right) = E_R\hat{E}_R + E_L\hat{E}_L.$$

This allows us to equate component-wise and find

$$E_R = \frac{E_\theta}{\sqrt{2}} - \frac{E_\phi}{\mathrm{i}\sqrt{2}},$$
$$E_L = \frac{E_\theta}{\sqrt{2}} + \frac{E_\phi}{\mathrm{i}\sqrt{2}}.$$

One important measure of the circularly polarized far fields is the axial ratio AR, which can help determine the quality of reception for receiving antennas of various polarizations. By [7] we can determine this measure as

$$AR = -\frac{|E_R| + |E_L|}{|E_R| - |E_L|}.$$

One issue we find with this definition is that each of its field-magnitude terms is dependent on an arbitrarily chosen observation distance, although the final result is not. We can reformulate this definition in terms of the functions N_θ, N_ϕ, L_θ, L_ϕ in order to avoid this dependence in practice.

Axial ratio calculation

Circularly-polarized antennas are sometimes of interest in cases where antenna orientation may vary, or where certain forms of noise and signal degradation must be overcome. Investigating the quality of a circularly-polarized antenna signal in simulation is of interest. For a signal with a given polarization ellipse, the axial ratio (AR) is the ratio of the lengths of the major and minor axes of the ellipse. AR ranges from $-\infty$ to $+\infty$. A perfectly right-hand circular polarized signal has AR = -1, a perfectly left-hand circular polarized signal has AR = +1. So, AR is a measure of quality for a signal which is designed and expected to be circular polarized.

The need for choosing an observation distance can be avoided when computing axial ratio. Combining definitions of $E_R, E_L, E_\theta, E_\phi$ in [7] and collecting certain terms,

$$E_R = \frac{k\exp(-\mathrm{i}kr)}{4\sqrt{2}\pi r}\left[-\mathrm{i}(L_\phi + \eta_0 N_\theta) - (L_\theta - \eta_0 N_\phi)\right],$$
$$E_L = \frac{k\exp(-\mathrm{i}kr)}{4\sqrt{2}\pi r}\left[-\mathrm{i}(L_\phi + \eta_0 N_\theta) + (L_\theta - \eta_0 N_\phi)\right].$$

Applying complex modulus,

$$\begin{aligned}|E_R| &= \left|\frac{k\exp(-\mathrm{i}kr)}{4\sqrt{2}\pi r}\right| \left|-\mathrm{i}(L_\phi + \eta_0 N_\theta) - (L_\theta - \eta_0 N_\phi)\right| \\ &= \left|\frac{k}{4\sqrt{2}\pi r}\right| \cdot \left|\exp(-\mathrm{i}kr)\right| \cdot \left|-\mathrm{i}(L_\phi + \eta_0 N_\theta) - (L_\theta - \eta_0 N_\phi)\right| \\ &= \frac{k}{4\sqrt{2}\pi r} \cdot 1 \cdot \left|-\mathrm{i}(L_\phi + \eta_0 N_\theta) - (L_\theta - \eta_0 N_\phi)\right|.\end{aligned}$$

Similarly,

$$|E_L| = \frac{k}{4\sqrt{2}\pi r} \cdot 1 \cdot \left|-\mathrm{i}(L_\phi + \eta_0 N_\theta) - (L_\theta - \eta_0 N_\phi)\right|.$$

Hence the definition

$$AR = -\frac{|E_R| + |E_L|}{|E_R| - |E_L|}$$

becomes

$$AR = -\frac{\frac{k}{4\sqrt{2}\pi r}\left|-\mathrm{i}(L_\phi + \eta_0 N_\theta) - (L_\theta - \eta_0 N_\phi)\right| + \frac{k}{4\sqrt{2}\pi r}\left|-\mathrm{i}(L_\phi + \eta_0 N_\theta) - (L_\theta - \eta_0 N_\phi)\right|}{\frac{k}{4\sqrt{2}\pi r}\left|-\mathrm{i}(L_\phi + \eta_0 N_\theta) - (L_\theta - \eta_0 N_\phi)\right| - \frac{k}{4\sqrt{2}\pi r}\left|-\mathrm{i}(L_\phi + \eta_0 N_\theta) - (L_\theta - \eta_0 N_\phi)\right|}.$$

Canceling common factor,

$$AR = -\frac{\left|-\mathrm{i}(L_\phi + \eta_0 N_\theta) - (L_\theta - \eta_0 N_\phi)\right| + \left|-\mathrm{i}(L_\phi + \eta_0 N_\theta) - (L_\theta - \eta_0 N_\phi)\right|}{\left|-\mathrm{i}(L_\phi + \eta_0 N_\theta) - (L_\theta - \eta_0 N_\phi)\right| - \left|-\mathrm{i}(L_\phi + \eta_0 N_\theta) - (L_\theta - \eta_0 N_\phi)\right|},$$

and we have arrived at a way of computing AR which does not depend on a chosen distance.

Radiation Efficiency

Another important measure is the radiation efficiency, which is defined as

$$\eta_a = \frac{P_{\text{rad}}}{P_{\text{del}}},$$

where P_{rad} is the total radiated power and P_{del} is the total power delivered to the antenna. Note that P_{rad} can be measured using the equivalent surface current data on S, and P_{del} can be found using measures of the voltage and current supplied to the antenna.

By [7], the total power radiated across the surface S can be found from the equivalent currents as

$$\frac{1}{2}\text{Re} \int_S \overline{\vec{J}^*} \times \vec{M}^* \cdot \hat{n}\, dS,$$

where $\hat{n}$ is the unit normal to the surface S. To discretize this integral, we have to consider the discretization of surface S, according to our grid choice.

6.1 Discretization and Updating

We now consider the determination of equivalent surface currents from simulation components. We allow the discretization of S to correspond to the domain discretization.

6.1.1 Discretization of the equivalent surface

Let the cuboid S have minimal and maximal corner node indexes $S_{Lx}, S_{Ly}, S_{Lz}, S_{Ux}, S_{Uy}, S_{Uz}$. That is, the $(-x)$-face corner nodes are at indexes (S_{Lx}, S_{Ly}, S_{Lz}), (S_{Lx}, S_{Uy}, S_{Lz}), (S_{Lx}, S_{Uy}, S_{Uz}), (S_{Lx}, S_{Ly}, S_{Uz}).

The $+x$-face corner nodes are at points (S_{Ux}, S_{Ly}, S_{Lz}), (S_{Ux}, S_{Uy}, S_{Lz}), (S_{Ux}, S_{Uy}, S_{Uz}), (S_{Ux}, S_{Ly}, S_{Uz}). Two diagonally opposed $-y$ face corners are $(S_{Lx}, S_{Ly}, S_{Lz}), (S_{Ux}, S_{Ly}, S_{Uz})$; and so on for the other faces. The $\pm x$-faces are divided into individual rectangles of area $dy \cdot dz$ which conform to the domain grid; the $\pm y$-faces are composed of rectangles of area $dx \cdot dz$; and the $\pm z$-faces are composed of rectangles of area $dx \cdot dy$. Note that this implies that the field component $H(S_{Lx}, S_{Ly}, S_{Lz})$ lies on the $(-x)$-face of S while $H(S_{Ux}, S_{Ly}, S_{Uz})$ lies just outside of it. Next we will consider the equivalent surface currents. We will locate these current components on the

centers of S face grids. This implies that for the $\pm x$ faces, there will be $(S_{Uy} - S_{Ly}) \cdot (S_{Uz} - S_{Lz})$ each of $y-$ and $z-$components for each of J and M. Similarly, for the $\pm y$ faces, each of $x-$ and $z-$ components for each of J and M total $(S_{Ux} - S_{Lx}) \cdot (S_{Uz} - S_{Lz})$; and for the $\pm z$ faces, these totals will be $(S_{Ux} - S_{Lx}) \cdot (S_{Uy} - S_{Ly})$.

6.1.2 Equivalent surface current calculation

Using these labels for the discretization of S, consider the determination of the equivalent surface currents $\vec{J}_S$, $\vec{M}_S$. On the $-x$-face, for example, we found that $M_y = -E_z$ and $M_z = E_y$. We locate the current components on the center of S face grids; each of these points is located between four neighboring nodes.

Equivalent magnetic currents

Recall that all discretized $\vec{E}$ components are located on edges in between nodes. So to obtain a value for $E_z = -M_y$ at a face center - say, correspnding to (S_{Lx}, S_{Ly}, S_{Lz}) - we take the average of the discretized E_z components at (S_{Lx}, S_{Ly}, S_{Lz}) and $(S_{Lx}, S_{Ly}, S_{Lz} + 1)$. More generally, choose a point on the $-x$ equivalent surface, which gives it indexes (S_{Lx}, j^*, k^*) such that $S_{Ly} \leq j^* < S_{Uy}$, and $S_{Lz} \leq k^* < S_{Uz}$. The corresponding discretized equation $M_y = -E_z$ is written as:

$$M_y(S_{Lx}, j^*, k^*) = -\frac{1}{2} \left(E_z(S_{Lx}, j^*, k^*) + E_z(S_{Lx}, j^* + 1, k^*) \right).$$

Similarly, discretizing $M_z = E_y$, the M_z components lie between discrete components $E_y(S_{Lx}, j^*, k^*)$ and $E_y(S_{Lx}, j^* + 1, k^*)$, such that we take

$$M_z(S_{Lx}, j^*, k^*) = \frac{1}{2} \left(E_y(S_{Lx}, j^*, k^*) + E_y(S_{Lx}, j^*, k^* + 1) \right).$$

The $+x$-face equivalent surface values for M_y, M_z are obtained with the same averaging, up to opposite signs and the x-index being S_{Ux}:

$$M_y(S_{Ux}, j^*, k^*) = \frac{1}{2} \left(E_z(S_{Ux}, j^*, k^*) + E_z(S_{Ux}, j^* + 1, k^*) \right),$$
$$M_z(S_{Ux}, j^*, k^*) = -\frac{1}{2} \left(E_y(S_{Ux}, j^*, k^*) + E_y(S_{Ux}, j^*, k^* + 1) \right).$$

On account of the similarity, the other equivalent current discretizations will only be considered for the "negative" respective faces. Also, we drop the asterisk on variable indexes; it should be understood that these indexes run between the limits of the corresponding discretized equivalent surface.

$$
\begin{aligned}
M_x(i, S_{Ly}, k) &= \frac{1}{2}\left(E_z(i, S_{Ly}, k) + E_z(i+1, S_{Ly}, k)\right), \\
M_z(i, S_{Ly}, k) &= -\frac{1}{2}\left(E_x(i, S_{Ly}, k) + E_x(i, S_{Ly}, k+1)\right), \\
M_x(i, j, S_{Lk}) &= -\frac{1}{2}\left(E_y(i, j, S_{Lk}) + E_y(i+1, j, S_{Lk})\right), \\
M_y(i, j, S_{Lk}) &= \frac{1}{2}\left(E_x(i, j, S_{Lk}) + E_x(i, j+1, S_{Lk})\right).
\end{aligned}
$$

Equivalent electric currents

The situation for equivalent electric currents differs slightly. Continuing to consider the $-x$ face of S, the applicable equations are $J_y = H_z$ and $J_z = -H_y$. The $\vec{H}$ components are centered on the faces of grid cells, unfortunately not the same faces as needed here. So in fact we need to average the four equidistant, neighboring $\vec{H}$ component terms to correctly locate the $\vec{J}$ component term. For example, take the same cell face with indexes ($S_{Lx}, j^*,\, k^*$) as before. The component $J_y(j^*, k^*)$ is centered between four z-faces, each with an associated H_z term:

$$
\begin{aligned}
J_y(S_{Lx}, j^*,\, k^*) = \frac{1}{4}(&H_z(S_{Lx}-1, j^*, k^*) + \\
&H_z(S_{Lx}, j^*, k^*) + H_z(S_{Lx}-1, j^*, k^*+1) + H_z(S_{Lx}, j^*, k^*+1)).
\end{aligned}
$$

Similarly,

$$
\begin{aligned}
J_z(S_{Lx}, j^*,\, k^*) = -\frac{1}{4}(&H_y(S_{Lx}-1, j^*, k^*) + \\
&H_y(S_{Lx}, j^*, k^*) + H_y(S_{Lx}-1, j^*+1, k^*) + H_y(S_{Lx}, j^*+1, k^*)).
\end{aligned}
$$

As with the magnetic currents described above, the same average is applicable up to the x-index and the negative, and we drop the asterisks in favor of understood index limits:

$$
J_y(S_{Ux}, j, k) = -\frac{1}{4}\left(H_z(S_{Ux}-1, j, k) + H_z(S_{Ux}, j, k) + H_z(S_{Ux}-1, j, k+1) + H_z(S_{Ux}, j, k+1)\right),
$$

$$J_z(S_{Ux}, j, k) = \frac{1}{4}\left(H_y(S_{Ux}-1, j, k) + H_y(S_{Ux}, j, k) + H_y(S_{Ux}-1, j+1, k) + H_y(S_{Ux}, j+1, k)\right).$$

We consider the other two negative faces:

$$\begin{aligned}
J_x(i, S_{Ly}, k) &= -\frac{1}{4}(H_z(i, S_{Ly}, k) + H_z(i, S_{Ly}-1, k) + H_z(i, S_{Ly}, k+1) + H_z(i, S_{Ly}-1, k+1)),\\
J_z(i, S_{Ly}, k) &= \frac{1}{4}(H_x(i, S_{Ly}, k) + H_x(i, S_{Ly}-1, k) + H_x(i+1, S_{Ly}, k) + H_x(i+1, S_{Ly}-1, k)),\\
J_x(i, j, S_{Lk}) &= \frac{1}{4}(H_y(i, j, S_{Lk}) + H_y(i, j, S_{Lk}-1) + H_y(i, j+1, S_{Lk}) + H_y(i, j, S_{Lk}-1)),\\
J_y(i, j, S_{Lk}) &= -\frac{1}{4}(H_x(i, j, S_{Lk}) + H_x(i, j, S_{Lk}-1) + H_x(i+1, j, S_{Lk}) + H_x(i+1, j, S_{Lk}-1)).
\end{aligned}$$

Recall that the above calculations yield time-domain equivalent currents; the auxiliary functions and potentials are defined in terms of the frequency-domain equivalent currents. So the discrete Fourier transform must be applied to the results.

6.1.3 Auxiliary function discretization

Now we consider the N and L functions. We describe some approximations to distances which assist our computation. Recall that $\vec{r}'$ is the vector between fixed domain center p' and a chosen source point p lying on surface S. Also recall that $\vec{r}$ is the vector between source point p and observation point q. Observing that $r'\cos\psi$ occurs in N and L functions, we can find a unit vector $\hat{r}$ in the direction of $\vec{r}$ and simply take $\vec{r}' \cdot \hat{r} = r'\cos\psi$.

As θ and ϕ locate the direction of q, we can write $\hat{r} = \sin\theta\cos\phi\hat{x} + \sin\theta\sin\phi\hat{y} + \cos\theta\hat{z}$. Suppose the center p' has node indexes (C_x, C_y, C_z), and suppose that p is centered on the cell face associated with indexes (p_x, p_y, p_z). At this point, we must declare which face of S we have chosen p to be on. Supposing p is on the $(-x)$-face of S, for example, we find $\vec{r}' = \Delta x(C_x - S_{Lx})\hat{x} + \Delta y(p_y + 0.5 - C_y)\hat{y} + \Delta z(p_z + 0.5 - C_z)\hat{z}$. Then

$$\vec{r}' \cdot \hat{r} = r'\cos\psi = \Delta x(S_{Lx} - C_x)\sin\theta\cos\phi + \Delta y(p_y + 0.5 - C_y)\sin\theta\sin\phi + \Delta z(p_z + 0.5 - C_z)\cos\theta.$$

Instead supposing that p is located on the $(+x)$-face, we instead have

$$\vec{r}' = \Delta x(S_{Ux} - C_x)\hat{x} + \Delta y(p_y + 0.5 - C_y)\hat{y} + \Delta z(p_z + 0.5 - C_z)\hat{z},$$

and

$$\vec{r}' \cdot \hat{r} = r' \cos\psi = \Delta x(S_{Ux} - C_x)\sin\theta\cos\phi + \Delta y(p_y + 0.5 - C_y)\sin\theta\sin\phi + \Delta z(p_z + 0.5 - C_z)\cos\theta.$$

Let us also consider the discretization of the integrals making up the $\vec{N}$ and $\vec{L}$ functions, which also differ by face. For a specific example, recall

$$N_\theta = \int_S (J_x^* \cos\theta\cos\phi + J_y^* \cos\theta\sin\phi - J_z^* \sin\theta)\exp(-\mathrm{i}|\vec{k}|r'\cos\psi)\, dS.$$

We will split the integral over S into six discretized integrals, by face. Consider $\pm x$ faces: we know the J_x component and its Fourier transform are zero. So we can cancel the first term which involves J_x^*. The discretized N_θ integral over the $(-x)$-face is then

$$N_\theta = \sum_{j=S_{Ly}}^{S_{Uy}-1} \sum_{k=S_{Lz}}^{S_{Uz}-1} \Delta y\Delta z \left(J_y^* \cos\theta\sin\phi - J_z^* \sin\theta\right) \cdot \ldots$$
$$\exp\left[-\mathrm{i}|\vec{k}|\left(\Delta x(S_{Lx} - C_x)\sin\theta\cos\phi + \Delta y(p_y + 0.5 - C_y)\sin\theta\sin\phi + \Delta z(p_z + 0.5 - C_z)\cos\theta\right)\right],$$

with the upper sum limits as they are due to S faces terminating on a node. And over the $(+x)$-face,

$$N_\theta = \sum_{j=S_{Ly}}^{S_{Uy}-1} \sum_{k=S_{Lz}}^{S_{Uz}-1} \Delta y\Delta z \left(J_y^* \cos\theta\sin\phi - J_z^* \sin\theta\right) \cdot \ldots$$
$$\exp\left[-\mathrm{i}|\vec{k}|\left(\Delta x(S_{Ux} - C_x)\sin\theta\cos\phi + \Delta y(p_y + 0.5 - C_y)\sin\theta\sin\phi + \Delta z(p_z + 0.5 - C_z)\cos\theta\right)\right].$$

The N_ϕ function, repeated: $N_\phi = \int_S (-J_x^* \sin\phi + J_y^* \cos\phi)\exp(-\mathrm{i}|\vec{k}|r'\cos\psi)\, dS$. Discretized over the $(-x)$-face, we zero J_x^* to obtain

$$N_\phi = \sum_{j=S_{Ly}}^{S_{Uy}-1} \sum_{k=S_{Lz}}^{S_{Uz}-1} \Delta y\Delta z \left(J_y^* \cos\phi\right) \cdot \ldots$$
$$\exp\left[-\mathrm{i}|\vec{k}|\left(\Delta x(S_{Lx} - C_x)\sin\theta\cos\phi + \Delta y(p_y + 0.5 - C_y)\sin\theta\sin\phi + \Delta z(p_z + 0.5 - C_z)\cos\theta\right)\right].$$

Over the $(+x)$-face,

$$N_\phi = \sum_{j=S_{Ly}}^{S_{Uy}-1} \sum_{k=S_{Lz}}^{S_{Uz}-1} \Delta y\Delta z \left(J_y^* \cos\phi\right) \cdot \ldots$$

$$\exp\left[-\mathrm{i}|\vec{k}|\left(\Delta x(S_{Ux}-C_x)\sin\theta\cos\phi+\Delta y(p_y+0.5-C_y)\sin\theta\sin\phi+\Delta z(p_z+0.5-C_z)\cos\theta\right)\right].$$

In this way, we have a total of four functions which need to be discretized over each of the six faces. Let us refrain from substituting the $r'\cos\psi$ term which differs across every face; each of the N and L functions are otherwise the same across opposing face pairs, so that we have only 10 more discretizations to define.

The functions L_θ and L_ϕ remain to be discretized on the $(\pm x)$-faces, where M_x^* is also zero:

$$L_\theta=\sum_{j=S_{Ly}}^{S_{Uy}-1}\sum_{k=S_{Lz}}^{S_{Uz}-1}\Delta y\Delta z(M_y^*\cos\theta\sin\phi-M_z^*\sin\theta)\exp(-\mathrm{i}|\vec{k}|r'\cos\psi),$$
$$L_\phi=\sum_{j=S_{Ly}}^{S_{Uy}-1}\sum_{k=S_{Lz}}^{S_{Uz}-1}\Delta y\Delta z(M_y^*\cos\phi)\exp(-\mathrm{i}|\vec{k}|r'\cos\psi).$$

For the $\pm y$-faces, we note that $J_y^*=M_y^*=0$. On the $-y$-face, we find

$$r'\cos\psi=\Delta x(p_x+0.5-C_x)\sin\theta\cos\phi+\Delta y(S_{Ly}-C_y)\sin\theta\sin\phi+\Delta z(p_z+0.5-C_z)\cos\theta,$$

and on $+y$,

$$r'\cos\psi=\Delta x(p_x+0.5-C_x)\sin\theta\cos\phi+\Delta y(S_{Uy}-C_y)\sin\theta\sin\phi+\Delta z(p_z+0.5-C_z)\cos\theta.$$

These can be substituted into the definitions

$$N_\theta=\sum_{i=S_{Lx}}^{S_{Ux}-1}\sum_{k=S_{Ly}}^{S_{Uy}-1}\Delta x\Delta z(J_x^*\cos\theta\cos\phi-J_z^*\sin\theta)\exp(-\mathrm{i}|\vec{k}|r'\cos\psi),$$
$$N_\phi=\sum_{i=S_{Lx}}^{S_{Ux}-1}\sum_{k=S_{Ly}}^{S_{Uy}-1}\Delta x\Delta z(-J_x^*\sin\phi)\exp(-\mathrm{i}|\vec{k}|r'\cos\psi),$$
$$L_\theta=\sum_{i=S_{Lx}}^{S_{Ux}-1}\sum_{k=S_{Ly}}^{S_{Uy}-1}\Delta x\Delta z(M_x^*\cos\theta\cos\phi-M_z^*\sin\theta)\exp(-\mathrm{i}|\vec{k}|r'\cos\psi),$$
$$L_\phi=\sum_{i=S_{Lx}}^{S_{Ux}-1}\sum_{k=S_{Ly}}^{S_{Uy}-1}\Delta x\Delta z(-M_x^*\sin\phi)\exp(-\mathrm{i}|\vec{k}|r'\cos\psi).$$

Finally, for the $\pm z$-faces, we note that $J_z^*=M_z^*=0$. On the $-z$-face, we find

$$r'\cos\psi=\Delta x(p_x+0.5-C_x)\sin\theta\cos\phi+\Delta y(p_y+0.5-C_x)+\Delta z(S_{Lz}-C_z),$$

and on the $+z$-face, we find

$$r' \cos\psi = \Delta x(p_x + 0.5 - C_x)\sin\theta\cos\phi + \Delta y(p_y + 0.5 - C_x) + \Delta z(S_{Uz} - C_z).$$

These can be substituted into the definitions

$$\begin{aligned}
N_\theta &= \sum_{i=S_{Lx}}^{S_{Ux}-1}\sum_{j=S_{Lz}}^{S_{Uz}-1} \Delta x\Delta z(J_x^*\cos\theta\cos\phi - J_y^*\cos\theta\sin\phi)\exp(-\mathrm{i}|\vec{k}|r'\cos\psi),\\
N_\phi &= \sum_{i=S_{Lx}}^{S_{Ux}-1}\sum_{j=S_{Lz}}^{S_{Uz}-1} \Delta x\Delta z(-J_x^*\sin\phi + J_y^*\cos\phi)\exp(-\mathrm{i}|\vec{k}|r'\cos\psi),\\
L_\theta &= \sum_{i=S_{Lx}}^{S_{Ux}-1}\sum_{j=S_{Lz}}^{S_{Uz}-1} \Delta x\Delta z(M_x^*\cos\theta\cos\phi - M_y^*\cos\theta\sin\phi)\exp(-\mathrm{i}|\vec{k}|r'\cos\psi),\\
L_\phi &= \sum_{i=S_{Lx}}^{S_{Ux}-1}\sum_{j=S_{Lz}}^{S_{Uz}-1} \Delta x\Delta z(-M_x^*\sin\phi + M_y^*\cos\phi)\exp(-\mathrm{i}|\vec{k}|r'\cos\psi).
\end{aligned}$$

These quantities together with the total radiatied power P_{rad} can be used to determine the directivity, by [7] with the formulas:

$$D_\theta = \frac{K^2}{8\pi\eta_0 P_{\mathrm{rad}}}|L_\phi + \eta_0 N_\theta|^2,$$

$$D_\phi = \frac{K^2}{8\pi\eta_0 P_{\mathrm{rad}}}|L_\theta - \eta_0 N_\phi|^2.$$

6.1.4 Example: Dielectric Resonating Antenna

The 2005 paper by B. Li and K.W. Leung [15] provides a suitable candidate for evaluating the far-field simulation capabilities of FDTD. We describe the geometry of the circular-polarized dielectric resonating antenna in [15].

The dielectric resonating antenna (DRA) illustrated here is a cuboid block of dielectric material with a high relative permittivity; its feed line is a thin strip of conducting material connected to ground by a soft voltage source 50Ω, and contacting the dielectric block on one side. A second conducting patch is also added on a face adjacent to the feeding strip. The geometry is given in [15], with minor departures in our simulation, and an image is reproduced below.

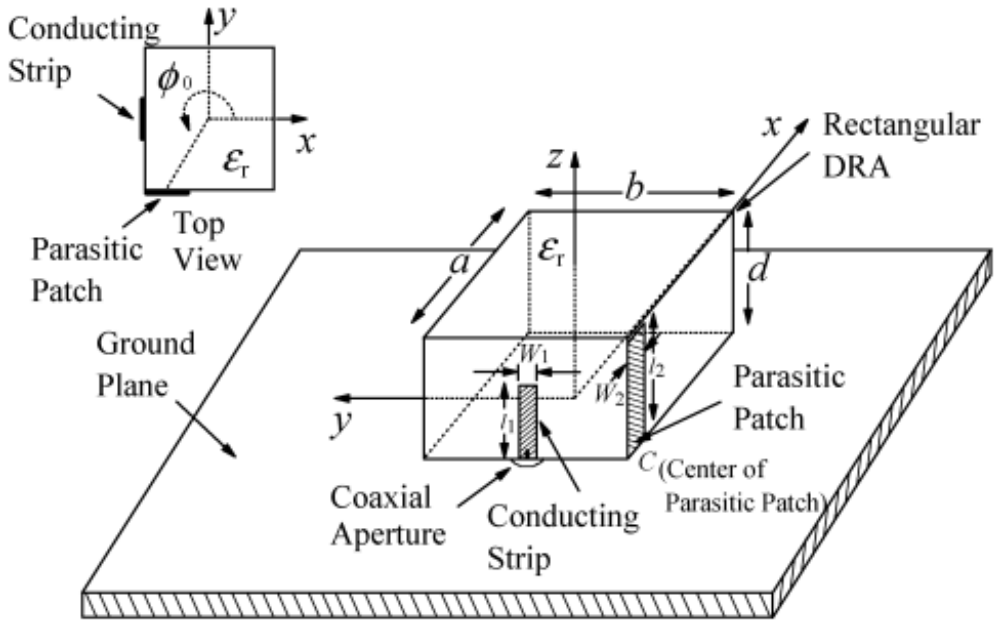

Figure 6.1: Design of strip-fed dielectric antenna with parasitic patch. This figure is reproduced from [15, Fig. 9].

The dielectric block is $24 \times 23.5 \times 12.34$ mm in x, y, z respectively. The feed line strip width $W_1 = 1$mm, and length $\ell_1 = 10$mm. The parasitic patch is added on the far $-x$ corner of its face, corresponding to a ϕ_0 value of 225.6°; $W_2 = 12$mm and $\ell_2 = 1$mm.

This antenna was found to be highly sensitive to the size of the ground plane, with the results approaching those in [15] more closely with larger ground plane sizes. However, computational resources quickly become an issue. The ground plane chosen for this simulation is 8.4 cm $\times$ 8.33 cm in x and y dimensions respectively, and a thin plate in z.

Ten air cells are allowed between all objects and the CPML layers for $\pm x$, $\pm y$, $-z$ boundaries. The $+z$ boundary was allocated twenty air cells between the nearest object, which is the $+z$ face of the DRA, and the CPML layer. The equivalent surface was chosen to lie five cells from the CPML layer on all sides.

Far field results were calculated for frequencies between 3 GHz and 4 GHz in 10 MHz steps. This includes directionality and axial ratio data for all angles of xy, xz, yz plane cuts. The primary aim was to compare results with those in [15], in particular Figs. 14 and 15 which characterize the response of axial ratio $\theta = 0$ or "boresight" direction to changes in patch length ℓ_1, ℓ_2. The following three figures illustrate that the boresight AR is insensitive to changes in the feed strip length and

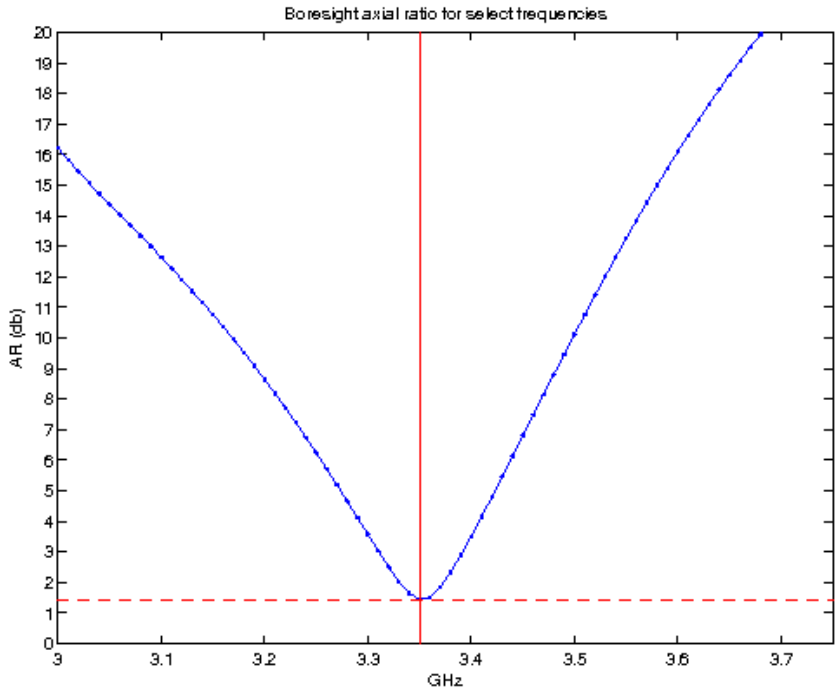

Figure 6.2: Boresight axial ratio of DRA with feed strip length 12mm, parasitic patch length 12mm.

Table 6.1: Boresight Axial Ratio by Feed Strip Length

Feed Strip ℓ_1 (mm)	Axial Ratio (dB) Minimum	Frequency (GHz)	Parasitic Patch ℓ_2 (mm)
12	1.4355	3.35	12
10	1.4406	3.35	12
8	1.4397	3.35	12

reaches a minimum AR of nearly 1 given a fixed parasitic patch length of 12mm, which agrees with the findings in Li [15]. However, the frequency at which we obtain this minimum is lesser by approximately 50 MHz. Experimentation seemed to indicate a sensitivity of this characteristic to the size of the ground plane, so it was chosen as large as available computation resources allowed.

6.1.5 Example: Microstrip Patch Antenna

We examine two strip-fed microstrip patch antenna simulations to verify three characteristics qualitatively. The simulation step sizes are each chosen to be 0.5 mm. The ground plate and dielectric for the square patch antenna are 40mm square in length and width, and the dielectric is 2mm thick (h) with permittivity 4. The antenna is square, $L = H = 10$mm. The feed strip is centered on a side of the patch antenna and extends 15 mm from the edge, and the source and

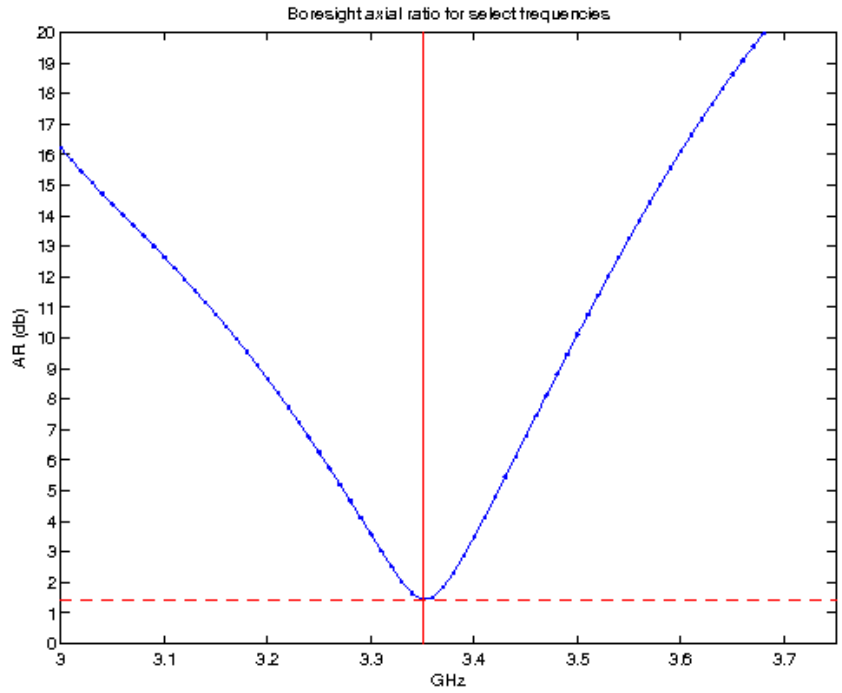

Figure 6.3: Boresight axial ratio of DRA with feed strip length 10mm, parasitic patch length 12mm.

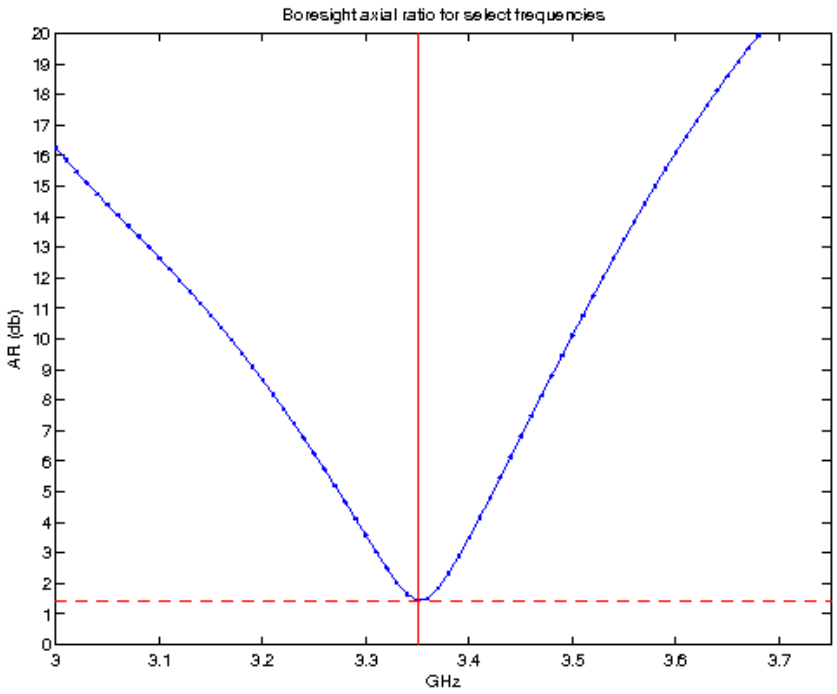

Figure 6.4: Boresight axial ratio of DRA with feed strip length 8mm, parasitic patch length 12mm.

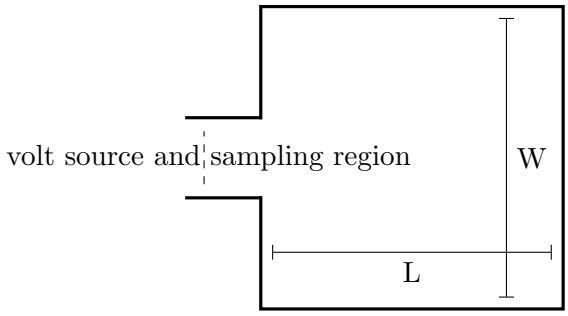

Figure 6.5: Top-down diagram of microstrip patch antenna layout.

sampling regions are located at its end. The source is driven with a cosine-modulated Gaussian signal centered at 7.5 GHz and with 7.5GHz of total bandwidth.

Let us briefly review the property of input impedance to an antenna. Much as with characteristic impedance examined above, we may find the input impedance by taking the ratio of frequency-domain sampled voltage to sampled current. For this configuration, we place our voltage and current sampling regions in the same space as the voltage source. The complex-valued input impedance is expected to be real at frequencies at which the antenna resonates. So, we calculate the input impedance $Z(\omega)$ much as before, and determine the frequency where its imaginary part imag(Z) is nearest to zero. Of course this method has a few problems: if we choose the wrong frequency spread, we may have no purely real values; if imag(Z) is nearly constant and near zero for a range of frequencies, then the resonant frequency becomes difficult to select. Resonant frequencies are the most efficient at converting supplied power into radiation, rather than reflecting it back toward the source. We have a second, more standard method to check for resonant frequencies, in S-parameters. For a port situated at the voltage source, the reflected wave and thus the S_{11} value will be much smaller at a resonant frequency. So, we calculate S_{11} for the input port and select its minimal value for the frequency spread. The resonant frequency is sharply indicated and in agreement as 7.23 GHz with both these methods. Calculating the input impedance has one advantage – assuming we find a resonant frequency, we can tune the power source to match the real part of the impedance. By doing so we minimize reflection and increase antenna efficiency. This design exhibits nearly real impedance $Z(7.23\text{GHz}) \approx 7.832\Omega$.

We also expect a majority of the power to be radiated upward perpendicular to the antenna plane. We examine the far-field directivity in the xy and xz planes and observe that this is present in simulation. The 120° spread centered at $\theta = 0$ shows a directivity above 0, indicating antenna

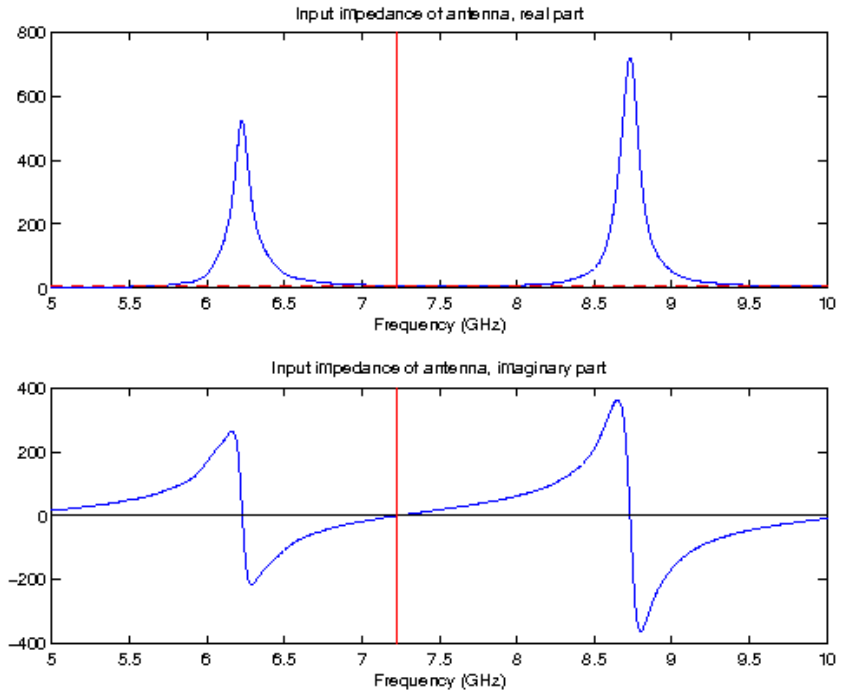

Figure 6.6: Input impedance of square patch antenna with resonant frequency 7.23 GHz indicated.

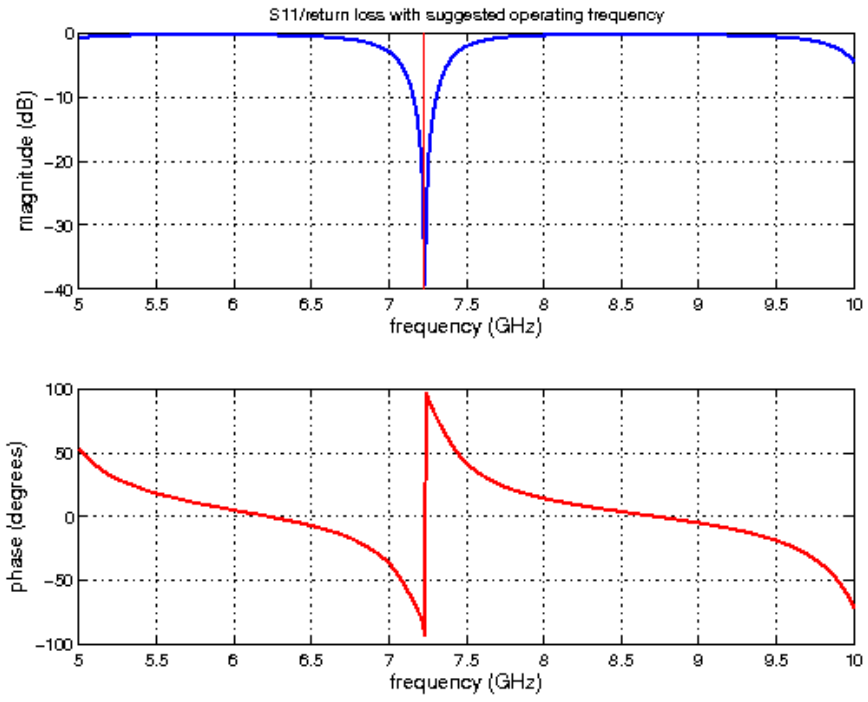

Figure 6.7: S-parameter of square patch antenna with resonant frequency 7.23 GHz indicated.

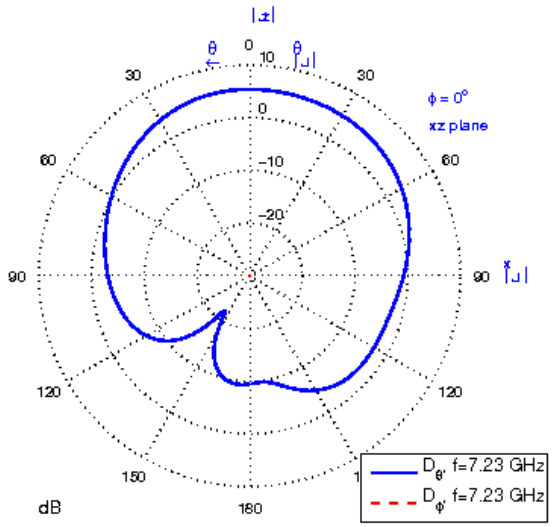

Figure 6.8: Far-field xz plane of square patch antenna at resonant frequency 7.23 GHz.

gain. As the ratio of length L to width W increases, we expect to see an increase in bandwidth and in input impedance. This is borne out with our second microstrip patch antenna design, which shares the same dimensions as the first but $L = 2W = 20$mm. The calculated resonant frequency using input impedance is clearly less reliable, and its value of 6.61 GHz disagrees with the S_{11} calculated resonant frequency of 6.76 GHz. At 6.76 GHz, the input impedance is almost real, and has a real part of 78.911Ω, revealing the expected increase.

Between about 6.3 GHz and 6.7 GHz, the S_{11} return loss takes on large negative values, indicating efficient energy transmission, and the far field directivity in the xz plane reveals the desirable antenna gain pattern near $\theta = 0$ is maintaned.

6.1.6 Example: Thin-wire dipole antenna

Finally we are now equipped to examine a dipole antenna using the thin-wire approximation. Using the rough approximation that the resonant wavelength λ is related to the length of the antenna as $\ell = \frac{0.95}{2\lambda}$ we design the antenna with a two-cell soft voltage source matched at 63.09Ω,

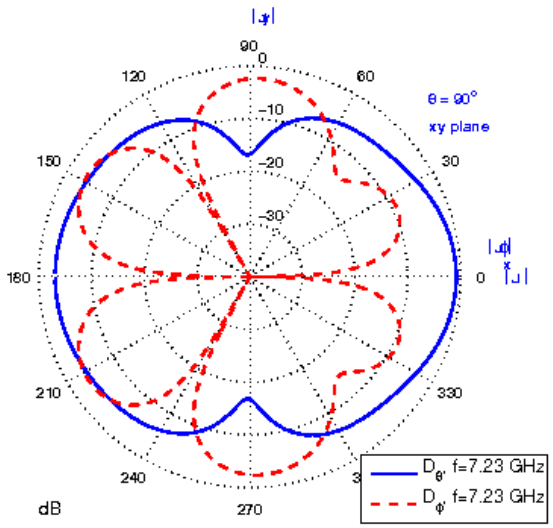

Figure 6.9: Far-field xy plane of square patch antenna at resonant frequency 7.23 GHz. Observe directivity values all lie below 0.

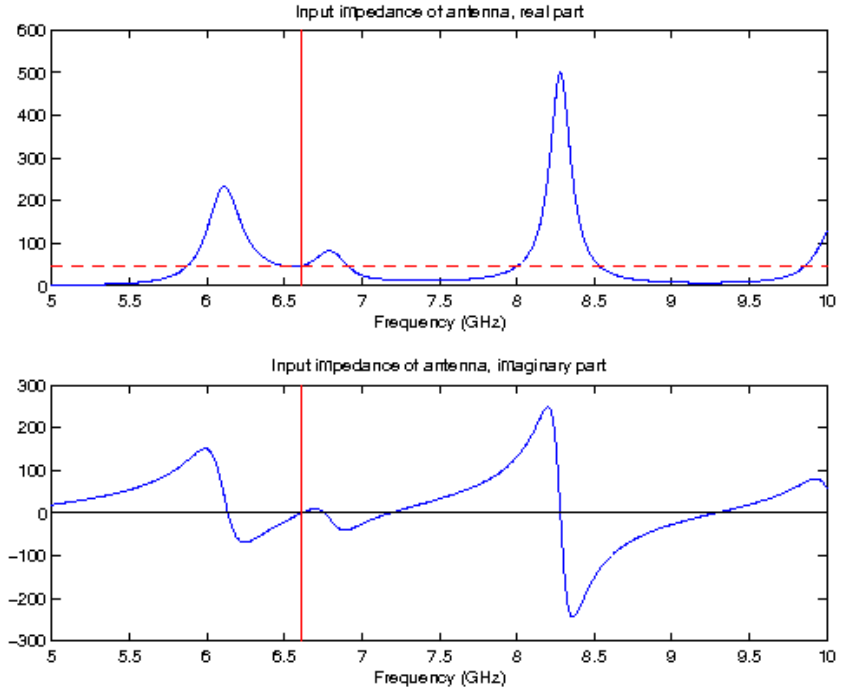

Figure 6.10: Input impedance of rectangular microstrip patch antenna.

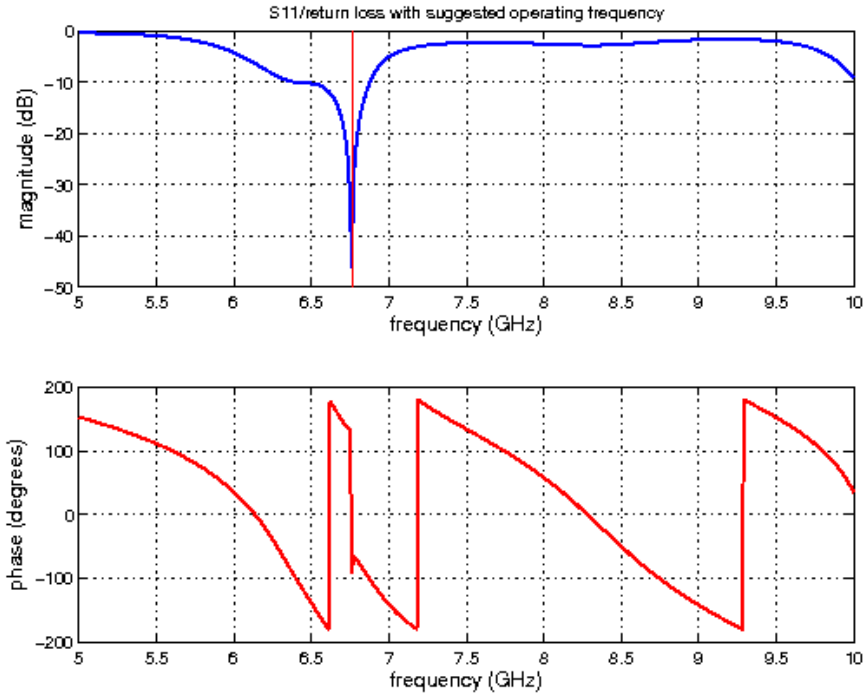

Figure 6.11: S-parameter of rectangular microstrip patch antenna.

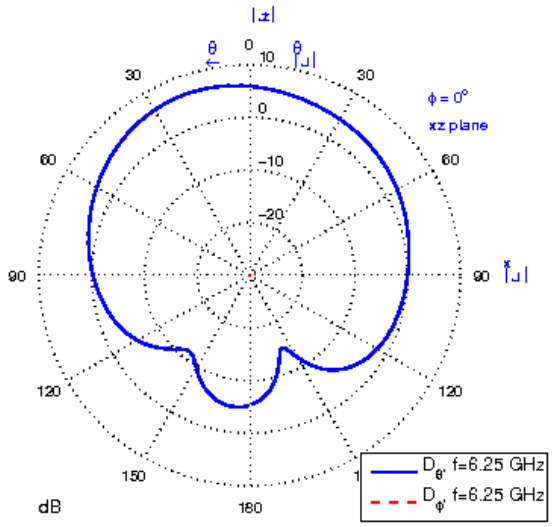

Figure 6.12: Directivity in xz plane of rectangular microstrip patch antenna, 6.25 GHz.

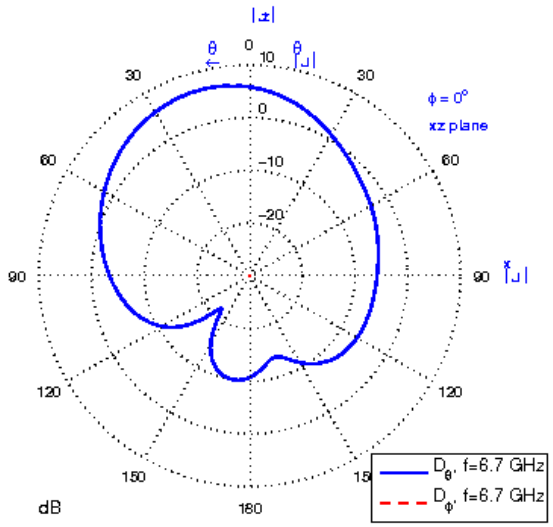

Figure 6.13: Directivity in xz plane of rectangular microstrip patch antenna, 6.7 GHz.

forming a path between two thin-wire lobes of equal length. We choose all step sizes to be 0.25 mm. The thin wires are chosen to be 0.02mm thick, oriented along x. Choosing an overall length 24mm leads to an expected resonant frequency just under 6 GHz.

The simulation is allowed to run up to about 3 ns, at 7000 timesteps, and is excited with a derivative-Gaussian pulse. The observed return loss bears out this estimation, showing a resonant frequency of 5.9 GHz. Likewise for this antenna we expect the yz-plane far-field directivity to show uniform radiation in all directions, and the xy-plane far-field directivity to show radiation dropping to zero as we near the axis of the antenna. The usefulness of the thin-wire approximation is proven in this example; we can successfully replicate the thin-wire behavior using ordinary PEC one cell in cross-section, but we need to drop the spatial step in y, z to 0.02 mm which causes the simulation to require about twelve times as long to run. If there were any other objects to model in simulation, we might face some significant difficulties with computational resources.

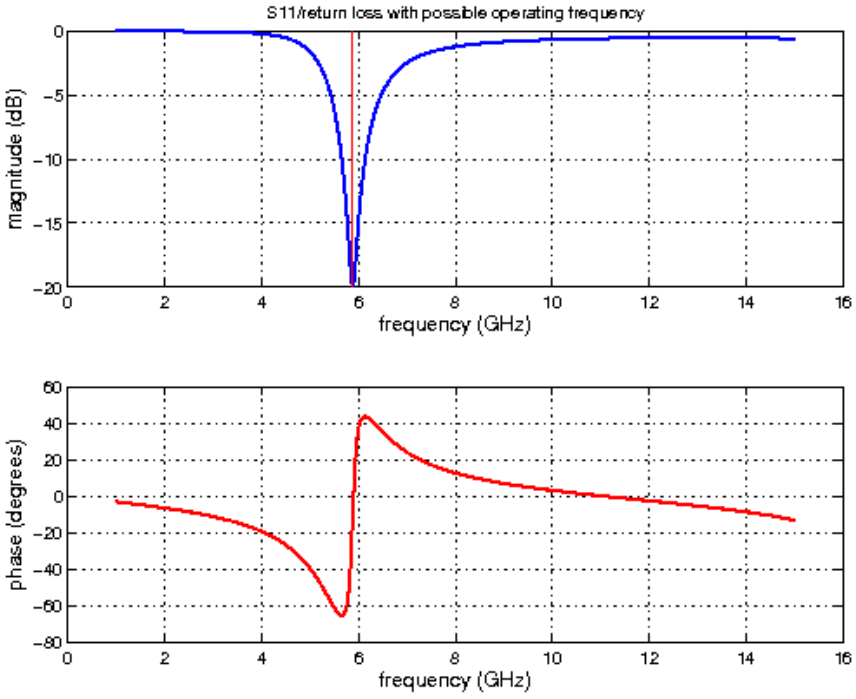

Figure 6.14: S-parameter of thin-wire dipole antenna.

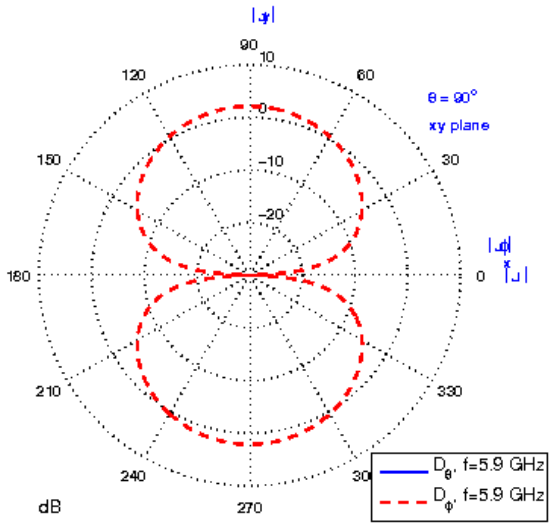

Figure 6.15: xy-plane far-field directivity of thin-wire dipole antenna.

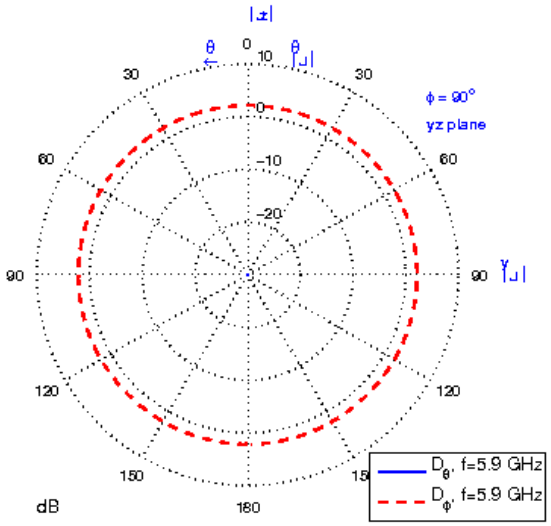

Figure 6.16: yz-plane far-field directivity of thin-wire dipole antenna.

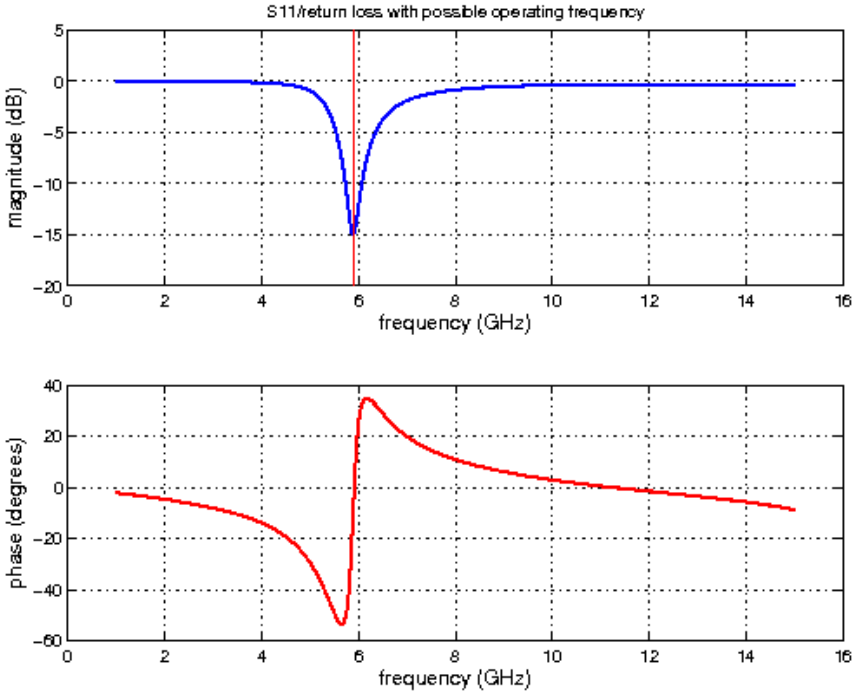

Figure 6.17: S-parameter of refinement-modeled dipole antenna.

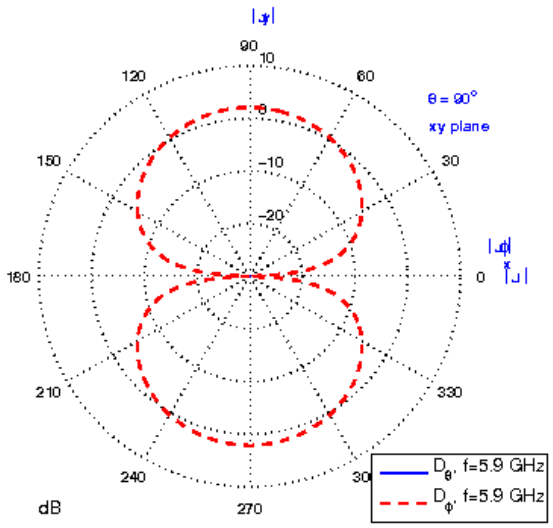

Figure 6.18: xy-plane far-field directivity of refinement-modeled dipole antenna.

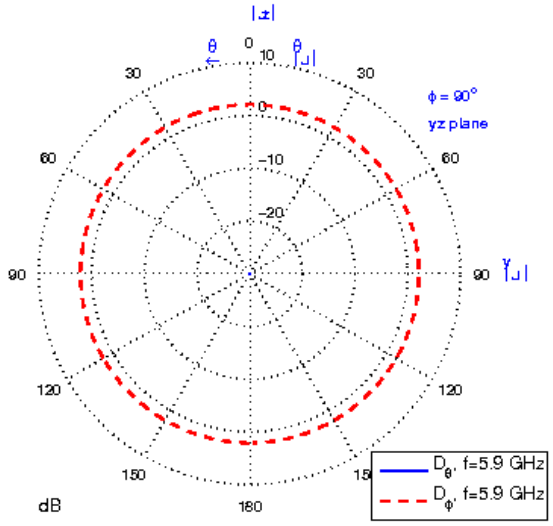

Figure 6.19: yz-plane far-field directivity of refinement-modeled dipole antenna.

6.2 Scattered Field Formulation

A common formulation of scattering problems is to assume that the scatterer material behaves linearly. Then we may consider analytically specified incident fields $\vec{E}_i$ and $\vec{H}_i$ and the scattering object's response, or scattered fields $\vec{E}_s$ and $\vec{H}_s$, separately. In particular, the incident fields are formulated as passing through empty medium, with no scattering objects present. We will assume that the surrounding medium is air or vacuum, such that the permittivity and permeability are as in vacuum:

$$\nabla \times \vec{H}_i = \varepsilon_0 \frac{\partial \vec{E}_i}{\partial t}, \tag{6.1}$$

$$\nabla \times \vec{E}_i = -\mu_0 \frac{\partial \vec{H}_i}{\partial t}. \tag{6.2}$$

The sums of the respective fields make up the total fields: $\vec{E}_{tot} = \vec{E}_i + \vec{E}_s$ and $\vec{H}_{tot} = \vec{H}_i + \vec{H}_s$.

Maxwell's equations are applicable to this total field formulation. By our linearity assumption, the total field can be rewritten as the sum of incident and scattered fields in and around the scatterer:

$$\nabla \times (\vec{H}_i + \vec{H}_s) = \nabla \times \vec{H}_i + \nabla \times \vec{H}_s = \\ \varepsilon \frac{\partial}{\partial t}(\vec{E}_i + \vec{E}_s) + \sigma^e(\vec{E}_i + \vec{E}_s) = \varepsilon \frac{\partial}{\partial t}\vec{E}_i + \sigma^e \vec{E}_i + \varepsilon \frac{\partial}{\partial t}\vec{E}_s + \sigma^e \vec{E}_s,$$

and

$$\nabla \times (\vec{E}_i + \vec{E}_s) = \nabla \times \vec{E}_i + \nabla \times \vec{E}_s \\ - \mu \frac{\partial}{\partial t}(\vec{H}_i + \vec{H}_s) - \sigma^m(\vec{H}_i + \vec{H}_s) = -\mu \frac{\partial}{\partial t}\vec{H}_i - \sigma^m \vec{H}_i - \mu \frac{\partial}{\partial t}\vec{H}_s - \sigma^m \vec{H}_s.$$

Now using the substitutions in (6.1) and (6.2), we obtain

$$\varepsilon_0 \frac{\partial \vec{E}_i}{\partial t} + \nabla \times \vec{H}_s = \varepsilon \frac{\partial}{\partial t}\vec{E}_i + \sigma^e \vec{E}_i + \varepsilon \frac{\partial \vec{E}_s}{\partial t} + \sigma^e \vec{E}_s,$$

and

$$-\mu_0 \frac{\partial \vec{H}_i}{\partial t} + \nabla \times \vec{E}_s = -\mu \frac{\partial \vec{H}_i}{\partial t} - \sigma^m \vec{H}_i - \mu \frac{\partial \vec{H}_s}{\partial t} - \sigma^m \vec{H}_s.$$

Rearranging, we find

$$\varepsilon\frac{\partial\vec{E}_s}{\partial t}+\sigma^e\vec{E}_s=(\varepsilon_0-\varepsilon)\frac{\partial\vec{E}_i}{\partial t}+\nabla\times\vec{H}_s-\sigma^e\vec{E}_i, \tag{6.3}$$

and

$$\mu\frac{\partial\vec{H}_s}{\partial t}+\sigma^m\vec{H}_s=(\mu_0-\mu)\frac{\partial\vec{H}_i}{\partial t}-\nabla\times\vec{E}_s-\sigma^m\vec{H}_i. \tag{6.4}$$

These expressions for the scattered field can be discretized as before, similarly to the equations (2.4) - (2.6). The discretized time derivatives on $\vec{E}_s$ and $\vec{H}_s$ allow us to solve for future timesteps of the scattered fields. Hence, these expressions yield updating equations for the scattered field in terms of past values of the scattered field, and past and current values of the incident field.

The discretized x component of vector equation (6.3) is solved for the future timestep of the scattered electric field. The result is given by

$$\begin{aligned}
E_{s,x}^{n+1}(i,j,k)=&\frac{2\varepsilon_x(i,j,k)-\sigma_x^e(i,j,k)\Delta t}{2\varepsilon_x(i,j,k)+\sigma_x^e(i,j,k)\Delta t}E_{s,x}^n(i,j,k)+\\
&+\frac{2\Delta t}{\Delta y(2\varepsilon_x(i,j,k)+\sigma_x^e(i,j,k)\Delta t)}\left(H_{s,z}^{n+\frac{1}{2}}(i,j,k)-H_{s,z}^{n+\frac{1}{2}}(i,j-1,k)\right)+\\
&+\frac{2\Delta t}{\Delta z(2\varepsilon_x(i,j,k)+\sigma_x^e(i,j,k)\Delta t)}\left(H_{s,y}^{n+\frac{1}{2}}(i,j,k-1)-H_{s,y}^{n+\frac{1}{2}}(i,j,k)\right)+\\
&+\frac{2(\varepsilon_0-\varepsilon_x(i,j,k))-\sigma_x^e(i,j,k)\Delta t}{2\varepsilon_x(i,j,k)+\sigma_x^e(i,j,k)\Delta t}E_{i,x}^{n+1}(i,j,k)+\\
&+\frac{2(\varepsilon_0-\varepsilon_x(i,j,k))-\sigma_x^e(i,j,k)\Delta t}{2\varepsilon_x(i,j,k)+\sigma_x^e(i,j,k)\Delta t}E_{i,x}^{n}(i,j,k).
\end{aligned}$$

Following the nomenclature in [7] as before, the above equation can be written as a sum of constant updating coefficient terms multiplied by their respective field terms:

$$\begin{aligned}
E_{s,x}^{n+1}(i,j,k)=&C_{ExE}(i,j,k)E_{s,x}^n(i,j,k)+\\
&+C_{ExHz}(i,j,k)\left(H_{s,z}^{n+\frac{1}{2}}(i,j,k)-H_{s,z}^{n+\frac{1}{2}}(i,j-1,k)\right)+\\
&+C_{ExHy}(i,j,k)\left(H_{s,y}^{n+\frac{1}{2}}(i,j,k-1)-H_{s,y}^{n+\frac{1}{2}}(i,j,k)\right)+\\
&+C_{ExEic}(i,j,k)E_{i,x}^{n+1}(i,j,k)+\\
&+C_{ExEip}(i,j,k)E_{i,x}^{n}(i,j,k),
\end{aligned}$$

with updating coefficients

$$C_{exe}(i,j,k)=\frac{2\varepsilon_x(i,j,k)-\sigma_x^e(i,j,k)\Delta t}{2\varepsilon_x(i,j,k)+\sigma_x^e(i,j,k)\Delta t},$$

$$C_{ExHz}(i,j,k) = \frac{2\Delta t}{\Delta y(2\varepsilon_x(i,j,k) + \sigma_x^e(i,j,k)\Delta t)},$$
$$C_{ExHy}(i,j,k) = \frac{2\Delta t}{\Delta z(2\varepsilon_x(i,j,k) + \sigma_x^e(i,j,k)\Delta t)},$$
$$C_{ExEic}(i,j,k) = \frac{2(\varepsilon_0 - \varepsilon_x(i,j,k)) - \sigma_x^e(i,j,k)\Delta t}{2\varepsilon_x(i,j,k) + \sigma_x^e(i,j,k)\Delta t},$$
$$C_{ExEip}(i,j,k) = \frac{2(\varepsilon_0 - \varepsilon_x(i,j,k)) - \sigma_x^e(i,j,k)\Delta t}{2\varepsilon_x(i,j,k) + \sigma_x^e(i,j,k)\Delta t}.$$

Note the occurrence of timesteps n and $n+1$ for incident fields; these arise from the time derivative applied to the incident field and are denoted by the subscripts ip for $incident - previous$ and ic for $incident - current$. In calculation, this suggests that two timesteps of the incident field must be available each time the scattered field is calculated.

We could choose to modify the scattering updating equation by splitting the sum across two calculation steps, the first involving only the nth timestep of the incident field and the second involving only the $(n+1)$th timestep of the incident field. That way, to save memory, we need store only one timestep of the incident field, and update the incident field between the scattering update steps.

The rest of the scattered field updating equations obtained from (6.3) are as follows.

E field, y component:

$$\begin{aligned} E_{s,y}^{n+1}(i,j,k) = {} & C_{EyE}(i,j,k)E_{s,y}^{n}(i,j,k) + \\ & + C_{EyHz}(i,j,k)\left(H_{s,z}^{n+\frac{1}{2}}(i-1,j,k) - H_{s,z}^{n+\frac{1}{2}}(i,j,k)\right) + \\ & + C_{EyHx}(i,j,k)\left(H_{s,y}^{n+\frac{1}{2}}(i,j,k) - H_{s,y}^{n+\frac{1}{2}}(i,j,k-1)\right) + \\ & + C_{EyEic}(i,j,k)E_{i,y}^{n+1}(i,j,k) + \\ & + C_{EyEip}(i,j,k)E_{i,y}^{n}(i,j,k), \end{aligned}$$

with updating coefficients

$$C_{exe}(i,j,k) = \frac{2\varepsilon_x(i,j,k) - \sigma_x^e(i,j,k)\Delta t}{2\varepsilon_x(i,j,k) + \sigma_x^e(i,j,k)\Delta t},$$
$$C_{EyHz}(i,j,k) = \frac{2\Delta t}{\Delta x(2\varepsilon_y(i,j,k) + \sigma_y^e(i,j,k)\Delta t)},$$

$$
\begin{aligned}
C_{EyHx}(i,j,k) &= \frac{2\Delta t}{\Delta z(2\varepsilon_y(i,j,k)+\sigma_y^e(i,j,k)\Delta t)},\\
C_{Ezyic}(i,j,k) &= \frac{2(\varepsilon_0-\varepsilon_y(i,j,k))-\sigma_y^e(i,j,k)\Delta t}{2\varepsilon_y(i,j,k)+\sigma_y^e(i,j,k)\Delta t},\\
C_{EyEip}(i,j,k) &= -\frac{2(\varepsilon_0-\varepsilon_y(i,j,k))-\sigma_y^e(i,j,k)\Delta t}{2\varepsilon_y(i,j,k)+\sigma_y^e(i,j,k)\Delta t}.
\end{aligned}
$$

E field, z component:

$$
\begin{aligned}
E_{s,z}^{n+1}(i,j,k) = {} & C_{EzE}(i,j,k)E_{s,z}^{n}(i,j,k)+\\
& + C_{EzHy}(i,j,k)\left(H_{s,y}^{n+\frac{1}{2}}(i,j,k)-H_{s,y}^{n+\frac{1}{2}}(i,j,k-1)\right)+\\
& + C_{EzHx}(i,j,k)\left(H_{s,x}^{n+\frac{1}{2}}(i-1,j,k)-H_{s,x}^{n+\frac{1}{2}}(i,j,k)\right)+\\
& + C_{EzEic}(i,j,k)E_{i,z}^{n+1}(i,j,k)+\\
& + C_{EzEip}(i,j,k)E_{i,z}^{n}(i,j,k),
\end{aligned}
$$

with updating coefficients

$$
\begin{aligned}
C_{exe}(i,j,k) &= \frac{2\varepsilon_x(i,j,k)-\sigma_x^e(i,j,k)\Delta t}{2\varepsilon_x(i,j,k)+\sigma_x^e(i,j,k)\Delta t},\\
C_{EzHy}(i,j,k) &= \frac{2\Delta t}{\Delta x(2\varepsilon_z(i,j,k)+\sigma_z^e(i,j,k)\Delta t)},\\
C_{EzHx}(i,j,k) &= \frac{2\Delta t}{\Delta y(2\varepsilon_z(i,j,k)+\sigma_z^e(i,j,k)\Delta t)},\\
C_{EzEic}(i,j,k) &= \frac{2(\varepsilon_0-\varepsilon_z(i,j,k))-\sigma_z^e(i,j,k)\Delta t}{2\varepsilon_z(i,j,k)+\sigma_z^e(i,j,k)\Delta t},\\
C_{EzEip}(i,j,k) &= -\frac{2(\varepsilon_0-\varepsilon_z(i,j,k))-\sigma_z^e(i,j,k)\Delta t}{2\varepsilon_z(i,j,k)+\sigma_z^e(i,j,k)\Delta t}.
\end{aligned}
$$

The scattered field updating equations obtained from (6.4) are as follows. H field, x component:

$$
\begin{aligned}
H_{s,x}^{n+\frac{1}{2}}(i,j,k) = {} & C_{HxH}(i,j,k)H_{s,x}^{n-\frac{1}{2}}(i,j,k)+\\
& + C_{HxEz}(i,j,k)\left(E_{s,z}^{n}(i,j+1,k)-E_{s,z}^{n}(i,j,k)\right)+\\
& + C_{HxEy}(i,j,k)\left(E_{s,y}^{n}(i,j,k)-E_{s,y}^{n}(i,j,k+1)\right)+\\
& + C_{HxHic}(i,j,k)H_{i,x}^{n+\frac{1}{2}}(i,j,k)+\\
& + C_{HxHip}(i,j,k)H_{i,x}^{n-\frac{1}{2}}(i,j,k),
\end{aligned}
$$

with updating coefficients

$$
\begin{aligned}
C_{HxH}(i,j,k) &= \frac{2\mu_x(i,j,k) - \sigma_x^m(i,j,k)\Delta t}{2\mu_x(i,j,k) + \sigma_x^m(i,j,k)\Delta t},\\
C_{HxEz}(i,j,k) &= \frac{2\Delta t}{\Delta y(2\mu_x(i,j,k) + \sigma_x^m(i,j,k)\Delta t},\\
C_{HxEy}(i,j,k) &= \frac{2\Delta t}{\Delta z(2\mu_x(i,j,k) + \sigma_x^m(i,j,k)\Delta t},\\
C_{HxHic}(i,j,k) &= \frac{2(\mu_0 - \mu_x(i,j,k)) - \sigma_x^m(i,j,k)\Delta t}{2\mu_x(i,j,k) + \sigma_x^m(i,j,k)\Delta t},\\
C_{HxHip}(i,j,k) &= -\frac{2(\mu_0 - \mu_x(i,j,k)) - \sigma_x^m(i,j,k)\Delta t}{2\mu_x(i,j,k) + \sigma_x^m(i,j,k)\Delta t}.
\end{aligned}
$$

H field, y component:

$$
\begin{aligned}
H_{s,y}^{n+\frac{1}{2}}(i,j,k) = {} & C_{HyH}(i,j,k)H_{s,y}^{n-\frac{1}{2}}(i,j,k) + \\
& + C_{HyEz}(i,j,k)\left(E_{s,z}^n(i,j,k+1) - E_{s,z}^n(i,j,k)\right) + \\
& + C_{HyEx}(i,j,k)\left(E_{s,x}^n(i,j,k) - E_{s,x}^n(i,j+1,k)\right) + \\
& + C_{HyHic}(i,j,k)H_{i,y}^{n+\frac{1}{2}}(i,j,k) + \\
& + C_{HyHip}(i,j,k)H_{i,y}^{n-\frac{1}{2}}(i,j,k),
\end{aligned}
$$

with updating coefficients

$$
\begin{aligned}
C_{HyH}(i,j,k) &= \frac{2\mu_y(i,j,k) - \sigma_y^m(i,j,k)\Delta t}{2\mu_y(i,j,k) + \sigma_y^m(i,j,k)\Delta t},\\
C_{HyEz}(i,j,k) &= \frac{2\Delta t}{\Delta x(2\mu_y(i,j,k) + \sigma_y^m(i,j,k)\Delta t},\\
C_{HyEx}(i,j,k) &= \frac{2\Delta t}{\Delta z(2\mu_y(i,j,k) + \sigma_y^m(i,j,k)\Delta t},\\
C_{HyHic}(i,j,k) &= \frac{2(\mu_0 - \mu_y(i,j,k)) - \sigma_y^m(i,j,k)\Delta t}{2\mu_y(i,j,k) + \sigma_y^m(i,j,k)\Delta t},\\
C_{HyHip}(i,j,k) &= -\frac{2(\mu_0 - \mu_y(i,j,k)) - \sigma_y^m(i,j,k)\Delta t}{2\mu_y(i,j,k) + \sigma_y^m(i,j,k)\Delta t}.
\end{aligned}
$$

H field, z component:

$$
H_{s,z}^{n+\frac{1}{2}}(i,j,k) = C_{HzH}(i,j,k)H_{s,z}^{n-\frac{1}{2}}(i,j,k) +
$$

$$
\begin{aligned}
&+ C_{HzEx}(i,j,k)\left(E^n_{s,x}(i,j,k+1) - E^n_{s,x}(i,j,k)\right) + \\
&+ C_{HzEy}(i,j,k)\left(E^n_{s,y}(i,j,k) - E^n_{s,y}(i,j+1,k)\right) + \\
&+ C_{HzHic}(i,j,k)H^{n+\frac{1}{2}}_{i,z}(i,j,k) + \\
&+ C_{HzHip}(i,j,k)H^{n-\frac{1}{2}}_{i,z}(i,j,k).
\end{aligned}
$$

with updating coefficients

$$
\begin{aligned}
C_{HzH}(i,j,k) &= \frac{2\mu_z(i,j,k) - \sigma^m_z(i,j,k)\Delta t}{2\mu_z(i,j,k) + \sigma^m_z(i,j,k)\Delta t} \\
C_{HzEx}(i,j,k) &= \frac{2\Delta t}{\Delta y(2\mu_z(i,j,k) + \sigma^m_z(i,j,k)\Delta t} \\
C_{HzEy}(i,j,k) &= \frac{2\Delta t}{\Delta x(2\mu_z(i,j,k) + \sigma^m_z(i,j,k)\Delta t} \\
C_{HzHic}(i,j,k) &= \frac{2(\mu_0 - \mu_z(i,j,k)) - \sigma^m_z(i,j,k)\Delta t}{2\mu_z(i,j,k) + \sigma^m_z(i,j,k)\Delta t} \\
C_{HzHip}(i,j,k) &= -\frac{2(\mu_0 - \mu_z(i,j,k)) - \sigma^m_z(i,j,k)\Delta t}{2\mu_z(i,j,k) + \sigma^m_z(i,j,k)\Delta t}
\end{aligned}
$$

6.2.1 Incident Waves

One primary goal of the scattered field formulation is to be able to introduce sources which may exist outside the domain. In this section, we examine incident plane waves as from a distant source, included in simulation by forcing of $\vec{E}_i$, $\vec{H}_i$. We must derive a way of introducing the analytically known incident waveform in simulation. However, our discussion will not cover methods to model the analytically known descriptions of point sources at finite distance.

We will use the same waveforms as covered in Chapter 3, as pulsed signals are equally effective for scattering problems. We use the convention of θ for polar angle and ϕ for azimuthal angle.

Incident Plane Waves

Similar to the section on the far-field transform, we will define the plane wave in terms of spherical components, and then convert back to Cartesian coordinates to obtain equations usable in simulation. In addition, we assume the external medium is air, such that propagation speed is c.

Choose a position $\vec{r}$ in space; let the magnitude of $\vec{r}$ be in units of meters. Let an EM plane wave be traveling in the direction of unit vector $\hat{k} = \hat{r} + \theta_i\hat{\theta} + \phi_i\hat{\phi}$. Then $\hat{k}\cdot\vec{r}$ denotes the scalar

distance between the origin and the point located by $\vec{r}$, in the direction the wave is traveling. So the quantity $\frac{1}{c}\hat{k}\cdot\vec{r}$ describes the time difference in seconds between a wavefront passing $\vec{r}$ and that same wavefront passing the origin. Of course, this time difference may be negative depending on the position of $\vec{r}$ and the orientation of $\hat{k}$.

Let plane wave's electric field amplitude at the origin describe a scalar function $f(t)$ of time in seconds. We can express the polarization of the incident wave in spherical coordinates using constant parameters E_θ and E_ϕ for the respective magnitudes of these components; then the full field at the origin is given by $\vec{E}_i(\vec{0}) = (E_\theta\hat{\theta} + E_\phi\hat{\phi})f(t)$. The amplitude at a fixed point $\vec{r}$, then, is given by

$$\vec{E}_i(\vec{r}) = (E_\theta\hat{\theta} + E_\phi\hat{\phi})f\left(t - \frac{1}{c}\hat{k}\cdot\vec{r}\right).$$

Note that the magnitude of $\vec{E}_i$ scales with both $\sqrt{E_\theta + E_\phi}$ and with the magnitude of f. By convention, we normalize such that $-1 \leq f \leq 1$.

We now determine how to calculate $\vec{E}_i, \vec{H}_i$ values throughout the domain for a chosen f waveform. We introduce two parameters t_0 and L to choose a time offset by which the wave is delayed. We allow two separate parameters for the same shift merely for readability of the algorithm: the L parameter is chosen as a function of the domain geometry, and the t_0 parameter chosen as a function of the waveform. Both the time and space considerations are necessary to ensure our initial incident fields are zero, and to avoid a jump at the plane wave's leading edge.

First, t_0 is chosen according to the waveform to be a sufficient delay to avoid jumps in incident field values. Now let $\vec{k}_1, \ldots, k_8$ point from the origin to the eight corners of the domain (in any order). We calculate L as the minimum of $\{\vec{k}\cdot\vec{k}_1, \ldots, \vec{k}\cdot k_8\}$. This scalar-valued distance is also multiplied by $1/c$ within the argument to f, and represents the largest time advancement of any domain corner. We delay the waveform by the same amount of time to ensure the entire $\vec{E}_i, \vec{H}_i$ fields start timestepping with zero values. So, with these chosen delays incorporated, we have

$$\vec{E}_i(\vec{r}) = (E_\theta\hat{\theta} + E_\phi\hat{\phi})f\left((t - t_0) - \frac{1}{c}(\hat{k}\cdot\vec{r} - L)\right).$$

In Cartesian, we observe that $\hat{k} = \sin\theta_i\cos\phi_i\hat{x} + \sin\theta_i\sin\phi_i\hat{y} + \cos\theta_i\hat{z}$. Also

$$E_\theta\hat{\theta} + E_\phi\hat{\phi} = (E_\theta\cos\theta_i\cos\phi_i - E_\phi\sin\phi_i)\hat{x} + (E_\theta\cos\theta_i\sin\phi_i + E_\phi\cos\phi_i)\hat{y} + (-E - \theta\theta_i)\hat{z}.$$

Then substitute this into the preceding. With $\vec{r} =< x, y, z >$, and using the abbreviation $f\left((t-t_0) - \frac{1}{c}(\sin\theta_i \cos\phi_i x + \sin\theta_i \sin\phi_i y + \cos\theta_i z - L)\right) = f(\tau)$,

$$\begin{aligned} E_{ix}(\vec{r}) &= (E_\theta \cos\theta_i \cos\phi_i - E_\phi \sin\phi_i) f(\tau), \\ E_{iy}(\vec{r}) &= (E_\theta \cos\theta_i \sin\phi_i + E_\phi \cos\phi_i) f(\tau), \\ E_{iz}(\vec{r}) &= (-E_\theta \sin\theta_i) f(\tau). \end{aligned}$$

These are the expressions which we use to determine the incident electric field component values at each timestep. Each component's location is plugged into $\vec{r}$ and the analytic expression used to evaluate f; parameters E_θ, E_ϕ, θ_i, ϕ_i plugged in to yield the full value E_{ix}, E_{iy}, or E_{iz}.

Now that we have this expression, it is most straightforward to use the relationship between $\vec{E}$ and $\vec{H}$ in freespace to derive the formulas for $\vec{H}_i$. Recalling that $\vec{k}$ is chosen in the direction of propagation, we use the impedance of freespace $Z_0 = \sqrt{\frac{\mu_0}{\varepsilon_0}}$ as the ratio of electric and magnetic field strengths to obtain

$$\vec{H}_i = \frac{1}{Z_0} \hat{k} \times \vec{E}_i.$$

Applying the cross product definition and simplifying the trigonometric expressions is laid out below:

$$\begin{aligned} H_{ix} &= \frac{1}{Z_0}\left(k_y E_{iz} - k_z E_{iy}\right) = \frac{1}{Z_0}\left(\sin\theta_i \sin\phi_i(-E_\theta \sin\theta_i) - \cos\theta_i(E_\theta \cos\theta_i \sin\phi_i + E_\phi \cos\phi_i)\right) f(\tau) \\ &= \frac{1}{Z_0}\left(-E_\theta \sin^2\theta_i \sin\phi_i - E_\theta \cos^2\theta_i \sin\phi_i - E_\phi \cos\theta_i \cos\phi_i\right) f(\tau) \\ &= -\frac{1}{Z_0}\left(E_\theta \sin\phi_i + E_\phi \cos\theta_i \cos\phi_i\right) f(\tau), \\ H_{iy} &= \frac{1}{Z_0}\left(k_z E_{ix} - k_x E_{iz}\right) = \frac{1}{Z_0}\left(\cos\theta_i(E_\theta \cos\theta_i \cos\phi_i - E_\phi \sin\phi_i) - \sin\theta_i \cos\phi_i(-E_\theta \sin\theta_i)\right) f(\tau) \\ &= \frac{1}{Z_0}(E_\theta \cos\phi_i - E_\phi \sin\phi_i \cos\phi_i) f(\tau), \\ H_{iz} &= \frac{1}{Z_0}\left(k_x E_{iy} - k_y E_{ix}\right) \\ &= \frac{1}{Z_0}\left(\sin\theta_i \cos\phi_i(E_\theta \cos\theta_i \sin\phi_i + E_\phi \cos\phi_i) - \sin\theta_i \sin\phi_i(E_\theta \cos\theta_i \cos\phi_i - E_\phi \sin\phi_i)\right) f(\tau) \\ &= \frac{1}{Z_0}\left(E_\theta \cos\theta_i \sin\theta_i \cos\phi_i \sin\phi_i(1-1) + E_\phi \sin\theta_i \cos^2\phi_i + E_\phi \sin^2\phi_i \sin\theta_i\right) f(\tau) \\ &= \frac{1}{Z_0}\left(E_\phi \sin\theta_i\right) f(\tau). \end{aligned}$$

Note that $f(\tau)$ uses the current time value, which is a half-integer for the magnetic f field.

6.2.2 Example: Dielectric sphere scattering

One classic problem is to obtain the responses of a dielectric sphere to an incident plane wave. That problem is briefly studied here. No far-field results are calculated, but the near-field is modeled and we can observe the cross-sectional planes through the origin.

Discrete Fourier transform

Again we will use the discrete Fourier transform to obtain important results in the frequency domain. We choose to find the frequency-domain scattered E_z field response for given f_c, so we take

$$E_z^*(\vec{x}, f_c) \approx \sum_{n=1}^{N} E_z^n(i,j,k)\Delta t \cdot \exp\left(-\mathrm{i}2\pi f_c n \Delta t\right).$$

However, for many problems of interest, storing the values of the entire domain for all timesteps is prohibitively expensive. Rather, we compute a running sum as timestepping proceeds, and avoid the need to store the complete field history. For the running sum, starting with $E_z^*(i,j,k,0,f_c) = 0$, at each timestep we calculate and store

$$E_z^*(i,j,k,n;f_c) = E_z^*(i,j,k,n-1;f_c) + E_z^n(i,j,k)\Delta t \cdot \exp\left(-\mathrm{i}2\pi f_c n \Delta t\right).$$

The transformed values for other fields can be computed analogously.

Problem description

Spatial steps are chosen as 0.02 m. The domain is empty except for the sphere, and is 4m in x by 2.2m in y by 4m in z centered on the sphere. The sphere chosen is 1m radius, is homogeneous with permittivity and permeability both equal to $\sqrt{1.5}$ and zero conductivity.

The incident plane wave is directed parallel to the x axis, and travels toward $+x$. The waveform chosen is a cosine modulated Gaussian centered at 0.667 GHz with bandwidth 1 GHz. The discrete frequencies sampled are 0.29979 GHz, 0.6 GHz, and 1 GHz. These correspond to the 2.4495 wavelength, 4.9024 wavelength, and 8.1707 wavelength problems respectively. The simulation was run for 2000 timesteps, corresponding to a final time of about 70 ns.

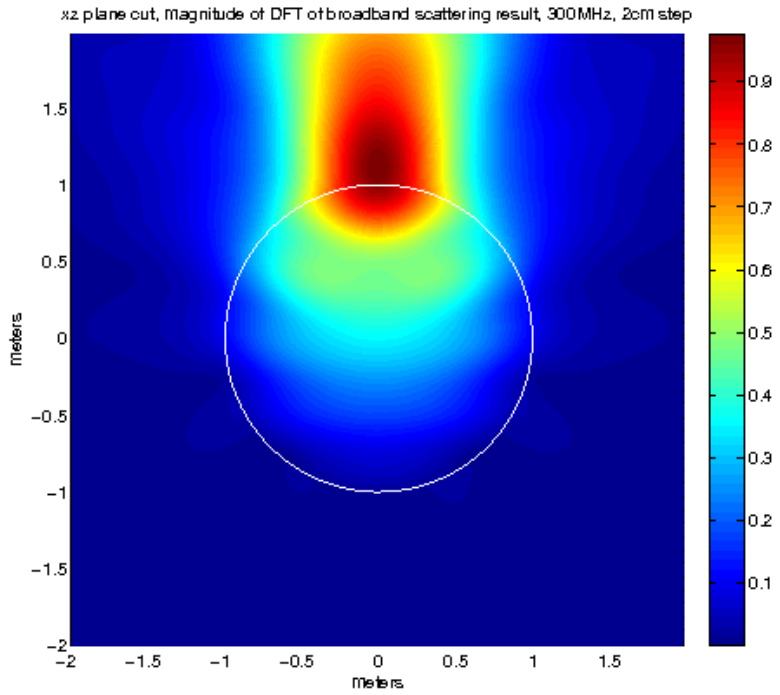

Figure 6.20: Frequency-domain dielectric sphere broadband signal scattering result, 300 MHz, xz plane cut

Simulations for this problem were also conducted with a monochrome sinusoidal source at each frequency of amplitude 1. The description is identical up to the waveform chosen for the incident field, which is a sine function, and that the monochromatic simulations were run for 3000 timesteps. Note that the magnitude of the frequency content in the broadband pulse differs, so we scale the broadband data to the monochrome data. The normalization factors and full-domain errors are collected in the following table.

Table 6.2: Dielectric sphere broadband result normalization and comparison to monochromatic signal result

Frequency (GHz)	Normalization coefficient ($\times 10^{-7}$)	Maximum nodal error ($\times 10^{-7}$)	L1 error	RMS error ($\times 10^{-8}$)
0.29979	1.8069	3.2688	0.094069	4.4359
0.6	2.3752	4.7217	0.10959	5.0106
1	3.8507	7.4755	0.099846	4.6466

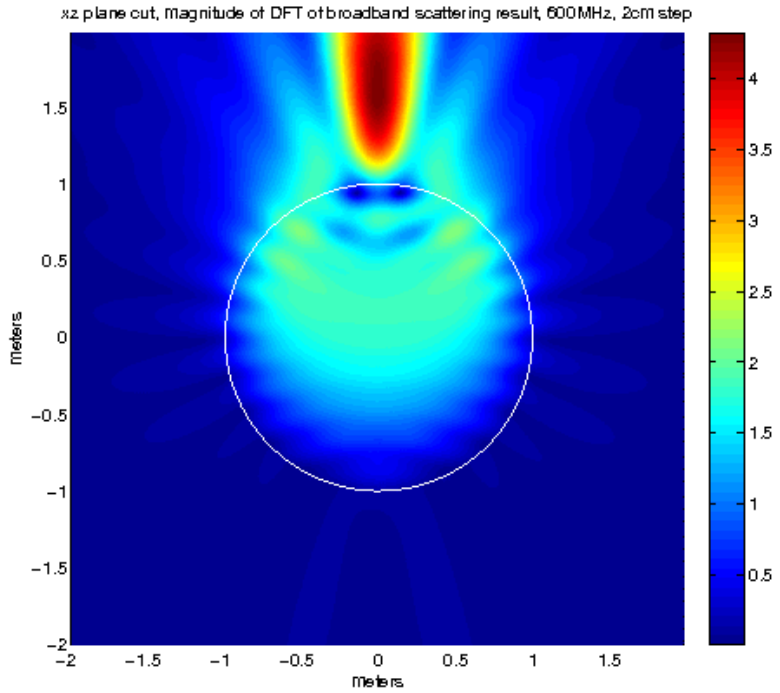

Figure 6.21: Frequency-domain dielectric sphere broadband signal scattering result, 600 MHz, xz plane cut

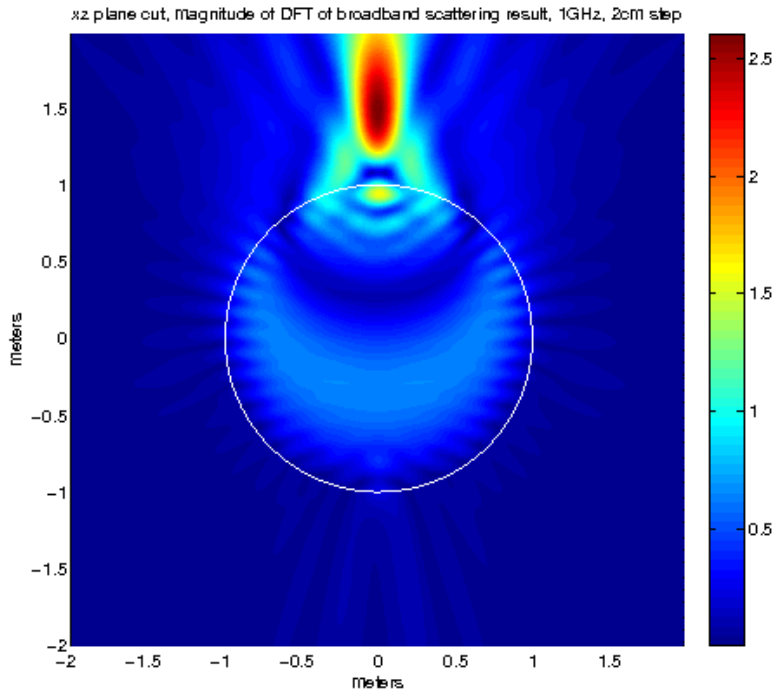

Figure 6.22: Frequency-domain dielectric sphere broadband signal scattering result, 1 GHz, xz plane cut

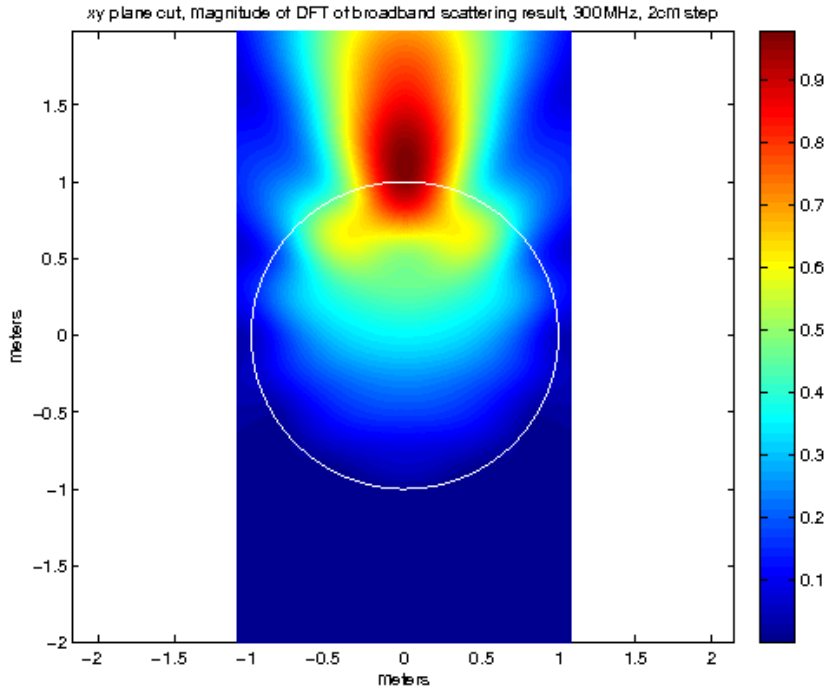

Figure 6.23: Frequency-domain dielectric sphere broadband signal scattering result, 300 MHz, xy plane cut

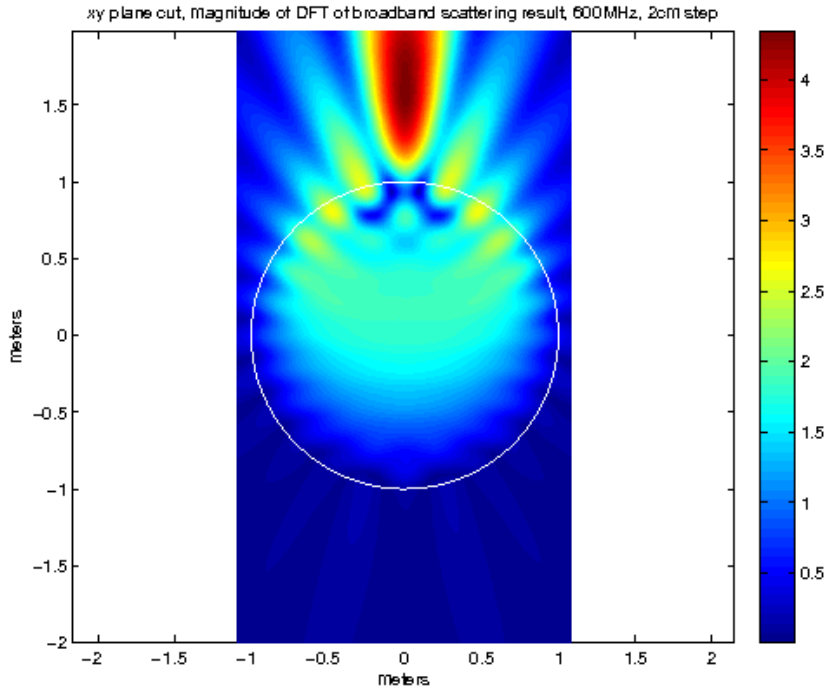

Figure 6.24: Frequency-domain dielectric sphere broadband signal scattering result, 600 MHz, xy plane cut

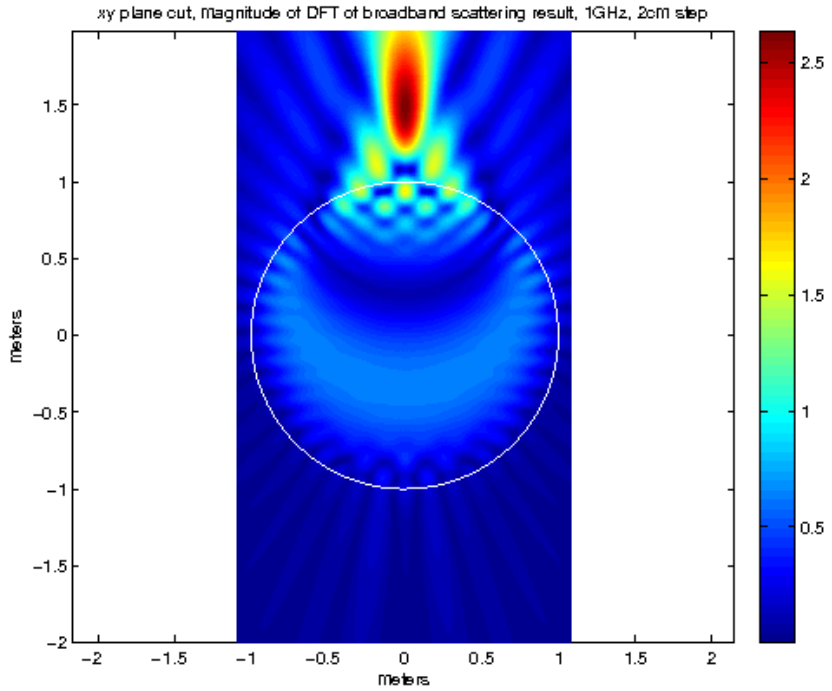

Figure 6.25: Frequency-domain dielectric sphere broadband signal scattering result, 1 GHz, xy plane cut

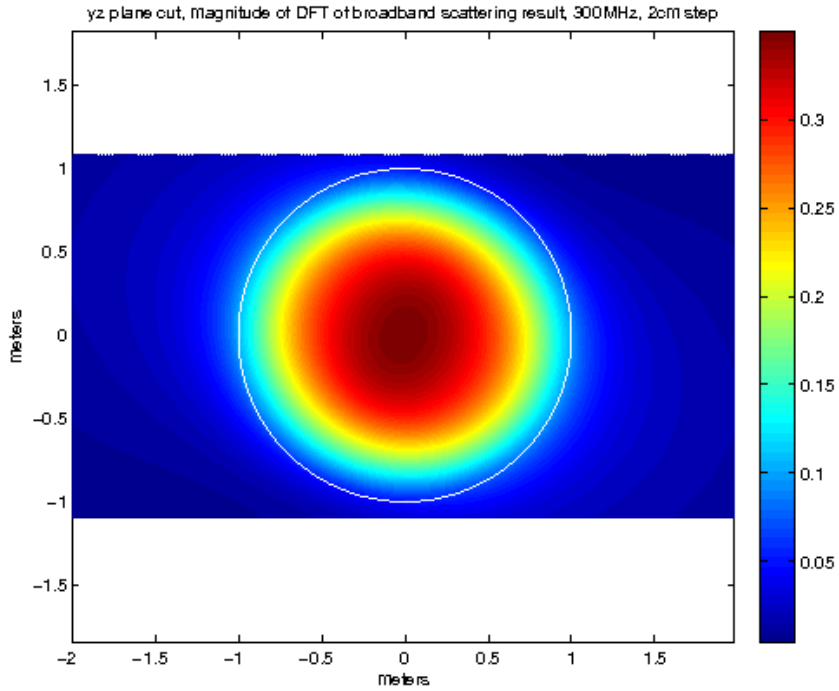

Figure 6.26: Frequency-domain dielectric sphere broadband signal scattering result, 300 MHz, yz plane cut

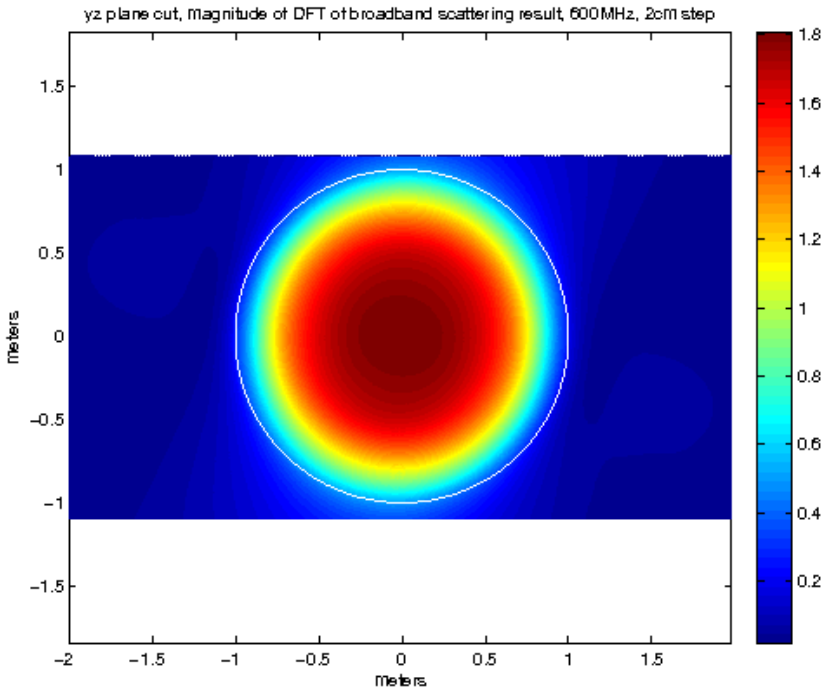

Figure 6.27: Frequency-domain dielectric sphere broadband signal scattering result, 600 MHz, yz plane cut

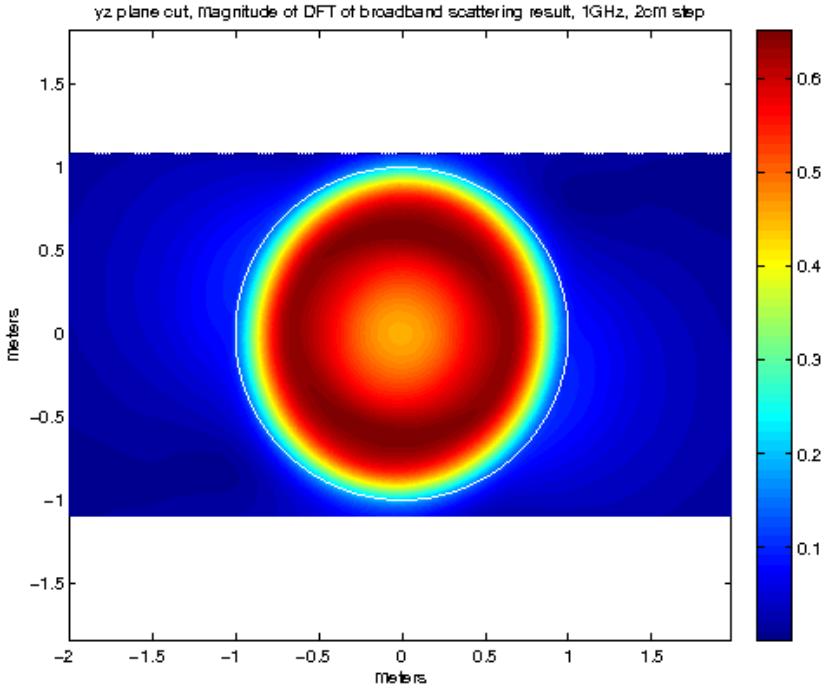

Figure 6.28: Frequency-domain dielectric sphere broadband signal scattering result, 1GHz, yz plane cut

CHAPTER 7

PARALLEL IMPLEMENTATION OF THE FDTD SCHEME

The FDTD scheme derived here is highly suitable for parallelization. As the availability of multi-core processors continues to increase, we are very interested in exploring the feasibility and implementation of parallel implementations of our FDTD scheme.

Consider the standard update equations, and the presence of updating coefficients. Each component update is conducted separately; these form the smallest parallel tasks which we will choose to consider. At this task level we have a strong data parallelism. We will find that the update process per component, per timestep is modest in the number of FLOPS it requires. So, in the design of resource-intensive simulations shown in previous chapters, memory tended to be the limiting resource over computation time.

The parallel simulations examined in this chapter are implemented using the Message Passing Interface (MPI) single-program multiple-data (SPMD) mode.

7.1 Memory Requirements and Work-Memory Ratio

For freespace regions of the domain, each cell requires six storage locations for $\vec{E}$ and $\vec{H}$ components, six for ε and μ parameters, six for σ^e and σ^m parameters, and eighteen (three per component) for updating coefficients. In addition, in problems where we use incident wave/scattered field formulation, we require storage for the phase data $\hat{k} \cdot \vec{r} - \ell_0$ at each component location, twelve incident component values total for past and previous timesteps, and a coefficient for each of those. We can free up twelve memory locations per node by observing that the material property fields are not needed after the updating coefficients are formed, and an additional twelve locations per node when we modify the incident fields to update in place.

We may also consider the memory consumed by auxiliary field storage in absorbing boundary and far-field schemes. The CPML scheme requires an additional updating coefficient and auxiliary field for each of two tangential components per boundary, totaling an additional four memory locations per CPML cell. Let us assume an eight cell thick layer on each boundary as has been

used in our simulations. The far-field algorithm requires four memory locations per cell, on a cubic equivalent surface internal to the domain; for simplicity let us assume the equivalent surface is the same size as the domain boundary.

Further, we also account for the extra components on the domain boundaries; $\vec{E}$ components which are tangential to a given boundary are extended by one, and $\vec{H}$ components which are normal to a given boundary are extended by one. This accounts for about $2N^2$ additional $\vec{E}$ components and N^2 additional $\vec{H}$ components per boundary.

Totaling up these requirements, for this FDTD formulation, in 3D simulations with a cubic domain N cells on a side, using incident plane wave, far-field and CPML techniques requires approximately $42N^3 + 219N^2$ memory locations. Of course, this will vary depending on the objects and sources within the domain, and departure from cubic dimensions.

We notice that updating coefficients contribute quite a bit to the memory requirements. Accordingly, let us briefly justify their use, setting aside the convenience in implementation of sources, elements, and other techniques. Counting the operations in a standard updating equation for a component of $\vec{E}$, our standard updating equation for $\vec{E}$ with updating coefficients requires nine memory references and seven FLOPS to calculate and store, assuming that the updating coefficients C are in memory. Stripping the detail from each coefficient so we may focus on resource consumption,

$$C_{ee} = \frac{2\varepsilon - \Delta t \cdot \sigma}{2\varepsilon - \Delta t \cdot \sigma},\ C_{eh} = \frac{2\Delta t}{2\varepsilon + \Delta t \cdot \sigma \cdot \Delta y},\ C_{eh} = \frac{-2\Delta t}{2\varepsilon + \Delta t \cdot \sigma \cdot \Delta y}.$$

The three updating coefficients themselves require a total of 16 memory references and 20 FLOPS to calculate. Recall also that we may choose to free up the material property fields before starting simulation timestepping.

The work-memory ratios ρ_{WM} of the two updating schemes are both close to 1, but the absolute number of references and FLOPS are significantly reduced by storing updating coefficients. So by storing the updating coefficients, we use only $3N^3$ more memory locations, reduce the memory references per component update by 64%, and reduce the FLOPS per component update by 74% in freespace. Note that the calculation of one half-timestep effectively limits the granularity of any parallel implementation of our FDTD scheme.

As complete data for $\vec{H}$ is required to update $\vec{E}$ components and vice versa, any partition of the data leads to a communication requirement after each half-timestep. In other words, the communication stage of each half-timestep is effectively serial: all cores must complete this before any can begin the next half-timestep.

7.2 Parallel Scheme

The data dependence of each cell for freespace and for all materials using the standard updating equations is only within the cell itself and the six cells neighboring its faces. This is the core reason why our derivation of the FDTD method can be parallelized to a large degree. We can separate the tasks of component updating by cell association, so that each process stores and manages a different portion of the domain. Referencing memory which is local to a process is usually much faster than communicating data between processes, due to the required transfers and MPI overhead. The most intuitive configurations, in which each core is assigned a contiguous volume of cells, also entail a desirable minimum of inter-core communication for common domain configurations. We will examine one component of these, in which the domain is split evenly along one dimension.

7.2.1 Standard Updating Equations

In the parallel implementations which follow, we partition the domain along the x-axis. In general, for a domain with $N \times M \times L$ cells in the x direction and P processes assigned to the task, we assign partitions of size approximately $(N/P) \times M \times L$ cells to each core, rounded to suit. Suppose the partition splits a domain at a cell with x-index n, with core 1 managing cells $m-1$, m and below in x, and core 2 managing cells m, $m+1$, and above in x.

Considering our definition of task as a single component update, we can view the load balancing in terms of tasks assigned per core. By splitting the number of cells as evenly as possible between cores, we split the tasks approximately evenly as well. We may expect to obtain good load balancing by this scheme, based upon our consideration so far. Observe that we have not accounted for partitioning the CPML or far-field tasks; this is described more in a later section. For now, note that we may expect these techniques to degrade the load balancing to only a slight degree, as the number of cores increases. We can observe good results for load balancing in the parallel

implementations described below.

The load balancing of a general parallel task is defined as $\beta \equiv T_{ave}/T_P$, where T_{ave} is the average time for all processors to complete the task, and T_P is the longest time required to complete the task, which sets total parallel runtime. A β-value of one suggests perfect balancing and is ideal, while extremely poor load balancing will be near zero. We calculate β-values given by the refinement of the dielectric sphere problem, based on time step timing data. Using each core's reported average time needed to complete one integer timestep, averaging these values provides T_{ave}.

Below we describe and show results of parallel implementation of two earlier examples. To consider load balancing we use a few figures from these examples. In the parallel version of our refined dielectric sphere scattering problem, which uses CPML on all boundaries and incident field and scattered field formulation, a parallel run on 12 cores yields $T_{ave} = 4.3630$ s and $T_P = 4.4134$ s, such that $\beta = 0.9886$. In the parallel version of our dielectric resonating antenna, which uses CPML on all boundaries and includes far-field processing, a parallel run on 12 cores yields $T_{ave} = 0.76538$ s and $T_P = 0.78063$ s, which yields $\beta = 0.9805$. This is evidence that our parallelization scheme, and choice of partitioning, produces respectable load balancing.

Let us consider some issues in a particular order, to emphasize importance to the parallel performance. We will consider updating the fields $\vec{E}$, $\vec{H}$ before we consider the formation of the updating coefficients. We will find that the data dependence of the standard updating equations require communication of elements tangential to the partitioned dimension: in our implementation, E_y, E_z, H_y, H_z components need to be communicated but E_x, H_x do not.

Suppose we are running a simulation usinc process count $P(\geq 3)$. For now assume that these cells contain only simple materials which use the standard updating equations. We can observe the data dependence by considering the updating equations at the appropriate locations for each component. First, consider H_y at a node with x-index m which is local to process 2. Suppose a partitioning point lies between nodes with x-indexes m and $m+1$, so that process 3 owns nodes with x-index $m+1$. The updating equation is repeated for convenience:

$$H_y^{n+\frac{1}{2}}(m,j,k) = C_{hyex}(m,j,k)\big(E_x^n(m,j,k) - E_x^n(m,j,k+1)\big) +$$
$$C_{hyez}(m,j,k)\big(E_z^n(m+1,j,k) - E_z^n(m,j,k)\big) +$$
$$+ C_{hyh}(m,j,k)H_y^{n-\frac{1}{2}}(m,j,k).$$

Notice that this update depends on $E_z^n(m+1,j,k)$, which is not local to process 2 but must be communicated from process 3. A similar observation for H_z at node m:

$$H_z^{n+\frac{1}{2}}(m,j,k) = C_{hzey}(m,j,k)\big(E_y^n(m,j,k) - E_y^n(m+1,j,k)\big)+$$
$$+ C_{hzex}(m,j,k)\big(E_x^n(m,j+1,k) - E_x^n(m,j,k)\big)+$$
$$+ C_{hzh}(m,j,k)H_z^{n-\frac{1}{2}}(m,j,k).$$

We notice dependence on $E_y(m+1,j,k)$ which is also local to process 3. However, observe H_x at node m:

$$H_x^{n+\frac{1}{2}}(m,j,k) = C_{hxez}(m,j,k)\big(E_z^n(m,j,k) - E_z^n(m,j+1,k)\big)+$$
$$+ C_{hxey}(m,j,k)\big(E_y^n(m,j,k+1) - E_y^n(m,j,k)\big)+$$
$$+ C_{hxh}(m,j,k)H_x^{n-\frac{1}{2}}(m,j,k).$$

This update equation does not depend on any data from node $m+1$ or beyond, but only data that is local to process 2.

Now, let us step to process 3, and consider updating E_y at node $m+1$. Repeated for convenience:

$$E_y^{n+1}(m+1,j,k) = C_{eyhx}(m+1,j,k)\big(H_x^{n+\frac{1}{2}}(m+1,j,k) - H_x^{n+\frac{1}{2}}(m+1,j,k-1)\big)+$$
$$+ C_{eyhz}(m+1,j,k)\big(H_z^{n+\frac{1}{2}}(m,j,k) - H_z^{n+\frac{1}{2}}(m+1,j,k)\big)+$$
$$+ C_{eye}(m+1,j,k)E_y^n(m+1,j,k).$$

We notice dependence on the term $H_z^{n+\frac{1}{2}}(m,j,k)$ which is local to process 2 rather than process 3. Omitting the other two updating equations, the pattern is as with the $\vec{H}$ fields: the y and z components require communication with process 2, and the x component does not. This pattern holds for each partition point.

We address this nonlocal data dependency with inter-process communication and what we will call 'local data redundant regions'. Each process' local partition of $\vec{H}$ data is appended on the $-x$ side with a redundant copy of the data needed to complete updates to $\vec{E}$; and each process' local partition of $\vec{E}$ data is appended on the $+x$ side with a redundant copy of the data needed

to complete updates to $\vec{H}$. These redundant regions are updated after each half-timestep using inter-process communication. Domain $-x$, $+x$ boundaries are exceptions where redundant data regions and communication are unnecessary.

Continuing with the previous example partition point, suppose our simulation is at timestep n. After process 2 completes its $n + \frac{1}{2}$ timestep update of $\vec{H}$, any required CPML calculation, and any required sampling, a call is made by process 2 to send the data $H_y(m, *, *)$ and $H_z(m, *, *)$ to process 3, where asterisks stand for the full extent of the field in the given dimension. Process 3 receives this data from process 2 and updates its redundant region, and sends analogous data on the next partition point to process 4, and so on. Process 2 receives analogous data from process 1 on the previous partition point.

The $n + 1$ timestep update can then proceed, as the redundant data regions contain the most current $\vec{H}$ data. After process 3 completes its $n + 1$ timestep update of $\vec{E}$, any required CPML calculation, any required lumped-element calculations, and any required sampling, a call is made by process 3 to send the data $E_y(m+1, *, *)$ and $E_z(m+1, *, *)$ to process 2. Process 2 receives this data from process 3 and updates its redundant region, and sends analogous data on the previous partition point to process 1.

For a cubic domain, each of these communication events is a transfer of $2 \times N \times N = 2N^2$ data values, per partition point, per timestep.

Now consider the initial setup of the domain and formation of the material property fields. Recall from Chapter 2 that we form the ε and μ arrays as averages of nearby material properties. On either side of a partition point, this averaging technique depends on data from both sides, so we have nonlocal dependency while setting up the material grid. Choosing the strategy here, we may opt for some simplicity: the complete material index grid is distributed to all cores. This is practicable for problems of modest size for three reasons: first, it is a one-time process which happens only at initialization. Second, for a cubic domain the data is only N^3 in size, rather than $3N^3$, as the material index data is representative of whole Yee cells. Third, the data is not needed after the material property grid is assembled, and can be cleared from memory. As mentioned earlier in this chapter, the same strategy is adopted for the material property grids $\varepsilon, \mu, \sigma^e, \sigma^m$ themselves. After the dependent updating coefficients are calculated, we also clear the material property grids from memory. We may note that for problems of extremely large size, even the N^3

communication and storage overhead may be unacceptable. In such a case we simply note that the relevant material index averages are either 2×1 cells or 2×2 cells in size, and so our data dependence is of nearly the same format as we saw in the field updating equations. The layout of data dependence is similar to what we saw of the $\vec{E}$ and $\vec{H}$ fields, and we may resort to a similar pattern of communication as outlined above to address it. After communication of the material index grid, the material property grids and the updating coefficients can then be calculated in parallel with no non-local dependency.

In summary, in order to complete an update to $\vec{H}$, the $\vec{E}$ perpendicular components at each partition point must be communicated to the process "below", in the sense of x-indices. In order to complete an update to $\vec{E}$, the $\vec{H}$ perpendicular components at each partition point must be communicated to the process "above" in the sense of x-indices.

This portion of the parallelization scheme leads to the large majority of the communication required. We will find that the far-field technique requires comparatively little extra communication, and CPML, incident wave/scattered field formulation, and lumped elements require none.

7.2.2 Additional Communication Requirements

The communication overhead required by extensions to the scheme is surprisingly small. For example, the lumped elements previously considered can span a partition point with no additional communication beyond what is required for the standard updating equations.

Lumped Elements

The lumped source, resistor, capacitor, and inductor elements are all easily extended to a parallel implementation. Consider the resistor and capacitor: as shown in Chapter 3, these passive elements only require a modification of existing updating coefficients. Thereafter, the standard updating algorithm is applied with these modified coefficients. Most importantly, there is no new data dependence beyond the standard updating equations. Hence, a resistor or capacitor element can cross a domain partition and function as intended with no additional code or communication overhead.

Inductor, voltage, and current source elements all require auxiliary fields as well as a modification of updating coefficients. As observed in Chapter 3, an inductor in the cell labeled (i, j, k)

requires storage of the previous current flux through the cell, $J_i^{n-\frac{1}{2}}(i,j,k)$ in order to update to the $n+\frac{1}{2}$ timestep. Yet, this is the only additional data dependency - and it's a local auxiliary field, computed using same-cell E values. So we have no additional data dependency between processes and can update with the standard update redundancy.

Circumstances are similar for voltage sources; rather than computing $J_i^{n+\frac{1}{2}}(i,j,k)$ from $\vec{E}$ field values, we assign the term a waveform to timestep through. The waveform is precalculated and not affected by grid values, so there are no additional data dependencies between processes for voltage or current sources.

CPML Boundaries

Examining a sample updating equation for E_x in a CPML region (adjacent to any of $\pm y$ or $\pm z$), and returning to our hypothesized partition point at $i = m$:

$$\begin{aligned} E_x^{n+1}(m,j,k) = {} & C_{exe}(m,j,k)E_x^n(m,j,k) + \\ & + C_{exhz}(m,j,k)\big(H_z^{n+\frac{1}{2}}(m,j,k) - H_z^{n+\frac{1}{2}}(m,j-1,k)\big) + \\ & + C_{exhy}(m,j,k)\big(H_y^{n+\frac{1}{2}}(m,j,k) - H_y^{n+\frac{1}{2}}(m,j,k-1)\big) + \\ & + C_{\Psi exy}(m,j,k)\Psi_{exy}^{n+\frac{1}{2}}(m,j,k) + C_{\Psi exz}\Psi_{exz}^{n+\frac{1}{2}}(m,j,k). \end{aligned}$$

Observing the dependence of this equation, we see that the dependencies of the usual updating equation are in play – in this case of E_x, no non-local data dependence. The additional terms of $C_{\Psi exy}(m,j,k)\Psi_{exy}^{n+\frac{1}{2}}(m,j,k)$, $C_{\Psi exz}\Psi_{exz}^{n+\frac{1}{2}}(m,j,k)$ refer to the auxiliary fields which are partitioned and stored the same way as the fields they act on. Hence, these CPML adjustments add no additional non-local data dependence, and no additional communication requirement.

Scattered Field and Incident Field Formulation

Recall that the scattered field formulation follows naturally after implementation of the incident field; the standard updating equations refer to the scattered $\vec{E}$ and $\vec{H}$ fields without modification. So, a scattered field formulation does not alter the data dependency of standard updating equations.

Also as observed in Chapter 6, the incident field is calculated analytically at each point. This process depends only on phase data $\hat{k}\cdot\vec{r}-\ell_0$, the scalar choice of waveform, and the timestep. The

required incident fields and phase data are distributed across cores with the same partitioning as the updating coefficients and $\vec{E}$, $\vec{H}$ data, up to redundancy. Hence there is no new non-local data dependence added when updating a scattered field and incident field formulation.

Far Field Transformation

Recall our equivalent surface S from Chapter 6, and let us examine the original point (S_{Lx}, j, k) and another cell face in addition to the one previously chosen. On the $-x$ face of S, the equivalent magnetic current component M_y is given by E_z, which we must take a spatial average to find:

$$M_y(S_{Lx}, j, k) = -\frac{1}{2}\left(E_z(S_{Lx}, j, k) + E_z(S_{Lx}, j, k+1)\right).$$

Similarly, the equivalent electric current component J_y is given by H_z, which we must average to find:

$$J_y(S_{Lx}, j, k) = \frac{1}{4}\left(H_z(S_{Lx}-1, j, k) + H_z(S_{Lx}, j, k) + H_z(S_{Lx}-1, j, k+1) + H_z(S_{Lx}, j, k+1)\right).$$

In the calculation of M_y the x index remained constant, which means if we assign all M_y values for the $-x$ face to the process that owns x-index S_{Lx}, then we have only local data dependence. Unfortunately we will not be able to arrange local data dependence for all components and faces.

Examining the calculation of J_y above we notice references to both x-indexes S_{Lx}, $S_{Lx}-1$. If it happens that these indexes are separated by a partition point, we need to consider the data dependency. Here, we notice that we require $x-$adjacent H_z components. If we assign our J_y field to the upper process, the one which owns x-index S_{Lx}, we find that its redundant data region already contains the required $S_{Lx}-1$ data, due to the standard updating equation dependences.

So far, we have not incurred any extra communication requirements. By comparison with Chapter 6 far-field component equations, we may verify that this situation holds for most of the components. Unfortunately when we examine J_z as it occurs on $\pm y$ and $\pm z$ faces, we find that there is an unavoidable non-local data dependency in the field averages. Considering the $-y$ face of equivalent surface S, we have that $J_z = H_x$, and we must form the average

$$J_z(i, S_{Ly}, k) = \frac{1}{4}\left(H_x(i, S_{Ly}-1, k) + H_x(i, S_{Ly}, k) + H_x(i+1, S_{Ly}, k) + H_x(i+1, S_{Ly}-1, k)\right).$$

We observe the dependence on nodes at x index i as well as $i+1$. Recall that the standard updating equations do not require communication of H_x components, so we need to conduct a custom communication of these components. For this $-y$ face, we may initially expect to communicate data of size $2(S_{Uz} - S_{Lz} + 1)$ memory locations per timestep. However, realizing that we only need the sum of components rather than their individual values, we choose to sum two components prior to communication and reduce the communication to $S_{Uz} - S_{Lz} + 1$ values. A nearly identical consideration applies to the $+y$ face and the J_z component.

We also find unavoidable non-local data dependency in J_y for the $\pm z$ faces. Considering the $-z$ face, we obtain $J_y = -H_x$ and we must take average

$$J_y(i, j, S_{Lz}) = -\frac{1}{4}\left(H_x(i, j, S_{Lz} - 1) + H_x(i + 1, j, S_{Lz} - 1) + H_x(i, j, S_{Lz}) + H_x(i + 1, j, S_{Lz})\right).$$

As before, this requires communication of H_x components; here we must transfer $S_{Uy} - S_{Ly} + 1$ values.

So, the total additional communication required to update a far field surface is $2(S_{Uy} - S_{Ly} + 1 + S_{Uz} - S_{Lz} + 1)$ per partition point. We consider the worst-case approximation that S is the same size as the domain boundaries, and we assume our domain is cubic, N grid cells on a side. Then our far-field communication requirement is approximately $2(N + N) = 4N$ per partition point, per timestep. The standard updating equation requirements of $2N^2$ per partition point, per timestep, and we see that the far field communication requirements are small in comparison.

7.3 Parallel Results

Where the timing $T_1$for a one-process run is available, we report the speedup. The speedup for P cores is defined as $\frac{T_1}{T_P} \equiv S_P$, and the parallel efficiency, E_P, defined as $\frac{S_P}{P}$. Higher efficiency numbers indicate better performance, with $E_P = 1$ being exactly linear speedup.

Dielectric sphere scattering problem

The dielectric sphere scattering problem described at the end of Chapter 6 was run with the parallel scheme described above.

Table 7.2: Dielectric sphere refinement parallel timing results

Cores	Total time (s)	Average time per timestep (s)	Speedup	Parallel Efficiency
1	135293.6116	34.9862	-	-
3	50000.1718	12.7985	2.7059	0.9020
6	29190.591	6.9525	4.6348	0.7725
12	17524.074	4.3630	7.7204	0.6434

Table 7.3: Dielectric resonating antenna refinement 1, boresight axial ratio by parasitic patch length

Feed Strip ℓ_1 (mm)	Axial Ratio Minimum (dB)	Frequency (GHz)	Parasitic Patch ℓ_2 (mm)
10	1.1436	3.34	12
10	4.1898	3.49	10
10	4.6995	3.81	8

Table 7.1: Dielectric sphere parallel timing results

Cores	Total time (s)	Average time per timestep (s)	Speedup	Parallel Efficiency
1	9825.917	5.1753	-	-
3	4306.5268	2.2036	2.2816	0.7605
6	3360.9238	1.6781	2.9236	0.4873
12	2414.6489	1.1683	4.069	0.3391

The same dielectric sphere scattering problem was run with a refinement of the grid: the problem description is identical up to the spatial step sizes, which is chosen to be uniformly 0.01 m. This leads to a timestep of half of its previous value, so the problem was run to 4000 timesteps. The xz cross sections at 300MHz, 600 MHz, 1GHz are illustrated below.

Dielectric resonating antenna refinement 1

The dielectric resonating antenna simulations were run with a refined grid, with step sizes $\Delta x = 0.25$mm, $\Delta y = 0.245$mm, $\Delta z = 0.25$mm. This results in a timestep half of the original, hence we run for 30000 timesteps.

We calculate the boresight axial ratio by frequency and find the minimum, tabulated below. For the points calculated, the $\ell_2 = 12, 10$mm results agree within about 10% of the data charted in [15, Fig. 15], and the $\ell_2 = 8$mm result agrees within about 30%. The full data are charted below. Unfortunately due to exceeding allotted computation time, the results for 3 and 6 core runs for

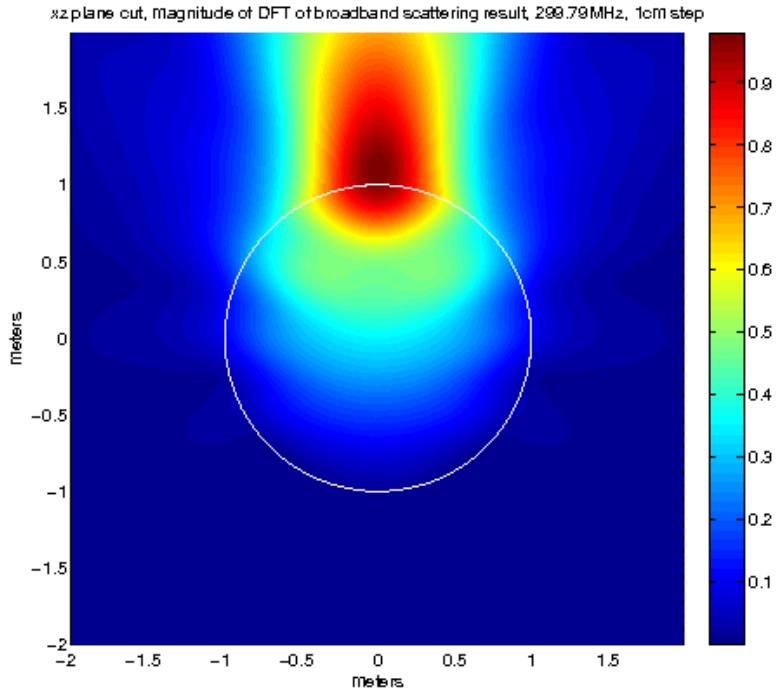

Figure 7.1: Frequency-domain dielectric sphere refinement, scattering result, 300 MHz, xz plane cut

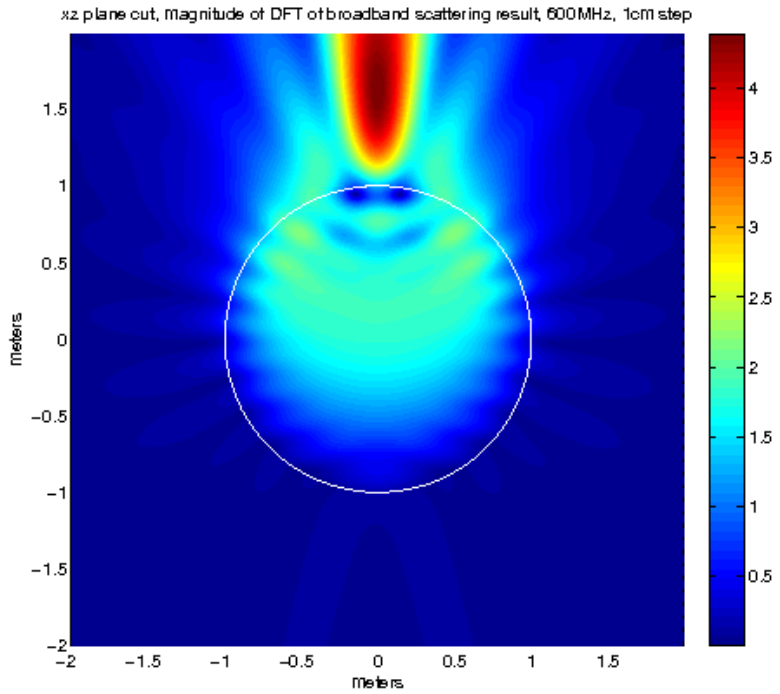

Figure 7.2: Frequency-domain dielectric sphere refinement, scattering result, 600 MHz, xz plane cut

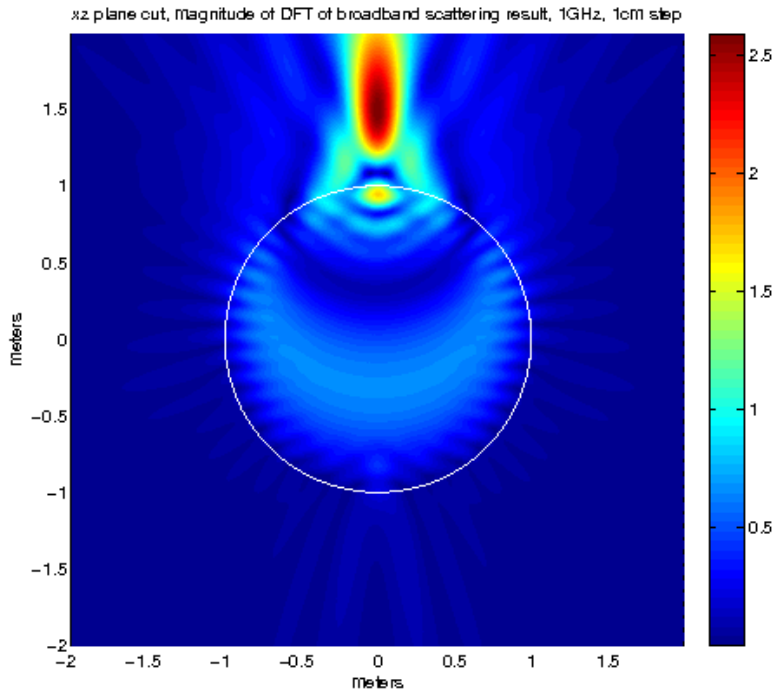

Figure 7.3: Frequency-domain dielectric sphere refinement, scattering result, 1 GHz, xz plane cut

$\ell_2 = 8$mm are unavailable.

Dielectric resonating antenna refinement 2

The dielectric resonating antenna simulations were run with a refined grid, with step sizes $\Delta x = 0.125$mm, $\Delta y = 0.1225$mm, $\Delta z = 0.125$mm. This results in a timestep one-quarter of the original, hence we run for 60000 timesteps. Unfortunately, for all runs involving 1 and 3 cores, the simulation exceeded allotted time and the results were unavailable.

Table 7.4: Dielectric resonating antenna refinement 1 parallel timing results

Cores	Total time (s)	Average time per timestep (s)	Speedup	Parallel Efficiency
Feed strip $\ell_1 = 10$ mm, parasitic patch $\ell_2 = 12$ mm				
1	217082.4286	6.6586	-	-
3	79449.5648	2.2653	2.7323	0.9108
6	51596.0062	1.4960	4.2073	0.7012
12	40268.6279	1.1346	5.3909	0.4492
Feed strip $\ell_1 = 10$ mm, parasitic patch $\ell_2 = 10$ mm				
1	220538.2762	6.7151	-	-
3	78936.6303	2.2283	2.7939	0.9313
6	51296.3603	1.4476	4.2993	0.7165
12	41336.8736	1.1191	5.3351	0.4446
Feed strip $\ell_1 = 10$ mm, parasitic patch $\ell_2 = 8$ mm				
1	221993.858	6.6905	-	-
3				
6				
12	39956.1142	1.0741	5.5559	0.4630

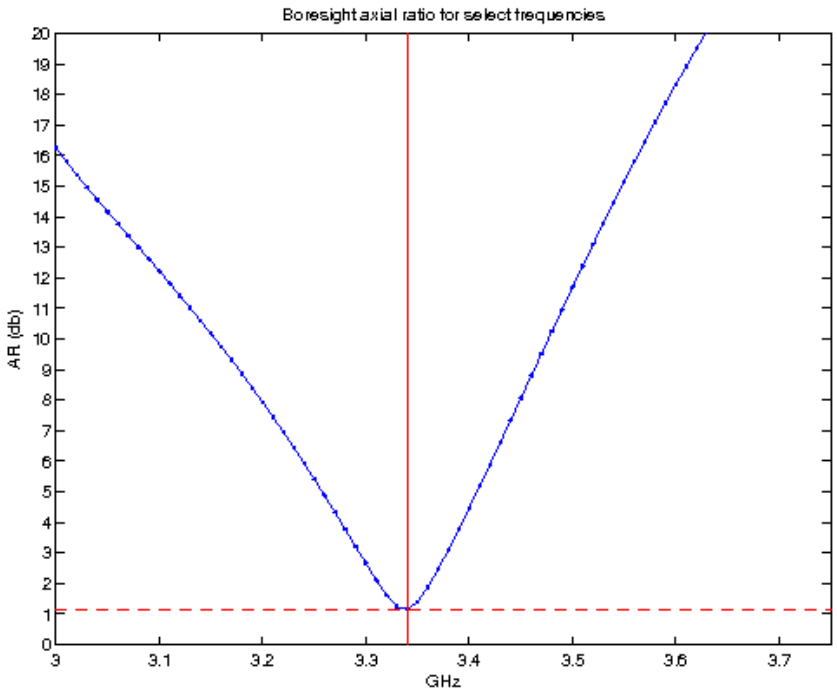

Figure 7.4: Boresight axial ratio of DRA refinement 1 with feed strip length 10mm, parasitic patch length 12mm.

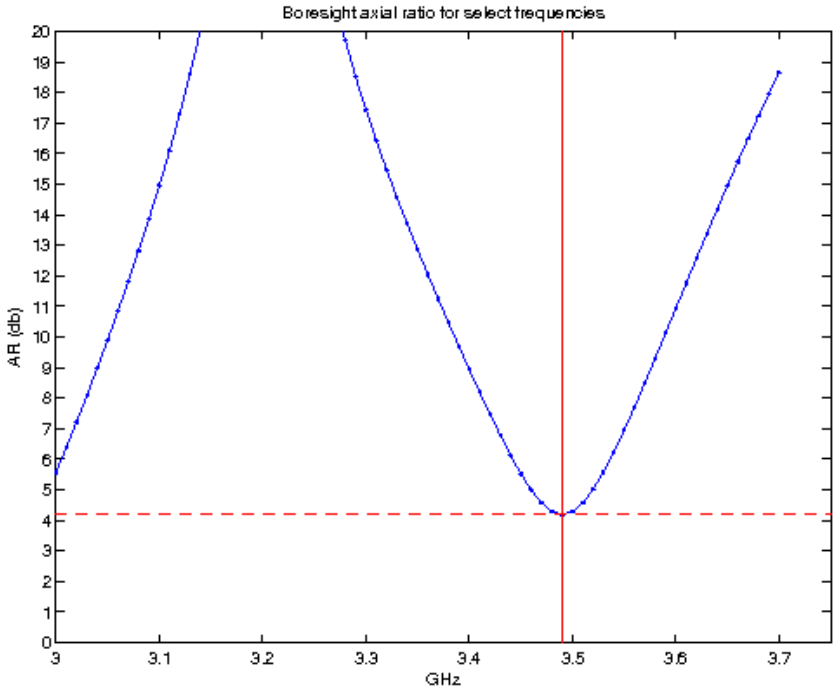

Figure 7.5: Boresight axial ratio of DRA refinement 1 with feed strip length 10mm, parasitic patch length 10mm.

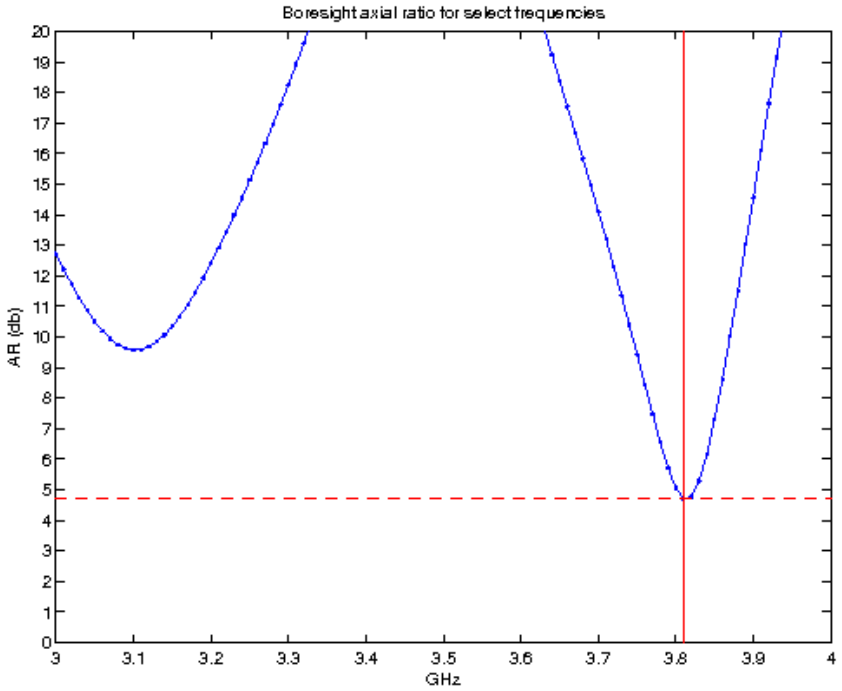

Figure 7.6: Boresight axial ratio of DRA refinement 1 with feed strip length 10mm, parasitic patch length 8mm.

Table 7.5: Dielectric resonating antenna refinement 2 parallel timing results

Feed strip $\ell_1 = 10$ mm, parasitic patch $\ell_2 = 12$ mm		
Cores	Total time (s)	Average time per timestep (s)
1		31.4327
3		10.6686
6	445207.5573	6.6999
12	340292.5074	4.7712
Feed strip $\ell_1 = 10$ mm, parasitic patch $\ell_2 = 10$ mm		
1		31.9647
3		10.9776
6	440284.84	6.2266
12	333927.3864	4.6316
Feed strip $\ell_1 = 10$ mm, parasitic patch $\ell_2 = 8$ mm		
1		
3		
6	450036.2665	6.7287
12		

REFERENCES CITED

[1] J.-P. Berenger. A perfectly matched layer for the absorption of electromagnetic waves. *Journal of Computational Physics*, 114(2):185–200, 1994.

[2] J.-P. Berenger. Three-dimensional perfectly matched layer for the absorption of electromagnetic waves. *Journal of Computational Physics*, 127(2):363–379, 1996.

[3] J.-P. Berenger. *Perfectly Matched Layer (PML) for Computational Electromagnetics*. Morgan & Claypool, 1st edition, 2007.

[4] W. C. Chew and W. H. Weedon. A 3D perfectly matched medium from modified Maxwell's equations with stretched coordinates. *Microwave and Optical Technology Letters*, 7(13):599–604, 1994.

[5] Q.-X. Chu, Z.-H. Chen, and Y.P. Zhang. FDTD modeling of matched impedance terminating a microstrip line. *International Journal of RF and Microwave Computer-Aided Engineering*, 15(3):325–328, 2005.

[6] W.R. Eisenstadt and Y. Eo. S-parameter-based IC interconnect transmission line characterization. *Transactions on Components, Hybrids, and Manufacturing Technology*, 15(4):483–489, 1992.

[7] A. Elsherbeni and V. Demir. *The Finite-Difference Time-Domain Method for Electromagnetics with MATLAB Simulations*. SciTech Publishing, Inc, 1st edition, 2009.

[8] J. Fang and D. Xeu. Numerical errors in the computation of impedances by FDTD method and ways to eliminate them. *IEEE Microwave and Guided Wave Letters*, 5(1):6–8, 1995.

[9] D.J. Griffiths. *Introduction to Electrodynamics*. Prentice-Hall of India, 3rd edition, 1999.

[10] M.A.R. Gunston. *Microwave Transmission-Line Impedance Data*. Van Nostrand Reinhold Company Ltd, 1st edition, 1972.

[11] U.S. Inan and R.A. Marshall. *Numerical Electromagnetics: The FDTD Method*. Cambridge University Press, 1st edition, 2011.

[12] J.D. Jackson. *Classical Electromagnetics*. John Wiley & Sons, Inc, 2nd edition, 1975.

[13] K. Kurokawa. Power waves and the scattering matrix. *IEEE Transactions on Microwave Theory*, 13(2):194–202, 1965.

[14] M. Kuzuoglu and R. Mittra. Frequency dependence of the constitutive parameters of causal perfectly matched anisotropic absorbers. *IEEE Microwave and Guided Wave Letters*, 6(12):447–449, 1996.

[15] B. Li and K. W. Leung. Strip-fed rectangular dielectric resonator antennas with/without a parasitic patch. *IEEE Transactions on Antennas and Propagation*, 53(7):2200–2207, 2005.

[16] J. Roden and S. Gedney. Convolution PML (CPML): an efficient FDTD implementation of the CFS-PML for arbitrary media. *Microwave and Optical Technology Letters*, 27(5):334–339, 2000.

[17] S. A. Schelkunoff. Some equivalence theorems of electromagnetics and their application to radiation problems. *Bell System Technical Journal*, 15:92–112, 1936.

[18] D. Sheen, S. Ali, M. Abouzahra, and J. Kong. Application of the three-dimensional finite-difference time-domain method to the analysis of planar microstrip circuits. *IEEE Transactions on Microwave Theory*, 38(7):849–857, 1990.

[19] A. Taflove and S. C. Hagness. *Computational electrodynamics: the finite-difference time-domain method*. Artech House, Inc., 3rd edition, 2005.

[20] F. L. Teixeira and W. C. Chew. On causality and dynamic stability of perfectly matched layers for FDTD simulations. *Transactions on Microwave Theory and Techniques*, 47(6):775–785, 1999.

[21] K. R. Umashankar, A. Taflove, and B. Beker. Calculation and experimental validation of induced currents on coupled wires in an arbitrary shaped cavity. *IEEE Transactions on Antennas and Propagation*, AP-35(11):1248–1257, 1987.

[22] K. Yee. Numerical solution of initial boundary value problems involving Maxwell's equations in isotropic media. *IEEE Transactions on Antennas and Propagation*, 14(3):302–307, 1966.

[23] X. Zhang, J. Fang, and K.K. Mei. Calculations of the dispersive characteristics of microstrips by the time-domain finite difference method. *IEEE Transactions on Microwave Theory and Techniques*, 36(2):263–267, 1988.

[24] H. Zhao, S. Crozier, and F. Liu. A high definition, finite difference time domain method. *Applied Mathematical Modeling*, 27:409–419, 2003.